THE USE OF MULTIPLE ANTENNA TECHNIQUES FOR UWB WIRELESS PERSONAL AREA NETWORKS (UWB-MIMO WPANs)

Mr. Mason Adam

Submitted in Partial Fulfilment of the Requirements of the Degree of Doctor of Philosophy, October 2014

Contents

LIST OF FIGURES

List of Tables

Abbreviations

DC 32-QAM	Dual Carrier 32 Quadrature Amplitude Modulation
DCM	Dual Carrier Modulation
UWB	Ultra Wide Band
QPSK	Quadrature Phase Shift Keying
8PSK	Eight Phase Shift Keying
OFDM	Orthogonal Frequency Division Multiplexing
MB-OFDM	Multiband Orthogonal Frequency Division Multiplexing
CSI	Channel State Information
RMS	Root Mean Square
ML	Maximum Likelihood
ZPS	Zero-PaddedSuffix
MSB	Most Significant Bit
SISO	Single Input Single Output
MIMO	Multiple Input Multiple Output
OFDM	Orthogonal Frequency Division Multiplexing
G1	Group One containing five interleaved and coded bits
G2	Group two containing 2nd five interleaved and coded bits
PSK	Phase Shift Keying
PLCP	Physical Layer Convergence Protocol
PPDU	PLCP Packet Data Unit
PSDU	Physical Service Data Unit
FCC	Federal Communications Commission
LLR	Log Likelihood Ratio
TDS	Time Domain Spreading

FDS	Frequency Domain Spreading
TFI	Time Frequency Interleaving
FFI	Fix Frequency Interleaving
TFC	Time Frequency Coding
FFT	Fast Fourier Transform
FEC	Forward Error Correction
STBC	Space-Time Block Code
STTC	Space-Time Trellis Codes
AWGN	Additive White Gaussian Noise
IEEE	Institute of Electrical and Electronics Engineers
IEEE 802.15	Working Group of IEEE
IFFT	Inverse Fast Fourier Transform
BCJR	Bahl Cocke Jelinek and Raviv algorithm
Log-MAP	Logrithmic Maximum A Posteriori decoding
SOVA	Soft Output Viterbi Algorithm
ECMA-368	ECMA international Standard for UWB technology
PER	Packet Error Rate
LOS	Line Of Sight propagation
BER	Bit Error Rate
NLOS	Non Line Of Sight propagation
SNR	Signal to Noise Ratio

Abstract

The research activities over the three years were presented in this thesis. The work centred on the use of multiple spatial elements for Ultra wide band wireless system in order to increase the throughput, and for wireless range requirement applications, increases the coverage area. The challenges and problems of this type of implementation are identified and analysed when considered at the physical layer. The study presents a model design that integrates the multiple antenna configurations on the short range wireless communication systems. As the demand for capacity increases in Wireless Personal Area Networks (WPAN); to address this issue, the framework of the Wi-Media Ultra Wide Band (UWB) standard has been implemented in many WPAN systems. However, challenging issues still remain in terms of increasing throughput, as well as extending cellular coverage range. Multiple Input Multiple Output (MIMO) technology is a well-established antenna technology that can increase system capacity and extend the link coverage area for wireless communication systems. The work started by carrying out an investigation into integrated MIMO technology for WPANs based on the Wi-Media framework using Multi-band Orthogonal Frequency Division Multiplexing (MB-OFDM). It considered an extensive review of applicable research, the potential problems posed by some approaches and some novel approaches to resolve these issues. The proposed ECMA-368 standard was considered, and a UWB system with a multiple antenna configuration was undertaken as a basis for the analysis. A novel scheme incorporating Dual Circular 32 - QAM was proposed for MB-OFDM based systems in order to enhance overall throughput, and could be modified to increase the

coverage area at compromise of the data rate. The scheme was incorporated into a spatial multiplexing model with measured computational complexity and practical design issues. This way the capacity could be increased to twice the theoretical levels, which could pay the way to high speed multi-media wireless indoor communication between devices. Furthermore, the range of the indoor wireless network could be increased in practical wireless sensor networks. The inherent presence of spatial and frequency diversity that is associated with this multiple radiators configuration enlarge the signal space, by introducing additional degrees of freedom that provide a linear increase in the system capacity, for the same available spectrum. By incorporating the spatial elements with a Dual Circular modulation that is specified within the standard, it can be shown that a substantial gain in spectral efficiency could be possible. A performance analysis of this system and the use of spatial multiplexing for potential data rates above Gigabit per second transmission were considered. In this work, a model design was constructed that increases the throughput of indoor wireless network systems with the use of dual radiating elements at the both transmitter and receiver. A simulation model had been developed that encapsulate the proposed design. Tests were carried out which investigate the performance characteristics of various spatial and modulation proposals and identifies the challenges surrounding their deployments. Results analysis based on various simulation tests including the IEEE802.15.3a UWB channel model had shown a lower error rate performance in the implementation of the model. The proposed model can be integrated in commercial indoor wireless networks and devices with relatively low implementation cost. Further, the design used in future work to address the current challenges in this field and provides a framework for future systems development.

1Introduction

1.1 Overview

The Wireless Personal Area Network (WPAN) is a short range communication system that interconnects various applications in the home and office environments. WPAN networking technology has grown considerably in the last few years, partly because of the advances in the underlying technology and partly due to its commercial merits penetrating the consumer market. Nevertheless, since the Federal Communication Commission's (FCCs) decision to allow unlicensed UWB operation in the 3.1-10.6GHz spectrum with power restrictions [1], there has been a surge in the number of commercially available short range wireless portable products. There has also been a growing interest in the technology from the academic community due to the potential benefits of wireless short range communications. There are currently various wireless communication networks that includes cellular, GPS, Military, Emergency and public services all of which had been assigned to a particular part of the frequency spectrum. The decision to allow unlicensed WPANs in the UWB spectrum has presented at the same time an opportunity and a challenge for RF designers. In a design approach, the flexibility over the physical layer has meant that different protocols at different layers could be implemented based on specific

applications tailored to a specific environment. The difficulty on the other hand stems from the spectral mask that has been defined in the proposal. This is because the federal authority requirements concerning the radiated power have made it very challenging to design receivers that distinguish between noise and signal data at very low power levels. Highly sensitive receivers, by their very nature require complicated design and hence increase the processing cost as well as the financial cost. The IEEE have established the IEEE 802.15.3a standards group based on previous research work by [2], in order to develop a standard model for the UWB PAN physical layer proposal and to meet the growing demands in UWB applications with high data rates. Although, the proposed standard has been dropped due to a disagreement between two subgroup proposals, the model has considered fundamental characteristics of the propagation channel which has been used in other proposals and standards. One practical challenge has been surrounding UWB communications for a while which is how to emulate the wireless medium. For example, could a deterministic model based on only measured data be enough to describe the wireless channel. The IEEE 802.15.3a standard has combined a number of data analyses for different measurement campaigns in a stochastic model and these were based on common propagation parameters that define many of the UWB wireless communication systems. Another key element to consider in the design of a channel model is the representation of multipath propagation in which the IEEE 802.15.3a standard has represented in terms of clustering using the Saleh-Valenzuela (SV) modified model. This representation resembles the arrival of multipath components of real measurement data of UWB waveforms. This type of observation has helped significantly in the way modern channel models can be developed in simulation.

Also, the large bandwidth that defines UWB systems has facilitated numerous

approaches to utilising the spectrum for short range wireless data communication. One classic approach had used all the available spectrum of the signal at very low power with very with very short duration to transmit information, where additional capacity could be obtained by incorporating a pseudo random spreading sequence with the signal pulse. Such approach makes use of the spatial property of these pulses in combating signal fading. Furthermore, there is no need for a carrier signal in this method as it tends to consume power and spectrum both of which are very scarce. Although this type of transmission scheme has been the traditional approach, the single band nature of its communication has remained a point of discussion in industry and research communities. In [3], a discussion regarding the physical layer has highlighted the concept behind the multiband design. Here, the model has been one which divides the large spectrum into sub-bands of 500 MHz or more and modulating the signal information using Orthogonal Frequency Division Multiplexing (OFDM). OFDM has been used for many years in conventional RF communications and has proved its effectiveness. Moreover, the underlying technical knowledge has been familiar to designers and researches alike, and hence made more sense for the scheme to be considered in research studies. Nevertheless, there is a major difference between OFDM in the narrowband and ultra wideband applications. In narrowband systems, OFDM symbols are transmitted over a single band, while in UWB domains, the symbols are interleaved over different bands. This inevitably requires reconsideration of the physical layer protocol, and should take into account coding and transmission design procedures.

The Multiband OFDM Alliance Special Interest Group (MBOA-SIG) of industrial consortia had supported the Multiband OFDM transmission scheme for UWB

applications. The industrial backing of this scheme has shaped consumer electronics in the UWB domains and has resulted in its integration on the Universal Serial Bus (USB) and Bluetooth-SIG systems. In addition, the publication of the ECMA-368 standard [4] by the Wi-Media Alliance has forwarded the technology into the commercial market and facilitated worldwide recognition. The ECMA-368 standard defines the physical layer and Medium Access Control (MAC) sub layer interface for short range wireless high speed communications. It was very important to standardise the free license in order to push the technology developments forward. When considering antenna technology for UWB systems a combination of frequency division and Multiple Input Multiple Output (MIMO) antenna schemes could be used in WPANs. The benefits of implementing MIMO technology in wireless communications have been well proven and documented for narrow band systems. The rapid increase in indoor multimedia networked applications from high-definition television (HDTV) to fully integrated home and office devices that rely on short range wireless links have highlighted the need for the multiple antenna technology in the UWB domain. If MIMO had been incorporated in the physical layer, then the received power could be enhanced as well as the range without violating the low emission levels imposed by the regulation authorities. Due to the large bandwidth available in UWB systems, frequency diversity tends to exists in such configuration which could be used in the information coding process to increase the rate of transmission. Although MIMO technology seems to represent an obvious solution for increasing the capacity of UWB applications, there has been a slow progress in its integration in commercial products. One of the key challenges for the technology has been the increase in the complexity and cost to the front end RF modules as well as the signal processing algorithms. On the one hand wireless portable devices for personal communications tend to be small in size and require minimum embedded

complexity. On the other hand, multiple antennas need special transmission coding and demodulation, and that increases the processing in the transmitter and receiver. Nevertheless, the rapid demand for WPAN in the last few years has raised the technology profile in the commercial world, and that has fostered more research in PANs. However, and more importantly, MIMO systems and their implementation have moved a long way in the last decade with the developments of more advanced signal processing algorithms. These developments have in turn enabled RF engineers to pursue very complex wireless link designs and introduce novel concepts in the transmission layer protocols.

1.2 Research aim and Objectives

The aim of this research was to propose a multiple spatial simulation model at the physical layer that operate in the Ultra wide band domain for Wireless personal Area Networks to enable an increase in the transmission rate to a maximum of dual the current available rate without an increase in the transmission power, or a reduction in the error performance. In addition, it facilitates an improvement in the data rate for capacity sensitive applications, and becomes configurable in order to enable an

increase in the wireless communication link for wireless range sensitive applications. For these applications, it was possible to increase the transmission range at the expense of the available data rate by a modification to the receiving algorithm. The proposed model would have the ability to vary the information rate in the link depending on the status of the channel. The scheme makes use of the channel diversity to reduce the fading correlation factors and improve the error performance of the wireless model. This research deals with the standard model that had been implemented in real commercial and consumer electronics. Due to the strong backing by various industrial consortia, the ECMA-368 standard had been developed and adapted in many commercial products. Hence, the intended model considers the ECMA-368 standard physical layer requirements and conditions in the implantation process. In particular, a method of integrating MIMO with MB-OFDM transmission was developed. Although developments in MIMO technology for narrow band systems had produced a large number of research papers in the literature, the volume of literature containing these techniques in application to UWB remain very scarce.

The area of concern governs this research manifest itself in the design and implementation of MIMO model with orthogonal frequency division modulation that fits within the WPAN-UWB systems. The model would be tested against an appropriate channel model test-bed in order to validate this proposed work. Hence, the model was evaluated using the defined standard channel model proposed by the Institute of Electrical and Electronics Engineers namely the IEEE 802.15.3a

standard, as well as stochastic channel model. The standard model produced by the IEEE was well suited to simulation and there were useful properties that would assist in finalising the models design. Statistical models aim to analyse certain channel parameters that describe the propagation mechanism. The use of multiple antennas in WPANs would be evaluated and an implementation process would be developed reflect the other area of concern. Spatial multiplexing would be explored and a novel method that optimises the multiple antenna schemes for the system would be developed. The MB-OFDM scheme enables symbol modulation in the frequency domain using spectral multiplexing, and incorporating the independent fading across different spectrum. Therefore, the spreading of the transmitted data into different frequencies optimises the cross correlation between spectrum tone signatures leading to improvement in the system performance, and allows efficiency in increasing the information rate. In addition, by combining the spatial and frequency domains, the signal space would significantly enlarge, and that would provide a foundation for rich media content transmission eventually approaching gigabit rates. Furthermore, an evaluation of the encoding on the signal data using spatial multiplexing as well as spatial and frequency diversity would be carried out to maximise the transmission range, and optimising the system capacity. This takes into account the introduction of spatial degree of freedom in the signal space, as a result of multiple antennas introduction in the physical space. The design would cultivate the multi-radiating elements advantages across the multiple dimensions coding in the physical layer protocol. The model requirements encapsulate a design that is practically feasible and able to adapt to different system design specifications. It would contain a scalability function that allows future requirements to be incorporated in the system design.

The specific objectives of the proposed model in this research were to induce an algorithm that combines multi-antenna with multiband UWB WPAN systems. It should produce a suitable MIMO technique for the operation in Wireless personal area network communication systems. The new concept had to be conformed to the ECMA-368 standard and the multiple spatial configuration should be integrated at the physical layer of the standard. The design should facilitate a readjustment in the model structure to enable increase in the wireless coverage area by encapsulating the communication range requirement in wireless sensor networks. Therefore, it was a requirement to produce a simulation model that covers the design requirements, and enabling verification of this proposed concept. This evaluation should be carried out against an approved industrially recognised model.

1.3 Thesis Contributions

The contribution to knowledge from this research is anticipated to be presented at the physical layer and focusing in two specific areas. The first is integrating MIMO technique with DC-32QAM in WPAN. The model design would contribute to the available capacity by increasing the theoretical throughput without increasing the spectrum of operation for UWB-WPAN systems. The second would be facilitating adjustment to the model in order to increase the transmission range of the communication with the specified transmission power available for legacy wireless system devices and single radiating element within wireless networks intended for indoor applications. This increase in the coverage area would be specific to wireless sensor network application where the range is more critical than the throughput.

1.4 MIMO Design Implementation

The naturally inherent dense environment that exists for indoor wireless communication presents a solid platform to explore the spatial, temporal and frequency diversities. MIMO technology has been proven to increase the system data rate for intensive media applications, and further enhance the available communications range. Furthermore, the technology has been used in narrow band systems and single band transmission processes. In this research, multiple antenna techniques will be implemented for UWB applications with a multiband OFDM transmission scheme. Firstly, the modulation of the signal information will be optimised to enable fast coding processes and transmission rates. The data frames will be spread across the antenna elements and then radiated at the same time which will increase the system efficiency considerably. This is an important contribution to WPAN systems in which a multi-antenna algorithm has been embedded in a multiband spectrum to enhance the overall capacity. Increasing the models capacity will have a direct impact on all forms of short range wireless communications. For example, a multimedia transmission between a set box and a television could be enabled without degrading the quality or increasing the compression coding. Alternatively, a network of several portable devices could be launched where devices perform different operations all at the same time. It could also further extended to the automotive industry where inboard entertainment systems could be facilitated, and more applications and functions could be realised. The implication of MIMO technology on home and office wireless systems is a robust communication link

between peripheral devices at very high data rates.

1.5 Modelling challenges of physical channel

UWB spectrum is very board and due to that, there is a variation in the frequency response of the system operating in these frequency bands. This challenge makes it very hard for RF designers to develop a channel model that satisfies the whole spectrum of the transmission link. Therefore, UWB applications have been designed based on a predefined model that specified for that particular wireless link system and its defined spectrum band of operation. This was then applied across the channel domain, and therefore the modelling of the channel had combined stochastic approach as well as actual channel measurements. Short range wireless portable devices operating on this channel should be designed so as to operate across the frequency bands, and should overcome the channel fading signatures differences between high and low end of the spectrum. In order to give an accurate account for the proposed design, the final concept in this project should deliver good performance across different channel models. The work proposed in this research would tackle this channel propagation challenge; and it is anticipated that accuracy in

identifying the multiple paths in indoor environments would have to be enhanced and optimised. In particular how the scattering signals could be reflected in the multipath model and the impulse response of the channel. Furthermore, how this response could be interpreted in the receiver block and how to create a novel design that represents this physical property. The stochastic model representation would be reviewed in order to have a better representation of the signal delay spread, and how the received power of these waves is disturbed. In existing literature, the statistical analysis so far has been hampered by very narrow studies of the propagation mechanism in ultra wideband domains.

However, this work would be widening the boundary of the study to include different environmental scenarios. Therefore, the modelling would consider diffraction, reflection and scattering effects in the evaluation process. In addition, it is intended that this research will present a novel model that encapsulate different propagation scenarios, and will bridge the physical layer design barrier that limit Ultra wide band devices within severely and hostile indoor channel propagations. The enhancement of the proposed concept should allow the integration of several WPAN peripheral devices resulting in an optimisation to the technology as well as reducing design costs. Further, it opens opportunities for future research into new applications other than the current office and home based applications. It is common knowledge that there are new short range wireless applications becoming available across different technology fields, each of which has a special interest in replacing wired communication links between devices in ever more crowded networks. Hence, the work proposed in the physical channel would contribute to various forms of future

wireless propagation.

1.6 Research limitations

The research into the physical layer of UWB communication systems has reached a level of maturity over the last decade, but nevertheless, there are a number of open research questions that needed to be addressed. The physical layer encompasses the encoding of data, the RF modules that enable the transmission and reception of data, and the generic generation of wireless signals. Research into the first layer of the UWB communications link had been bounded by the limited number of available measurements obtained from the environment. The work here takes this into account, and will therefore attempt to analyse the available experimental data that exists for indoor wireless links. Although the modelling and simulation proposed in this research handles various multipath channels that reflect certain geometric configurations in home and office environments, there are some additional observations that needed to be addressed. Firstly, the limited research in this field makes it very challenging to obtain a comprehensive approach to the problems at the physical layer. Secondly, the narrow focused nature of previous research into the

spectrum had limited the available results to specific frequencies and not across the entire spectrum. In some commercial applications, the research into wireless links had focused on the lower bands of the UWB spectrum, and this reflected in the development of much specialised models. Channel propagation is a physical phenomenon that depends on objects scattering signals in all directions and this creates an infinite number of dimensional representations.

However, research into the electromagnetic waves propagation, and the energy distribution of the channel paths was very difficult. Modelling of the propagation physical phenomenon and its representation for wireless indoor and office environment is particularly challenging. All the currently available models based on measurements and statistical representation included a data base of different types of building furniture and decoration material etc. However, all of these representations are still limited and do not account for every scenario. More importantly, because of the relatively small wavelength that characterise UWB applications, scattering from some materials tends to create a different frequency response when interacting with these objects. This in turn, makes it very hard to design a simulation process that absorbs these effects, and hence limit the accuracy of the design model.

A further limitation is that the MIMO configuration we aim to adopt relates to the physical layer transmission scheme that operates on narrow band spectrum. Due to the widespread use of the ECMA-368 standard in commercial applications, the

multi-antenna system proposed in this research has been designed to comply with this particular standard. Therefore, the proposed MIMO algorithm would require further modification and optimisation in the case of a new standard's requirement. This is because the standard uses the MB-OFDM scheme for the transmission process and hence all the research work has been based on this type of spectrum segmentation.

Advanced in information theory in the last decade had introduced a very high class performance codes in the field of forward error correction class of codes. Due to the high data rates required by this research, and the limitation in the complexity requirements at low power wireless personal area network systems, the available coding methods and coding rate had to be in consistent with the standard specification. As such, iterative decoding algorithms that required feedbacks would not be used in this research. These types of codes that required additional cost in transmitter and receiver structures would limit the research objectives in introducing these types of codes. A review of the advanced available methods as the turbo decoding would be highlighted but not taken to optimise the coding process. Forward error correction coding would be the used as the source of coding algorithm in conformance with the standard.

Also, the ultra-wideband system generally requires very high speed clocks, and this requires advanced digital signal processing. This presents a very practical challenge as there are limitations in the model design and simulation that have to be

considered. Designing pulses with very short periods operating at low energy level presents a challenging software and hardware prerequisite. In addition, the cost of developing hardware electronics for this type of application increases rapidly. In order to maintain higher data transmission, proper decoding of the received symbols should be realised which in turns requires complex processing units. Accurate synchronisation is also very important for the digital signal processing block, however the cost factor should be considered in these applications. Furthermore, another key challenge is the interference that is created in this type of communications link. On the one hand, there are power constraints on the transmitted signals that tend to adversely reflect on the signal to noise ratio. On the other hand, the error margin increases considerably as the information rate of the system increases. In this research, some effort will be made to address all of the above challenges and come up with useful solutions. Although, it is intended that the resulting outcome will accomplished these prerequisites, there are observations that will need to be identified.

1.7 The proposed structure of the thesis

The contents of the proposed thesis will be divided into chapters that identify specific topics. A summary of these chapters has been provided in the following:

Chapter two will provide a review of the past and current literature of the various concepts that underpin WPAN. It will analyse current research work in the UWB channels and experimental studies into specific environments. A review of previous channel propagation models will be summarised to identify certain results that are of key interest to this work. Published studies into the area of multiple antenna technology will be reviewed and relevant results to this project will be highlighted. The design methodologies behind channel modelling and multiple antenna techniques will also been outlined in the assessment. A review of the modulation methods would be provided along with their implementation.

Chapter three presents the design concept used in this work. The proposed model

applies multiple radiating elements in the physical layer of the ECMA standard. MIMO scheme would be designed so as to operate on Ultra wide channel model. Different channel models would be used to evaluate the induced concept used in this research. Explanation of the model will be firstly discussed in detail as well as the reasoning for the design. The background to stochastic concepts behind the model will be discussed and a comprehensive explanation to them will be included. The scope of the scheme will cover the coding algorithm, mathematical algorithm, and the simulation design procedure. The multiple antenna design will have been presented covering the transmission protocol. The integration procedure of the multiple antennas techniques in the physical layer would be explained. This includes specifically induced design algorithm that allow multiple radiators to be absorbed in both the transmission and demodulation schemes. The optimisation process to the model design which was implemented in the developed system would then present. Additional system requirements had been discussed including optional physical layer requirements.

Chapter four presents the implementation method of the proposed work. In this chapter, the implementation of the design had been considered and explanation to the concept formulation was given. This implementation was carried out in the simulation environment based on Matlab software package. The receiver's implementation was followed with explanation to the integration of the proposed model on the wireless receiving structure, and the test bed requirements for the simulation. A proposal to optimise decode method was explained that further enhance the system performance.

The final chapter will provide a conclusion to the research project by highlighting the obtained results from the system model. It will outline the contribution of this work for the short range WPAN technology and how it can be integrated in future research. It will also identify areas in the research which could be incorporated in future studies in PANs. A review of the validation process for the multiple antenna system would be discussed along with comparative tests with existing approved practical models. A detail analysis will be discussed to project the merits of the design model. A review of standardised models will also be carried on to identify a viable test method.

1.8 Research methodology

The purpose of this section is to outline the research methodology used in the production of multiple antennas model for Ultra wide band system used in the Wireless Personal Area Network systems. It describes six phases including identification, designing model, implementation, Optimisation, testing and verification of the proposed model that was presented in this project. The adopted research methodology for this work had been illustrated graphically in the following figure.

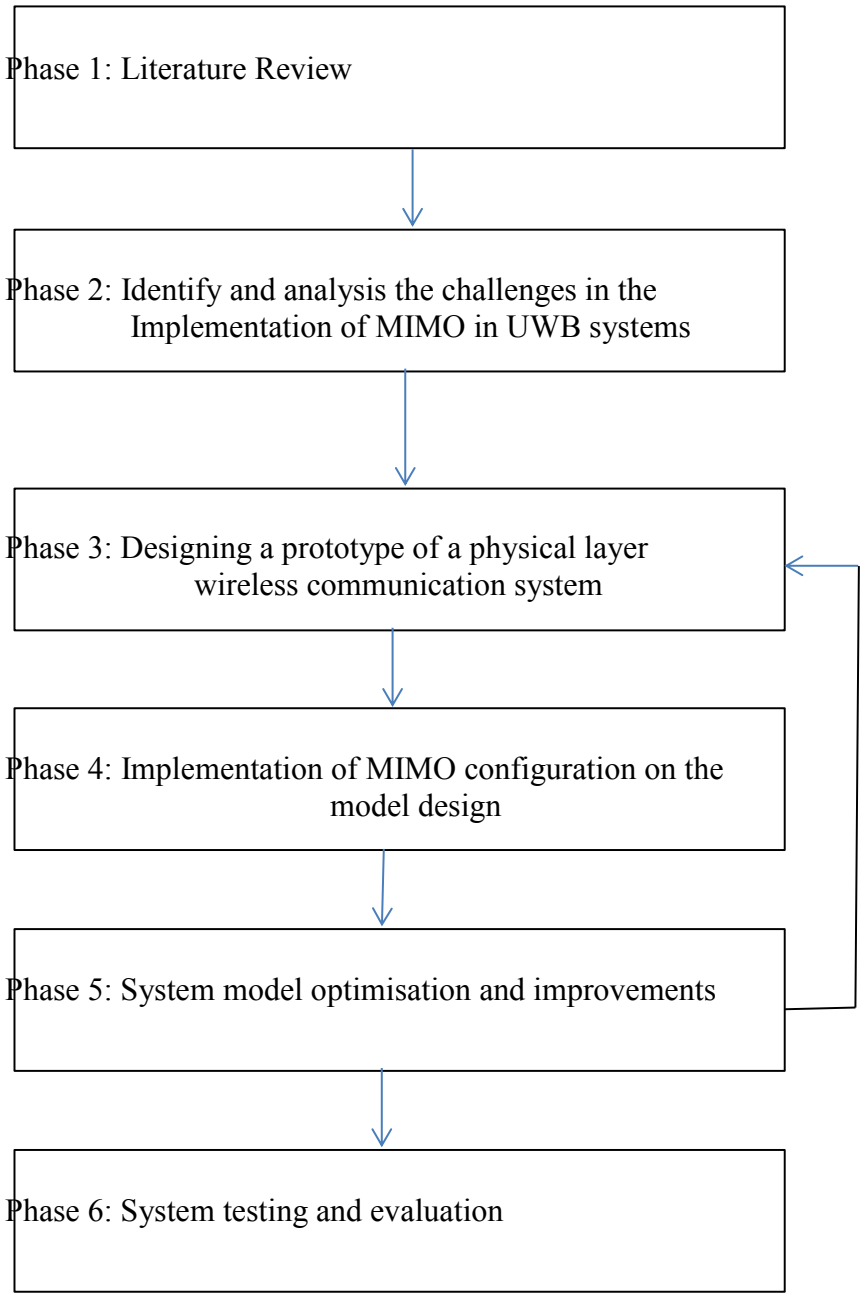

Figure 1: Research methodology

Six phases approach were identified in defining an appropriate research program structure. These are as follows

Phase 1 (Literature Review): This phase covers previous works on the implementation of MIMO techniques on Ultra wide band wireless systems. The focus would be on identifying the main problems and challenges that encapsulate the technology. Various concepts would be looked at and explored to facilitate new design models.

Phase 2 (Identifying related problems): In this section, the emphasis would be on identifying tangible problems in the design and implementation of spatial elements in hostile indoor environments. Challenging channel behaviours and problems would be induced and considered for research work.

Phase 3 (Designing a prototype of a physical layer Wireless communication system): In this stage, a prototype design model would be constructed to enable the linking of the various physical layer blocks of the wireless system and producing a functional and operational design model. This interconnection allows for observation of the blocks parameters and the system performance.

Phase 4 (Implementation of MIMO configuration on the model design): MIMO construction would take place in this section and would be integrated in the simulation model. The algorithm for implementation would be tested to verify the system performance. The design concept would be implemented to infer the theoretical analysis.

Phase 5 (System model optimisation and improvements): The modelling design would be improved and optimised. Further analysis would be carried out to improve the performance and reduce the complexity involves.

Phase 6 (System testing and evaluation): In this step, the various scenarios would be tested and the model would be observed to finalise the design. Evaluation would be performed on each block within the simulation model and all the results would be documented.

2 Background Research

2.1 ECMA-368 Specifications

The ECMA standard specifies OFDM modulation with multiple bands in which the spectrum had been segmented into a collection of lower frequency bands. It divides the unlicensed spectrum into sub-bands each of which consists of a 528MHz bandwidth, and combines a tuple of bands in Band Groups (BG1 – BG5) except for the last two bands [5], and figure (2.1.1) gives a description of this spectrum division. A flexible feature of the model is the variable transmission rate in which the standard supports data rates of 53.3, 80, 106.7, 160, 200, 320, 400, 480 Mb/s. The MB-OFDM scheme has been used in

this model, and where every band has been allocated equal number of subcarriers. Frequency and time spreading with forward error correction coding techniques has been used to vary the data rates. In addition the Inverse Fast Fourier Transform (FFT) has been implemented in the construction of the OFDM symbol. In order to apply OFDM modulation, the targeted spectrum had been firstly divided according to the standard specification. The transmission across multiple bands had been implemented in Time-Frequency Code (TFC), which makes good use of the band segmentation within the ECMA standard. The segmentation of every band groups had been shown, and where different modulation schemes could be applied.

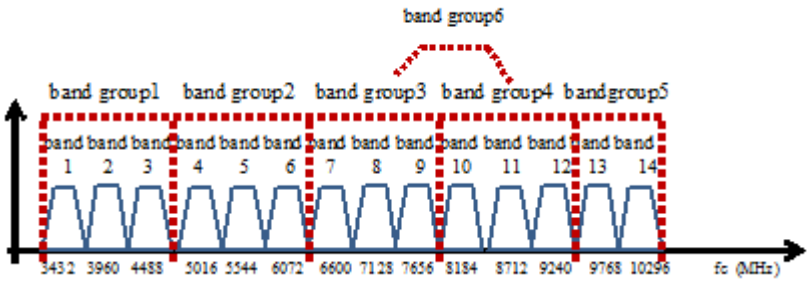

Figure (2.1.1): Spectrum division into band groups: Taken from [3]

As the standard specified PHY and MAC layer protocol, the physical layer had

defined Physical Layer Convergence Protocol (PLCP) sub-layer to interface between this layer and the upper MAC counterpart [6]. This sub-layer provides a method for converting PHY Service Data Unit (PSDU) into PLCP Packet Data Unit (PPDU). The PPDU structure consists of the PLCP preamble that includes the Channel Estimation and Packet synchronisation sequences, the PLCP header, and the PSDU. Further error detection and correction were added to improve the wireless communication links.

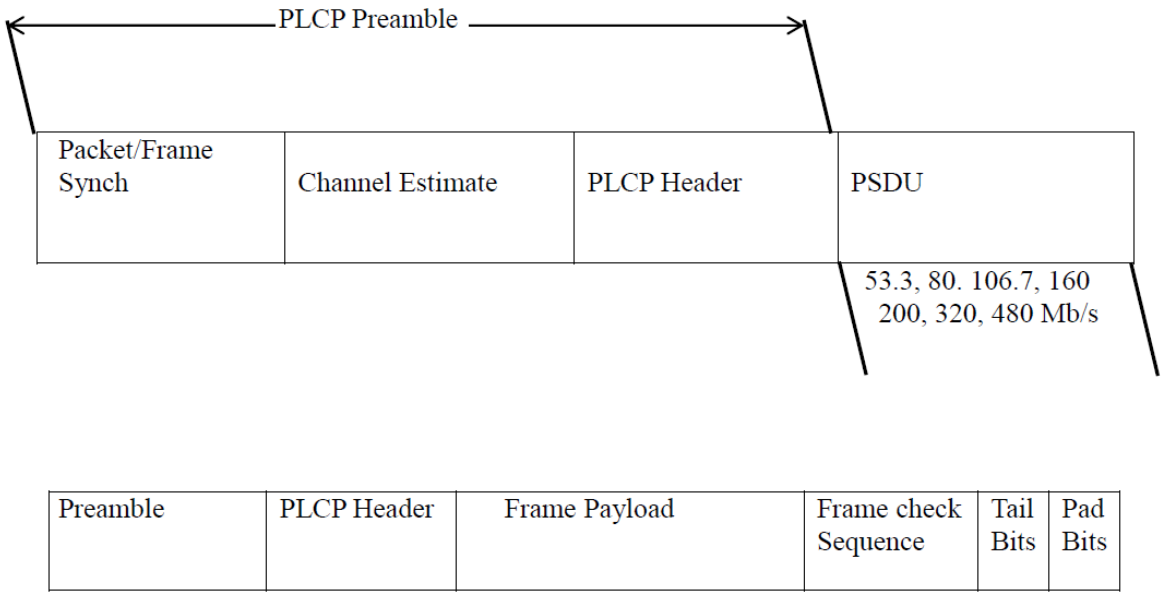

Figure (2.1.2) PPDU and PLCP structure: Taken from [4]

The process of transmission consists of collect a number of packets (or frames) in which a predefined number of modulated OFDM symbols forming the message packet. As it had been stated, frequency domain spreading, time domain spreading and Forward Error Correction (FEC) are used to vary the data rate. There are three specified types of TFC, the first one is where the

coded information is interleaved over three bands and that termed as Time-Frequency Interleaving (TFI) [7]. The second coding is where the coded information is interleaved over two bands, and this referred to as TF12. The third one in which the transmission was done over signal band where the term Fix Frequency Interleaving (FFI) was used for this type of coding. Four time-frequency codes within the first four and six bands group make use of TFI, and three time-frequency codes uses TFI2 and FFI coding, giving support of ten channels in each band group. In the case of the fifth band group, two time-frequency codes uses FFI and one uses TFI2. On the other hand in the six band group, FFI channels and one of the TFI2 channels overlap with the channels in the third and fourth band groups. In order to allow range regularity and radio coexistence within the standard, a mechanism for nulling the OFDM subcarriers in the TFC operations had been provided. Frequency Domain Spreading (FDS), and Time Domain Spreading (TDS) were been facilitated in order to expand the bandwidth for the modulation schemes. Further, the various coding rates were assigned to different coding and modulations depending on the applications. Table (2.1) gives description of the different coding, Data rates, and modulation in the PSDU.

Data Rate (Mb/s)	Modulation	Coding Rate	FDS	TDS	Coded Bits/6OFDM Symbol	Info Bits/ 6 OFDM symbol
53.3	QPSK	1/3	Yes	Yes	300	100
80	QPSK	1/2	Yes	Yes	300	150
106.7	QPSK	1/3	No	Yes	600	200
160	QPSK	1/2	No	Yes	600	300
200	QPSK	5/8	No	Yes	600	375
320	DCM	1/2	No	No	1200	600
400	DCM	5/8	No	No	1200	750
480	DCM	3/4	No	No	1200	900

Table (2.1): The defined data rates and modulation parameters in ECMA standard

In mathematical form, the transmit signal could be describes as follows [8]

$$x_{RF}(t) = Re\left\{\sum_{c=0}^{N-1} x_n(t - nT_{SYM}) \exp(j2\pi f_c(p(n)))\ t\right\} \qquad (2.1.1)$$

In the above formula, $x_n(t)$is the baseband signal representation for the nth symbol of within the transmitted packet, and since these are time limited signals, then $s_n(t)$will equal to zero outside time frame (0 - T_{SYM}). The function $p(n)$ maps the nth symbol to the appropriate frequency band, and f_c is the centre frequency for that frequency band. The OFDM symbol length T_{SYM} includes the Zero Padded Suffix (ZPS). These extra suffix sequences provide a mechanism to mitigate the effect of multipath and a guard interval to allow sufficient time for the transceivers to switch between centre frequencies of bands. Figure (2.1.3) shows TFC with modulated symbols including the additional ZPS used in the transmission.

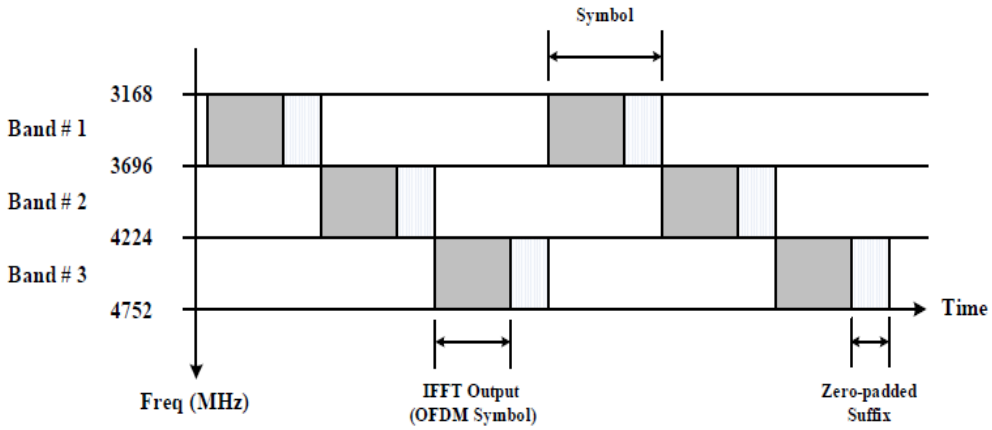

Figure (2.1.3): Modulated symbol interleaving over three bands with ZPS

2.2 MIMO System

Multiple Input Multiple Output (MIMO) techniques consist of using multiple antennas at both ends of the communication channel to exploit spatial diversity and add another degree of freedom to the system capacity [9], [10]. The technique combines the temporal, spatial and frequency diversities in the transmission scheme to increase the link throughput. MIMO enables the transmission of data over multiple channels and hence increases the available data rate of the system [11]. This in turn produces a linear increase in capacity without the need for bandwidth expenditure [12]. Furthermore, it doesn't require additional transmission power and this single factor makes it very attractive for short range wireless communication networks [13]. This is because of the astringent power regulation imposed by federal regulators (e.g. the FCC in the USA).

The spectrum allocation in MIMO multiband systems has been constructed by supplying each user a sub band (with a minimum bandwidth of 500 MHz) and all the transmitting antennas operate in the same band for each user at that particular time duration. The encoding process has been applied across all of the antennas, the number of subcarriers within one symbol and the number of OFDM symbols that forms blocks or frames for transmission. This way, each complex symbol could be identified by the subcarriers of the particular

spectrum at the specified antenna element during a known OFDM period of a marked frame. Due to the encoding format, a matrix representation is used in multi-spatial systems to simplify its mathematical representation. The sequences allocated to each user and for each antenna were designed such that they were orthogonal to each other or the correlation factor is zero between them [14]. This independent property ensures the formulation of a diagonal matrix which simplifies the detection process at the receiver side and reducing the hardware and complexity costs. The transmitted based band signal (d) represented by each symbol to be transmitted on antenna z has been interpreted mathematically as follows [15].

$$d_z(t) = \sqrt{\frac{E}{A}} \sum_{s=0}^{S-1} b_z(s)\, e^{-j2\pi s\Delta f}\ (t - T_{AP}) \qquad (2.1.2)$$

Where E, A , b, T and f represent the total energy, the total number of antennas, the complex symbol, the duration of the added prefix (this could be Cyclic prefix or Zero-padding) and the sub frequency spacing between two subcarriers. The energy of all the transmitted signals has been normalised to eliminate the number of radiating elements, and in addition satisfying the spectrum mask regulations [16]. A total number of Z blocks consisting of OFDM symbols are transmitted from all the antennas forming a code word

matrix B and for each radiating element a number of symbols have been allocated. That is for the a^{th} antenna, a number of complex code weights forms a matrix $X_a$representing the duration of the OFDM symbol for the particular block z. Furthermore, there were A antennas forming a matrix U of all the blocks and the complex symbols. Within the symbol duration, a total of S subcarriers are used to modulate the symbol. The channel operates across all the subcarriers of the symbol, all symbols within the block and across all the antennas forming a matrix CH. For every receiving antenna, a channel vector $CH_i$of dimension ZSA x 1 has been formed consisting of a superposition to the physical link response weights from the spatial elements [17], [18].

$$B = [B_0 , \quad B_1 \ , \dots \quad B_{(Z-1)}] \tag{2.1.3}$$

$$X_a^z = [X_a^z\,(0), \quad X_a^z\,(1) , \dots \quad X_a^z\,(S-1)] \tag{2.1.4}$$

$$CH = [CH_1 , \quad CH_2 \ , \dots \quad CH_U] \tag{2.1.5}$$

$$CH_i = [CH_{i1} , \quad CH_{i2} \ , \dots \quad CH_{iA}] \tag{2.1.6}$$

The sub channel weights of the radiating elements in CH can be represented statistically as a random variable with a magnitude having the form of the log normal or Nakagami distribution [19]. The convolution process between the transmitted signal and the channel results in a received signal that is

statistically distributed due to the statistical nature of the channel. The fact that, there are multiple spatial elements, the received signal is represented in a matrix form as follow [20], [21], [22].

$$U = \begin{vmatrix} X_1^1 X_1^2 \ldots & X_1^A \\ X_2^1 X_2^2 \ldots & X_2^A \\ X_3^1 X_3^2 \; X_3^3 \ldots & X_1^A \\ X_1^1 X_1^2 \ldots & X_1^A \end{vmatrix}, \quad R = \begin{vmatrix} R_{11} R_{12} \ldots & R_{1A} \\ R_{21} R_{22} \ldots & R_{2A} \\ R_{31} R_{32} \ldots & R_{3A} \\ R_{A1} R_{A2} \ldots & R_{AA} \end{vmatrix} \quad (2.1.7)$$

Where R_{ji} represent the J^{th} transmitting antenna and the i^{th} receiving antenna

Due to the effects of the channel, each receiving antenna in the MIMO configuration would receive copies of the neighbouring antenna's signals [23]. One of these weights represents the correct signal between the pair of transmitter and receiver and the rest could be considered to be interference [24], and for analytical purposes all the channel weights could be represented by a vector G (of dimension AS x 1). In addition, the multipath effect produces multiple copies for each transmitted signal and hence every channel $G_i$is expanded by a number of multipath components of length Q [25]. Additional assumptions have been applied by [26] to simplify the computation and state that all the radiating elements have the same number of multipath signals.

$$G = [G_1, \quad G_2 \; , \ldots \quad G_A \;] \qquad (2.1.8)$$

$$G_i = [G_1(1), \quad G_2(2) \, , \ldots \quad G_A(Q) \;] \qquad (2.1.9)$$

In the frequency domain, the channel could be decomposed into its Fourier coefficients consisting of the subcarrier weights and the multipath components forming a matrix F of dimension S x Q. The received signal at the i^{th} antenna would form a vector Y constructed from the channel Fourier matrix F and the transmitted signal vector X [27], [28]. The power spectral density of the received signal would form a Hermitian matrix H which could be decomposed to its unitary and diagonal matrices using the single value decomposition.

$$F = [F_{s0q0}, \quad F_{s0q1} \ldots F_{s0(q-1)}; F_{s1q0}, \ldots F_{s1(q-1)}, \ldots \quad F_{(s-1)(q-1)}] \qquad (2.1.10)$$

$$G = F.G, \quad Y_i = (F.G).X$$

$$H = E[Y_i . (Y_i)^t] = V A V^t, \quad A = \text{diag}[a_1 \ldots. \quad a_k]$$

The eigenvalues of the received signal power is represented by the diagonal matrix A and is used to provide a measure of the signal power at the receiver. This power measure is then used to evaluate the system performance in terms of the signal to noise power ratio, and as a further analysis tool to measure the coverage area. The addition of the noise to the received signal power would increase the amount of distortion in the received OFDM symbols, and hence affecting the bit error rate of the system. Additive White Gaussian Noise (AWGN) has been used in the modelling and design simulation in previous research work [29], [30], [31]. The inherent rich diversity that encapsulates indoor wireless communication [32], and the frequency selectivity property of the UWB channel has led researchers to come up with further statistical

assumptions [33]. These have assumed that the spectrum of each sub band that the symbol hops across was independent of each other and were not correlated. Implementing this assumption for the evaluation of the MIMO model performance, has shown that using the multiband approach with symbol hopping increases the system performance and provides an additional degree of freedom in the frequency domain. Nevertheless, further research is needed to be carried out concerning the operation of multiband transmission plans in the UWB systems. This includes determining more accurate statistical models for the MIMO capacity in the physical medium, and the spectrum power for each of the sub bands across each band group.

2.2.1 Alamouti Scheme Space-Time Block Code (STBC)

The growing demand for more channel capacity had led to research in the spatial domain to add an extra degree of freedom to the capacity. The break through that was captured by Alamouti scheme [34], which had opened a new area of research into the MIMO techniques.

The scheme uses two transmit antennas, two time intervals, and a novel complex orthogonal principle that uses space-time technique to increase the performance without increasing the signal power. A code-word matrix was formed from two consecutive symbols (s1,s2), and their complex conjugate counterparts in a dual time pins as follows

$$\boldsymbol{X} = \begin{bmatrix} s1 & -s2^* \\ s2 & s1^* \end{bmatrix} \qquad (2.2.1)$$

The scheme using two symbol periods to transmit the dual symbols from two antennas, and therefore in essence the original content information would be transmitted twice across the time intervals. The original principle was formation of the matrix$\boldsymbol{X}$, which is a complex orthogonal matrix as

$$\boldsymbol{X}\,\boldsymbol{X}^H = \begin{bmatrix} |s1|^2 + |s2|^2 & 0 \\ 0 & |s1|^2 + |s2|^2 \end{bmatrix}$$

$$= |s1|^2 + |s2|^2 * \boldsymbol{I}_2 \qquad (2.2.2)$$

This orthognality of the matrix of rank two gives the Alamouti code a diversity gain of 2. The diversity analysis was based on the Maximum likelihood detection. Nevertheless, there is a critical condition that fading should remain invariant of the two consecutive symbol periods for every spatial code.

$$\begin{bmatrix} y_1 \\ y_2^* \end{bmatrix} = \begin{bmatrix} h_1 & h_2 \\ h_2^* & -h_1^* \end{bmatrix} \begin{bmatrix} x_1 \\ x_2 \end{bmatrix} + \begin{bmatrix} n_1 \\ n_2^* \end{bmatrix} \qquad (2.2.3)$$

At the receiver, estimating the channel coefficients will lead to multiplying the received noisy signal vector with the channel matrix will lead to the following

$$\begin{bmatrix} h_1^* & h_2 \\ h_2^* & -h_1 \end{bmatrix} \begin{bmatrix} y_1 \\ y_2^* \end{bmatrix} = \begin{bmatrix} h_1^* & h_2 \\ h_2^* & -h_1 \end{bmatrix} \begin{bmatrix} h_1 & h_2 \\ h_2^* & -h_1^* \end{bmatrix} \begin{bmatrix} x_1 \\ x_2 \end{bmatrix} + \begin{bmatrix} h_1^* & h_2 \\ h_2^* & -h_1 \end{bmatrix} \begin{bmatrix} n_1 \\ n_2^* \end{bmatrix}$$

$$\begin{bmatrix} \hat{y}_1 \\ \hat{y}_2^* \end{bmatrix} = [|h_1|^2 + |h_2|^2] \begin{bmatrix} x_1 \\ x_2 \end{bmatrix} + \begin{bmatrix} h_1^* n_1 + h_2 n_2^* \\ h_2^* n_1 + h_1 n_2^* \end{bmatrix} \quad (2.2.4)$$

Due to the orthognality of Alamouti code, simple ML receiver would estimate the transmitted symbol as follows

$$\hat{x}_j = Error\ function\left(\frac{\hat{y}_j}{|h_1|^2+|h_2|^2}\right) = Q\left(\frac{\hat{y}_j}{|h_1|^2+|h_2|^2}\right) \quad (2.2.5)$$

It is important to note that, the two main objectives in using orthogonal space-time code were to increase the diversity order, and reducing the complexity of symbols detection at the receivers. Further, the complex orthogonal codes would not exists for a number of spatial elements that is greater than two with the defined objective goals mentioned before. STBC could be further improved in terms of its coding gain by using convolutional encoders as in what is termed as Space-Time Trellis Codes (STTC).

2.3 The Physical Channel

There has been a significant amount of research concerning the channel measurements for Ultra-wide band applications stemming from the practical and theoretical difficulties these systems present. The measurement approach has been carried out based on two distinctive domains, the time domain approach which evaluates and measures the impulse response of the medium; whereas the frequency domain methods deals with the channel transfer function based on spectrum evaluation. In the time domain, channel sounders have been implemented by using either short or high energy pulses, or more robust methods using correlative channel sounders [35]. The latter uses wide band signal with low Signal to Noise Ratio (SNR) to avoid interfering with the surrounding wireless systems (e.g. narrowband applications). At the other end, a PN sequence is used in the correlation process where the original transmitted signal is then induced. In order to extract the channel parameters, different measurement procedures have been performed. Two high resolution algorithm methods that have been used in practice and have been highlighted in research papers [36]. The first is the CLEAN algorithm which is based on an iteration process. Received pulses are first correlated with a known pulse shape in order to extract the strongest pulse and then iteratively extract the following dominant pulse components until a threshold of energy level is reached. The

SAGE algorithm [37] is the other method which uses a maximum likelihood estimate using the parameters applied with iteration process. The Vector Network Analyser (VNA) technique is a widely used measurement method in the frequency domain [38]. It uses a frequency sweep of sinusoidal waveform to excite the channel and then measure its transfer function. The inherent averaging makes it less affected by noise and interference and can perform large band width measurements. However, due to the slow operation of frequency stepping, this process can take a long time for dynamic channels. Furthermore, the wiring issues tend to limit the measurements to short area ranges. Scalar Network Analyser is a modified method that measures only the magnitude of the transfer function and hence reduces the operation time that VNA takes.

Measured data has shown that for the indoor channel, the scattered objects tend to be distributed in the form of clusters between the transmitters and receivers [39]. Furthermore, within each cluster the arrival ray tends to be non-uniformly distributed. One important implication of the clustering assumption is the Saleh-Valenzuela (SV) model in which multipath components follow a Poisson distribution with inter arrival times that is exponentially distributed [40]. Moreover, the model has a cluster and ray arrival times as well as a decay factor value for each of them and hence provides a great flexibility in modelling different scenarios.

The IEEE has established various standardisation groups to develop standard

models each of which covers certain applications under common specifications of its physical layer proposal. These models have been developed based on measured data and the simulation of identifiable prerequisite requirements for system design. These were common primary characteristics of the multipath channel such as the power delay profile, RMS delay and the number of multipath components, and data that requires an agreement between the measured data and the standardised models realisations.

In this section, two models that frequently mentioned in research papers are highlighted (namely the IEEE 802.15.3.a and IEEE 802.15.4a).

For office and residential indoor environments, the IEEE 802.15.3a task group have been established with communication ranges of less than 10 m [41]. The model parameters were based on measurements and define four separate radio environments with different ranges (LOS 0-4m CM1, NLOS 0-4m CM2, NLOS 4-10m CM3, MPCs CM4). The IEEE 802.15.3a standard is based on the SV model with large and small scale fading being modelled as lognormal distribution with similar standard deviation values. The channel impulse response of the standard had been modelled as follows:

$$h(t) = X \sum_{c} \sum_{y} B_c, y \, e^{j\theta_{c,y}} \, \delta(t - T_c - \tau_{c,y}) \qquad (2.3.1)$$

Where X is lognormal distributed random variables

Inside this model, there are three random variables with three distributions representing the amplitude, the phase, and the time (arrival time). The first random variable is the amplitude and represented by Rayleigh Distribution in the original SV model. The coefficients in the path represent the amplitude (gain = ampl of I + Q components) and were modelled as Log-normal distribution instead of the above Rayleigh distribution [42].

$$f_{c,y}(B_{c,y}) = (2B_{c,y}/\bar{B}^2_{c,y})\, e^{-B_{c,y}/\bar{B}^2_{c,y}} \qquad (2.3.2)$$

Where $\bar{B}^2_{c,y}$ *is the average power (variance)*

$\bar{B}^2_{c,y}$ is the average power that is statistically distributed and every arrival pulse will have its own power. The distribution here is the Exponential distribution and could represent two average power values. The first one is the average power of each ray (y) within the cluster, and the second is the average power of each cluster (c) (Each cluster is compared in terms of its power in comparison with other clusters i.e. The first 2 or 3 clusters normally will have more power than the later ones). The second random variable is the phase (Theta) which is assumed to follow Uniform distribution between [0, 2π]. The third random variable represents time, and here there are two time of arrivals, one for the cluster arrival time and the other for the ray arrival time within a cluster, both of which follow a Poisson distribution [43].

$$f_{Tm}(T_m|T_{m-1}) = \Lambda \exp\{-\Lambda (T_m - T_{m-1})\}, \quad m > 0 \qquad (2.3.3)$$

$$f_{\tau m}(\tau_{p,m}|\tau_{(p-1),m}) = \lambda \exp\{-\lambda (\tau_{p,m} - \tau_{(p-1),m})\}, p > 0 \qquad (2.3.4)$$

Although these results have been used in existing research and have gained acceptance in the academic community, there are still very limited measurements that have been taken to date when considering the free spectrum channel. Hence, further investigation is needed before these assumptions could be taken as a realistic representation of the channel behaviour. In this research, the above channel model would be used as basis for modelling the physical medium and further analysis would be carried out to investigate the channel parameters that have been identified in the literature.

2.4 MIMO-OFDM wireless system block model

As engineering designers was able to implement multicarrier in the discrete time domain using inverse fast Fourier transform acting as modulator and its corresponding fast Fourier projection in the frequency domain representing the

demodulation, block representation becomes a useful representation tool in the design and implementation of complex wireless system. Representing the model into a number of interconnected blocks allows for systematic design, implementation and evaluation of wireless projects. MIMO wireless model consists of a number of integrated blocks at the transmitting and receiving sides [44]. These are the coding module which provides Forward error correction codes that helps reducing the channel noise distortion, and the modulation block where the desired signal was mapped across the constellation. This constellation was associated with the specified modulation scheme. The resulted complex symbols was then modulated and translated in the time domain using frequency transform according to the IFFT, and then passed to Digital to Analogue conversion (D/A). At the receiving block, the opposite operation was carried out, by estimating the original wireless signal using the decoding and demodulation blocks. Figure (2.4.1) gives a description of the multiple antennas wireless model used in the design and modelling of real wireless systems.

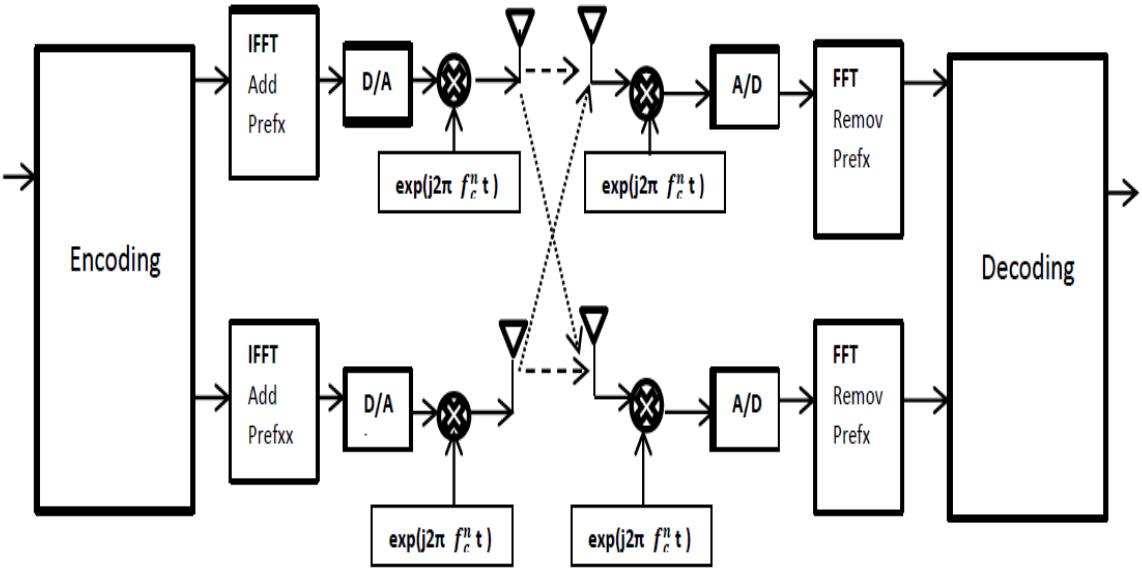

Figure (2.4.1): MIMO wireless block model system: Taken from [33]

2.5 Convolutional Coding

There are considerable performance improvements in using coded transmitted signals over un-coded signals in wireless communication system. The Convolutional coding process produces coded signal out of un-coded message sequence, and uses parity bits computed from message bits. Convolutional code is specified by the number of input bits (i), the number of output bits (o),

and the number of memory registers (o, i, m) [45]. Since there are a number of parity bits, the code rate (r) of the encoder is (i / o), and this quantity represents the efficiency of the code. The number of inputs and outputs normally range from 1 to 8 in practical application, whereas the number of registers takes values ranging from 2 to 10. Convolutional encoder contained core quantities, and these are the constraint length, and the generator polynomials. The constraint length (L) represents the number of bits in the encoder memory that effect the output coded signal. Increasing the constraint length would increase the resilience to bit errors. Although the downside is that it takes longer time to decode. The numbers of generator polynomials are equal to the number of parity bits in every sliding window. The convolutional code is generated by convolving the desired message signal with the generator polynomial. The output code normally specified by constraint length and the code rate as (r*L). Convolutional encoders sometimes defined as systematic and non-systematic encoders. Systematic encoders are very easy to implement in hardware and have simple look up table. Further, the errors in these encoders dose not propagate catastrophically. On the other hand, in the case of non-systematic encoders, the output symbols do not include the input data. A block diagram for the convolutional encoder was shown in figure (2.5.1), highlighting the main components of the encoder. It shows the input, outputs, generator polynomial, and memory registers. The polynomials are used in the modulo-two adders operation between input signal and the memory registers reflecting the constraint length were used in the production of the output codes. The generator polynomials are critical in generating code with good error protection properties, and there are well defined polynomials in

standardised real time wireless application.

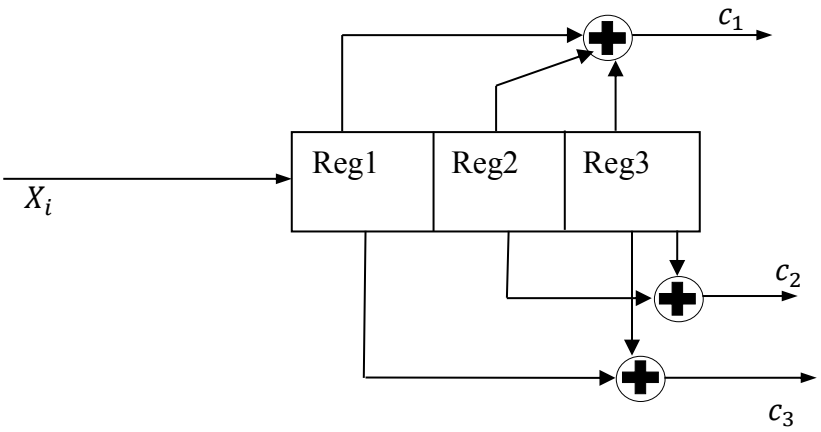

Figure (2.5.1): Block diagram of main components in convolutional encoder

The code rate of the encoder could be altered by the use of Puncturing. Puncturing uses dummy bits in the encoding and decoding process. The advantage of using Puncturing is that the coding rate could be changed dynamically in a flexible way depending on the channel condition, which affects the received signal power. The encoder finite state machine operation could be projected by the use of Trellis diagram. Trellis diagram gives linear time sequence of events, and shows the states, the inputs, and outputs in relation to time figure (2.5.2). Trellis structure normally initialise at zero states to simplify tracking within the diagram. If the path metric going down words then the input is one bit, and going up words then the input bit for the encoding is the binary zero.

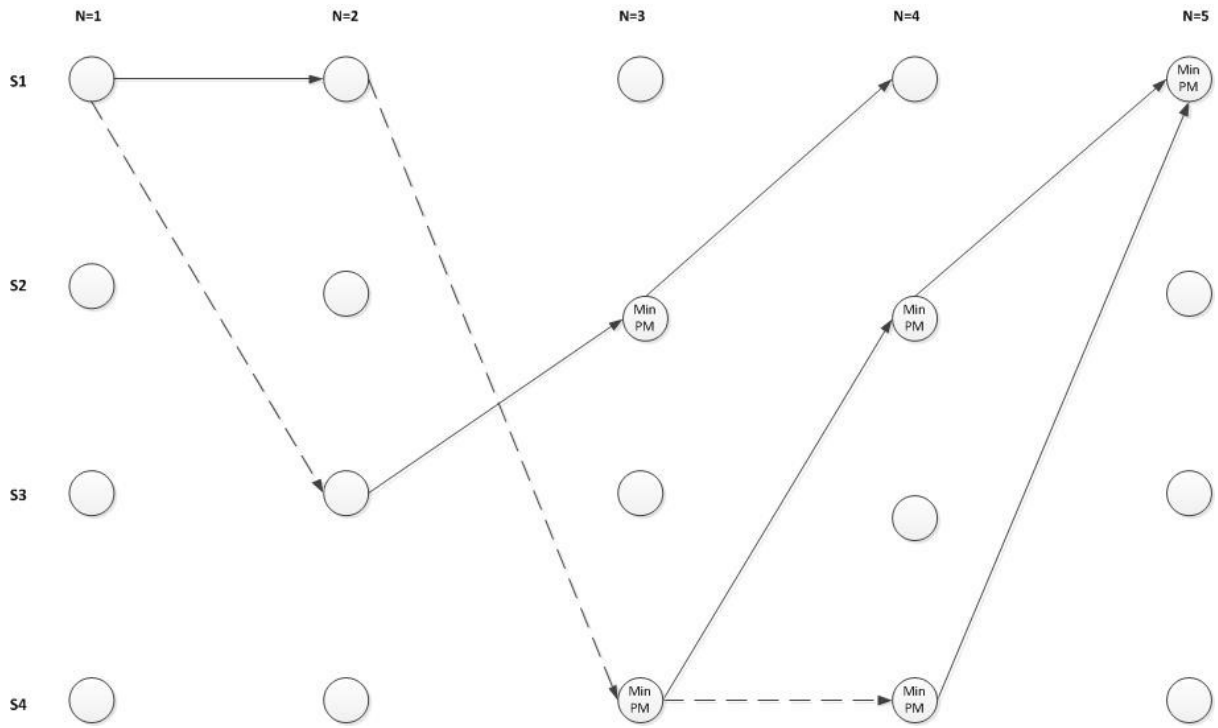

Figure (2.5.2): The trellis Diagram structures in discrete intervals

2.6 Viterbi Decoding

Viterbi decoder is a powerful and widely applicable algorithm that uses soft Maximum likelihood decoding on the trellis structure [46]. The decoding algorithm maximising the probability condition of the received symbol given the transmitted signal, by choosing the nearest symbol based on minimisation of the Euclidean metric. The Viterbi algorithm have two sequential phases, the first includes calculation of the trellis metrics (the branch metric, path metric, and decision bits), and the second represents the trace-back in time to identify the most likely sequence of symbols. Look up table are generated and used by the decoding algorithm across the trellis structure, therefore there are memory limitation for the traceback that control Viterbi process. The Branch Metric (BM) calculates and stores the output difference between the observed parity bits, and the estimated parity bits (this estimated output bits depend on the input to the encoder and the current state of the encoder). The Path Metric (PM) represents a value on the state node indicating the path weight at that particular node and particular time (a node may have many path coming to it, but the one with the highest value, represents the weight of that node at that particular time). This weight value project the number of bit errors detected when comparing observed and the most likely message up to that particular time. However, when traversing through the trellis to estimate the most likely

path, at any particular time interval, the decision would be picking the node at that particular time with the smallest path metric among the entire node within that time index. Traversing in the forward direction could have multipath with the equal PM, and therefore the backward process enables to find the most likely path. The backward process starts at the last time interval, and chooses the node with lowest PM, and then traverses backward from that states. This way, all the multiple paths are removed and only the survive path would be left representing the most likely sequence. Figure (2.6.1) below shows the survivor path based on the implementation of the Viterbi algorithm.

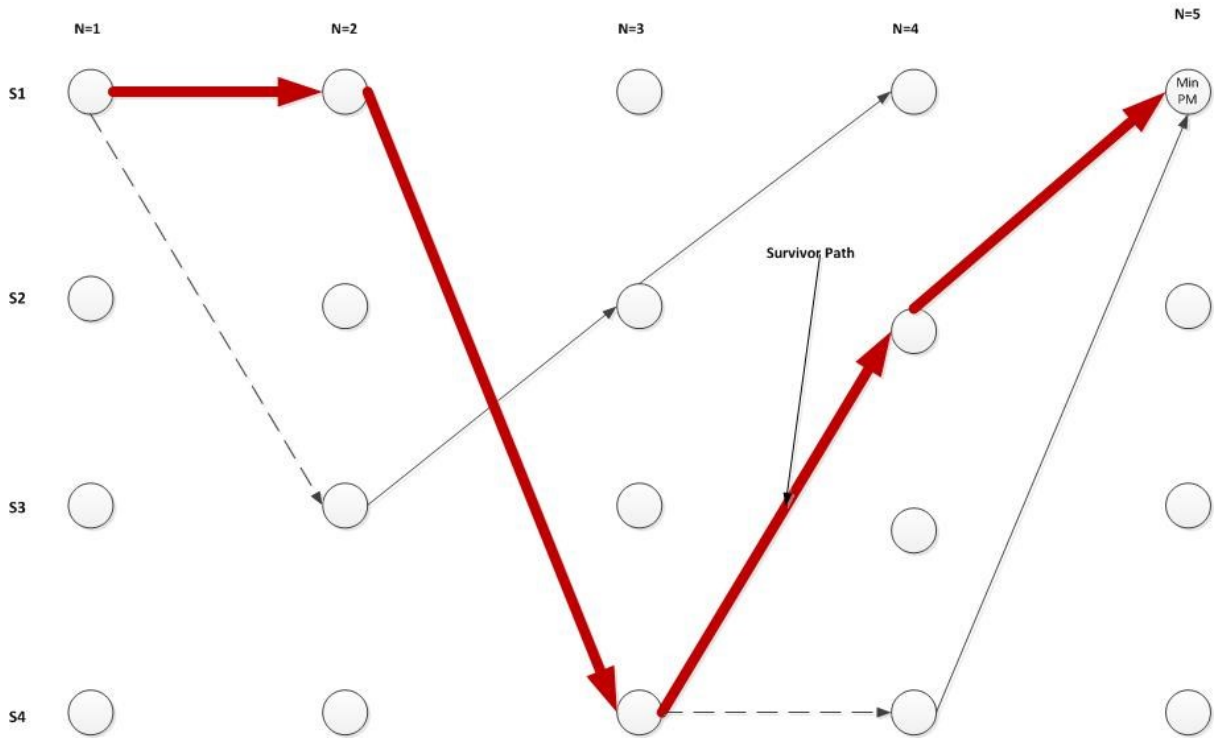

Figure (2.6.1): The survivor paths of a trellis diagram based on Viterbi Decoding

2.7 BCJR algorithm and its challenges

This algorithm was proposed by Bahl Jelinek Cocke and Raviv (BCJR) to maximise the posterior decoding defined on the trellis structure of the convolutional code [47]. This is an iterative decoder based on the forward error correction code, and principally is a soft output algorithm used for Markov chain based structure. It is important to note that, convolutional code exhibits Markov chain since it's a finite state machine. In Viterbi algorithm, the error probability is minimised between the transmitted and received code-word, while the aim in BCJR method is to minimise the bit error probability. It is very clear that, the latter algorithm gives better performance in terms of the error performance. The two vectors for the encoders are the input sequence signal to the encoderX_i, and the output signal sequence from the encoderX_o. Considering the states of the encoder, there are a number of states for every encoder based on the memory registers of that particular encoder. While transmitting, the encoder transit from one state to another with every instant of time project three main statesS_{prev},S_{cur}, and S_{nex} (S_{prev}indicating the previous state, S_{cur}refer to the current state, and S_{nex}indicating the next state for the encoder). The encoder moves (jump) between states depending on the input source information sequence (the original voice or data sequence required for transmission). The posterior log likelihood ratio of the input signal

depending on observed finite and limited received signal could be defined as flows

$$L(x\_i) = \log\left\{\frac{P(x\_i = 1|Y)}{P(x\_i = 0|Y)}\right\} \qquad (2.7.1)$$

Therefore, the scheme could also be referred to as Maximum Posteriori Probability (MAP) decoder. However, since there is a convolutional encoder that applied to the input signal, then the output transmitted signal (x) will depends on the input signal and the states of the encoder. Including these states in the conditional formula would be as flow

$$L(x\_i) = \log\left\{\frac{\sum_{u,p;x\_i=1} P(S_{k-1} = u, S_k = p|Y)}{\sum_{u,p;x\_i=0} P(S_{k-1} = u, S_k = p|Y)}\right\} \qquad (2.7.2)$$

In the transition between the previous state (S_{k-1}) and the current state (S_k), all the paths through the branches as result of an input one ($x\_i = 1$) would be summed together in the numerator expression for the posterior likelihood (eq. 2.7.2), while all the state transitions from (u to p) as result of an input zero to the convolutional encoder ($x\_i = 0$) would be summed in the denominator. Furthemore, the observed sequency (Y), could be divided into three segments, the past, current and the future ($Y_{y<k}$, $Y_{y=k}$, and$Y_{y>k}$,). The likelihood expression could be segmented based on its probability components relating the encoder states. In the use of Bay's theorem and Markov property, the

individual probabilities forming the expression could be expressed by certain quantities that needed to be calculated within the iterative process.

$$P\left(S_{k-1}=u,S_k=p\middle|\hat{Y}_{1,k}\right) = P\left(S_{k-1}=u\middle|\hat{Y}_{1,k-1}\right)P\left(S_k=k,\hat{Y}_k\middle|S_{k-1}=u\right)P(\hat{Y}_{k+1,k}|S_k=p)$$

$$P(S_{k-1}=u,S_k=p,\hat{Y}_{1,k}) = P(S_{k-1}=u,\hat{Y}_{1,k-1})\,P\left(S_k=k,\hat{Y}_k\middle|S_{k-1}=u\right)P(\hat{Y}_{k+1,k}|S_k=p)$$

$$P(S_{k-1}=u,S_k=p,\hat{Y}_{1,k}) = \alpha_{k-1}(u)\;\gamma_k(u,p)\;\beta_k(p) \tag{2.7.3}$$

$$\alpha_{k-1}(u) = P(S_{k-1}=u,\hat{Y}_{1,k-1}) \tag{2.7.4}$$

$$\gamma_k(u,p) = P\left(S_k=p,\hat{Y}_k\middle|S_{k-1}=u\right) \tag{2.7.5}$$

$$\beta_k(p) = P(\hat{Y}_{k+1,k}|S_k=p) \tag{2.7.6}$$

The forward calculation starting from the initial sate to the end involves (α), and the backward path calculation involves (β), while the transition between states related to (γ) labelled in figure (2.7.1). It is important to note, the reverse path (backward) only calculated recursively after the whole Y sequence had been received.

The MAP algorithm for the BCJR decoding steps as follows:

1- Initialising the forward and backward recursion for alphas and betas $(\alpha_0[S], \beta_k[S])$

2- Calculating the branch metrics Gammas $\gamma_k(u,p)$

$$\gamma_k(u,p) = P\left(S_k = p, \hat{Y}_k \middle| S_{k-1} = u\right)$$

$$= P(S_k = p | S_{k-1} = u).\ P\left(\hat{Y}_k \middle| S_{k-1} = u, S_k = p\right)$$

$$\gamma_k(u,p) = P(p|u)\ P\left(\hat{Y}_k \middle| u,p\right) = P\left(X_{i,k}\right) p\left(\hat{Y}_k \middle| X_{o,k}\right)$$

$$= P\left(X_{i,k}\right)\left(\sqrt{\frac{E_s}{\pi\sigma^2}}\right)\ e^{-\left(\frac{\left\|\hat{Y}_k - X_{o,k}\right\|^2}{\sigma^2}\right)}$$

It is important to note that for the BCJR algorithm, the noise variance σ^2corresponding to the specified branch should be calculated. In the other hand, the noise variance was not required in the Viterbi scheme and that reduces the algorithm complexity.

3- Calculating the forward recursion in terms of alphas (α)

$$\alpha_k(p) = \log\left\{\frac{\sum_u \alpha_{k-1}(u).\gamma_k(u,p)}{\sum_u \sum_p \alpha_{k-1}(u).\gamma_k(u,p)}\right\} \qquad (2.7.7)$$

4- Calculating the backward recursion in term of betas

$$\beta_k(p) = \log\left\{\frac{\sum_u \beta_{k+1}(u).\gamma_k(u,p)}{\sum_u \sum_p \alpha_k(u).\gamma_k(u,p)}\right\} \qquad (2.7.8)$$

5- Computing the likelihood of the input as follows

$$L(x_i) = \log\left\{\frac{\sum_{u,p;x_i=1} \alpha_{k-1}(u).\gamma_k(1,u,p).\beta_k(p)}{\sum_{u,p;x_i=0} \alpha_{k-1}(u).\gamma_k(0,u,p).\beta_k(p)}\right\} \qquad (2.7.9)$$

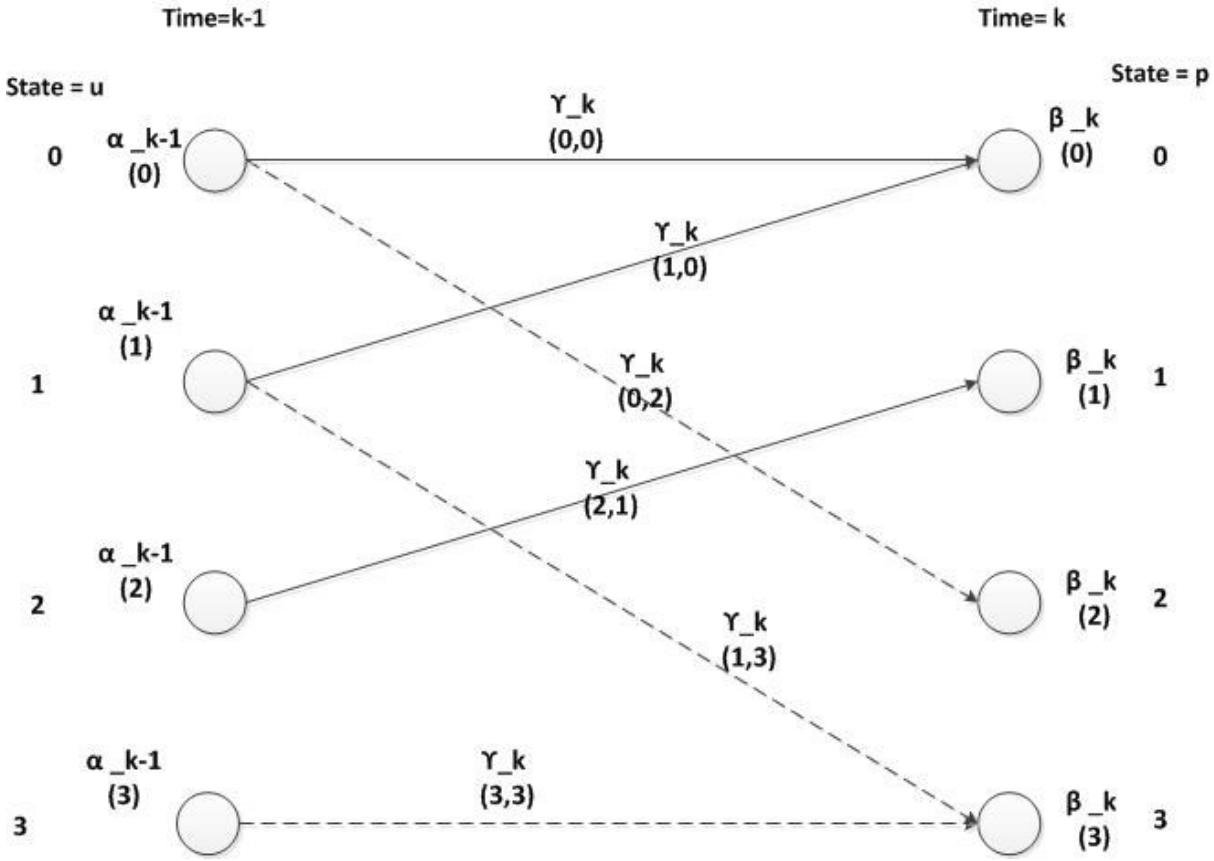

Figure (2.7.1): The BCJR algorithm parameters in the trellis

Further approximation could be used to the BCJR algorithm in the name of Log-MAP and Max-Log-MAP, which make use of the logarithmic property to give an efficient implementation. The Max algorithm gives further reduction in the complexity by removing the exponential term in the Log-MAP method. Therefore, the latter algorithm gives an optimal computational performance in comparison to the original scheme. In conclusion, BCJR algorithm works in a recursion process by depending on joint events (previous, current, and expected future events), and therefore has a complexity issue as well as overhead cost. This is one of the major challenges in applying these non-linear algorithms in low cost wireless applications. This is because, for every observed received signal vector, there would a multiple computations regarding the states of the encoder with evaluation to the relation between the input signal vector, and the estimated trellis states. The numerical instability of underflow and overflow due to design errors in the iteration process makes this algorithm less favourable to be implemented in wireless indoor application.

2.8 Turbo code and its cost of implementation

Turbo have a convolutional structure with two encoders applied for every input sequence (original information signal), separated by an inter-leaver [48]. These are recursive systematic convolutional encoders (figure 2.8.1). At the receiving side, there are two Soft-Input Soft-Output (SISO) decoders separated by inter-leaver to reformat the second encoder at the transmitter. Figure (2.82) gives a description of the decoding structure used in the turbo algorithm. The implementation of SISO algorithm could be based on SOVA or the more optimise but involved MAP method, with passing extrinsic information in the implementation. The turbo algorithm is an iterative decoder, and therefore it's critical to determine the number of iteration for every cycle within the method. Choosing a large number of iteration would increase the cost exponentially, and if there is no threshold limit, the algorithm will run to infinite loop and would result in failures. This particular problem of iteration is one of the main disadvantages in applying this algorithm in WPAN systems.

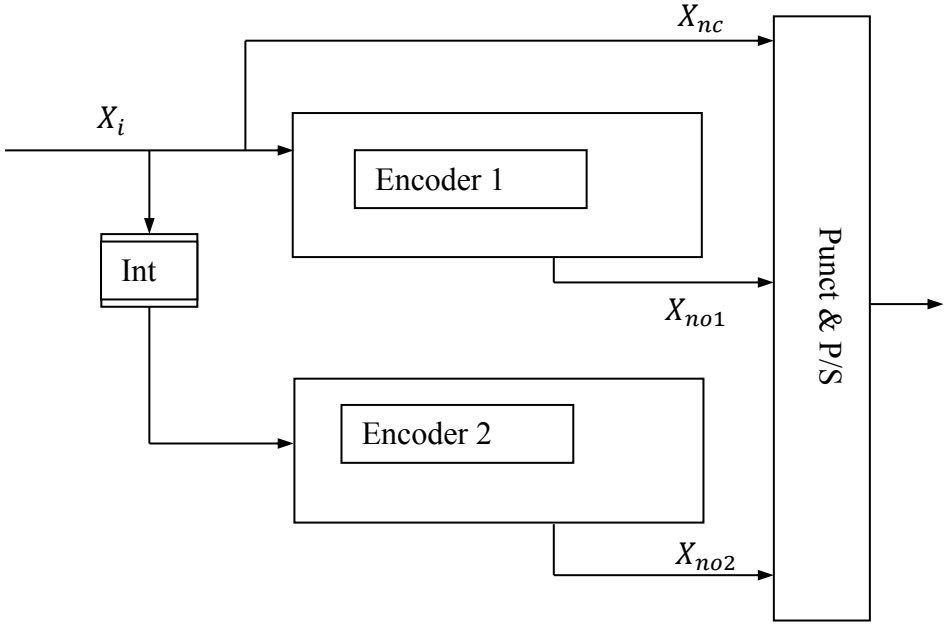

Figure (2.8.1): The encoding structure of the Turbo scheme

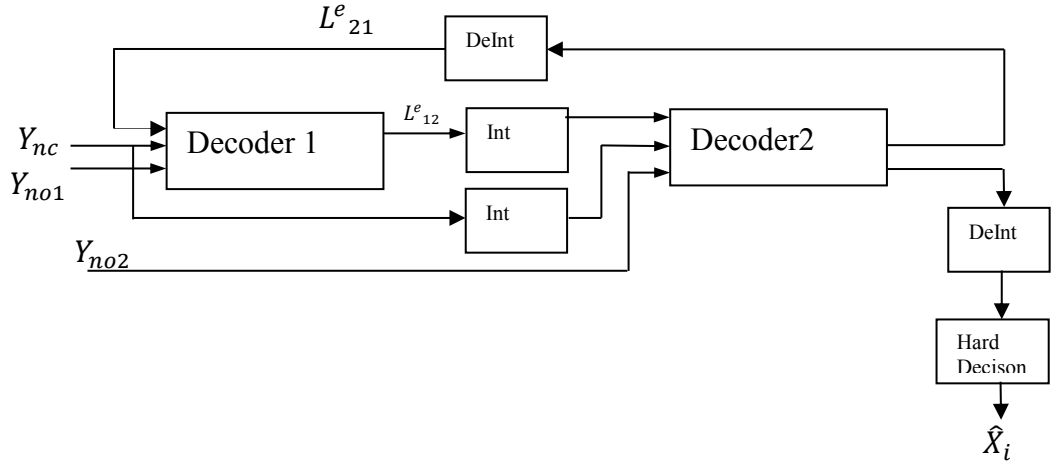

Figure (2.8.2): Block diagram structure of the Turbo Decoder

2.9. Modulation Schemes

The modulation schemes that have been used in the UWB Multiband wireless communications standards were based on Quadrature Phase Shift Keying (QPSK) and Quadrature Amplitude modulation (QAM) including 16-QAM & 32-QAM. The ECMA-368 standard has defined Quadrature Phase Shift Keying (QPSK) modulation for up to 200 Mbps and Dual Carrier Modulation (DCM) for the higher rate schemes [49], [50]. The various modulation schemes that have been proposed in the literature and undertaken in previous research work are summarised in this section.

2.9.1. Quadrature Phase Shift Keying

This scheme had been assigned for control signals at the packet header and for the lower transmitting rate less than 320 Mb/s (53.3 Mb/s, 80 Mb/s, 106.7 Mb/s, 160 Mb/s, and 200 Mb/s). QPSK modulation has been accomplished by dividing the coded bit sequences into groups of 2 bits forming a complex number that have In-phase and Quadrature components (figure 2.9.1), and uses the normalisation factor ($M = \frac{1}{\sqrt{2}}$) expressed as follow.

$$s[k] = M \times [(2 \times b[2k] - 1) + j(2 \times b[2k+1] - 1)\,] \qquad (2.9.1.1)$$

Time-domain spreading (TDS) and Frequency-domain spreading (FDS) are used in QPSK modulation to vary the data rates and create the necessary diversity required for the scheme [51]. The diversity in the spectrum has been implemented by taking fifty QPSK symbols and their other fifty conjugate counterparts and then mapping them both onto 100 OFDM subcarriers, and hence allowing the transmitter to operate on the real part of the IFFT tones [52]. In the case of time domain, the same QPSK symbols would be transmitted at different time slots.

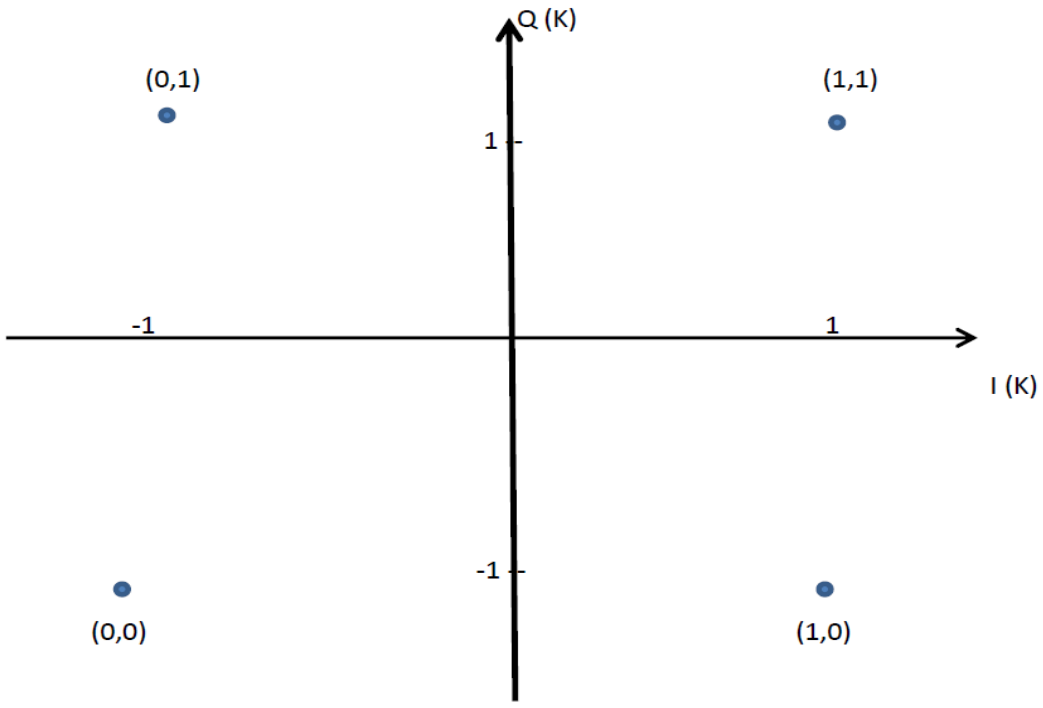

Figure (2.9.1): Quadrature Phase Shift Keying Mapping

Due to the frequency hopping specification with QPSK modulation, the channel fading tends to be independent the frequency bands and that gives it more performance strength in regards to the error correction. At the receiver, once the equalisation had been carried out, the data coming from the two OFDM symbols are demodulated by QPSK. Euclidean metrics (d_p,d_s) were used in soft decoding by calculating the distances between the received symbol and constellation symbols based on spreading or without spreading (Y_{s_k}, Y_{p_k}, and S_n) as follows

$$d = \sqrt{(r_1 - x_2)^2 + (r_2 - y_2)^2} = \sqrt{(x_1 - x_2)^2 + (y_1 - y_2)^2} \qquad (2.9.1.2)$$

$$d_p = \sqrt{\left(Re(Y_{p_k}) - Re(S_n)\right)^2 + \left(Im(Y_{p_k}) - Im(S_n)\right)^2} \qquad (2.9.1.3)$$

$$d_s = \sqrt{\left(Re(Y_{s_k}) - Re(S_n)\right)^2 + \left(Im(Y_{s_k}) - Im(S_n)\right)^2} \qquad (2.9.1.4)$$

2.9.2. Dual Carrier Modulation

DCM has been suggested by [53] to accommodate the need for higher data rate applications as part of the ECMA standard. It uses frequency diversity by allocating the DCM symbol (which consists of four bits) to two separate subcarriers separated by 200 MHz The idea behind DCM is to use frequency diversity in a large symbol bandwidth by transmitting the same information in parallel and with 50 tones separation within the same symbol. If one subcarrier experiences a deep fade, the probability of another subcarrier carrying the same information but separated by relatively large bandwidth to experience the same deep fade is realistically very small. A total number of 100 complex symbols are mapped to 100 IFFT subcarriers in the transmitter block before transmission [54]. This method groups the bits in two sections each having a length of 50 with 100 bits. It then takes a subgroup of 2 bits as (b[g(k)], b[g(k) + 50]) and (b[g(k) +1], b[g(k) + 51]). These groups of 4 bits are then converted to 2 QPSK symbols (table 2.9.2). A pair of 16-QAM constellation maps was used to perform the dual modulation and transform each pair of symbols into a DCM symbol (figure 2.9.2).

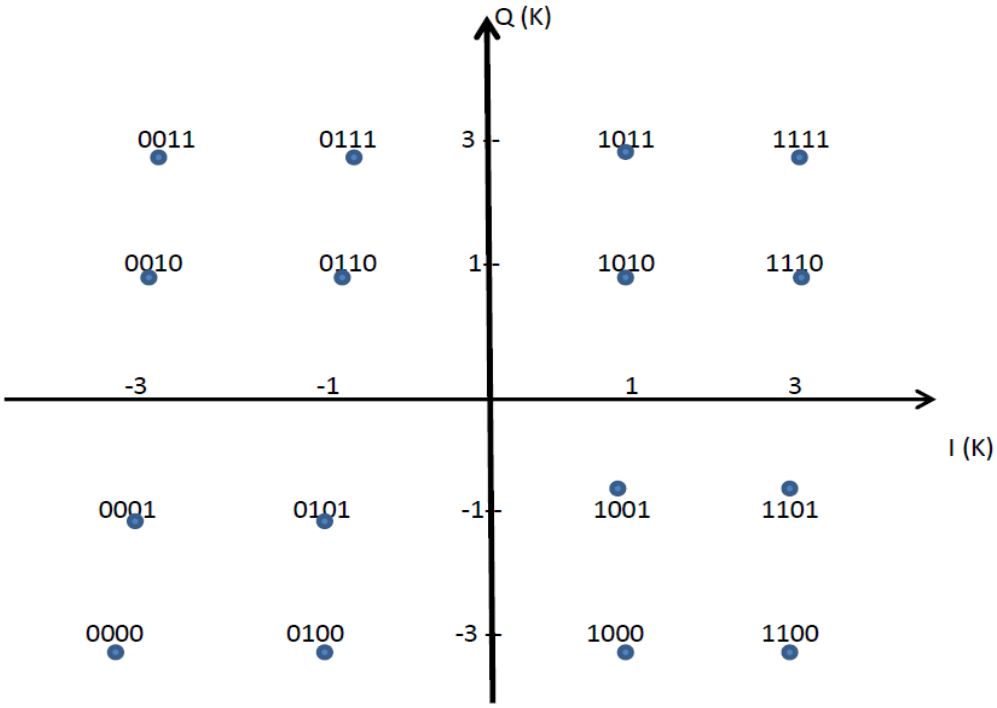
Q (K)
I (K)
0011
0111
1011
1111
0010
0110
1010
1110
0001
0101
1001
1101
0000
0100
1000
1100
3
1
-1
-3
-3
-1
1
3

(A1): S [K] = [I (K), Q (K)]

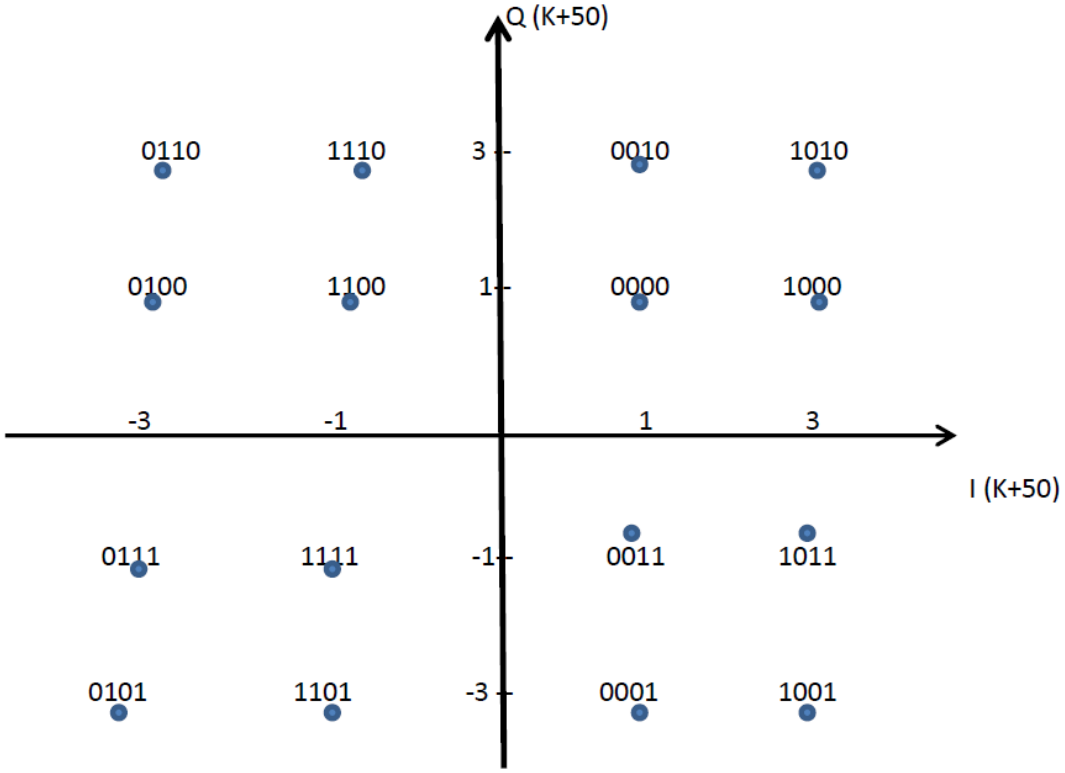

(A2): S [K+50] = [I(K+50), Q(K+50)]

Figure (2.9.2): Constellation mapping of DCM: (A1) = S [N]; (A2) = S[N+50]

Input Bit b[g(k)], b[g(k)+1], b[g(k)+50], b[g(k)+51]	I[k]	Q[k]	I[k+50]	Q[k+50]
0 0 0 0	-3	-3	1	1
0 0 0 1	-3	-1	1	-3
0 0 1 0	-3	1	1	3
0 0 1 1	-3	3	1	-1
0 1 0 0	-1	-3	-3	1
0 1 0 1	-1	-1	-3	-3
0 1 1 0	-1	1	-3	3
0 1 1 1	-1	3	-3	-1
1 0 0 0	1	-3	3	1
1 0 0 1	1	-1	3	-3
1 0 1 0	1	1	3	3
1 0 1 1	1	3	3	-1
1 1 0 0	3	-3	-1	1
1 1 0 1	3	-1	-1	-3
1 1 1 0	3	1	-1	3
1 1 1 1	3	3	-1	-1

Table (2.9.2): The DCM mapping signal across the constellation maps

The de-mapping process at the receiver uses the two constellation maps and combines the subcarriers that represent the same symbol. Each two subcarrier containing the I and Q quadrature components of the particular symbol had been separated by 50 FFT tones, and hence this diversity produces two different signals with various power strength for the symbol [55]. When combining these signals, one constellation map would be required to represent the two bits, and the other one would identify the next two bits. Originally,

each subcarrier represents four bits that had been mapped in such way so as to make the linear combination of two subcarriers would produce only two bits in each constellation branch. The starting point was the combining of two subcarriers with total of 8 bits in each constellation, and then after the combining process, each output of a constellation branch ending with two bits. The top branch would contain the first and third bits (b1,b3), and the lower branch would represent (b2,b4) as [56].

2.9.3. Dual Circular 32-QAM

Although ECMA-368 standard offers 480 Mb/s transmission rate, it is difficult to achieve this data rate in real life due to poor channel conditions which causes drop packets. This in turns results in lower throughputs and retransmission was needed in this instance. Furthermore, although this rate could be adequate for data and voice communications, for intensive media, video conferencing and live streaming contents, a higher transmission rate

would be needed to enable successful communication for these types of applications. The DC 32-QAM scheme had been proposed in order to increase the system throughput by mapping more information on each subcarrier of the 100 IFFT data tones [57]. The scheme takes 1500 interleaved and coded bits and then divides them into 250 bits, then further division is carried out by forming 50 groups of 5 reordered bits (b_g(k), b_g(k)+ 50, b_g(k) + 51, b_g(k) + 100, b_g(k) + 101) to be mapped over two symbols using 2 8-ary PSK constellations (figure 2.9.3). The first four bits are mapped to two QPSK symbol similar to the DCM, while the fifth bit is used to conform the mapping to two 8-ary PSK-like constellations. To further enhance the interleaving process, the first and the hundredth bits are combined together and the same process for the second bit from the first fifty pair with the second forming the next fifth pair as follow

$$(2\, b\_g(k) + 50 - 1) + j\,(2\, b\_g(k) + 100 - 1)$$

$$(2\, b\_g(k) + 51 - 1) + j\,(2\, b\_g(k) + 101 - 1)$$

Due to the nature of 8-ary PSK constellation, all the constellation points have equal amplitude which adds another advantage to DC 32-QAM in comparison to the 2 16-QAM DCM scheme in terms of constant power ratio. Furthermore, this type of modulation conforms to the specification of ECMA-368 and have the same DCM frequency planning by using two individual OFDM data carriers separated by 50 tonnes (subcarriers) with 200 separation for the diversity purposes, and each subcarrier have 4 bandwidth standard

requirements.

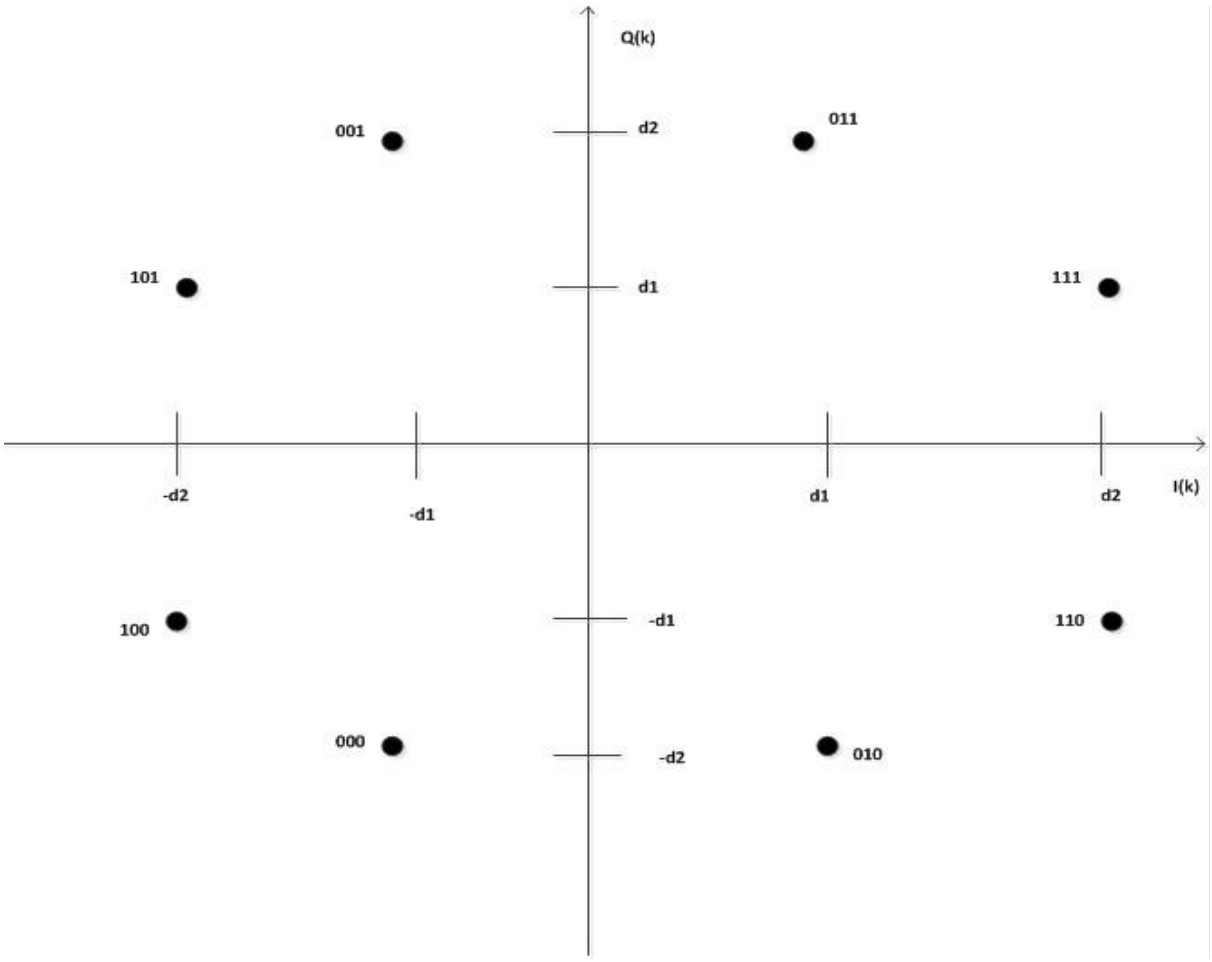

(B1): S [K] = [I(K), Q(K)]

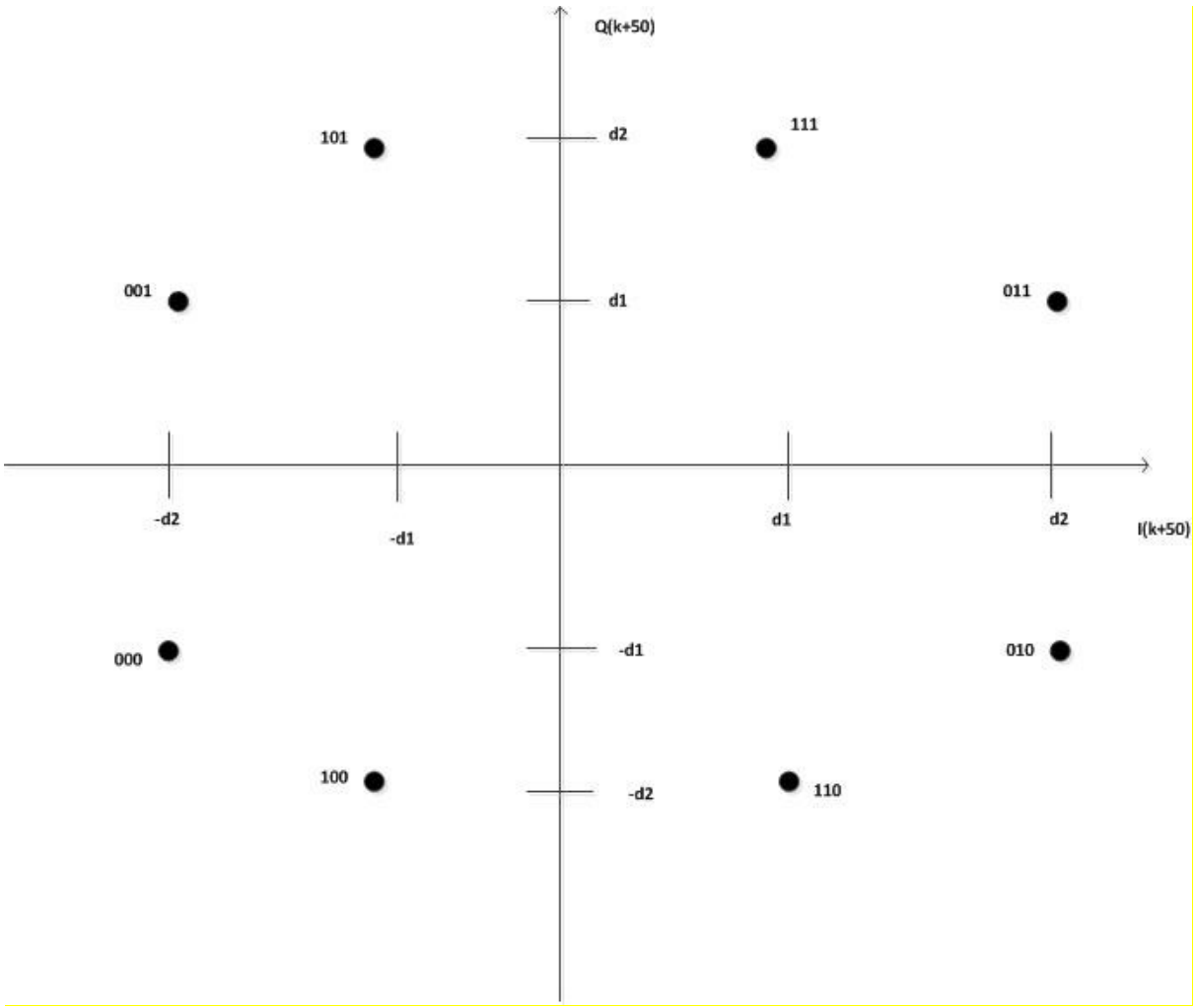

(B2): S [K+50] = [I(K+50), Q(K+50)]

Figure (2.9.3): Constellation mapping of DC 32-QAM: (B1) = S [K]; (B2) = S[K+50]

In the demodulation process, a soft bit de-mapping has been proposed for I & Q components that had been transmitted on two different subcarriers. Each

subcarrier represented by a symbol consisting of the four bits that formed the 2 QPSK symbols, plus the fifth bit which de-mapped according to each of the two DC 32-QAM symbols (S(k) , S(k + 50)). In the case of the S(k) constellation, the fifth bit is considered zero valued if the received symbol is close to the constellation point along the Q axis, else it takes a value of one if it's close to the I axis. For the constellation of S(k + 50) the opposite is applied, that is the fifth bit is considered to be a one if the received symbol is close to the constellation point along the Q axis, otherwise its zero. Channel State Information (CSI) had been used to further improve the decoding process. System simulation for both DCM and DC 32-QAM has shown that the latter outperforms the DCM in terms of both throughput and transmission range. The results of these previous researches will be used in the developments of the design model and further work will be carried out to develop a more optimised modulation scheme.

3. Design

3.1 Introduction

In this chapter, the designs of the proposed MIMO model have been described including the development phases. An overview of the design scheme is then summarised in the first part. In the second section, the transmitting design scheme was then explained and instructions to the design steps taken had been highlighted. The modulation scheme is analysed from a design prospective and a detail methodology to the principle concept is then given. The receiving model design was then followed on the next section, where a description to this phase was undertaken. The design principle was explained and schematic analysis was then produced. A configuration for receiver structures that allows the model to increase the coverage area was shown. This construction provided conformation of the model to wireless range demand applications. The last section gives a mathematical analysis the performance of the proposed model. In this part, a mathematical treatment to the concept of the design was given including performance metric measures. Concluding remarks is then summarising the design work.

3.2 Design Overview

The model design of a physical layer MIMO-UWB wireless communication system operating in the free spectrum requires a number of interconnected modules representing the transmitter, receiver and the physical channel. The project had been divided into layers and each one has its own requirements and operational functions. The design tasks have been spread across these layers with various degrees of complexity. The structure involves the transmitting module, the physical channel model and the receiver part, and this arrangement was embedded in the design. Encompassing this design structure, it is ability of backward compatibility for legacy systems with lower transmission rate. The scheme uses the inherent spatial and frequency diversities to boost the system performance by increasing the capacity, and facilitates higher throughput that dynamically varies to accommodate both the physical conditions and the type of wireless transmissions (data, videos, etc.).

The first layer of the design framework includes a transmitting module consisting of two spatial elements with initial design requirements. The second part of this phase constitutes a multipath fading channel model designed to test and evaluate the system performance in terms of the spatial and frequency

diversity presence. This in turn introduces more channels for the transmitted signal, and so improving the link budget. The receiving module represents the last sub-system within this layer, and includes the decoding and estimation algorithms, as well as objects link requirements. The aim design for this layer was to evaluate the proposed concept and how to develop theoretical algorithms into working wireless systems. Therefore, a predefined metrics conditions was evaluated at the output of the receivers. In the case of not satisfying the test requirements, the design is then readjusted and modified until certain conditions are satisfied. This method enables the development in stages with ascending order in term of complexity forming a bottom up hierarchy.

Once this phase was completed, the next layer would include an advanced MIMO transmitting and receiving sub-systems. An additional Standardised IEEE802.15.3a channel model would be included. The transmitting block includes the objects within the pervious developed transmitting block, as well as stringent modulation and spatial requirements. The receiving block in this phase would include an optimised decoding and equalisation algorithms that meet the desired requirements. The validation of the research hypotheses would be met at this stage, and hence an iterative approach would be applied. The results error performance was then compared with previous work and identified pre-set levels in the signal power. System optimisation was the third phase and covers the improvements to the model design and performance. The packet error rate (PER) for the communication link of both LOS and NLOS was further reduced in this sub-system. The complexities in the receiver were studied to make further improvement, and the overall design complexity was

optimised. Testing of the application included verification of particular conditions, by the simulation of hypothesised scenarios in order to test the fitness of the model. Additional requirements had been embedded into the model and then examined for approval purposes. Further development to the design was carried out in this stage so as to ensure practical feasibility of the system in real time environments.

The evaluation phase involves multiple tests of various indoor scenarios in order to full fill all the design requirements. Experimental analysis was applied to the final version of the developed design in order to validate the simulated design model against standardised and recognised approved models.

Predefined parameters had been used to test various fitness tests and systems requirements such as the time delay, bit error rate (BER), the signal to noise ratio (SNR) and the power profile. The necessity for this step was to match the system requirements with the achieved results and approves theoretical concepts. These results approved the design concept in increasing the link capacity, by the use of spatial element and contribute to the knowledge in this field. Figure 3.1 below gives an overview to the design framework.

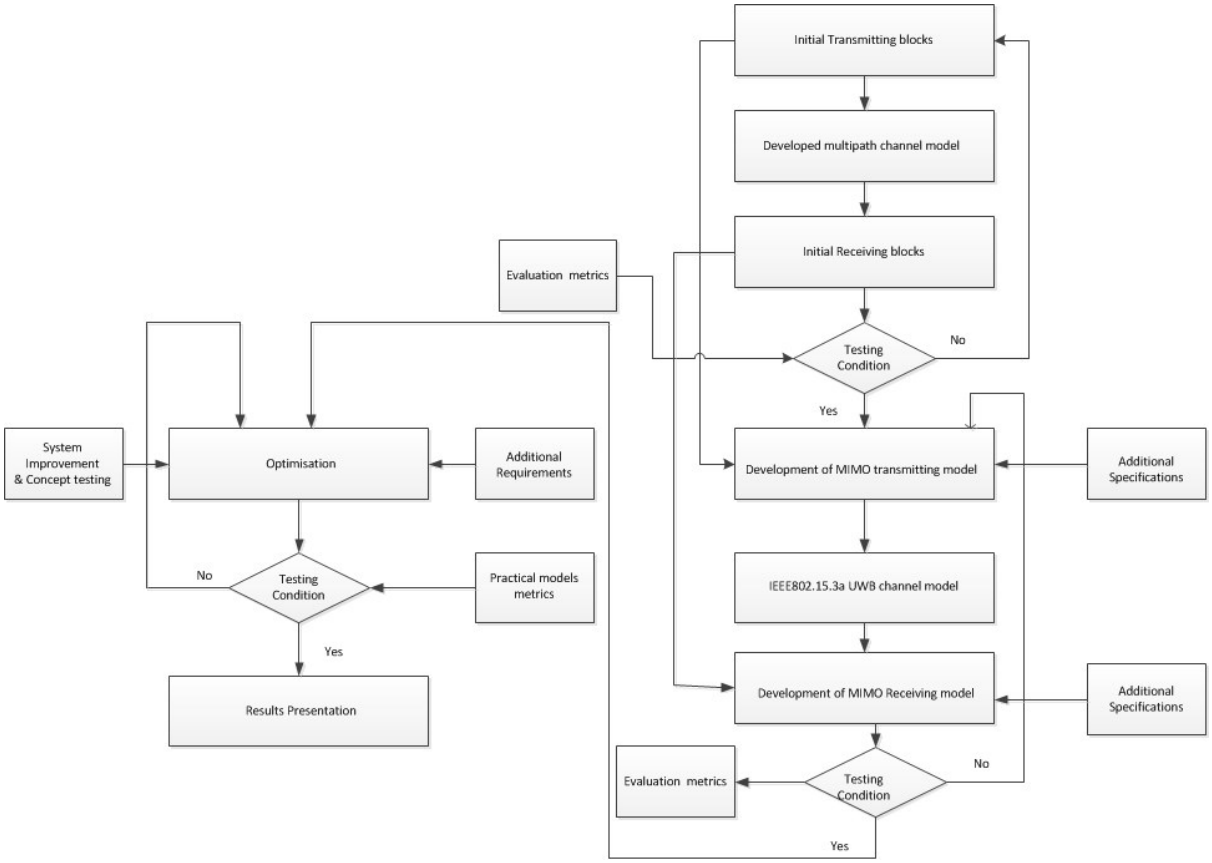

Figure (3.1): Scheme of the Design development

3.3 Design Method

3.3.1 The Transmitting Model Design

The design architecture of the modulation scheme consists of two branches, each of which contains dual QPSK constellations that convert the input stream into two sequences of complex symbols. Then, the pair of symbols within every branch was reordered by interchanging the In-phase components of this complex numbers. This transformation expands the fading diversity across the modulated symbols within the code-word, and improves the performance across the spatial and frequency domains. This form of implementation enforces frequency selectivity and fading variation across the desired signal components. The next stage in this transmitting design was to increase the spectral efficiency (bps/Hz) of the modulation scheme. For this purpose, a method for achieving high end wireless link with large modulation scheme that convert the two bits symbol into a large dimension symbol was developed. Incorporation of dual circular 8 points constellation maps in the name of 8-ary PSK modulation would results in an increase the modulation dimension and facilitates high data rate transmission. The equal decision region for symbol

bits gives this particular modulation an advantage in terms of Peak to Average Power Ratio (PAPR). Furthermore, increases the number of bits within a symbol and that increases the symbol rate by enabling high data rate transmission.

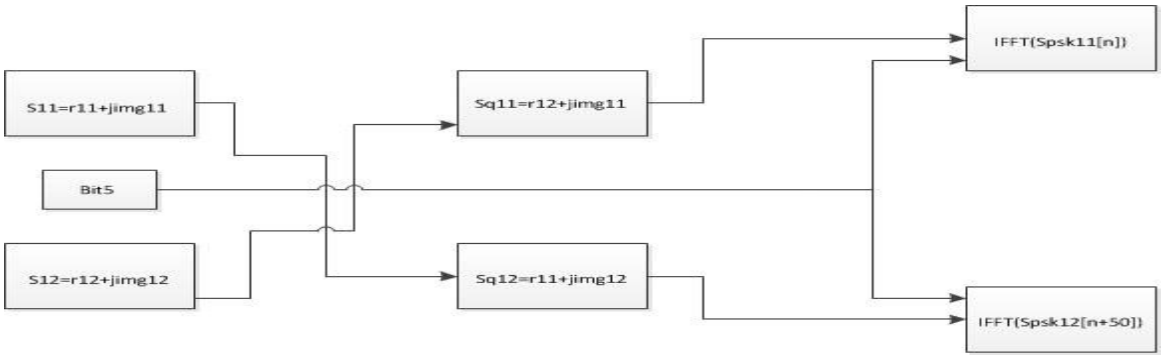

Figure (3.2): The formation of the modulation across the dual complex symbols

The scheme applied on the two branches with the same order and formulation, and hence enabling legacy systems and devices to be included in this design. Every branch represented a group of five bits, four of which relates to the dual complex symbols and the fifth bit was used for the control part. The process takes the interchanged complex symbols (coming from the dual QPSK symbols) and the fifth bit representing that particular group (G1 for the first branch, and G2 for the second branch). The constellations of these 8-ary PSK was designed so that there are two distinct distance metrics across the

orthogonal In-phase and Quadrature domains on the four quadrants scatter diagram. The eight signal points were distributed across the two orthogonal domains based on these dual Euclidean metrics.

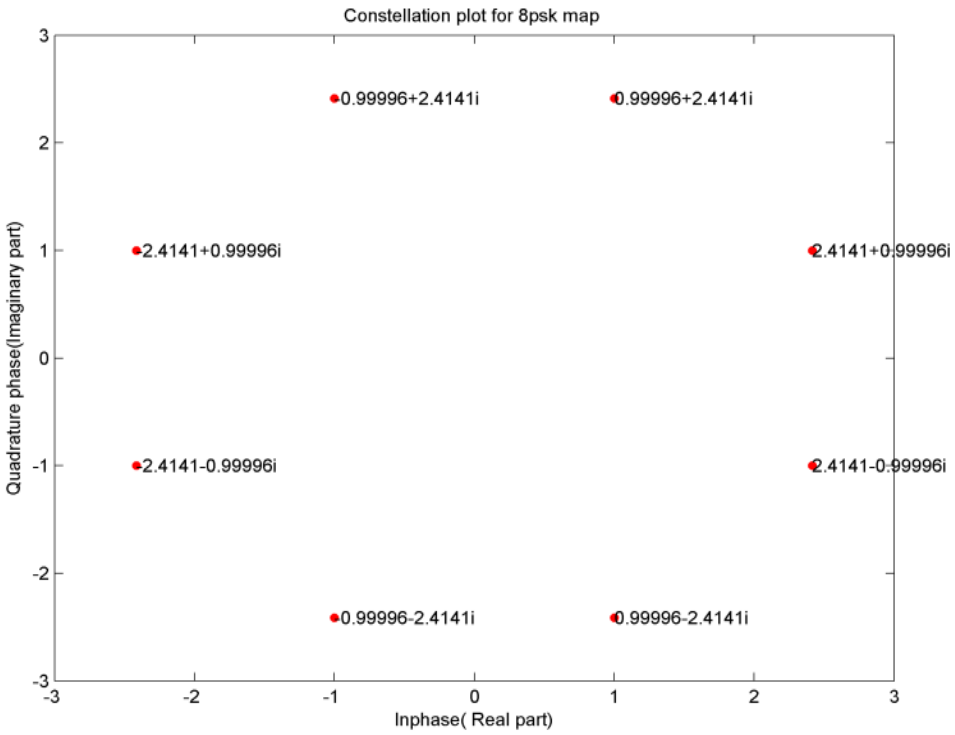

Figure (3.3): The two distance metrics across the 8 signal constellation points

In this 8-ary PSK modulation with constant amplitude modulation, the positions of symbols were rotated around the circle by $\frac{j2\pi}{16}$ (22.2 degrees), so as to ensure that only two distance metrics (d1, d2) from the origin across the real and imaginary axes in the complex plane contains the constellation points.

These metric locations was used to position the four QPSK complex signals using the driving bit (b5) located in each of the two sub groups(G1,G2) . For the first branch, the two output complex symbols from the four point modulation (QPSK modulation) was multiplied by the distance metrics so as to be transformed into PSK complex symbols ready to be distributed across the eight point maps. The first complex symbol was assigned to the first PSK constellation, while the second symbol representing the third and fourth bits within G1 was a located to the second constellation. The binary value of the fifth bit represents the most significant bit of the PSK symbol (three bits symbol), and was used as a reference to identify the particular signal point on the map in which these symbols represents. In a similar manner, these steps were applied across the second branch in parallel to achieve the spectral efficiency of the system. The original four quadrature symbols represented as follows

$$\mathrm{s}_{qpsk_1^{G1}} = x^{G1}{}_{c(n)} + jx^{G1}{}_{c(n)+50} \qquad (3.1)$$

$$\mathrm{s}_{qpsk_2^{G1}} = x^{G1}{}_{c(n)+1} + jx^{G1}{}_{c(n)+51} \qquad (3.2)$$

$$\mathrm{s}_{qpsk_1^{G2}} = x^{G2}{}_{c(n)} + jx^{G2}{}_{c(n)+50} \qquad (3.3)$$

$$\mathrm{s}_{qpsk_2^{G2}} = x^{G2}{}_{c(n)+1} + jx^{G2}{}_{c(n)+51} \qquad (3.4)$$

Where $$c(n) = \begin{cases} 2n & n \in \{0 \ldots .24\} \\ 2n + 50 & n \in \{25 \ldots .49\} \end{cases}$$

The metrics d1 and d2 were interchanged between the symbols based on b5 binary value. In the case of the first group, the following operation was done on the dual constellations.

For the first constellation

If b5 == 0

$$s_{psk_1^{g1}}(m) = d1 * real\left(s_{qpsk_1^{g1}}\right) + d2 * imag\left(s_{qpsk_1^{g1}}\right)$$

Else

$$s_{psk_1^{g1}}(m) = d2 * real\left(s_{qpsk_1^{g1}}\right) + d1 * imag\left(s_{qpsk_1^{g1}}\right)$$

For the second constellation

If b5 == 0

$$s_{psk_2^{g1}}(m) = d2 * real\left(s_{qpsk_2^{g1}}\right) + d1 * imag\left(s_{qpsk_2^{g1}}\right)$$

Else

$$s_{psk_2^{g1}}(m) = d1 * real\left(s_{qpsk_2^{g1}}\right) + d2 * imag\left(s_{qpsk_2^{g1}}\right)$$

End

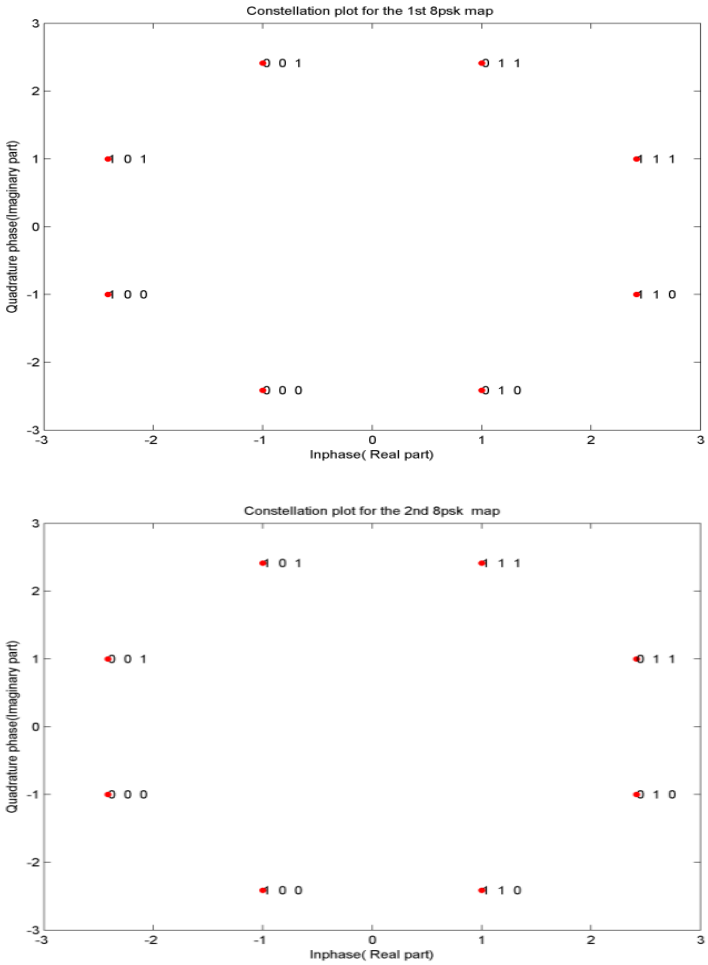

Figure (3.4): The constellation maps used for the dual 8-ary PSK symbols

The formulated PSK symbols were then allocated to different IFFT subcarriers with spatial variation and over 50 MHz frequency separation. It is important to mention that, due to the use of MIMO and transmitting the dual symbols from every branch across two antennas, the actual frequency separation would be much greater, and insures maximum degree of separation in terms of the spectral fading across these symbols. The second transmitting branch would be subjected to the same process, which enables backward compatibility with the proposed ECMA-368 standard. The figure below illustrate this construction

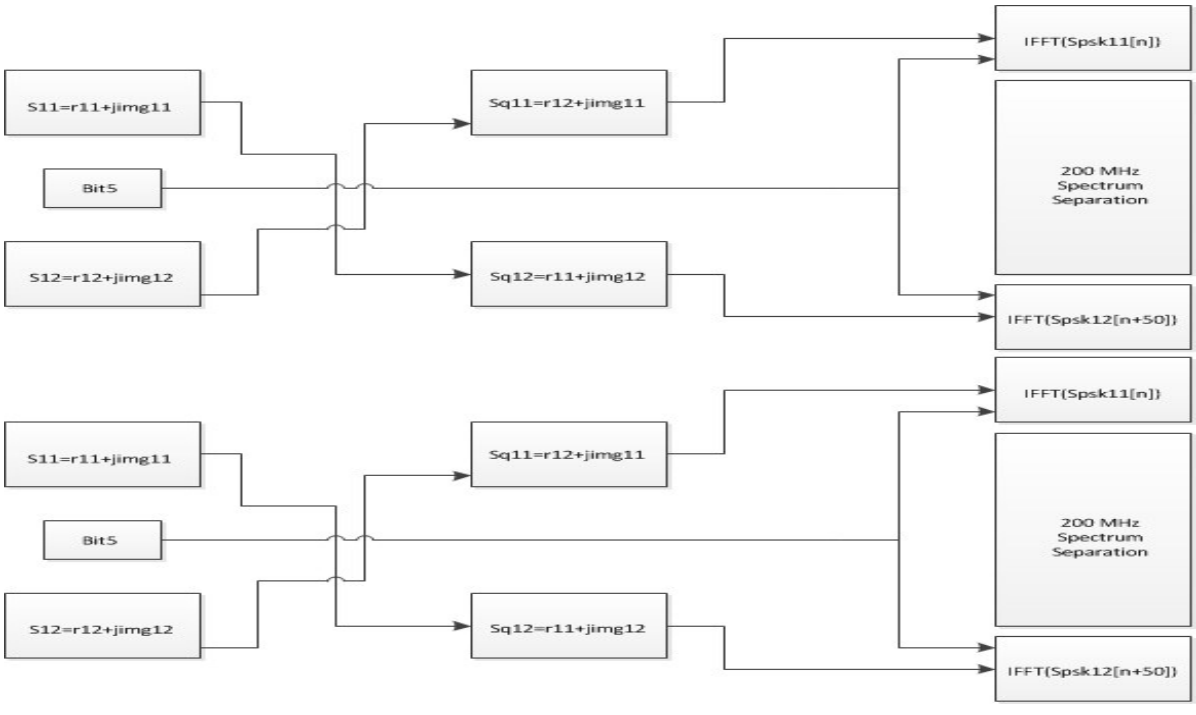

Figure (3.5): The transmitting configuration design across the two antennas

3.3.2 The Receiving model Design

The receiver architecture consists of two branches, and there are dual 8-PSK constellations in every branch. A cross interchanging was applied to the In-phase components with the four received complex symbols. This process was undertaken by taking the real amplitude of the first complex symbol within the second branch, and inserted in place of the In-phase component of the first symbol within the first receiver branch. In the same time, the amplitude of the first symbol within the first branch replaces the amplitude of the first complex symbol within the second receiving branch. In a similar process, the second received 8-PSK symbol within the first receiving branch was readjusted by replacing its real amplitude with its counterpart of the second symbol within the second receiving block. In across exchange, the second received 8-ary PSK complex symbol was modified by inserting the In-phase of the second symbol of the first branch in place of its real amplitude. Therefore, all the received signals carried by the four complex symbols were readjusted in this process, and figure (6) describes this design scheme. The recived signals at both dual receivers had been expressed by the following received symobls.

$$R_{k(n)}^{psk_1^{A1}}(\mathrm{m}) = H_{k(n)}^{A1} S_{k(n)}^{psk_1^{A1}}(\mathrm{m}) + \mathrm{z}_{k(n)}^{A1} \qquad (3.3.1)$$

$$R_{k(n+50)}^{psk_2^{A1}}(\mathrm{m}) = H_{k(n+50)}^{A1}\, S_{k(n+50)}^{psk_2^{A1}}(\mathrm{m}) + \mathrm{z}_{k(n+50)}^{A1} \qquad (3.3.2)$$

$$R_{k(n)}^{psk_1^{A2}}(\mathrm{m}) = H_{k(n)}^{A2} S_{k(n)}^{psk_1^{A2}}(\mathrm{m}) + \mathrm{z}_{k(n)}^{A2} \qquad (3.3.3)$$

$$R_{k(n+50)}^{psk_2^{A2}}(\mathrm{m}) = H_{k(n+50)}^{A2}\, S_{k(n+50)}^{psk_2^{A2}}(\mathrm{m}) + \mathrm{z}_{k(n+50)}^{A2} \qquad (3.3.4)$$

Where $H_{k(n)}^{i}$ and $H_{k(n+50)}^{i}$ were the channel spectrums for the first anad second sections of the ith receiver.

Channel equlaisation was carried out to remove the specturm distrubance caused by the filtring effect of the medium. This channel fading minmisation is a critical step for the system performance, and a good channel estimater implementation is an essential requirment in mulitple antennas wirelss model. In the presence of channel weights estimaters W_i^j , the following formulas was enduced.

$$\tilde{R}_{k(n)}^{psk_1^{A1}}(\mathrm{m}) = W_n^{A1}\, R_{k(n)}^{psk_1^{A1}}(\mathrm{m}) \qquad (3.3.5)$$

$$\tilde{R}_{k(n+50)}^{psk_2^{A1}}(\mathrm{m}) = W_{k(n+50)}^{A1}\, R_{k(n+50)}^{psk_2^{A1}}(\mathrm{m}) \quad (3.3.6)$$

$$\tilde{R}_{k(n)}^{psk_1^{A2}}(\mathrm{m}) = W_n^{A2}\, R_{k(n)}^{psk_1^{A2}}(\mathrm{m}) \quad (3.3.7)$$

$$\tilde{R}_{k(n+50)}^{psk_2^{A2}}(\mathrm{m}) = W_{k(n+50)}^{A2}\, R_{k(n+50)}^{psk_2^{A2}}(\mathrm{m}) \quad (3.3.8)$$

The noise term z was assumed to be AWGN reprsenting the recivers' entiteis such as thermol noise, and therefore multiplication by the channel estimator would not change the statiscal propoty of this term. Taking this into account, the noise power determine the practical snr for a useble error rate performance. To elaporate on the mathematics, one could assume the noise power to be amargenlaised quantity by ignoring the additional z term from the received symbol formula. It is important to mension here, this assummtion was done to highlight the channel effect at this junction. In reality, the noise term always exists and there is no way to completely remove the nosie from the system. All the availabe alogrithms would minimise the noise term, but will not remove the noise completely. These process would be repeated across the the dual antennas and then the transmitted symbols could be estimated. It is sufficient to mention the estimation process within one radiating element. Hence, the estimated transmitted symobl for one of the receiving antennas $\bar{\bar{R}}_i^j$ could be

recoverd in the presence of frequency and spatial divresities with the follwing formula.

$$\bar{\bar{R}}_{k(n)}^{psk_1^{A1}}(\mathrm{m}) = \left(h^{*A1}_{\ n} h_n^{A1}\right)^{-1} . \tilde{R}_{k(n)}^{psk_1^{A1}}(\mathrm{m}) \qquad (3.3.9)$$

$$\bar{\bar{R}}_{k(n+50)}^{psk_2^{A1}}(\mathrm{m}) = \left(h^{*A1}_{\ k(n+50)} h_{k(n+50)}^{A1}\right)^{-1} \tilde{R}_{k(n+50)}^{psk_2^{A1}}(\mathrm{m}) \quad (3.3.10)$$

It was clear that, each of the received symbol had bits coming from different channel spectrum. The differences in the channel fading signatures were due to the two degrees of freedom in the diversity presence that were located in UWB channels. If only the inherent of diversity effect had been constraind to the frequency domain as it was the case for classical DC modulation, then induced correlation between the channel coffeicints presented in the medium specturm would effect the dual received signals of the same symbol. The additional degree of freedom encapsulated by the spatial diveristy would minmise this correlation factor, and results had shown the advanteges of this additional degree of freedom in the diversity to the overall system performance.

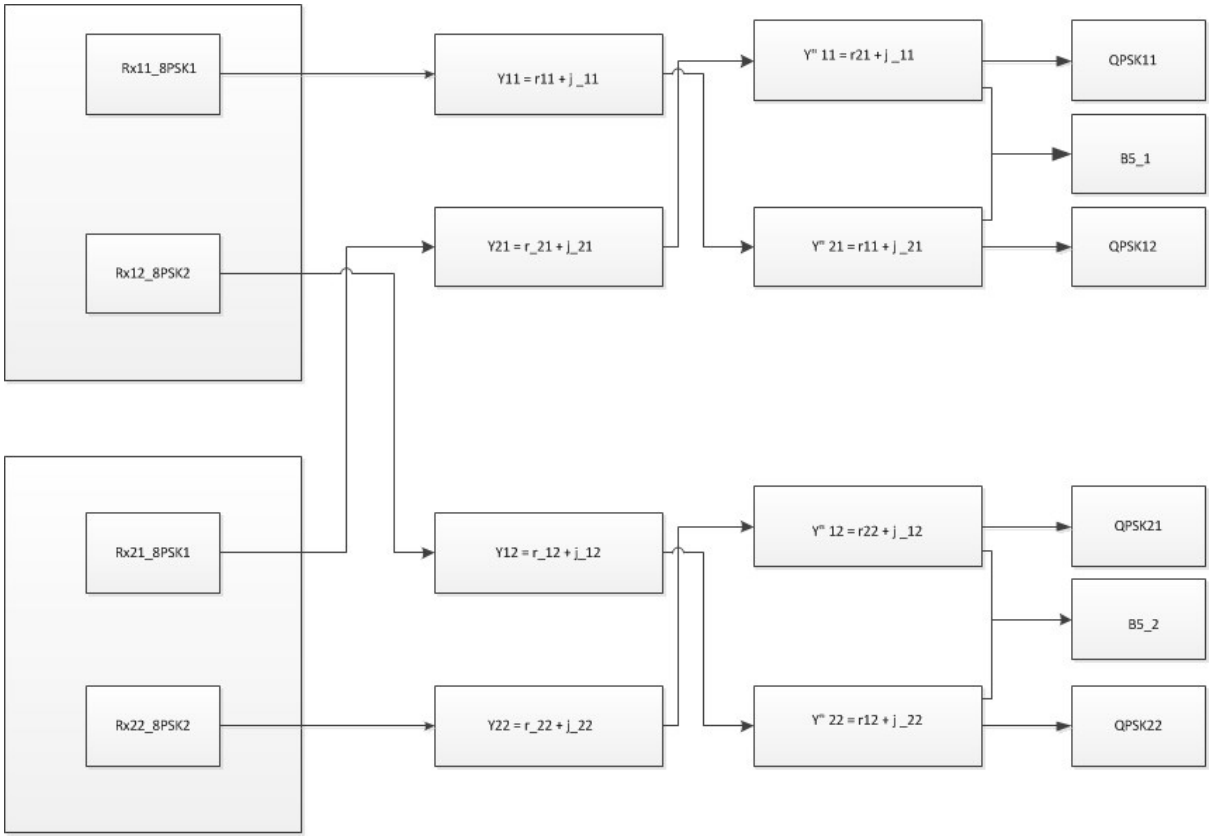

Figure (3.6): The design scheme of the dual receivers

3.3.3 Modification to the Receiving model Design

In wireless applications where the coverage area is a critical requirement, the model could be configured to full-fill this criteria. In wireless sensor networks, the wireless range demand plays a crucial component for system validation, and its eclipses the throughput requirement. In this context, the model could be configured to replace the multiplexing technique by a full use of diversity across the spatial and frequency domains. This modification allows for increase in the signal power without a violation to the FFC regulation, or an increase in the radiation power. The transmitting structure remains the same, but the receiving model would be readjusted by adding a combiner module to combine the received symbols from the dual receiving antennas. This increase in the coverage area comes at expense of the throughput, which gives an optimum performance for wireless range sensitivity systems. Figure (3.7) gives a block description of the receiving configuration. The rest of the de-mapping and decoding algorithm remains the same.

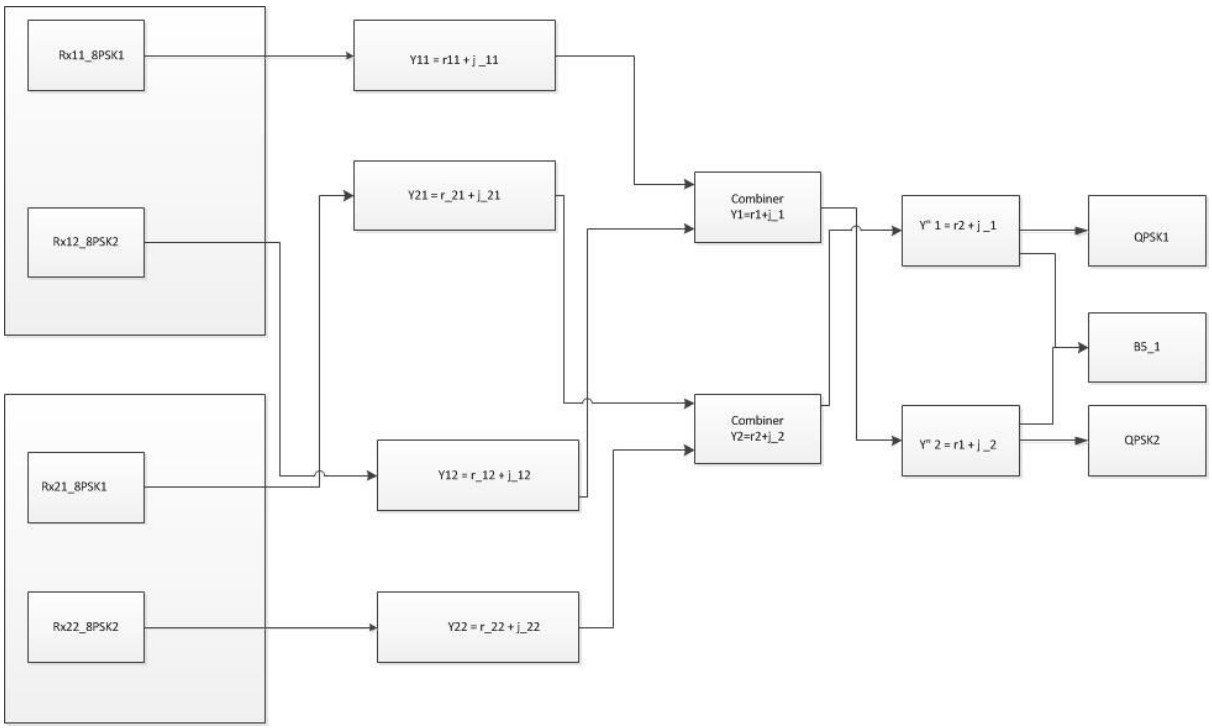

Figure (3.7): The design scheme for the modified dual receivers

3.4 Mathematical Analysis

One of the main aims in using MIMO system is to improve the data rate through the introduction of Spatial Multiplexing Gain (SMG). In this analysis, a numerical derivation of the error performance for the proposed model was presented. Analytical formulation was carried out to drive the performance of the scheme in the presence of noise and fading channel effects. The first section drives an average probability of error in multipath environment with direct and non-line of sight channel coefficients. In the second section, the distribution of the noise was used to measure the model performance and drive a mathematical expression for the error bound based on this observation. A numerical derivation of the Pair-wise Error Probability PEP was driven based on the probability density of the pairwise distance metric between symbol pair combination. This method enables to formulate an error measure metric that could be applied to different channel fading properties.

3.4.1 Analysis of Average Probability of Error

Although the coding and mapping of the symbols would affect the error detection in the receiving process, it adds further complexity to induce a close form analytical formula for the probability of error. This could be noticed if Gray coding for example had been considered, where the probability of detection decreases significantly when shifting away from neighbouring symbols in the constellation map. Therefore, assumption of equal symbol error condition in the constellation map would be observed here. The average error performance would dependent on the fading parameter in the SNR and governs its probability density$P_{ch}(ch)$. In this work, the Nakagmi-n model consisting of (γ, n, σ) as channel parameters, and with $P_{Nch}(\gamma; n, \sigma)$ as it its probability density function would be used to describes a scenario with a combination of line of sight and non-line of sight multipath fading components. Therefore, the average probability of error $P(E)$ could be redefind in the following form

$$P(E) = \int_0^{\infty} P_{e|H_i}\, P_{Nch}(\gamma; n, \sigma)\ d\gamma \qquad (3.4.1)$$

Considering the conditional error probability and with the conditional approximation formula would lead to

$$P_{e|H_i} = \frac{1}{\pi}\int_0^{\frac{\pi}{2}}\prod_{r=1}^{R} e^{-\left(\frac{\bar{\bar{\beta}}_r}{\sin^2\theta}\right)}\ d\theta \tag{3.4.2}$$

$$P(E) = \int_0^{\infty}\frac{1}{\pi}\int_0^{\frac{\pi}{2}}\prod_{r=1}^{R} e^{-\left(\frac{\bar{\bar{\beta}}_r}{\sin^2\theta}\right)}\ \frac{\gamma}{\sigma^2}\ e^{-\left(\frac{\gamma^2+n^2}{2\sigma^2}\right)}\ I_0\left(\frac{\gamma n}{\sigma^2}\right)\ d\gamma \tag{3.4.3}$$

Let the SNR $\bar{\bar{\beta}}_r$

$$\bar{\bar{\beta}}_r = \gamma$$

Introducing the MGF $f(b,\rho)$ would lead to the follwing

$$f(b,\rho) = \int_0^{\infty} P_\rho(\rho)e^{b\rho}\ d\rho \tag{3.4.4}$$

$$P(E) = \frac{1}{\pi}\int_0^{\frac{\pi}{2}}\prod_{r=1}^{R} f_{Rac}\left(-\left(\frac{k}{\sin^2\theta}\right),\bar{\bar{\beta}}_r\right)\ d\theta \tag{3.4.5}$$

$$f_{Rac}\left(-\left(\frac{k}{\sin^2\theta}\right),\bar{\bar{\beta}}_r\right) = \int_0^{\infty} P_{\bar{\bar{\beta}}_r}(\bar{\bar{\beta}}_r)e^{\frac{k}{\sin^2\theta}\bar{\bar{\beta}}_r}\ d\bar{\bar{\beta}}_r \tag{3.4.6}$$

$$f_{Rac}\left(-\frac{k}{2\sin^2\theta},\bar{\bar{\beta}}_r\right) = \frac{(1+n^2)\sin\theta^2}{(1+n^2)\sin\theta^2 + k\,\bar{\bar{\beta}}_r}\ e^{\left(-\frac{n^2 k\,\bar{\bar{\beta}}_r}{(1+n^2)2\sin^2\theta + k\,\bar{\bar{\beta}}_r}\right)} \tag{3.4.7}$$

$$P(E) = \frac{1}{4\pi} \int_0^{\frac{\pi}{2}} \prod_{r=1}^{R} \left(\frac{(1+n^2)\sin\theta^2}{(1+n^2)\sin\theta^2 + k\,\bar{\bar{\beta}}_r} \, e^{\left(-\frac{n^2 k\,\bar{\bar{\beta}}_r}{(1+n^2)2\sin^2\theta + k\,\bar{\bar{\beta}}_r} \right)} \right) d\theta \quad (3.4.8)$$

With a few assummptions

$$P(E) = \frac{1}{4\pi} \int_0^{\frac{\pi}{2}} \left(\frac{(1+n^2)\sin\theta^2}{(1+n^2)\sin\theta^2 + k\,\bar{\bar{\beta}}_r} \, e^{\left(-\frac{n^2 k\,\bar{\bar{\beta}}_r}{(1+n^2)2\sin^2\theta + k\,\bar{\bar{\beta}}_r} \right)} \right)^R d\theta \quad (3.4.9)$$

There are multiple symbols being transmitted simultaneously from multiple antennas in the presence of dual spatial and frequency diversities. In order to analyse the performance of MIMO system, vector notation would be introduce to obtain the transmission of multiple symbols across the radiating antennas. Each transmitted vector would belong to the sub-space set of message signals represented as follows

$$\boldsymbol{v}_i \in S \; where \; S = \{\boldsymbol{v}_1, \boldsymbol{v}_2 \ldots . \boldsymbol{v}_S\} \, , \boldsymbol{v} = \begin{bmatrix} s1 \\ \vdots \\ s4 \end{bmatrix}$$

Making use of the Upper bound condition, the code word error would be observed one the receivers detect erroneously a vector within the sub-set that differs from the original vector across all the symbols. Numerically, this could be projected for the MIMO Dual Carrier Modulation (DCM & 32-DC) as

$$\boldsymbol{v}_{SER} = SER(C1).SER(C2).SER(-C1^*).SER(-C2^*)$$

$$\boldsymbol{v}_{SER} = P_{S1}(C1).P_{S2}(C2).P_{S3}(-C1*)P_{S4}(-C2*)$$

$$\boldsymbol{v}_{SER} = \prod_{i=1}^{4} SER(S_i)$$

$$\boldsymbol{v}_{SER} = \left(\sum_{i=1}^{3} PEP_i(C1)\right).\left(\sum_{i=1}^{3} PEP_i(C2)\right).\left(\sum_{i=1}^{3} PEP_i(-C1^*)\right).\left(\sum_{i=1}^{3} PEP_i(-C2^*)\right) \quad (3.4.10)$$

Due to the symmetry between the quadrature components within the complex symbol, the calculation could be simplified when considering the dual bits symbol for either perpendicular phase components. Hence, considering the In-phase quadrature part would lead to the following

$$\boldsymbol{v^I}_{SER} = \left(\sum_{i=1}^{3} SER^I{}_i(C1)\right).\left(\sum_{i=1}^{3} SER^I{}_i(C2)\right).\left(\sum_{i=1}^{3} SER^I{}_i(-C1*)\right).\left(\sum_{i=1}^{3} SER^I{}_i(-C2*)\right) \quad (3.4.11)$$

$$\boldsymbol{v^I}_{SER} = \prod_{j=1}^{4}\left(\sum_{i=1}^{3} SER^I{}_i(C_j)\right)$$

$$P^I{}_{S|H}(C) = \sum_{i=1}^{3} SER^I{}_i(C) = Q\left(\sqrt{\frac{E}{No}\sum_{\substack{i=1 \\ i\neq k}}^{3}\left\|\mathrm{H}_i(\bar{\mathrm{S}}_i{}^t - \bar{\mathrm{S}}_k{}^t)\right\|^2}\right) \quad (3.4.12)$$

Let the symbol difference metric equal to $\beta^2{}_{ik}$ and the symbol difference by δ_i as follows

$$\delta_i = (\bar{S}_i^{\,t} - \bar{S}_k^{\,t})$$

$$\beta^2{}_{ik} = \left\| H_i(\bar{S}_i^{\,t} - \bar{S}_k^{\,t}) \right\|^2 = \|H_i\delta_i\|^2 = \|H_i\|^2\|\delta_i\|^2$$

Therefore,

$$P^I{}_{S|H}(C) = Q\left(\sqrt{\frac{E}{No}\sum_{i=1}^{3}\|H_i\|^2\|\delta_i\|^2}\right)$$

And the conditionl probablity could be expressed in terms of βas

$$P^I{}_{S|\beta}(C) = Q\left(\sqrt{\frac{E}{No}\sum_{\substack{i=1\\ i\neq k}}^{3}\beta^2{}_{ik}}\right) \tag{3.4.13}$$

$$P^I{}_{S|\beta}(C) = \frac{1}{\pi}\int_0^{\frac{\pi}{2}} e^{-\left(\frac{\sqrt{\frac{E}{No}\sum_{\substack{i=1\\ i\neq k}}^{3}\beta^2{}_{ik}}}{\sin^2\theta}\right)}\, d\theta \tag{3.4.14}$$

Expanding the above expression to represent the complex symbol with its quadrature components would lead to

$$P_{S|\beta^I,\beta^Q}(C)$$

$$= \frac{1}{4\pi}\int_0^{\frac{\pi}{2}} e^{-\left(\frac{\sqrt{\frac{E}{No}\left(\sum_{\substack{i=1\\ i\neq k}}^{3}\beta^{I2}{}_{ik}+\sum_{\substack{i=1\\ i\neq k}}^{3}\beta^{Q2}{}_{ik}\right)}}{\sin^2\theta}\right)}\, d\theta \tag{3.4.15}$$

In order to determine the overall probability of error, integration across the

distributions of SNR is required as the following.

$$P_S(E) = \int_0^{\infty} \int_0^{\infty} P_{S|\beta^I,\beta^Q}(C)\, P_{\beta^I}(\beta^I)\, P_{\beta^Q}(\beta^Q)\, d\beta^I\ d\beta^Q \qquad (3.4.16)$$

The squared magnitude of the channel $\|\mathrm{H}\|^2$ would determine the exhibited distribution of β^2, and hence the squred magnitude summation of independent ecludian metric resemples the distribution as the weights of its channel where

$$\|\mathrm{H}\|^2 = (|h_1|^2 + |h_2|^2 + \ldots. + |h_L|^2)$$

And $\|\mathrm{H}_i\|^2$ that was considered to be a CHI-SQUARED random variable with 2L degree of freedom. The density function of this distribution had been defined as

$$P_\beta(\beta) = \frac{1}{(L-1)!}\, \beta^{L-1}\, e^{-\beta} \qquad (3.4.17)$$

Let

$$\bar{\bar{\beta}}_z = \sqrt{\frac{E}{No}\left(\sum_{\substack{i=1 \\ i\neq k}}^{3} {\beta^z}^2_{ik}\right)}\ , and\ z = I, Q,\ k = \frac{2(M-1)}{3\log(M)}\ , M = 16\ ,32$$

Then, the average probability of error would be defined as

$$P_S(E) = \frac{1}{4\pi}\int_0^{\infty}\int_0^{\infty}\int_0^{\frac{\pi}{2}} e^{-\left(\frac{\bar{\bar{\beta}}_I+\bar{\bar{\beta}}_Q}{\sin^2\theta}\right)} \frac{1}{[(L-1)!]^2}\, \bar{\bar{\beta}}_I^{\,(L-1)}\, \bar{\bar{\beta}}_Q^{\,(L-1)} e^{-(\bar{\bar{\beta}}_I+\bar{\bar{\beta}}_Q)}\, d\theta\, d\bar{\bar{\beta}}_I d\bar{\bar{\beta}}_Q \quad (3.4.18)$$

Expand the expression and assuming independent symbol error across all the radiating elements would lead to

$$P(E) = \frac{1}{4\pi}\int_0^{\infty}\dots\int_0^{\infty}\int_0^{\frac{\pi}{2}} e^{-\sum_{r=1}^{R}\left(\frac{\bar{\bar{\beta}}_I+\bar{\bar{\beta}}_Q}{\sin^2\theta}\right)} \prod_{r=1}^{R}\left(P_r(\bar{\bar{\beta}}_{Ir}), P_r(\bar{\bar{\beta}}_{Qr})\right)\, d\bar{\bar{\beta}}_{I1}..d\bar{\bar{\beta}}_{IR,} d\bar{\bar{\beta}}_{Q1}\dots d\bar{\bar{\beta}}_{QR}\, d\theta \quad (3.4.19)$$

$$P(E) = \frac{1}{4\pi}\int_0^{\infty}\dots\int_0^{\infty}\int_0^{\frac{\pi}{2}} e^{-\sum_{r=1}^{R}\left(\frac{\bar{\bar{\beta}}_I+\bar{\bar{\beta}}_Q}{\sin^2\theta}\right)} \frac{1}{[(RL-1)!]^{2(RL)}}\, \bar{\bar{\beta}}_I^{\,R(L-1)}\, \bar{\bar{\beta}}_Q^{\,R(L-1)} e^{-R(\bar{\bar{\beta}}_I+\bar{\bar{\beta}}_Q)}\, d\theta\, d\bar{\bar{\beta}}_I d\bar{\bar{\beta}}_Q \quad (3.4.20)$$

3.4.2 Error performance measure based on the noise statistic

In order to validate a wireless model, it is importunate to envisage its response to different transmitted signals and this condition could not fulfilled by a deterministic wireless signal. Therefore its well-known to transmit stochastic signals for the analysis proposes. Based on this observation, the transmitted signal X was a random variable, and given that the channel H was assumed to be statistically distributed according to the specific environment, then the received signal Y would also be a random variable. The joint entropy H(X,Y) would be

$$H(X,Y) = \sum_x \sum_y P(x,y).\log\frac{1}{P(x,y)} \qquad (3.4.21)$$

$$= \sum_x \sum_y P(x,y).\log\frac{1}{P(x,y)}$$

$$= -\sum_x \sum_y P(x,y).\log P(x)$$

$$-\sum_x \sum_y P(x,y).\log(y|x)$$

$$= -\sum_x P(x).\log P(x) + H(Y|X)$$

$$= H(X) + H(Y|X) \qquad (3.4.22)$$

The mutual information I(X; Y) is

$$I(X;Y) = H(X) - H(X|Y) = H(Y) - H(Y|X)$$

And

$$f(y) = f(X;H) + f(N)$$

$$f(y) - f(X;H) = f(Y|X,H) = f(N)$$

Where f(Y), f(Y|X,H) and f(N) is the Probability Density Function (PDF) of the received signal vector, the conditional PDF of the received signal and the PDF of the noise respectively.

The conditional pdf of the received signal vector given the joint channel and the transmitted signal vectors would be as

$$f(Y|X,H) = f(N) = \prod_{t}^{T}\prod_{r}^{R}\frac{1}{\pi}\exp(-|N_t^r|^2)$$

$$= \frac{1}{\pi^{R\,T}}\exp\left(-\sum_{t}^{T}\sum_{r}^{R}|N_t^r|^2\right) \quad (3.4.23)$$

Where R are the number of receiving antennas, T the number of transmitting antennas

Hence,

$$f(Y|X,H) = \frac{1}{\pi^{RT}} \exp\left(-tr\left(N\,N^{H}\right)\right) \quad (3.4.24)$$

Maximising the above conditional PDF would result in the Maximum likelihood (ML) of C_{ML} (the transmitted code word), and reduces the error probability of the system as follow

$$C_{ML} = \arg\max_{x} f(Y|X,H)$$

$$C_{ML} = \arg\max_{x} \frac{1}{\pi^{RT}} \exp\left(-tr\left(\left(Y-\sqrt{\frac{E_x}{N_0N_t}}\,HX\right).\left(Y-\sqrt{\frac{E_x}{N_0N_t}}\,HX\right)^{H}\right)\right) \quad (3.4.25)$$

$$C_{ML} = \arg\min_{x} tr\left(\left(Y-\sqrt{\frac{E_x}{N_0N_t}}\,HX\right).\left(Y-\sqrt{\frac{E_x}{N_0N_t}}\,HX\right)^{H}\right) \quad (3.4.26)$$

The probability of symbol error would be obtained where difference metric of the predicted erroneous code word $\hat{S}$ would be higher than the metric of the transmitted code word X. In a mathematical form, the above observation could be expressed as follows

$$tr\,(N.N^H) = \; tr\left(\left(Y - \sqrt{\frac{E_x}{N_0N_t}}\,H\hat{S}\right).\left(Y - \sqrt{\frac{E_x}{N_0N_t}}\,H\hat{S}\right)^H\right)$$

$$\geq \; tr\left(\left(Y - \sqrt{\frac{E_x}{N_0N_t}}\,HX\right).\left(Y - \sqrt{\frac{E_x}{N_0N_t}}\,HX\right)^H\right) \qquad (3.4.27)$$

And the noise could be related to the probability of error and the Euclidean metric.

$$tr\,(N.N^H) \propto P(E) \propto \; tr\left(\left(Y - \sqrt{\frac{E_x}{N_0N_t}}\,H\hat{S}\right).\left(Y - \sqrt{\frac{E_x}{N_0N_t}}\,H\hat{S}\right)^H\right)$$

Since Y represents the correct received word, the expression could be combined as follows

$$tr\,(N.N^H) = tr\left(\left(\sqrt{\frac{E_x}{N_0N_t}}\;hx + N - \sqrt{\frac{E_x}{N_0N_t}}\,h\hat{S}\right).\left(\sqrt{\frac{E_x}{N_0N_t}}\;hx + N - \sqrt{\frac{E_x}{N_0N_t}}\,h\hat{S}\right)^H\right)$$

$$tr\,(N.N^H) = tr\left(\begin{array}{l}\left(\sqrt{\frac{E_x}{N_0 N_t}}\,\left(h\hat{S} - hx\right) + N\right) \\ .\left(\sqrt{\frac{E_x}{N_0 N_t}}\,\left(h\hat{S} - hx\,\right) + N\right)^H\end{array}\right) \quad (3.4.28)$$

3.4.3 Numerical Evaluation of PEP

As there were variable coding methods, the weights of error probabilities normally varies and tends to be effected by the particular coding scheme. In the case of Gray coding, the weight of error estimation decreases sharply as the distance between the received and the estimated symbol increases. This is because nearby symbols would have high probability errors, and to get one bit of error in each symbol would require small amount of energy. In order to get more bits within a specific symbol, then high energy would be required to a

achieve that. The high energy of errors would accommodate outer symbols in the decoding sphere on the scatter diagram. The energy of errors and the probability of errors have an inverse relationship when quantifying the decoding algorithm. In addition to this observation, the various modulation schemes spread the symbols on the constellation diagram with different energy separation. That is to say, for Quadrature amplitude type modulation, the energy between the symbols and the origin point on the constellation map had variables values. While, the Phase Shift keying method, have an equal energy values between the symbols and the origin of the scatter diagram. For a single symbol s transmitted from antenna t, the error would result in detecting one the M-1 neighbouring symbols (7 for 8-PSK) within the constellation. It could be noticed that the larger the sphere decoding the more neighbouring symbols to choose from, and therefore there were more erroneous symbols available for selection. This in turns increases the probability of error and reduces the system performance. On the other hand the small radius that could be envisaged in the second smaller sphere contained small number of erroneous symbols. That leads to a small percentage in the probability of error, which lead to a more optimised system with good error performance property. A point to mention here that, the term erroneous symbols was used to indicate the process of estimating wrongly transmitted symbols in a map with only correct symbol in a collection of noisy received symbols.

In the current proposal, a dual antennas configuration using Dual Carrier based on Circular and Quadrature modulation (in the form of 8-ary PSK

constellations) were used in the PEP derivation. The probability of error was derived based on Maximum Likelihood (ML) metric symbol estimation. Initially the symbols across the constellation had been assumed to have equally likelihood probability with maximum a posteriori (MAP) detection. Therefore, from a transmitting point of view and with blind prior knowledge of the user signal, it was reasonable to assume equate the symbol probabilities within the constellation. As the desired signal was a random variable based on a stochastic process, there should be an equal probability weights across all the signal points. Introducing the Union bound principle for this evaluation and having the number of points within a specific scatter diagram as M, and then the probability of error $P_s(E)$ for a single transmitted symbol would be

$$P_S\left(\bigcup_{s=1}^{S} P_s\right) \leq P_{s=s1}(E) + P_{s=s2}(E) \ldots\ldots + P_{s=S}(E)$$

$$P_S(E) \leq \sum_{s=1}^{S} P_s(E) \qquad (3.4.29)$$

As there were M number of symbols across a particular constellation map, and with equal transmitting probability, then the symbol error probability could be obtained based on the bound formulation as

$$P_S(E) \leq \frac{1}{M} \sum_{i=1}^{M} P_i(E) \qquad (3.4.30)$$

Having obtained M symbols for transmission, then by introducing pairwise symbol error which could interpreted by $P(s,e)$, then having send the symbol s as one of the signal within the M map, then an erroneous detection of symbol e as an element of this map would correspond to this pair error combination. The joint Probability of erroneous symbols would translated as

$$P_S(E) \leq \frac{1}{M}\sum_{s=1}^{M}\sum_{s\neq e} P(s,e) \qquad (3.4.31)$$

In the case of upper bound on the Probability error at the receiver, there would be M.M combination of pair error probability, therefore

$$P_S(E) \leq \frac{1}{M.M}\sum_{e=1}^{M}\sum_{\substack{s=1\\ s\neq e}}^{M} P(s,e) \qquad (3.4.32)$$

Having defined multiple symbols across the radiating element within a multiple spatial configuration, the error performance could be bounded for this multi-dimensional modulation. Expanding the above expression for the case of multiple antennas, then the probability of symbol error across all the radiating elements would be

$$P_S(E) \leq \frac{1}{T.M.M}\sum_{t=1}^{T}\sum_{e=1}^{M}\sum_{\substack{s=1\\ s\neq e}}^{M} P^t(s,e) \qquad (3.4.33)$$

In order to evaluate the proposed model in term of the pairwise error performance, it was critical to analysis the probability of error within the received signal. In the presence of channel Information CI metric (it is variable entity which could exhibits distortions due to noisy coefficients) that determine the equalisation process at the receiver, and given a well-known prior knowledge of the state channel, the receiving signals would be processed. This could be done by investigating the statistical behaviour of the received signal components. As it was more involve getting a close form equation for the error measures, a practical approximation was needed to induce a systematic pairwise error probability formula. Hence, an error bound had been introduce by assuming that all the receiving symbols vectors were in an error, and all the symbols were independent from each other. This assumption was a realistic measure as the transmitted signal and the noise both of which were independent and identically distributed entities. This leads to the following PEP formula

$$P(E) = \prod_{p=1}^{A1,A2} \prod_{n=1}^{N} \prod_{s=1}^{M} P_{n,s}^{p}(E) \qquad (3.4.34)$$

Introducing the upper bound principle in order to evaluate the PEP for the system model would give a maximisation limit for the error performance. Therefore, the upper bound pairwise error probability across all the symbols within the MIMO configuration could be defined in terms of the Euclidean energy metric $D(s,e)$between the transmitted s and the erroonus detected e symbols as

$$P(E) \leq \prod_{p=1}^{A1,A2} \prod_{n=1}^{N} \prod_{s=1}^{M} \exp - \left(D_{s,n}^{p}(s,e) \right) \qquad (3.4.35)$$

In the case of erroneous detection of all the N symbols that spans the OFDM block across the pairwise construction within the T and R antennas, would define the PEP metric within the following condition

$$D(s,e) = \sum_{r=1}^{R} \sum_{n=1}^{N} \left\| \sum_{t=1}^{T} h_{t,n}^{r} \Delta_{n}^{r}(s,e) \right\|_{F}$$

$$D(s,e) = \sum_{r=1}^{R} \sum_{n=1}^{N} \left(\sum_{t_2=1}^{T} \left(h_{r,n}^{t_2} \Delta_{n}^{t_2}(s,e) \right)^{\dagger} \sum_{t_1=1}^{T} h_{r,n}^{t_1} \Delta_{n}^{t_1}(s,e) \right) \qquad (3.4.36)$$

Where $\Delta \equiv$ *the error magnitude metric between c &e*

Assumming that the channel fading remain constant over the N symbols that spanning an OFDM block. Then, the formula could be readjusted as

$$D(s,e) = \sum_{r=1}^{R} \sum_{t_2=1}^{T} \left(\sum_{t_1=1}^{T} \left(h_{r}^{t_2} \right)^{\dagger} h_{r}^{t_1} \sum_{n=1}^{N} \left(\Delta_{n}^{t_2}(s,e) \right)^{H} \Delta_{n}^{t_1}(s,e) \right)$$

$$D(s,e) = \sum_{r=1}^{R} \sum_{t_2=1}^{T} \sum_{t_1=1}^{T} \left(h_{r}^{t_2} \right)^{\dagger} h_{r}^{t_1} \sum_{n=1}^{N} \left(\Delta_{n}^{t_2}(s,e) \right)^{H} d_{n}^{t_1}(s,e) \qquad (3.4.37)$$

Manipulating the channel fading coefficients within the summations would reproduce the following term

$$H_r \;=\; \sum_{t_2=1}^{T} h_{t_2}^{q}$$

Considering the pairwise distance energy between the transmitted symbol and the erroneous estimated symbols which represented the second term in the exponential part of $D(s,e)$ in a matrix form (K) that consisting of all the pair combinations that maximises the error qunity. Then, a single row matrix would be defined as

$$K^{t_2,t_1} \;=\; \sum_{n=1}^{N} \left(\Delta_n^{t_2}(s,e)\right)^{\dagger} \;\Delta_n^{t_1}(s,e)$$

Since the power of the pairwise distance forms a nonnegative definite matrix and the components were independent and identically distributed**,** then the square matrix K that contained the pair distances of symbols across all the radiating elements would exhibit a Harmitian property and the square root of this matrix could be expressed as

$$K^{1/2} \;=\; \begin{bmatrix} \Delta_1^1 & \Delta_2^1 & \dots & \Delta_N^1 \\ \Delta_1^2 & \Delta_2^2 & \dots & \Delta_N^2 \\ \vdots & \vdots & \ddots & \vdots \\ \Delta_1^T & \Delta_2^2 & \dots & \Delta_N^T \end{bmatrix} \qquad (3.4.38)$$

Applying matrix decomposition on the matrix K, then a formation of unitary matrices A and its conjugate such that multiplication by its conjugate results in an identity matrix (AA*=I) contained on its columns the eigenvectors of the symbol pairs difference matrix, and a diagonal matrix Σ would be induced to describe the original complex entity matrix. The power of the matrix K was governed by the non-negative diagonal matrix Σ containing its eginvlues $\lambda_t, \{t = 1, \dots T\}$ on its diagonal positions. This operation transfer the pair-wise combination into the following form

$$K = A^{\dagger} \Sigma A \quad , and \quad \Sigma = \sum_{t=1}^{T} \lambda_t$$

Therefore, D(s,e) was redefined as

$$D(s,e) = \sum_{r=1}^{R} (H_r)^{\dagger} K H_r = \sum_{r=1}^{R} (H_r)^{\dagger} A^{\dagger} \Sigma A H_r \qquad (3.4.39)$$

The fading coefficeints h was a random variable that been governed by the statiscal property of the the medium in which the wireless system operates. An imporatant observation to mention was that, the stochatical behaviour of the random variable parameter encapsulate the probablity density of any other term was multiplied with it (ie: H* A). Thefore, introducing another paramter ϕ that reprents the multiplication of the unitry matrix A with the channel coefficients.

$$\phi = H A$$

Therefore, the channel fading effect embadded in the eculdian metric would translate this experssion to the following

$$D(s,e) = \sum_{r=1}^{R} \phi_r^{\dagger} \Sigma \phi_r$$

$$D(s,e) = \sum_{r=1}^{R}\sum_{t=1}^{T} \lambda_t \ |\phi_r^t|^2 \qquad (3.4.40)$$

Due to the presence of the Gaussian distribution, the conditional error probability of the receiving symbol vector in the proposed dual antenna configuration could be expressed in terms of the derived Euclidean matrix with the following formula

$$P(E|H) = Q\left(\sqrt{\frac{E_x}{2N_0N_t}}\frac{\|D(s,e)\|_F^{\ 2}}{4}\right)$$

$$P(E|H) = Q\left(\varphi \sum_{r=1}^{R}\sum_{t_2=1}^{T}\sum_{t_1=1}^{T} \left(h_r^{t_2}\right)^{\dagger} h_r^{t_1} \ A^{t_2,t_1} \Sigma \left(A^{t_2,t_1}\right)^{\dagger}\right) \qquad (3.4.41)$$

Where $\varphi = \sqrt{\frac{E_x}{8N_0N_t}}$

Applying the Chernoff bound on the q-function, and then this experssion could refomulated by expanding the upper bound in terms of pair-wise error probability across the symbols with thir corresponding antennas in this bounded form. Therefore in the presence of multiple antennas and DC symbols configuration, the conditional error probability formula could be upper bounded as

$$P(E|H) \leq \frac{1}{2} \exp\left(-\varphi \sum_{r=1}^{R}\sum_{t_2=1}^{T}\sum_{t_1=1}^{T}\left(h_r^{t_2}\right)^{\dagger} h_r^{t_1} \quad A^{t_2,t_1}\,\Sigma\,(A^{t_2,t_1})^{\dagger}\right) \qquad (3.4.42)$$

The channel statistics would govern the power term and affect the error performance in the particular environment. The derived formula would be altered depends on the channel fading, and therefore could be applied to various channel conditions. Rayleigh channel had been used in the numerical evaluation for two important reasons; one is the ability to measure the metric performance including the error rate, the diversity effect, and throughput of the proposed models. These measures allow for a clear distinction between the various wireless models in the simulation environments. The second reason comes from practical challenges, and that to do with the difficulty in getting a close form mathematical expression for this multiple antennas model. In applying this Rayleigh model, there is only one exponential term in its

probability density function and that reduces the complexity burden of the software and hardware running environment. As the effect of channel remain constant when the same channel fading was used across wireless systems, then an accurate comparison had been performed between this proposed model with pervious proposed wireless model. Including the channel distribution within the error formula and taking the average probability to remove the uncertainty introduced by the random variable within the expression would translate the derived conditional equation to the following

$$P(E) \leq \int_{0}^{\infty} P(E|H) \quad P(H)$$

$$P(E) \leq \int_{0}^{\infty} |\mathrm{H}| \exp\left(\varphi \sum_{r=1}^{R} \sum_{t_2=1}^{T} \sum_{t_1=1}^{T} \left(h_r^{t_2}\right)^H h_r^{t_1} \quad A^{t_2,t_1} \Sigma \left(A^{t_2,t_1}\right)^* \right) \exp(-|H|^2) \; dH \quad (3.4.43)$$

Where the pdf of the channel was

$$P(H) = 2 \; |H| \; e^{(-|H|^2)}$$

$$P(E) \leq \int_{0}^{\infty} |\mathrm{H}| \; \exp\left(\varphi \sum_{r=1}^{R} \sum_{t=1}^{T} \lambda_t \;\; \phi_t^r \right) \exp(-|H|^2) \;\; dH \qquad (3.4.44)$$

$$P(E) \leq \int_{t=1}^{T} |\mathrm{H}| \prod_{r=1}^{R} \prod_{t=1}^{T} \exp(\varphi \ \lambda_t \ \phi_t^r) \ \exp(-|H|^2) \quad dH \quad (3.4.45)$$

$$P(E) \leq \int_{t=1}^{T} |\mathrm{H}| \prod_{r=1}^{R} \prod_{t=1}^{T} \exp\left(-\sqrt{\frac{E_x}{2N_0N_t}}\lambda_t \ \phi_t^r - |H|^2\right) \quad dH \quad (3.4.46)$$

$$P(E) \leq \int_{0}^{\infty} |\mathrm{H}| \prod_{r=1}^{R} \prod_{t=1}^{T} \exp -\left(\sqrt{\frac{E_x}{2N_0N_t}}\lambda_t \ \phi_t^r + 1\right)|H|^2 \quad dH \quad (3.4.47)$$

Lets

$$\left(\sqrt{\frac{E_x}{2N_0N_t}}\lambda_t \ \phi_t^r + 1\right) = \Psi$$

$$P(E) \leq \int_{0}^{\infty} |\mathrm{H}| \prod_{r=1}^{R} \prod_{t=1}^{T} \exp -(\Psi)\,|H|^2 \quad dH \quad (3.4.48)$$

Introducing the following Laplace transform expression into the above equation would lead to the next expression for the average error

$$\int_0^{\infty} exp^{-sy}\ dy = \frac{1}{s} \quad , s > 0$$

$$P(E) = \prod_{r=1}^{R}\prod_{t=1}^{T} \frac{1}{\Psi} = \prod_{r=1}^{R}\prod_{t=1}^{T} \frac{1}{\left(\sqrt{\frac{E_x}{2N_0N_t}}\lambda_t\ \phi_t^r + 1\right)} \qquad (3.4.49)$$

3.5 Concluding Remarks

In this chapter, the design steps taken to produce this novel model was explained and described in details. A flowchart to the design plan was given with an overview description the scheme was highlighted. The transmitting and receiving models for the design were reviewed, explained, prepared and issued. A configuration to the receivers was shown that allows the model to increase the coverage at the expense of the through put for wireless range demand applications. A mathematical analysis of the proposed model was then developed in terms of the error performance. The next chapter would cover the implementation of this design, and gives the instructions required to execute the various algorithms across the design flowchart. The implementation of OFDM with MIMO within UWB wireless system would be performed and analysed. The finalisation of the channel model that simulated the rich multipath environment would be covered.

4. Implementation

4.1 Introduction

In this chapter, the implementation of the design had been considered along with an explanation to the concept formulation. This implementation was carried out in the simulation environment based on Matlab software package. The physical layer setting was conducted and conformed based on the ECMA-368 standard. The chapter was divided into sections, where the second section considered the construction of the transmitters. This included the coding and modulation for the desired signals. The next section had considered the model channel that was used to infer the indoor distortion that attach with wireless signals in this close environment. The receiver's implementation was followed with explanation to the integration of the proposed model on the wireless receiving structure, and the test bed requirements for the simulation. A proposal to optimise decode method was explained that further enhance the system performance in the next section. Concluding remarks is then summarised this chapter.

4.2 Implementation on transmitters

In this proposal, modulation was carried out across two antennas with two frames containing 1500 coded and interleaved bits each. In the presence of frequency diversity, these frames were divided into six blocks at every branch spreading across the dual radiating elements. In this scheme, spatial diversity was used to further enhance the system performance and reduces the effect of fading. The implementation of the scheme was based on parallel formulation, so as to ensure backward compatibility, and reduces the cost and complexity of high speed hardware clocks at a slight expense of the extra RF modules. In every branch, a block of 250 codded and interleaved signal bits were divided into 50 groups, and every group contains 5 bits. The spreading of every group exhibit multiplexing and diversity properties in sub-optimum manner, and hence the dual 8-ary PSK symbols on every radiating elements forms two separate OFDM frames separated by 50 MHz spectrum, and spatial separation that adds another degree of freedom. The 100 signal subcarriers were used to modulate an equal number of 8PSK symbols, and hence there were a

distinction between the DCM modulation where the dual OFDM symbol frames within a branch carry exactly the same signal information, in this scheme the frames were independent and carried different parts of the bit's group information. Therefore, the formation of the frames project signals multiplexing. Encoding was added to the standard in order to limit the signal errors at receivers. Convolutional coding with 7 registers, 2 inputs, and 3 outputs was implemented. As the coding rate could be varied by the use of dummy zeroes as part of the puncturing process, the defined rate had been achieved by the use of this method. The puncturing pattern [1 1 1 0 0 1] was used to retransform the original encoder rate to the specified rate for this model. The generated data was then passed to a convolutional encoder of a rate ¾, with a constraint length of 7 coming from the memory registers (with each memory holding 1 bit used to perform the convolutional algorithm). A data generation file was created to produce three vectors of bits sequence with length 450, 450, and 225 bits. These bits were then passed to half rate convolutional encoder resulted in producing new vectors with length 900, 900, and 450 bits. These vectors were then passed to the above puncturing process resulting in the required vectors with 600, 600, and 300 sequence bits. Modulo-2 adders with the corresponding polynomial generators were used to produce the output encoded information data. These generated codes had been projected based on specified trellis structure. The trellis structure represents an important parameter in the optimisation of coding and therefore this structure had to be specified in a predefined format. The predefined standard Matlab library function Poly2trellis had been used to define the trellis structure based on this model design, and therefore its entries had to be adjusted for this

proposal. The encoded information data were then passed to an interleaving procedure, as to strength the robustness against deep fade distortion.

4.3 Modulation of symbols

The incoming bits streams were mapped into modulated symbols, and that involved a number of processes in the implementation phase. The serial data stream was converted into truncated vectors of parallel sequences of equal size, and then passed to a Fourier transform functions for time domain translation. The interleaved signal information bits were initially segmented into super frames, and there were F number of frames. The frame contained D data symbols, and this sequence was encoded into a codeword matrix by dividing it into B OFDM blocks and every block has a length of K subcarriers. Then, these blocks were mapped across the A transmitting elements forming a matrix of BK x A.

$$\mathrm{M} = [M_0^0 \quad M_1^1 \quad \ldots\ldots\ldots M_{B-1}^{F-1}] \qquad (4.3.1)$$

$$\mathrm{M} = [M_0 \quad M_1 \quad \ldots \quad M_{F-1}] \qquad (4.3.2)$$

In which the matrix related to a block b within frame f was then defined as

$$M_f^b = \begin{bmatrix} s_1^b(0) & s_1^b(1) & \cdots & s_1^b(K-1) \\ s_2^b(0) & s_2^b(1) & \cdots & s_2^b(K-1) \\ \vdots & \vdots & \ddots & \vdots \\ s_A^b(0) & s_A^b(1) & \cdots & s_A^b(K-1) \end{bmatrix} \qquad (4.3.3)$$

Every radiating element had been divided into two branches, and every branch had a number of B OFDM blocks of signal sequence to be transmitted. Then for the i[th] branch, $\boldsymbol{s}_i^1 \quad \boldsymbol{s}_i^2 \quad \ldots\ldots\ldots \boldsymbol{s}_i^B$ was sent serially in OFDM blocks 1, 2… B, as part of the encoding scheme across all the antennas, and where $\boldsymbol{s}_i^j$ represents a vector of length K. The coded blocks had been forwarded to the IFFT where inverse frequency transformation was performed. In this design, there were four radiated symbols, and hence there were four parallel signals transmitted at the same time. In every symbol vector within a transmitting branch, K-point IFFT was applied for the transformation. Therefore for the first branch, the dual OFDM symbol vectors were

$$\boldsymbol{S}_b^{Tx1} = \quad [\boldsymbol{v}_b^1 \quad \boldsymbol{v}_b^2\ ]^T$$

$$\boldsymbol{S}_b^{Tx1} = \begin{bmatrix} s_b^1(0) & s_b^1(1) & \dots & s_b^1(K-1) \\ s_b^2(0) & s_b^2(1) & \dots & s_b^2(K-1) \end{bmatrix} \qquad (4.3.4)$$

For the second branch,

$$\boldsymbol{S}_b^{Tx2} = \quad [\boldsymbol{v}_b^3 \;\; \boldsymbol{v}_b^4\,]^T$$

$$\boldsymbol{S}_b^{Tx2} = \begin{bmatrix} s_b^3(0) & s_b^3(1) & \dots & s_b^3(K-1) \\ s_b^4(0) & s_b^4(1) & \dots & s_b^4(K-1) \end{bmatrix} \qquad (4.3.5)$$

The space frequency coding that had been proposed in the implementation scheme for this configuration was described in the figure (1). At the t instant of time, the fours 8-ary PSK symbols $s_b^1(t)$, $s_b^3(t)$), ($s_b^2(t)$, $s_b^4(t)$) was assigned to the f(k), and f(k+50) subcarriers within the b block across both transmitting antennas.

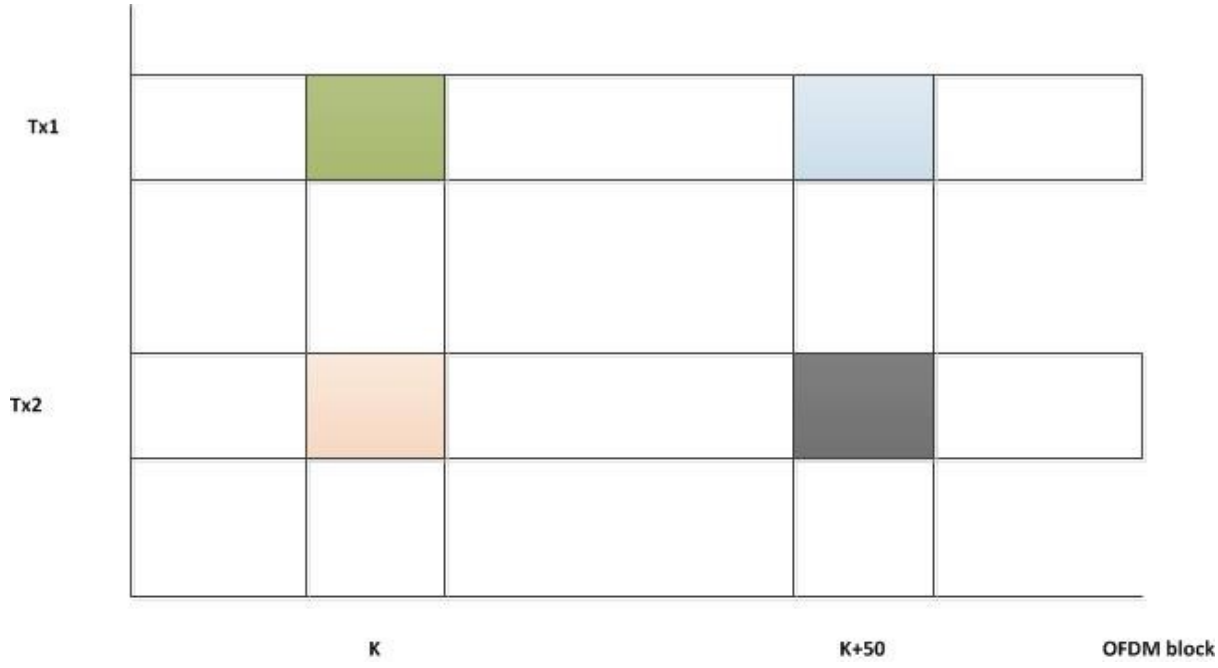

Figure (4.1): Space Frequency division within an OFDM block

The transmitted signal frame for a transmitting branch across an antenna within the b OFDM block was represented as follows

$$x_b^a(t) = \sqrt{\frac{E_x}{A}} \sum_{k=0}^{K-1} s_b^a(k)\ \mathrm{e}^{\mathrm{i}2\pi \mathrm{f}_k(\mathrm{t}-T_{sym})} \qquad (4.3.6)$$

Where T_{sym} was the duration of the OFDM symbol ($T_{sym}=KT_s$), T_s was the time duration for a subcarrier symbol, $\sqrt{\frac{E_x}{A}}$ was a normalisation factor for the average transmitted energy across the antennas.

The information stream across the multiple transmitting branches was modulated across orthogonal sub-band channels forming the frequency data

subcarriers of the OFDM symbols. The samples data was developed in the frequency domain, and therefore the signal spectrum had to be transformed to the time domain through the inverse frequency transform using IFFT. OFDM process is easily implemented in the digital domain. OFDM was bandwidth efficient since the spectrum was divided into narrow bands for transmitting more information data. In addition, it overcomes fading selectivity by the formation of these narrow band channels. Guard intervals within OFDM make it more robust to the effect of ISI, and this parallel formation of sub-channels makes it less susceptible to impulse noise. Furthermore, when using parallel transmission as a pose to serial counterpart, that makes this scheme more dynamics in terms of resource allocation, and hence the data rate could be varied by transmitting at different sub-channels with variable fading. In the second stage of modulation, the transmitted signal was shifted up in the frequency domain to the carrier spectrum by filtering and up-conversion. The OFDM carrier frequencies consist of orthogonal functions, each of which was used to carry a complex symbol representing an information signal. OFDM overlaps the subcarriers and that make use of the available spectrum in an efficient way. It could be noted that the transmitted formula for the symbol have two parts, one is the information part and the second represents the carrier function. This process results in a new pass-band signal as follows

$$x_b^a(t) = \sum_{k=0}^{K-1} Re(x_b^a(t))\ \mathrm{e}^{\mathrm{i}2\pi \mathrm{f}_k(\mathrm{t}-T_{sym})} \qquad (4.3.7)$$

4.4 IFFT OFDM implementation on the MIMO configuration

In the implementation scheme, there were dual transmitting and receiving antennas, with an OFDM modulation that consists of 128 subcarriers in which 100 tonnes (Ds) were used to carry the information signals. These modulation carries was designed and arranged to accommodate the serial to parallel (S/P) converted and encoded message samples. It was useful to note that, ifft function folds the signal across the origin, and hence shifting the signals before the Fourier transformation was necessary. Therefore, the samples were readjusted in a developed function (SigShift) that fold these signals and add

redundancy guards (ngs, nps) in each block of 128 processed samples. This result in signals vectors that were divided into two sections consisting of fifty data carries on both halves of the spectrum before applying the inverse function. The upper section of samples were swapped and shifted into the first spectrum location, and the lower part were placed in the upper spectrum location, while the middle frequency space was allocated to a sixteen zero frequency samples. This formation ensures that the ODFM vector spectrum centred at the zero frequency and runs form –N/2 to N/2 period. Therefore, the symmetry of the vector had been changed by making the positive and negative frequencies symmetric around the zero frequency point. Table 1 gives a description of the parameters used in the transformation.

Parameters	Description	Values
nps	Number of pilot subcarriers	12
ngs	Number of guard subcarriers	10
N	Total number of IFFT tones	128
Ds	Number of Data subcarriers	100

Table (4.1): Frequency transformation parameters

The duration of an individual IFFT block was defined as 242.42ns (nanosecond), which represents the frame of subcarriers periodT_{fs}. In addition,

these orthogonal IFFT signals have f_n a sub-frequency spacing of 4,125MHz between carries as defined in the ECMA standard. The sampling frequency for every IFFT tone contained in the function $\phi(t)$ (this function relate to a particular subcarrier within the OFDM symbol, and there were 128 functions within this symbol) runs at 528 MHz (fs), and the function could be illustrated as follows

$$\phi(t) = \begin{cases} \sum_{n=-\frac{128}{2}}^{\frac{128}{2}-1} e^{i2\pi f_n(t-T_{sym})}, 0 < t \leq T_{fs} \\ 0\ , \qquad else\ where \end{cases} \qquad (4.4.1)$$

The symbol duration includes the frame subcarriers of length of 242.42 ns, and the zero-padded subcarriers of 70.08 ns time laps (GI duration), totalling 312.5 ns, and this period duration would define the parallel transmission of the signal information. A point to mention in OFDM modulation was the reduction in receiver complexity attached with this multiple spatial configuration, and this manifest it's self in the orthognality condition which ensure any two pins with the Fourier function $\phi(t)$ satisfy the condition, and therefore ensure simple cross-correlation receiving process.

$$\sum_{t=-\frac{N}{2}}^{\frac{N}{2}-1} e^{i2\pi p\frac{t}{N}} * e^{i2\pi q\frac{t}{N}} = 0, \forall p \neq q \qquad (4.4.2)$$

Although the discrete signal x(n) was spread across the IFFT branches, it's a part of a transmission frame and clearly represents N-point discrete Fourier transform of symbol data. Once the data and redundancy subcarriers had been added to the symbol vector, then the b^{th} OFDM symbol of the i^{st} branch of length K was summarised as follows

$$s_b^i(n) = \frac{1}{\sqrt{128}} \left(\sum_{c=0}^{99} A(c)\, e^{i2\pi U_d(c)\frac{n}{128}} + R \right) \qquad (4.2.3)$$

Where R was defined as

$$R = \sum_{c=0}^{9} G(c)\, e^{i2\pi U_g(c)\frac{n}{128}} + \sum_{c=0}^{11} P(c)\, e^{i2\pi U_p(c)\frac{n}{128}}$$

Where $A(c)$, $G(c)$, *and* $P(c)$ *were the Actual information subcarries, the Guard subcarries, and the Pilot subcarries respectively.* U_d, U_g, *and* U_p *were the functions that maps the indices [0-99],[0-9], and [0-11] to the logical frequency subcarriers.*

Additional Guard interval was applied to mitigate the ISI, and used to compensate for the jitters in the transmission channel. The variation in the delay of the received OFDM symbols requires this GI to overcome this jittering effect. The final implementation stage within the transmitting block was extending the length of the OFDM symbols (extending the time duration) within every frame across all the four parallel transmitting frames (Nsm). This was done by inserting an additional 37 zeroes guard samples (Zp). In

completion of this process, the signals were then transmitted across the wireless channel and every symbol having a rate of (Fsm). The transmitting parameters were summarised in table 2 below.

Description	Value
Coding rate	3/4
Puncturing pattern	[1 1 1 0 0 1]
T_{sym} Symbol duration	312.5 ns
IFFT OFDM period (T_{fs})	242.42 ns
GI duration	70.08 ns
fs sampling frequency	528 HMz
f_n subcarrier frequency spacing	4,125MHz
Nsm Total number samples within a symbol	165
Fsm The symbol rate	3,2 MHz
Zp the number of samples in Zero-padding	37

Table (4.2): Transmitting parameters

4.5 The implemented Channel model

In this implementation, different hypothesis were considered to test the fitness of the proposed multi-antennas wireless model. In order to propose a wireless model, it was necessary to define and implement a channel model that emulates the specific environment in which this designed concept operate on. The choice of the channel model in this design was very important to ensure a reliable simulation that was based on a recognised and verified UWB channel model. Specific scenarios were covered to ensure the practical feasibility of the design. Additional verifications were used to test the proposed design. A standardised channel model was used to infer the performance merits of the system. The model has been used to simulate the physical channel effects on the wireless signal. In this section, the channel model was implemented to satisfy the indoor medium characteristics. Previous measurements had shown that Indoor Ultra wide band channel impulse response behaves in clustering manners. The observation had shown that log normal distribution fits the measurement data for the UWB channel amplitudes. Furthermore, the phase components of the impulse response were considered to be redundant as they were rotated within the absolute of 90 degrees.

In order to validate any work, it had to be subjected to a well-known and verified standard model. As result, the proposed DC-32QAM had been subjected to the IEEE803.15.3a model for validation and verification. . Modelling channel behaviour in the time domain deals with continuous time events. As it was the case, these continuous time events needed to be discretise in the simulation process, and therefore it was imperative to define this discretisation stage where the UWB transmission have high temporal resolution. One of the challenges in a simulation work was how to validate a particular novel design while clarifying very clearly the very distinct contributions in simulation environment. To this end, the well approved standardised channel model was used in the verification, and then modified based on a proposal concept. In the development stage, the simulation was carried out using the first two propagation scenarios of the model, namely line of sight and non-line of sight for short ranges (ch1, ch2). It had been useful to consider the transmitted signals as a time limited event and the channel response as multipath cloud with various power coefficients spanning different time resolution. These events needed to be transferred from its continuous time domain to the discrete version for the modelling purposes. The specified channel uses very small sampling times for the discretisation process of the UWB continuous channel, in order to convert it to discrete sample model. Furthermore, Nyquist theorem states that for a successful sampling operation, the sampling frequency has to be twice the largest frequency in the signal, and hence to capture of the spectrum content within the targeted signal, the sampling frequency should be chosen to be much greater than the maximum frequency. This in turn reduces the sampling resolution window and increases

the number of samples. Taking these notes into account, adjustment for the IEEE model was needed to absorb the requirements of this work. This was reflected in the reduction of the simulation time and a reduction in complexity of the algorithm by focusing on the behaviour of a limited number of multipath channel coefficients without losing the bulk of the spectrum content. The amplitudes of the multipath fading in the SG3a UWB model reflect the signal distribution at the receivers, resulting from the filtering effect by the channel. The characteristic of the received signal cloud was obtained by actual measurements and stochastic analysis for the indoor environment in the standard. This standardised model uses a sampling period of 0.167 ns (nanosecond) for the discretisation process of the UWB channel response, translating this continuous response into discrete samples model. It was important to keep the channel characteristic of the model the same by keeping all the main channel parameters to its original values. The cluster arrival rate, ray arrival rate, cluster attenuation constant, ray attenuation constant, The overall standard deviation of the multipath shadowing with a lognormal distribution, standard deviation of lognormal shadowing for the clusters, standard deviation of lognormal shadowing for the rays within a particular cluster, the mean excess delay, the number of significant paths within 10dB of peak power (NP_10dB), the Power Delay Profile (PDP), and the RMS delay spread should all be consistent with the standard requirements.

The specified model produces impulse response consisting of 100 channel

realisations, each of which had a multipath cloud containing over 600 paths. The first step here was to average these multipath channels across each time pin to form an average channel, that encapsulate the medium behaviour. As this was time varying channel, this averaging gave more accurate response than a single channel response representation. Noting that, the UWB channel response of the standard was discretised version with equal time pins across the entire channel, and hence averaging will not change the time index. In the discretisation stage, a search for the maximum delayed coefficient (ch(t_max)) was firstly obtained. It was noted that different scatters and indoor structures resulted in various time delay pins, and hence a number of significant pins was identified by combination of measurements and stochastic process. This ensures that all other weights occurred within this time window, as these events were not periodic and have specified time resolution. Next, a sampling time (ts) was chosen which facilitate capturing the core content of the multipath amplitudes. The sampling time was very critical for indoor wireless transmission due to the unlimited bandwidth, resulted from the randomness property of the arrival times. This governs the signal wave's propagation and results in high resolution signals. From simulation analysis, it was found that the sampling time for these models should be at least smaller than four times the significant path that represented the smallest time duration. In addition, finding suitable sampling window would depends on the user requirements as well as the software and hardware limitations, but the smaller the value, the more accurate the signalling process analysis. To illustrate this operation, consider h1 (the first channel coefficient) with a maximum time delay tm, then the sampling time (ts) was chosen much smaller that tm by at least half of its

value (Figure 4.2). Then, in order to discretise h1, the length of h1 was expanded in the discrete domain based on the following syntax

h1 = 1+ floor (tm / ts)

h1 samples at k times its frequency f(h1) ==> fs = k*f(h1) , so N = k

ch = 100 (there were 100 channels),

np = NP (for each ch there were a number of multipath NP)

To discretise path(n)_time_cont , then

Ch=n , np(ch=n)= NP paths , path(n)_time_cont = L ns (L nano-seconds)

Now, storing these discrete time indices in an array(t_Nfs) as

t_Nfs = 1 + floor (Path_time_discrete)

The above expression, could expanded to store all the discrete samples corresponds to all continuous time array (path(1:end)_time_cont) as follows

t_Nfs = 1 + floor(path(1:end)_time_cont / ts)

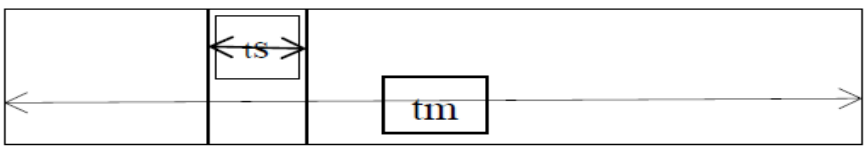

Figure (4.2): Time window for discretisation

A vector of equally space discrete samples with a maximum length corresponding to the largest path delay was then created to allocate all the time pins within the temporal cloud. Then, each continuous time instance of a significant path had a corresponding discrete sampling value within this vector encapsulating its duration in the discrete domain. An array of channel amplitudes with the same time vector length was then created and populated with weights corresponding to these time pins. Thus, the largest delay path had its amplitude allocated at the last index in the array and hence preserving the distribution of the impulse response. These large spectrum content UWB channel response was passed through filtering operation in order to down sample it to a workable band limited spectrum by using a resample function. Although, some frequency response parts were eliminated and the spectrum shape had a marginal alteration, the core of channel behaviour was still persevered. The graphs below (Figure 4.3) provide a comparison of the two models, where it could be seen that the overall density and the statistical shape had been preserved.

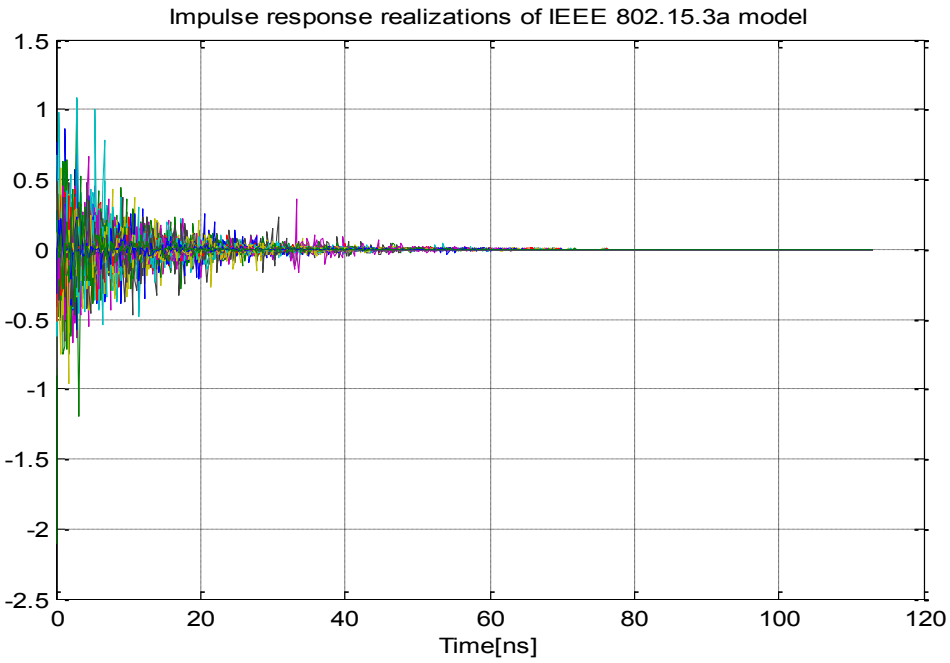

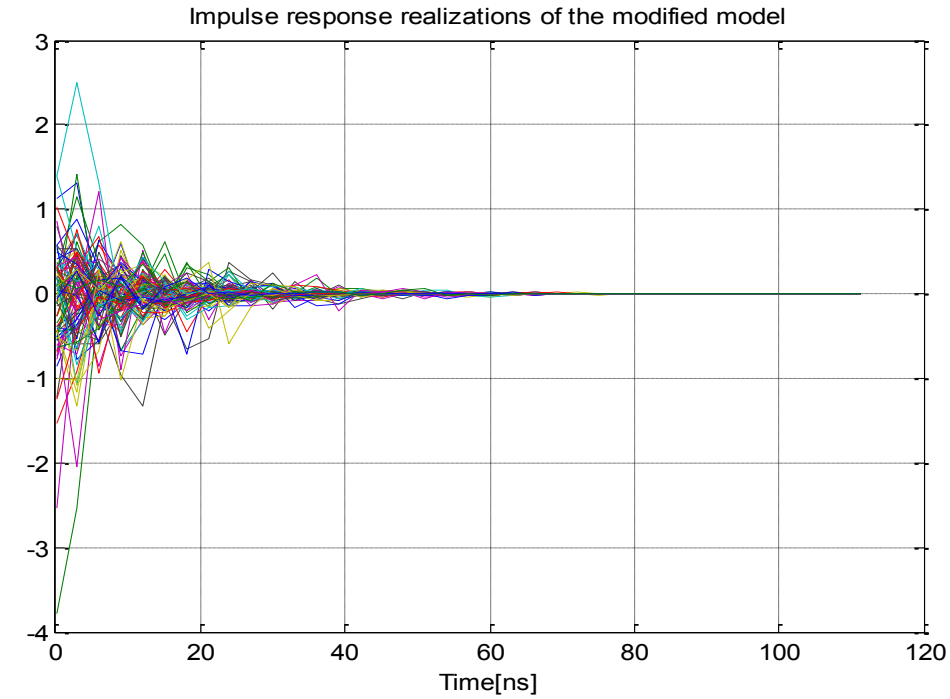

Figure (4.3): Comparison between IEEE803.15.3a model and its modified version

For simulation purposes, a down conversion with filtering and resampling was

undertaken by readjusting the sampling period. Hence, the implementation was performed by applying down sampling conversion with the aid of resampling using a time resolution of 3.006 ns. Resampling had produced a sampling period of 2.672 ns (0.167 * 16), which resulted from multiplying the sampling index by sixteen. This sampling time increases the resolution window sixteen times the original sampling index and reducing the sampling frequency by the same amount. Quantisation for the continuous time response was lead to formatting the desired resolution ts and a decimating factor of N. The value of N was an even quantity that was chosen to be a next power of two integers in the discretisation process. Similar responses with the same time index was added together, with transmit pulse filtering and band pass or low pass down conversion to fit the simulation requirements of the particular system (down conversion for this system). The resampling adjustment had to ensure the mitigation of the aliasing effect before the decimation by considering code with anti-aliasing filtering or complex down conversion. It was important to mention that, the sampling pins tend to store multipath coefficients and it was not practically feasible to store the entire continuous time multipath. In gernal, changing an event that elapse a very small period would mean oversampling with higher number of samples proportional to its spectrum in simulation test-beds. This in turns leads to a large number of weight coefficients in the convolution stage, and increases the costs of processing and memory requirements attached with the implementation. Furthermore, the proposed ECMA-368 standard specifies FFT size of 128 tones with 100 subcarriers for the transmitted signal at both transmitters and receivers sides.

As mentioned before, the resulting impulse response had over six hundred

paths which needed to be resampled in order to limit the simulation and facilitated the 128 fft frequency transformation. This domain translation had to match the transmitted signal transformation in the simulation. Fifty symbols were required for the signal in each subsection of the transmitter with 50 MHz spectrum separation between the two sections, and hence a maximum of fifty channel samples was required in the convolution process. Knowing that the FFT is periodic and symmetric in nature, there was a limitation in UWB channel samples available for DSP processing within the sampling environment. This was then justified the proposed sampling period expressed for this channel model. Figure 4.4 below show the channel impulse response in the time and frequency domains.

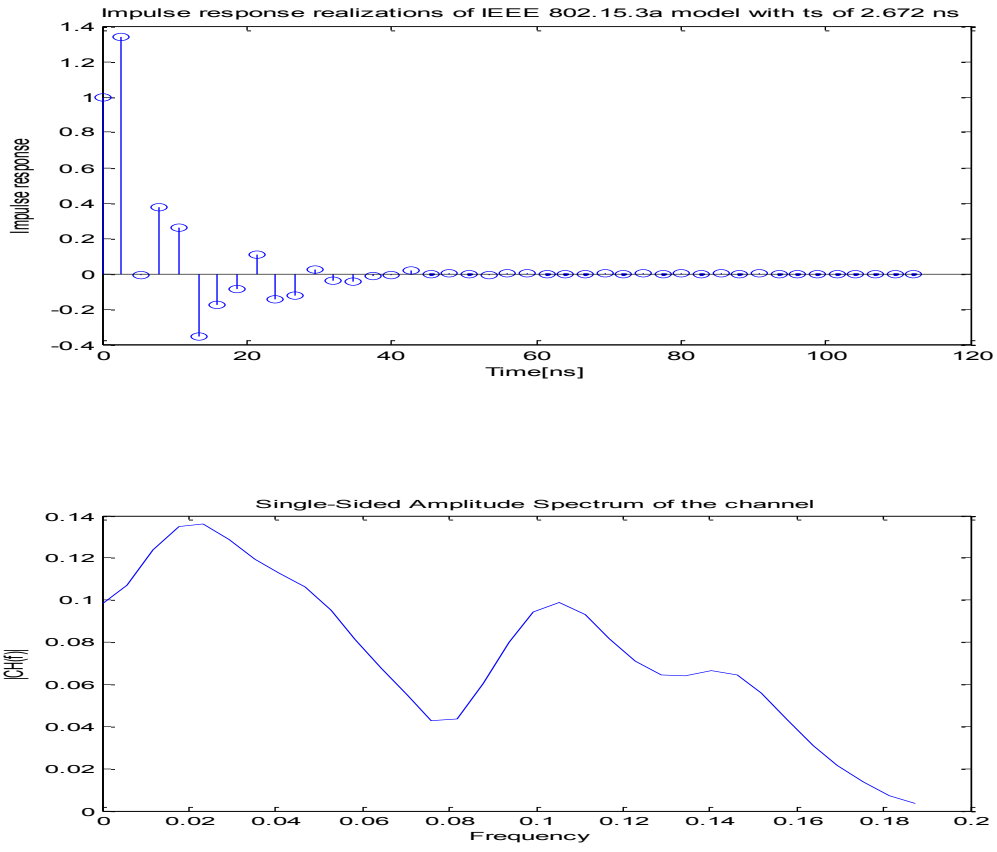

Figure (4.4): Time and frequency channel response

4.6 Receiver Implementation

The received noisy and distorted symbols had an additional length of Guard signal that did not contain information data, and had been used to reduce the ISI (Inter Symbol Interference). Therefore, the first step was to remove these redundancies from the OFDM symbol frame.

The guard intervals was copied and added to the header of the symbol frame in repetitive manner across the symbols, and therefore a specific function was implemented at the receive branches to remove these redundancies by reordering the received frames. The operation was done by initially creating a frame that consists of two vectors, one represents the last 37 samples of the particular received symbol, and the second part consists of 91 zero samples, and then 128 length vector was added to the first received 128 sample of the original frame.

The re-adjustment procedure had the following format

Y1 = Y0 (1:128)

Y2 = Y0 (128:165)

Y3 = zeros (1:91)

Y = Y1 + [Y2 Y3]

Once these additional guard intervals was removed from OFDM symbols, then Fast Fourier Transform FFT operation was performed across the symbols and the frame to translate the received signals into the frequency domain. The translation was performed on a noisy and corrupted symbols and expressed mathematically as follows

$$\bar{\bar{\mathrm{Y}}}(\mathrm{q}) = fft(y) = \frac{1}{N}\sum_{n=0}^{N-1}\left(\sum_{p=0}^{N-1} \mathrm{Y}_{l,D_{1,2}}^{A_a}(\mathrm{p})\ \mathrm{e}^{-\mathrm{i}2\pi\mathrm{pn}/\mathrm{N}} + z\right)\mathrm{e}^{\mathrm{i}2\pi\mathrm{nq}/\mathrm{N}} \qquad (4.6.1)$$

$$\bar{\bar{\mathrm{Y}}}(\mathrm{q}) = \quad Y(q)H(q) + Z(q) \quad , q = 0{,}2 \ldots 127 \qquad (4.6.2)$$

The process used 128 FFT bin size that was specified within the ECMA standard, and hence this implementation gives practical advantage in terms of hardware complexity. Equalisation had been followed for these frequency domain samples across symbol vectors and packet frames. In order to carry the equalisation process, accurate channel estimation in the name of CSI was critical. Hence in this part, two model scenarios was implemented one which had assumed perfect channel estimation procedure, and the other had

considered partial channel estimation (equalisation errors). Frequency transformation had to be applied for the channel coefficients, so as to carry out frequency domain equalisation. Since symmetrical frequency domains channel samples was required, a shift and swap between the upper and lower channel spectrum had been carried out. This ensures synchronisation with the received signal samples in the frequency domain, and avoids distortion in the equalisation. The implementation steps for the channel frequency transform were summarised as follows

$$\text{hf} = \text{fft}\left(\left[\text{h} \quad zeors\left(128 - length(h)\right)\right], 128\right)$$

$$\text{hf} = [\, hf(128{:}49) \;\; hf(2{:}51) \,]$$

A critical equalisation task was removing the channel spectrum distortion from the received signal components. In this case, received symbols were divided by the channel spectrum to eliminate the channel effect. Zero Forcing equaliser have a problem of noise enhancement for low SNR, and while a formulation for the model had used to constrain the complexity associated with MIMO implementation, it was imperative to address this shortfall within the simulation environment. The reconstruction had been conducted by transformation, in which the first PSK symbol within the second antenna was allocated in the first radiating element, and replacing the first slot of the second receiving branch by the corrosponding second symbol within the first antenna. Then, as the design proposal had stated that, the dual 8-ary PSK symbols across the two radiating elements had to be combined. This

tranformation induces new received symbols contained fading distrotions with additonal degree of freedom encapsuated from the spatial and frequency domain configration. Then a matlab file function (ReTransformConcept) were created to take the dual symbols across the 1500 symbols frame on every branch of the receiving antennas. The real components of the dual receiving branches were interchanged inducing modified symbols as result of the transformation. Then following this process, the resulting complex symbols in every branch across the dual radiating elements were divided with the magnitude of the quadrature components of its corroposnding symbols. These ulterd symbols were then soft decoded to infer the orignal transmitted QPSK symbols.

$$y_{k(n)}^{psk_1^{R1}} = d_1^{psk_1^{R1}} + jd_2^{psk_1^{R1}} \quad (4.6.3)$$

$$y_{k(n+50)}^{psk_2^{R2}} = d_1^{psk_2^{R2}} + jd_2^{psk_2^{R2}} \quad (4.6.4)$$

$$y_{k(n+50)}^{psk_2^{R1}} = d_1^{psk_2^{R1}} + jd_2^{psk_2^{R1}} \quad (4.6.5)$$

$$y_{k(n)}^{psk_1^{R2}} = d_1^{psk_1^{R2}} + jd_2^{psk_1^{R2}} \quad (4.6.6)$$

Applied cross insertion, the new complex symbols were then became

$$\bar{\bar{y}}_{k(n)}^{psk_1^{R1}} = \text{Real}\left(y_{k(n+50)}^{psk_2^{R2}}\right) + jd_2^{psk_1^{R1}} = d_1^{psk_2^{R2}} + jd_2^{psk_1^{R1}} \quad (4.4.7)$$

$$\bar{\bar{y}}_{k(n+50)}^{psk_2^{R2}} = \text{Real}\left(y_{k(n)}^{psk_1^{R1}}\right) + jd_2^{psk_2^{R2}} = d_1^{psk_2^{R2}} + jd_2^{psk_2^{R2}} \quad (4.4.8)$$

$$\bar{\bar{y}}_{k(n+50)}^{psk_2^{R1}} = \text{Real}\left(y_{k(n)}^{psk_1^{R2}}\right) + jd_2^{psk_2^{R1}} = d_1^{psk_2^{R2}} + jd_2^{psk_2^{R1}} \quad (4.4.9)$$

$$\bar{\bar{y}}_{k(n)}^{psk_1^{R2}} = \text{Real}\left(y_{k(n+50)}^{psk_2^{R1}}\right) + jd_2^{psk_1^{R2}} = d_1^{psk_2^{R2}} + jd_2^{psk_1^{R2}} \quad (4.4.10)$$

The orignal QPSK symbols were then determined as

$$\text{y}^{qpsk_1^{g1}} = \frac{\left(\bar{\bar{y}}_{k(n)}^{psk_1^{R1}}\right)}{\left|d_2^{psk_1^{R1}}\right|} = r^{g1}{}_{c(n)} + jr^{g1}{}_{c(n)+50} \quad (4.4.11)$$

$$\text{y}^{qpsk_2^{g1}} = \frac{\left(\bar{\bar{y}}_{k(n+50)}^{psk_2^{R2}}\right)}{\left|d_2^{psk_2^{R2}}\right|} = r^{g1}{}_{c(n)+1} + jr^{g1}{}_{c(n)+51} \quad (4.4.12)$$

$$\text{y}^{qpsk_1^{g2}} = \frac{\left(\bar{\bar{y}}_{k(n+50)}^{psk_2^{R1}}\right)}{\left|d_2^{psk_2^{R1}}\right|} = r^{g2}{}_{c(n)} + jr^{g2}{}_{c(n)+50} \quad (4.4.13)$$

$$\text{y}^{qpsk_2^{g2}} = \frac{\left(\bar{\bar{y}}_{k(n)}^{psk_1^{R2}}\right)}{\left|d_2^{psk_1^{R2}}\right|} = r^{g2}{}_{c(n)+1} + jr^{g2}{}_{c(n)+51} \quad (4.4.14)$$

The searching subspace of the paths metrics for the soft decoding alogirhm had been reduced by this receving design, and the transformation process results in lowering the signal constellation to four points scatter map. For

every received symbol, the In-phase and Qudarature components coming from different indenpent channels, and the demodulation were perfomed by examming these distance metrics to obatin the orignal two dimenstional (two bits symbol) transmitted symbols. These induced distorted complex numbers were then passed to a measure function (RecAntenDCMSoft_QPSK) which have the task of measuring the recovred actual eculidean distances on the two In-phase and quarduature orthognal domains. These actual noisy measurment were then used in the ML searching alogrithm to reconstruct the orignal signals. Its imporatn to mension here that, these two measurment values correposnds to the Second Most Significant bit (SMB) and the Least Significant Bit (LSB) of the 8-ary PSK symobls. The eculdian metrics evulation was done independnetly across the orthongal dimensions of the mdoified complex symbols. These metrics were then used in the demodulation process as soft decoding inputs to the Vierbi decoder. This reduction in the signal alphabate reduces combutation within the viterbi alogrithm. The reduction of the finite eculidean metric sets that spans the signal constellation, optimise the ML solution which was refltected in the number of paths metrics within the trellis. In the ML scheme, finding the minmum distance across a large set of signals was NP-hard optimisation problem and therefore a smaller set of path mertics makes this deocding alogirthm releasiable in paractical applications. A reduction in the complexity was observed by reducing the searching graph subspace for the demapper. This was then repeated for the 50 complex symbols across the receiveing branches. In mathematical form, the above process would be expersssed as follows

$$\widehat{\mathbf{D}}_{qps_r^{g1}}^{R(n)} = \arg\min_{d_{qps_r^{g1}}} \sum_{p=1}^{P} \left\| Re\left(y_p^{qps_r^{g1}} - c_p^{R(n)} s_p^{qps_r^{g1}} \right) \right\|^2 \quad (4.4.15)$$

$$\widehat{\mathbf{D}}_{qps_r^{g1}}^{I(n)} = \arg\min_{d_{qps_r^{g1}}} \sum_{p=1}^{P} \left\| Im\left(y_p^{qps_r^{g1}} - c_p^{I(n)} s_p^{qps_r^{g1}} \right) \right\|^2 \quad (4.4.16)$$

$$\widehat{\mathbf{D}}_{qps_r^{g2}}^{R(n+50)} = \arg\min_{d_{qps_r^{g2}}} \sum_{p=1}^{P} \left\| Re\left(y_p^{qps_r^{g2}} - c_p^{R(n+50)} s_p^{qps_r^{g2}} \right) \right\|^2 \quad (4.4.17)$$

$$\widehat{\mathbf{D}}_{qps_r^{g2}}^{I(n+50)} = \arg\min_{d_{qps_r^{g2}}} \sum_{p=1}^{P} \left\| Im\left(y_p^{qps_r^{g2}} - c_p^{I(n+50)} s_p^{qps_r^{g2}} \right) \right\|^2 \quad (4.4.18)$$

Where $\widehat{\boldsymbol{D}}_{qps_r^{g}}^{i}$ was the estimated ecludian distance matrix containing the magntiude of one the quadrature compoentents $i \in$ (R,I) for recived symbols frame, C^d was the channel estimate for that ecludian metric . $y_j^{qps_r^{g}}$ was the recived noise PSK symobl within the j spectrum section , and $s_p^{qps_r^{g}}$ was the PSK symobl in the constellation map.

The result complex symbols identifies the four allocated bits as ($b_{c(n)+50}, b_{c(n)+51}, b_{c(n)+100}, b_{c(n)+101}$) for that speceific group. The fifth bit within the group was then idenified in a soft decoding based on the position of the received PSK symbols allocated to the dual maps of that receiving antanna

branch. A point to mention here, that the most significant bit (MSB) within the dual PSK symbols for a branch, reperensted the fifth bit within the group across that link branch. Reducing the error estimation by strong decoding alogrithim was critical, and the system proframance degrades significantly if there was bit flibbing, or if the demdoulation method was not optimissed. In the case of the first PSK map, the bit was considered to have a value of 1 if the predicated symbol was located in the In-phase region, and considered 0 for the second map if belongs to the same region. If the perdicated symbol was located within the region of the vertical Qurdature axis of the frist map then the bit takes the 0 value, and takes the binary value of 1 for the second 8PSK constellation map.

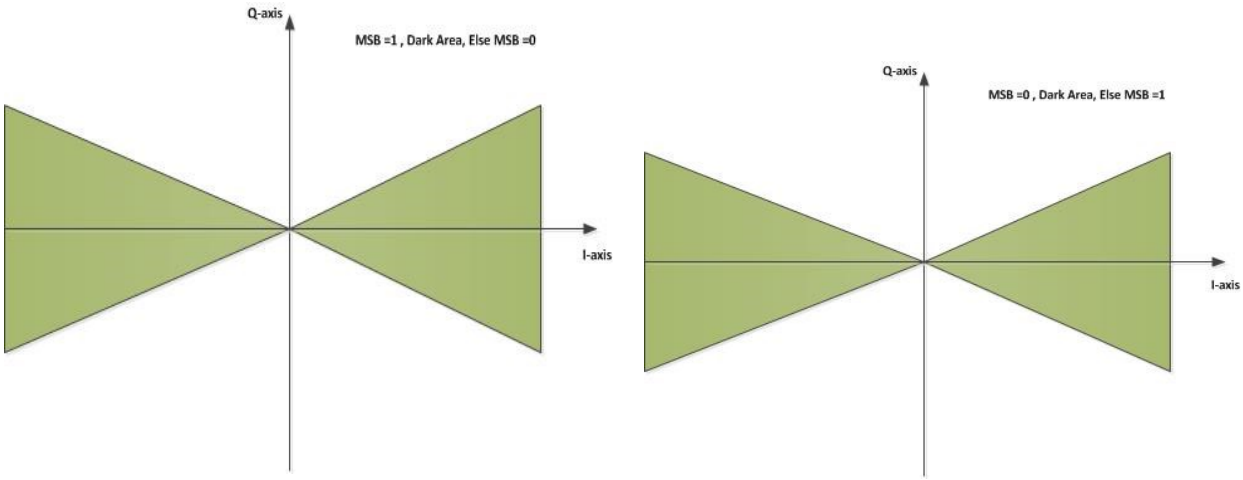

First 8PSK map Second 8PSK map

Figure (4.5): The decoding regions for the MSB of the PSK symbols

The doted diagonal line in the above figure (45 degree from the I domain) reperesented the base metric boundry in which the third bit binary value was detrmined. Since, the two distance metrics for the I and Q axis(d1,d2) were

equal across both orthognal domains. Then, a simple substraction of the received complex symbol real and imagnry parts from the $I_{d1}^{psk_1^a}$(d1), and $I_{d2}^{psk_1^a}$ (d2) determined the positon of the symbol within the above regions. Therefore, upon receiving the two symbols within each reciving block($y_{k(n)}^{psk_1^a}, y_{k(n+50)}^{psk_2^a}$), the follwing metrics used to infer the 3rd bit.

In the case of b3 = 0

The conditon for the first 8PSK map was

$$\mathrm{P1} = \sqrt{\left[Real\left|y_{k(n)}^{psk_1^a}\right| - I_{d1}^{psk_1^a}\right]^2 + \left[Imag\left|y_{k(n)}^{psk_1^a}\right| - I_{d2}^{psk_1^a}\right]^2} \quad (4.4.19)$$

$$\mathrm{P2} = \sqrt{\left[Real\left|y_{k(n)}^{psk_1^a}\right| - I_{d2}^{psk_1^a}\right]^2 + \left[Imag\left|y_{k(n)}^{psk_1^a}\right| - I_{d1}^{psk_1^a}\right]^2} \quad (4.4.20)$$

$\mathrm{P1} < \mathrm{P2}$

The condtion for the second 8PSK map

$$\mathrm{P1} = \sqrt{\left[Real\left|y_{k(n+50)}^{psk_2^a}\right| - I_{d1}^{psk_2^a}\right]^2 + \left[Imag\left|y_{k(n+50)}^{psk_2^a}\right| - I_{d2}^{psk_2^a}\right]^2} \quad (4.4.21)$$

$$\mathrm{P2} = \sqrt{\left[Real\left|y_{k(n+50)}^{psk_2^a}\right| - I_{d2}^{psk_2^a}\right]^2 + \left[Imag\left|y_{k(n+50)}^{psk_2^a}\right| - I_{d1}^{psk_2^a}\right]^2} \quad (4.4.22)$$

$P1 > P2$

In the other case of b3 = 1

The conditon for the first 8PSK map was

$$P1 = \sqrt{\left[Real\left|y_{k(n)}^{psk_1^a}\right| - I_{d1}^{psk_1^a}\right]^2 + \left[Imag\left|y_{k(n)}^{psk_1^a}\right| - I_{d2}^{psk_1^a}\right]^2} \quad (4.4.23)$$

$$P2 = \sqrt{\left[Real\left|y_{k(n)}^{psk_1^a}\right| - I_{d2}^{psk_1^a}\right]^2 + \left[Imag\left|y_{k(n)}^{psk_1^a}\right| - I_{d1}^{psk_1^a}\right]^2} \quad (4.4.24)$$

$P1 > P2$

The condtion for the second 8PSK map

$$P1 = \sqrt{\left[Real\left|y_{k(n+50)}^{psk_2^a}\right| - I_{d1}^{psk_2^a}\right]^2 + \left[Imag\left|y_{k(n+50)}^{psk_2^a}\right| - I_{d2}^{psk_2^a}\right]^2} \quad (4.4.25)$$

$$P2 = \sqrt{\left[Real\left|y_{k(n+50)}^{psk_2^a}\right| - I_{d2}^{psk_2^a}\right]^2 + \left[Imag\left|y_{k(n+50)}^{psk_2^a}\right| - I_{d1}^{psk_2^a}\right]^2} \quad (4.4.26)$$

$P1 < P2$

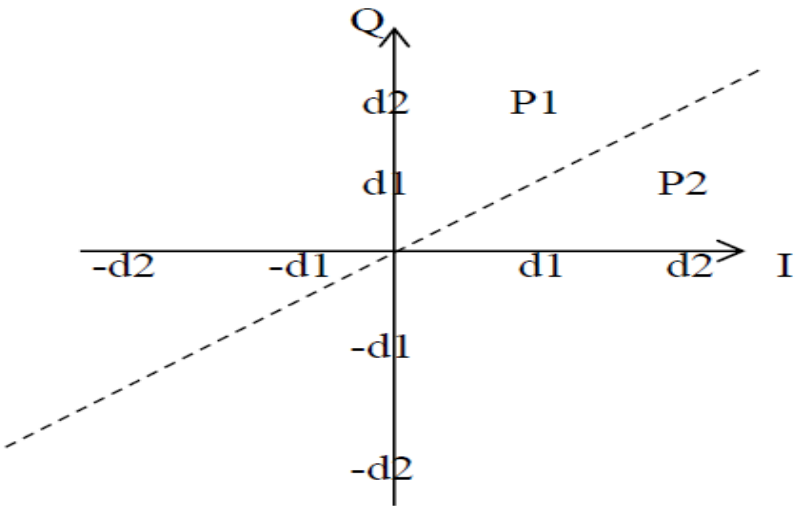

Figure (4.6): Expression of the metric length position

The viterbi alogrithm was undertaken by using a predfined function within a software backage (vitdec function within the Matlab library). The implementation had required to specify the input parameters for the function was based on the modulation method used on the transmitted symbols. These paramters were then used in the decoding process to estimate the binary singnal information. The trace back length through the trellis was set to 100, and the structure of the trellis was consistant with the transmitter convolutional structure. The use of unquant mode was applied to infer the soft decoding based on the actual calculated ecludian entries. This function itself had been used with the system paramters defined in table 3.

Vitdec function Parameters	Description	Values
tbln	track back length	100
tstr	The trellis describtion	poly2trellis(7,[133 171])
trunc	Truncating entry vector	Matlab definition (no delay)
unquant	Decoding type (soft)	Real input values

Table (4.3): Paramteters of Matlab viterbi function

The estimated and decoding symbols were then rearranged using arrangement function (Rearrangbits). The last stage was a compartive error function (ErrorCalc), where the number of erronouns bits were calcuated and then compared with the total number of bits to find the BER within the proposed model. Thereshold levels was set to control the simulation by limiting the number of errors for the wireless system. A completioning high degree of accuracy, these receiving steps were exhastivelly repeated over the simulation enviorment. Figure (4.7) gives a description of the proposed model.

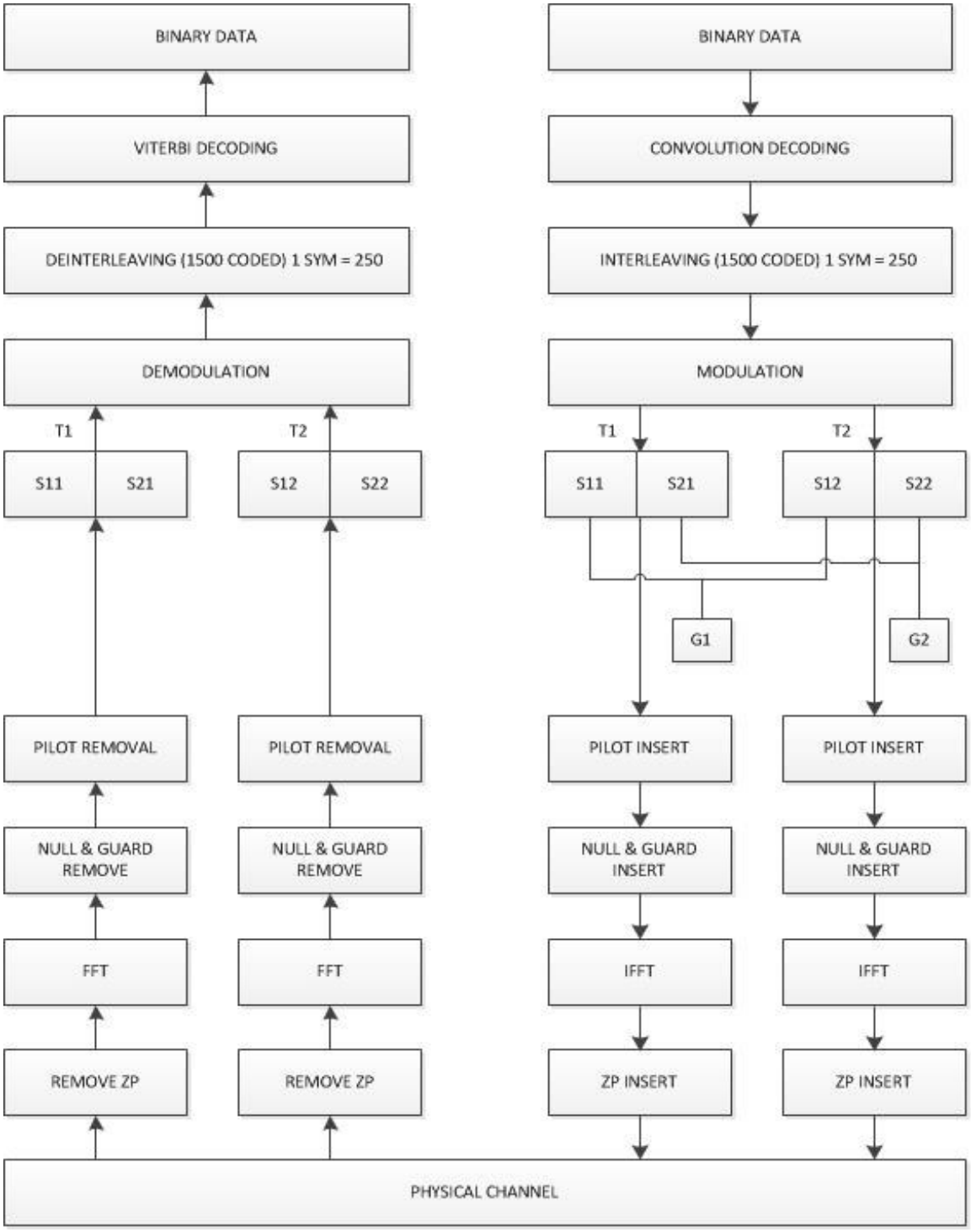

Figure (4.7): The proposed model

4.7 Optimisation for the Decoding method (LLR)

Introducing the LLR approach to optimise the soft decoding approach by ensuring the entry to the viterbi decoder had more certanty to the entry metric. Given the observed received symbols, the conditional probablity of the transmitted symbols could be used to infer the LLR formula. In the aid of Payes'Rule and with logrithmic tranformation, the LLR could be summerised as follows

$$L(x|y) = L(y|x)\, L(x)\, / L(y)$$

Since y was observed (known quanity), then

$$L(x|y) = L(y|x)\, L(x)$$

$$L(x|y) = L(y|x) + L(x)$$

The LLR represents a method for for identfying the most probable transmitted bits within a noisy received symbols that would be passed to the Vitrebi decoder. In the dual carrier configuration for each decoding block, there were

two receivd symobls($y^i_{k(n)}$, $y^i_{k(n+50)}$) corrpupted by different channel fadings according to the inherent frequency and spatial diversities within the UWB channels. Hence, the error performance for each of these received distotred symbols was different from each other, and this had been as a result of multivarite fading in the channel specturm that convloved with that particular symbol signal. Demapping of the control bit would follow the same process as the ML method, and the second copies of the received symbols would be passed to the tranfomration operation.The transformation concept at the receiving reduces the constellation dimension (down convert the eight points map to four points scatter). This process gives an important advanatages interms of the complexity reduction in the demapping and decoding alogrithms. Therefore, implmenting LLR demapping resulted in two soft quntities, MSB b_1(the Most Significant Bit), and LSB b_0(the Least Significant Bit). What is critical here was that, the MSB was related to the soft input to the decoder follwing the transformation and not related to the orignal received qunitiy. The constellation map was divided into regions related to each binary value carried by these symbol bits. A subset of values were located to a particular region corrosponding to one the significant bit value. The LLR demapping process across the first received transformed symbol $y^i_{k(n)}$ one of the dual reciving block was carried out in the follwing equations.

$$L\left(b_{MSB}^{qpsk_1^{g1}}\right) = \log\left\{\frac{P\left(b_{MSB}=1|y_{k(n)}^{qpsk_1^{g1}}\right)}{P\left(b_{MSB}=0|y_{k(n)}^{qpsk_1^{g1}}\right)}\right\}$$
$$= \log\left\{\frac{\sum_{s\in C_{MSB=0}} P(s|y_{k(n)}^{qpsk_1^{g1}})}{\sum_{s\in C_{MSB=1}} P(s|y_{k(n)}^{qpsk_1^{g1}})}\right\} \quad (4.7.1)$$

$$L\left(b_{LSB}^{qpsk_2^{g1}}\right) = \log\left\{\frac{P\left(b_{LSB}=1|y_{k(n)}^{qpsk_2^{g1}}\right)}{P\left(b_{LSB}=0|y_{k(n)}^{qpsk_2^{g1}}\right)}\right\}$$
$$= \log\left\{\frac{\sum_{s\in C_{LSB=0}} P\left(s\middle|y_{k(n)}^{qpsk_2^{g1}}\right)}{\sum_{s\in C_{LSB=1}} P\left(s\middle|y_{k(n)}^{qpsk_2^{g1}}\right)}\right\} \quad (4.7.2)$$

Where C_i correspnds to a subset of symbols that have the a bit position b_k having of one the binary values b_k E {0,1}.

Expanding these experssion with the presence of noise power, the noise distortion could be observed to effect the overall snr at the receiver and hence had to be minised in the error performance evulation.

$$\boldsymbol{L}(\boldsymbol{y}) = \log\left\{\frac{\sum_{s\in C_{b\forall 0}} e^{-\left[\frac{(s-y)^2}{\sigma^2}\right]}}{\sum_{s\in C_{b\forall 1}} e^{-\left[\frac{(s-y)^2}{\sigma^2}\right]}}\right\} \quad (4.7.3)$$

The vairance of the LLR formula would be calcuated by taking the variances of the two received symbols and inducing an estimate mean of the variance as

$$\sigma^2 = \frac{\sigma_{s1}^2 + \sigma_{s1}^2}{2} \qquad (4.7.4)$$

In a similar manner, the second spectrum in the DC demodulation within the same reciving block would be performed as follows

$$L\left(b_{MSB}^{qpsk_1^{g2}}\right) = \log\left\{\frac{P\left(b_{SSB}=1|y_{k(n+50)}^{qpsk_1^{g2}}\right)}{P\left(b_{MSB}=0|y_{k(n+50)}^{qpsk_1^{g2}}\right)}\right\} = \log\left\{\frac{\sum_{s\in C_{MSB=0}} P\left(s\left|y_{k(n+50)}^{qpsk_1^{g2}}\right.\right)}{\sum_{s\in C_{MSB=1}} P\left(s\left|y_{k(n+50)}^{qpsk_1^{g2}}\right.\right)}\right\} \qquad (4.7.5)$$

$$L\left(b_{LSB}^{qpsk_2^{g2}}\right) = \log\left\{\frac{P\left(b_{LSB}=1|y_{k(n+50)}^{qpsk_2^{g2}}\right)}{P\left(b_{LSB}=0|y_{k(n+50)}^{qpsk_2^{g2}}\right)}\right\} = \log\left\{\frac{\sum_{s\in C_{LSB=0}} P\left(s\left|y_{k(n+50)}^{qpsk_2^{g2}}\right.\right)}{\sum_{s\in C_{LSB=1}} P\left(s\left|y_{k(n+50)}^{qpsk_2^{g2}}\right.\right)}\right\} \qquad (4.7.6)$$

4.8 Conclusion

In this chapter, the implementation for the proposed simulation model had been considered. The transmitting, and receiving structures were given, and their implementation in a simulated environment had been explained. The channel that emulates the real indoor fading and distortion was considered, and implemented in the running program. A proposal to improve the demodulation and estimation of symbols was given, and the formation of this model within the physical layer standard had been highlighted.

5. Simulation

5.1 Introduction

In this chapter, the simulation of the proposed design was carried out to envisage the hypothesis of the scheme. In order to perform the different tasks and the required tests, a software application had to be considered which satisfied the research hypothecs. Matlab software application had been identified for this implementation. Matlab is software package that allows mathematical manipulation of various algorithms and functions. The communication toolbox within Matlab provides a laboratory environment where wireless communication system could be design, simulated and then evaluated in a controllable platform. The chapter covers a definition of the functions used in the simulation, specification of the wireless model scenario, implementation and result observations of the work. A conclusion notes on these results was given with future remarks on suggested work.

5.2 Overview of the simulation

The design and simulation process of the model had predicted the response of MIMO WPAN system to the inherent distortions, noise impairments and real-indoor wireless environment disturbances by quantitative and analytical measures. The proposed model design had to be evaluated in a simulation environment to induce the requirement hypothesis. Therefore, in this work a form of test-bed like environment were constructed to emulate the real life operational conditions. There were a number of parameters that had to be identified within the framework of the design. The actual measureable parameter in real time WPAN system is the ratio between the signal power and the noise power referred to as SNR. Thermal noise and other form of noise would be combined in AWAGN model. In this simulation design, the power spectral of the noise had been assigned in the algorithm in relation to the SNR. The second parameter was the channel coefficient related to each path within the ultra-wide band channel model. These had been generated randomly so as to represent the indoor medium condition. Hence, a stochastic model in the

form of Gaussian distribution had been used in the mathematical evaluation. The delay within the channel clusters had to be identified in the model parameters. Non direct line of sight paths in the multipath model, had incur time delay and hence these delay interval had been set up in the process. The followed result figures had been undertaken in multiple simulation conditions with various requirements.

5.3 Simulation functions

In order to facilitated and emulate this wireless model, a simulation test bed was required to be designed and created in which the requirements and specifications of this WPAN application was satisfied. In fulfilling these requirements, several functions and multiple elapsing methods had been created using similar principle to encapsulation in object oriented programming. This was achieved by separate various design and implementation methods and algorithms into separate functions, and all being called in one main object body. This allows optimisation, correction and modification while developing the model.

5.4 Specifications of the simulation process

Monte Carlo simulation had been considered in this evaluation method with analyses of the various degrees of freedom corresponding to the spatial, frequency and time domains included in the proposed design. The number of packet frames had been set to 2000 and the bit stream had been set with large sequential intervals so as to formulate a confidence margin in the accuracy of the simulation results. The source signal was generated from a pseudo random sequence generator. The frame length consists of 1500 interleaved and coded bits corresponding to DC32-QAM with additional length variability. The simulation setting had been carried based on two main distinct principles. The first uses interchanged simulation analysis between time and frequency domains on the transmitting and receiving structure. The second setting uses primarily frequency domain analysis to infer the design and implementation hypothesis. Specific simulation settings was summarised in the following table in accordance with specification requirements that was defined in the implementation chapter.

Simulation Initialisation settings	Description
[1 1 1 0 0 1]	Puncturing setting
¾ cr	Convolutional coding rate
Ch1 & ch2	IEEE803.15.3a standard channel model
1500 s/p	1500 symbols per frame for DC32QAM
Ch1 Model	LOS, distance 0-4m
Ch2 Model	NLOS, distance 0-4m
Nit= 1e2	Number of iteration associated with Eb/No
5.28 ns ch1 RMS	RMS delay in nano-second for LOS
8.03 ns ch2 RMS	RMS delay in nano-second for NLOS
dly1b = [0 3 5 6 8 14 16 18 19 20]	The delay samples for multipath fading
1000	The number of threshold errors (variable)
1e-6, 1e-9	The maximum number of errors per BER pin

Table (5.1): summery of specific simulation settings used in the simulation

5.5 Time-frequency implementation

In this section, the work was focused on implementing the proposed method in the frequency domain and then transferred to the time domain at the channel stage and finally translated the received signal component to the frequency domain at the receiver. Therefore, the transmitted symbol had been constructed as an OFDM symbol contains 100 IFFT frequency tones for the message signal and the additional 28 subcarriers were assigned for the standard requirements (10 guard carries, 12 pilots subcarriers and 6 nulling tones). To reduce ISI, addition padded zero had been used based on the requirement specification. The modulated symbols were then passed to128 standard inverse fast Fourier transform function defined in Matlab tool box with a known algorithm. The following figures (5.5.1, 1.5. 2) show the performance of dual antennas based on DCM and DC-32QAM, and then compared them to standard single antenna configuration. The model was developed based on the pervious functions along with a number of standard Matlab functions. The results for the system BER had been presented in the following graphs. The results show comparisons between dual antennas configuration and single transmitter systems. During simulation two channel models were applied, namely, the LOS CM1 model and NLOS CM2 model both of which are available from the IEEE 802.15.3a channel model standard. This standardised

model was applied because it captures the physical link behaviour in the UWB domain. Figure 5.5.1 shows that the MIMO model provides 8dB of improvement at 10^{-2} BER in comparison to the SISO DC 32-QAM. Furthermore, the BER curve for the SISO model diverges when reducing the BER threshold and moving at the upper region of the SNR which further highlights the increased signal strength that the MIMO configuration provides. The error rate performance tends to vary marginally at very low SNR in figure 5.5.2 with slight improvement when crossing the 14 dB level in the SNR for the DCM, although the increase remains very small.

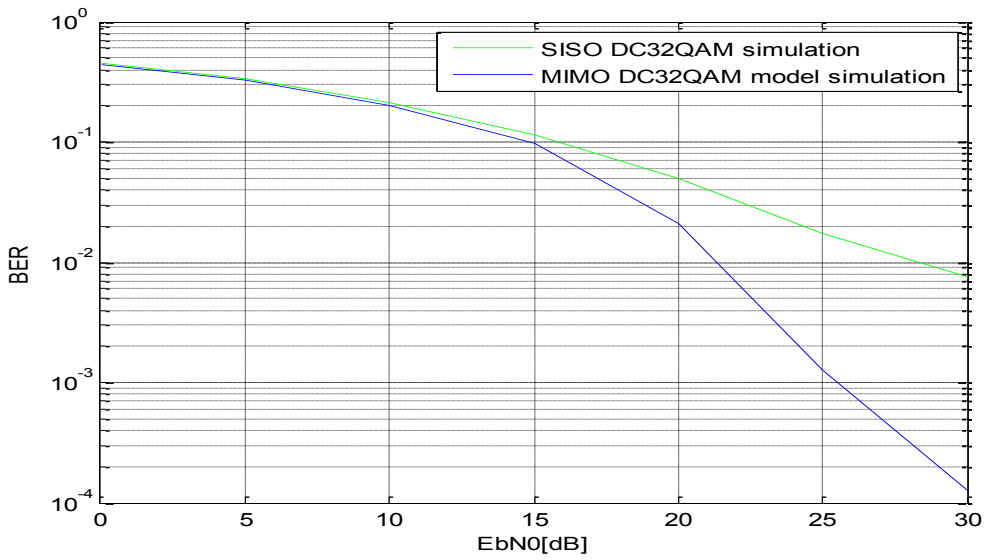

Figure (5.5.1): BER Simulation of MIMO DC32QAM vs SISO DC32QAM

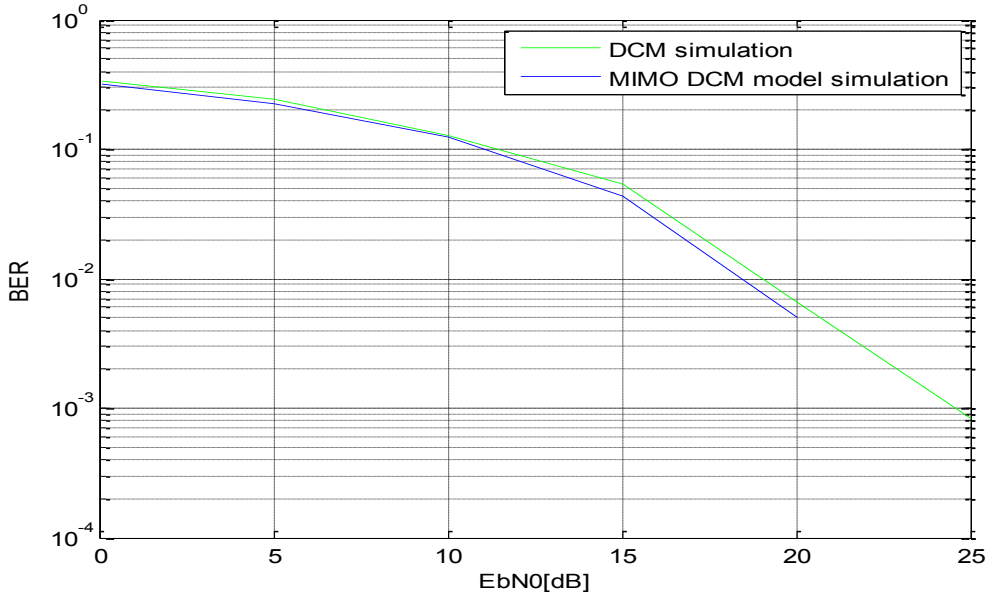

Figure (5.5.2): BER Simulation of MIMO DCM vs SISO DCM

In figure (5.5.3), a comparison between DCM and DC-32QAM had been carried out to evaluate the effect of the error performance when increasing the number of bits per symbol and how it relates to the proposed model. The small decrease in the BER curve indicates the effect of noise distortion in the constellation map at the decoder when the scattering density of symbols increases.

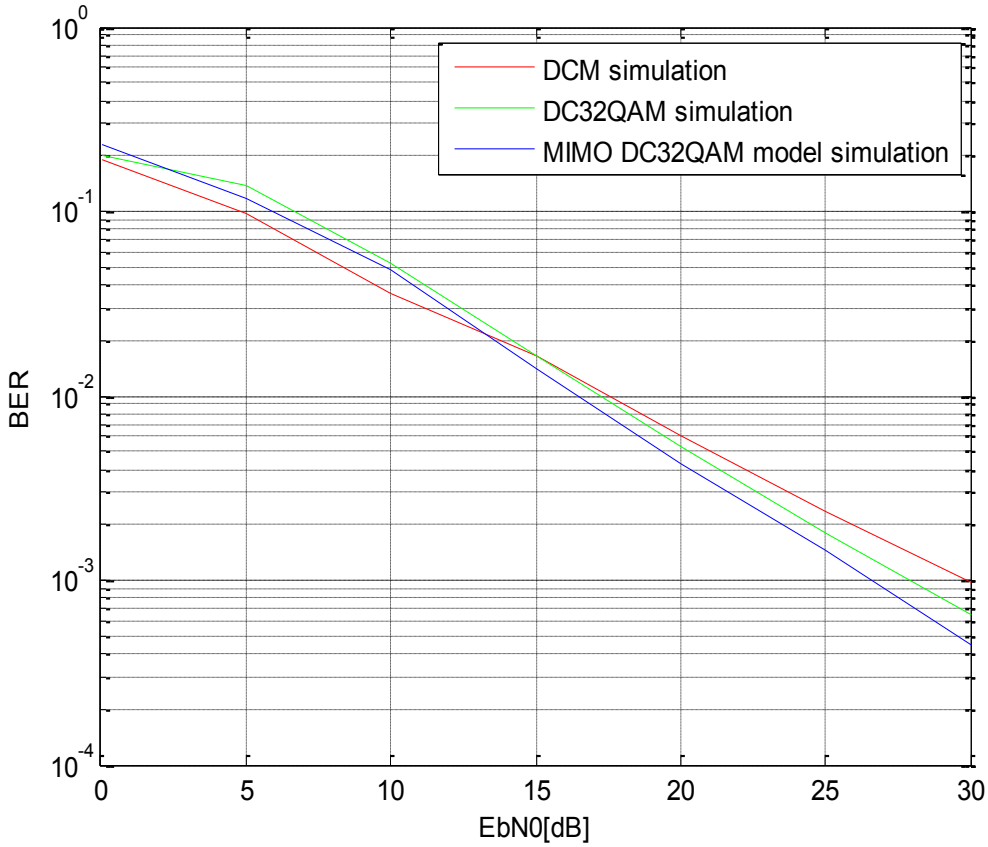

Figure (5.5.3): BER Comparison between DCM, DC32QAM and MIMO model

The following simulation in figure (5.5.4) shows the impulse response of UWB channel based on IEEE802.15.3a that measure the number of channel realisation, the time duration and the impulse response in 3D graphic.

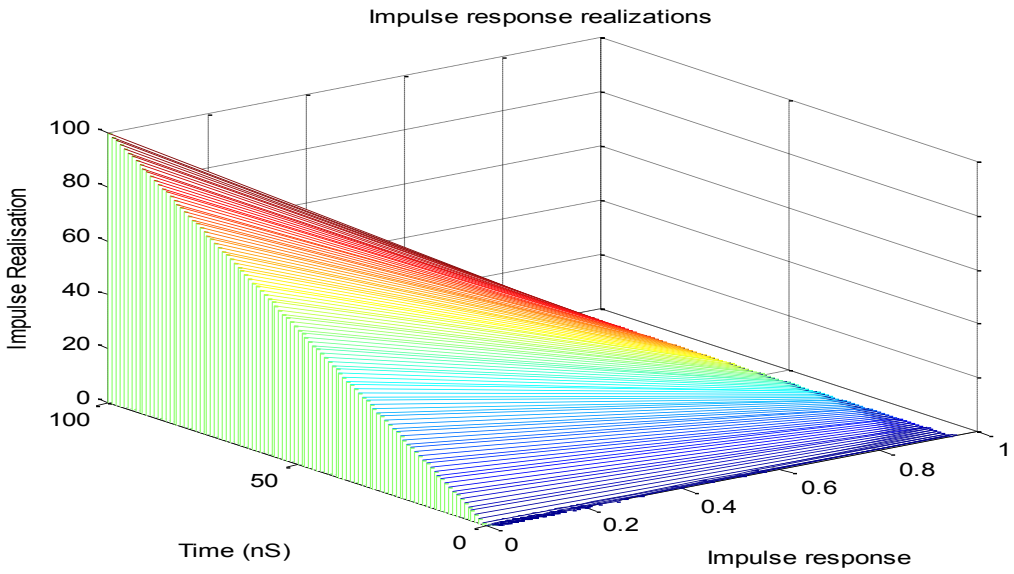

Figure 5.5.4: Impulse response with its time response and impulse realisation

The design had been evaluated in different channel conditions by constructing multipath channel model that encapsulate variation in the delay intervals and the fading power. Figure (5.5.5) shows the performance of the proposed design in the presence of Rayleigh channel model and compares this design with an analytical Rayleigh model. Stochastic tap delay line model had been used where an array of channel delay samples interval had been created. These delay interval run randomly in mathematical algorithm to emulate the random nature of the channel fading within the WPAN environment. The channel tap power profile was arranged to have maximum power of 0dB and could fluctuate to negative 30dB as a consideration of the fading power disturbance

that governs this hostile environment. The error performance had been compared in figure (5.5.6) where analytical and simulation models as well as DC 32-QAM had all been tested, and the results show close approximation between the analytical and simulation models.

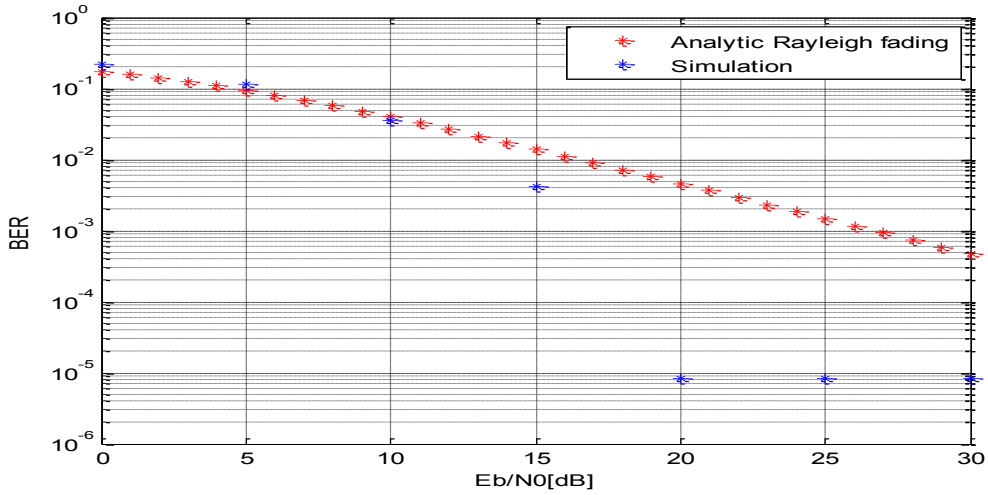

Figure (5.5.5): Comparison between analytical Rayleigh and Simulation models

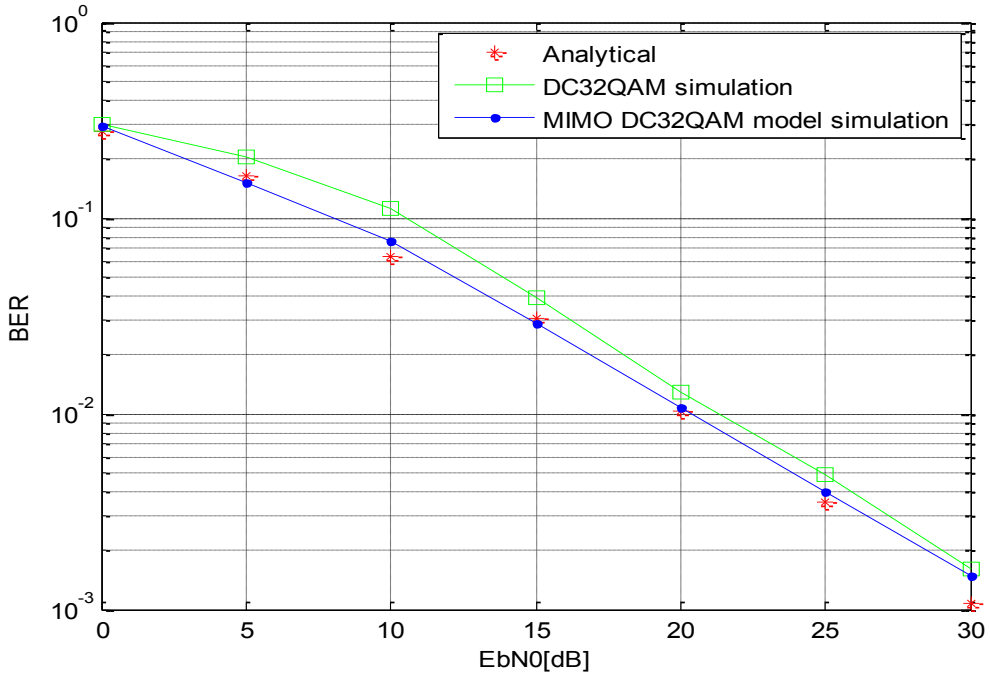

Figure (5.5.6): BER results of DC32QAM, Analytical and MIMO models

5.6 Simulation using coded modulation with hard decoding evaluation

In the evaluation process, it was important to cover different decoding algorithms and measure the response of the model in different implementation settings, and how its error performance compared. In particulare, if the model was used in a wireless application where the demodualtion at the receivers was based on hard alogrithm implemenation, how this model works in this setting. In this test, a test bench was developed to measure the model behaviour when decoding based on hard algorithm de-mapping. In the same setting, multipath fading based on complex and randomly distributed channel amplitude fading coefficients were generated to emulate the channel distortion. After which, the transmitted signals were convolved with the channel coefficients in the time domain, and then converted in the frequency domain where the receiving process had been performed. Figure (5.5.7) shows the results of the simulation of DC32-QAM-B-8PSK, MIMO-DC32QAM, and the new proposed concept of MIMO-DC-32QAM. As the SNR increases, the number of bits in errors

decreases sharply in comparsion to the other two models which reflected by the divergence of the purple curve. Furthemore, even at BER of 10^{-2} there were aroud 5 dB improvement in comparsion with DC-32-QAM and standard MIM0 DC32-QAM model. This results illustrated the advanteges of the proposed model event at conceptual wireless setting where hard alogirthm was implemented.

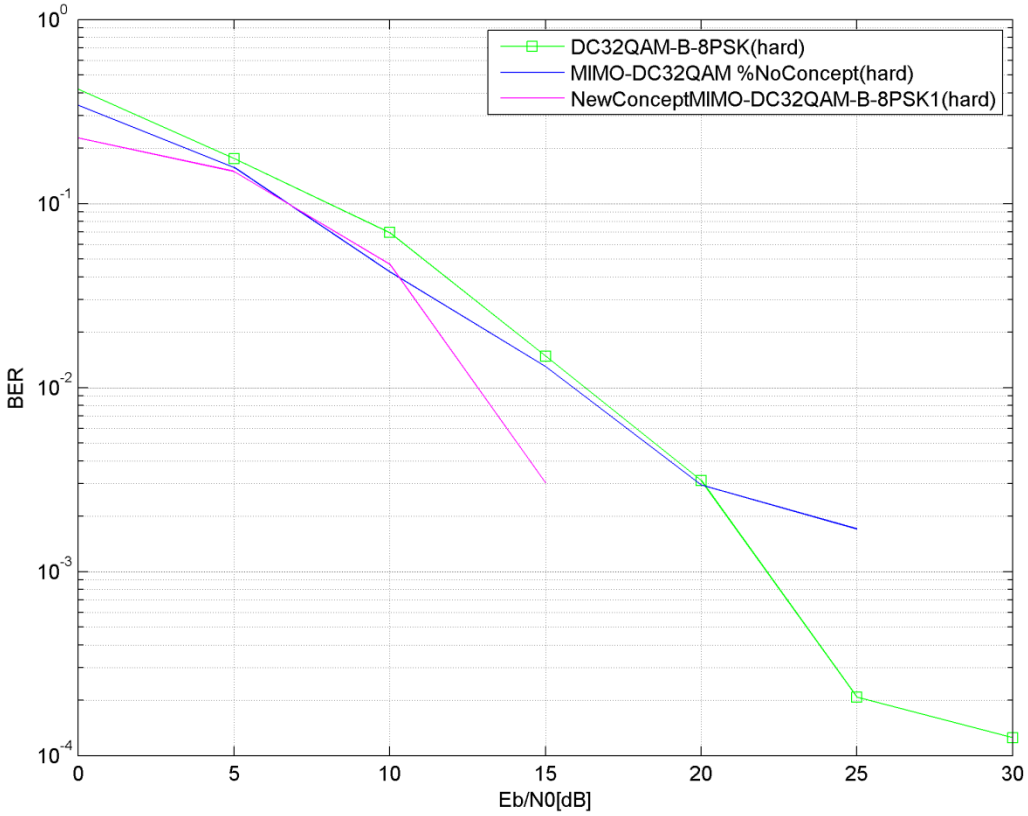

Figure (5.5.7): Comparion of the models error peromances using hard decoding

5.7 Simulation verification based on LLR implementation

In this section, Logarithmic implemenation based on the likelihood scheme was tested and evaluated to showed that the porposed model faciliated the use of different decoding plans depending on the specification of the wireless application. The soft metric in this scheme was evaluated using the likelihood scheme before passing it to the input viterbi function, and that in difference to the previous method where the induced ecludian metrics was directely passed as an inputs to the viterbi decoder. The originated LLR coming from the Gaussian channel was used in this scheme to increase the reliability of the input metrics to the Viterbi decoder. Maximum a posteriori probability was used in rising up the densities of the estimated symbols given the received signal. Simulation results had shown that, this additional method in the two stages signal estimation algorithm improved the error performance in

comparison to standard decoding scheme. In addition, since the design and implementation of the proposed model had resulted in a reduced signal constellation (map with four symbol points), the attached LLR complexity was significantly reduced. The likelihood metric in this simulation had two quantities that were forwarded to the vitedec decoder function. The first was the sign of the LLR indicating the binary decision, and the other represented the magnitude of the metric which reflected the confidence in the likelihood for the soft decoding algorithm. The variance used in the LLR expression was calculated from the variances coming from the two branches across the two receiving antennas. Since every input to the de-mapper (the new modified received symbol) had originally coming from two branches across the two radiating elements. The additional advantages of this likelihood scheme had been measured in the resulted error performance comparison shown by the BER curve in figure (5.5.8), where a measurable improvements had be shown as steps of SNR levels. The figure also highlighted the way the proposed scheme formulate the regions which the received symbols had been estimated, and this planning reduces the number of erroneous bits which reflected in steepens of the error curve. As the proposed de-mapping scheme had considered an approximation to the Likelihood formula in the consideration of noise, it was important to measure the significant of this approximation on the error performance. Monte Carlo simulation had shown that this modified Likelihood formula gives a good error performance and the approximation had relatively small degradation in the error curve.

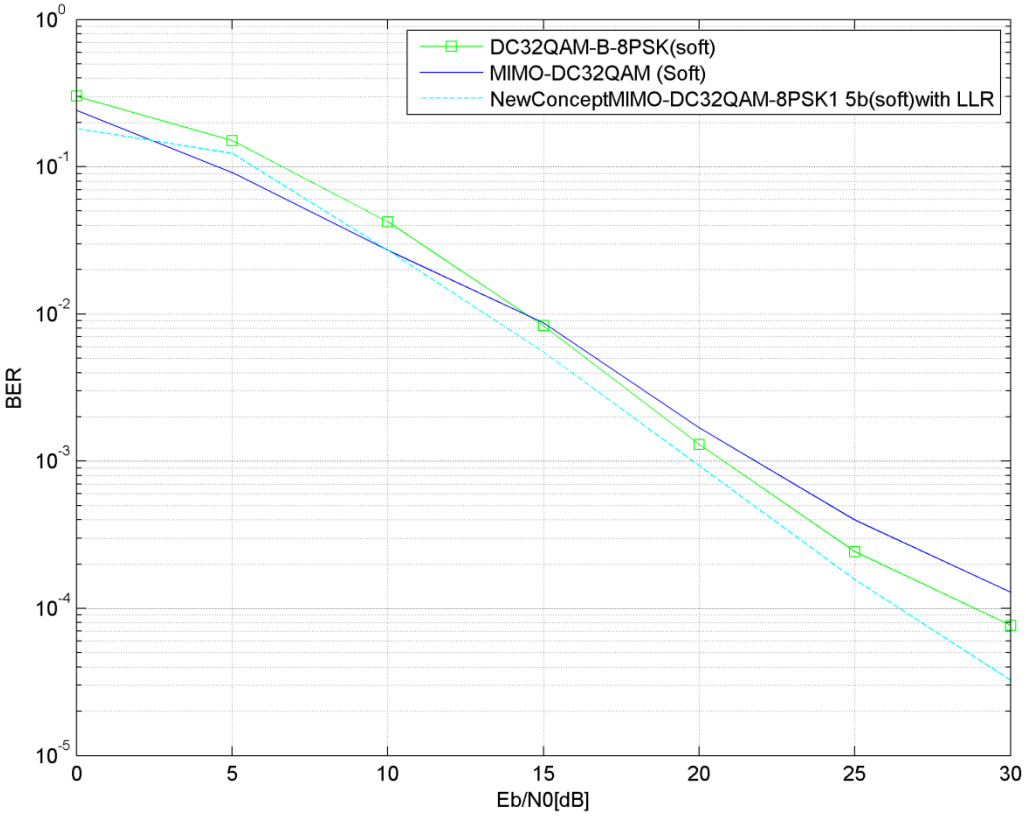

Figure (5.5.8): BER comparison of the model using LLR de-mapping method

5.8 Evaluation based on Comparison between ML & LLR methods

There are a number of soft decoding algorithms, and different wireless systems and applications had been declared based on these algorithms. What was important for any novel concept was to satisfy these systems by providing good error performance in all the available settings. Therefore, it was imperative to carry out an evaluation test based on well-known soft de-mapping methods that used in WLAN applications. In this simulation setting, a comparative in the model performance when applying ML soft metric and LLR de-mapping methods was conducted and evaluated. Simulation results had shown that the model performance equally when applying these soft decoding algorithm, and this clearly illustrate the advantages of implementing the proposed model on Indoor wireless systems. In figure (5.5.9), the single DC32-QAM-B-8PSK (green curve), stnadard MIMO-DC32QAM(blue curve), the proposed model with the ML soft demapping and its implemnation based on LLR demapping were shown. In the graph, the new proposed concept of MIMO-DC-32QAM LLR (cyan curve) using LLR method and the proposed

concept of MIMO-DC-32QAM Soft (blue-circle curve) with ML soft demapping showed a compariable resluts indicating the strength of the noval model. Additonal test had been carried out envisage the error performance at lower SNR between modulation models, and once again figure (5.5.10) showed that the prposed model gives good BER performance in comparsion with single dual carrier configuration model.

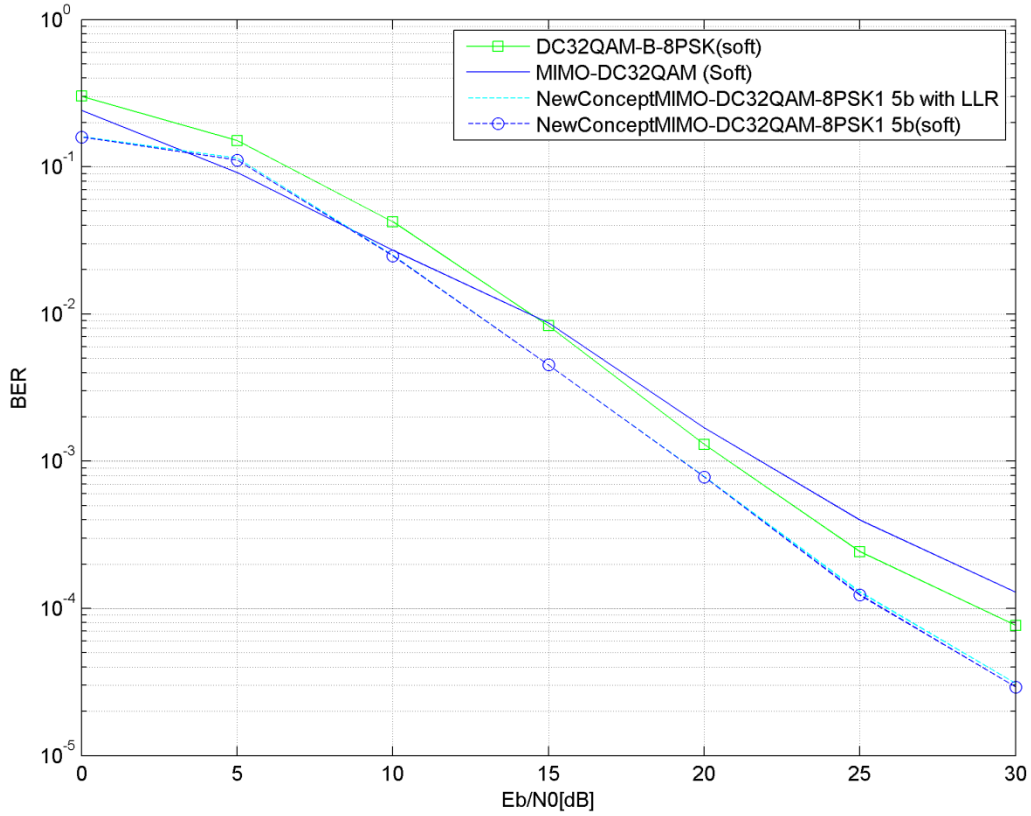

Figure (5.5.9): Comparison of BER performance between ML soft and LLR demapping methods

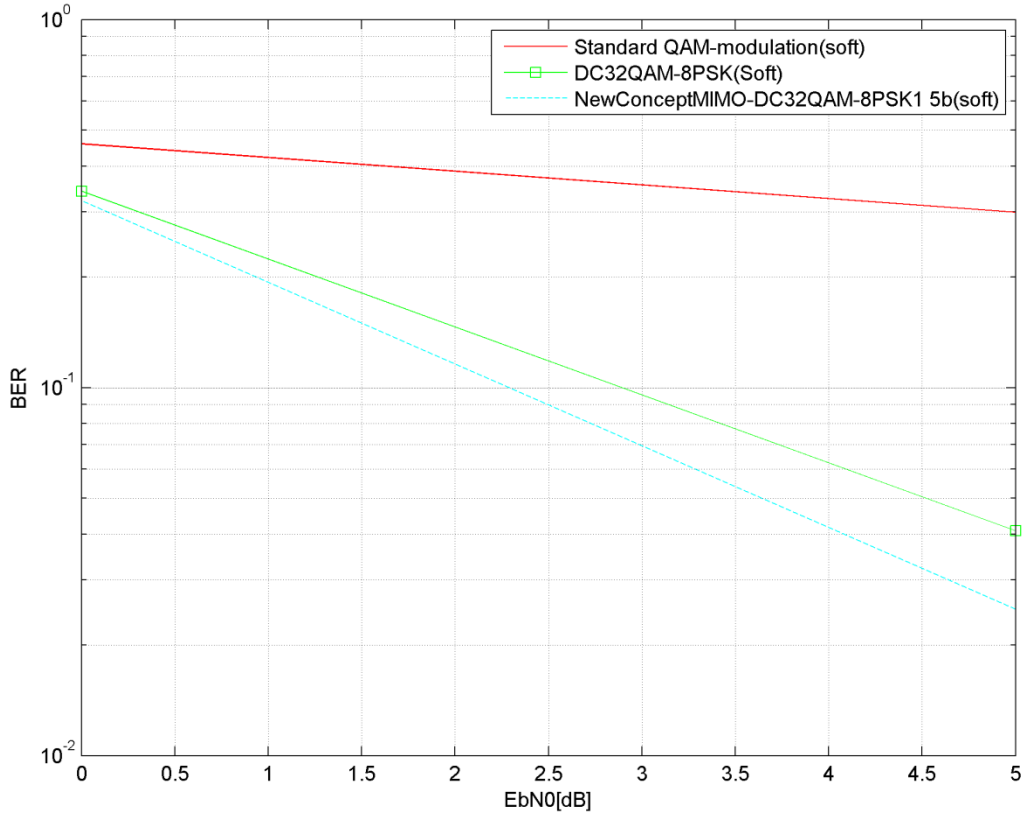

Figure (5.5.10): BER performance comparison for soft decoding at low SNR

5.9 Evaluation and verification of the spatial hypothesis

In this section, the model had been tested to determine the spatial diversity hypotheses that the MIMO configuration produce based on frequency domain analysis. Mathematical algorithm based on orthogonal configuration with the use of programming codes in Matlab environment was tested. The results were averaged over multiple packets in the SNR range of 0dB to 30dB. The behaviour of the system was analysed by implementing two transmitters and two receivers in the proposed multi-antennas model configuration. The results were then compared to the SISO DC 32-QAM model. Rayleigh fading channel with i.i.d. complex Gaussian entries was undertaken in the simulation to observe the model characteristic. Figure 5.5.11 shows that spatial diversity together with different channel spectrum for the MIMO model provides 7dB of improvement at 10^{-3} BER in comparison to the SISO DC 32-QAM. The frequency diversity ensures this additional gain in the SNR curve which reflects in the gradual improvements in the error performance of the model.

Furthermore, the BER curve for the SISO model diverges when reducing the BER threshold and moving at the upper region of the SNR which further highlights the increased signal strength that the MIMO configuration provides.

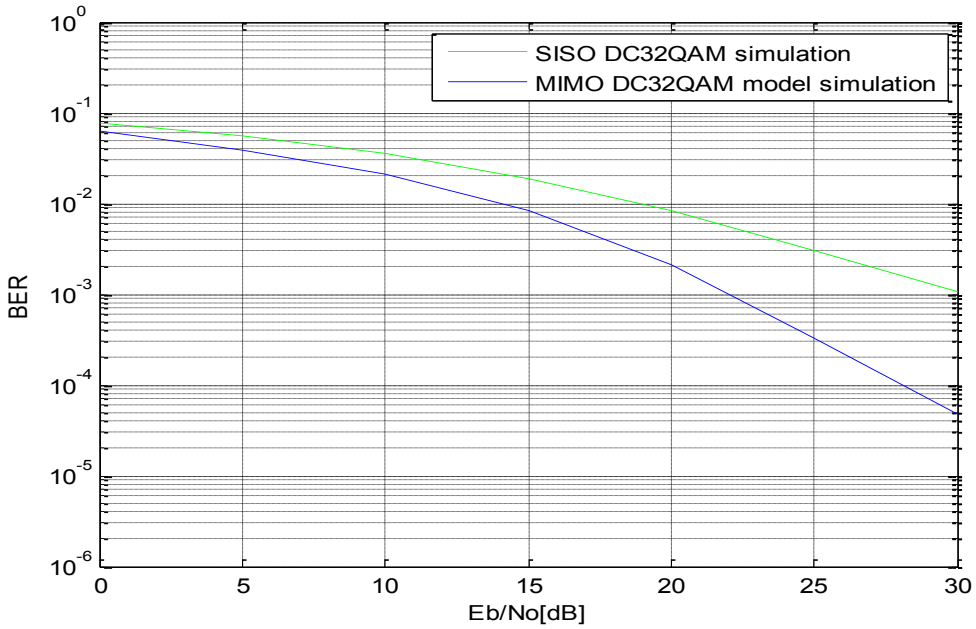

Figure (5.5.11): SISO DC32QAM vs MIMO DC32QAM BER evaluation

5.10 Evaluation based on CSI distortions

Figure (5.5.12) shows the case where the Channel State Information at the received is being corrupted and how the system perform in this circumstances. The CSI disturbance could be due to the nature of the dynamic environment in the indoor case scenario which normally very hostile, or could be due to the type of receiver being implemented. Furthermore, the mathematical algorithm being considered at the decoder would deviates the weight channel coefficients resulting in error estimation at the decoding process. At 10^{-3}BER, an improvement of 9dB could be observed when the decoder has enough knowledge of the pilot symbols for the model compared with noisy model. Regardless of the real implementing environment, the model had to show successful operation at all these scenario, hence the following graph indicate the performance of the design.

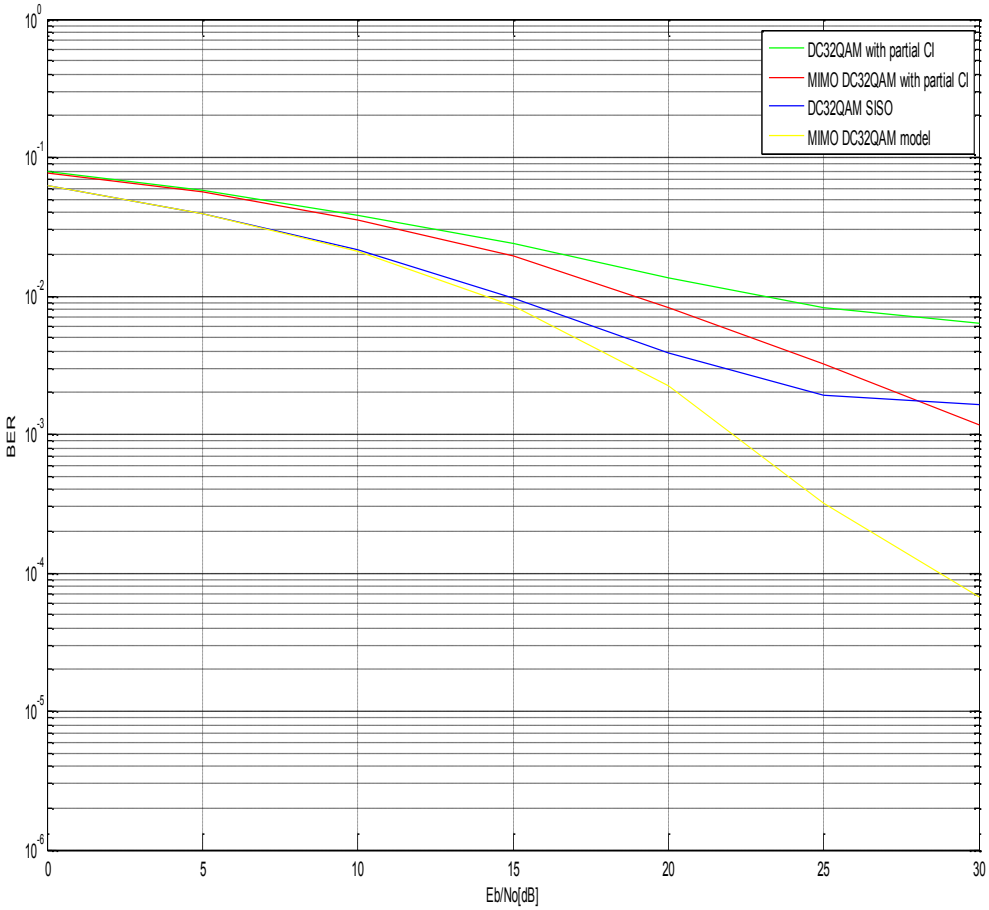

Figure (5.5.12): Models comparison with impairments in the CSI

5.11 Performance variation based on spatial configuration

The next figure (5.5.13), a test had been carried out to investigate the effect of the symbol conjugation on the model performance. In this simulation, two configurations had been taken, one with alternate conjugation in the complex plane. In the second configuration, the symbol pair transmitted from both antennas was omitted from the negative conjugation in the spatial domain. It could be noticed very clearly that the red curve representing the second configuration deviate deeply as the SNR increases and performance deteriorate rapidly. Moreover, the error rate figures increases and overshoot the standard DCM model with single radiating element.

.

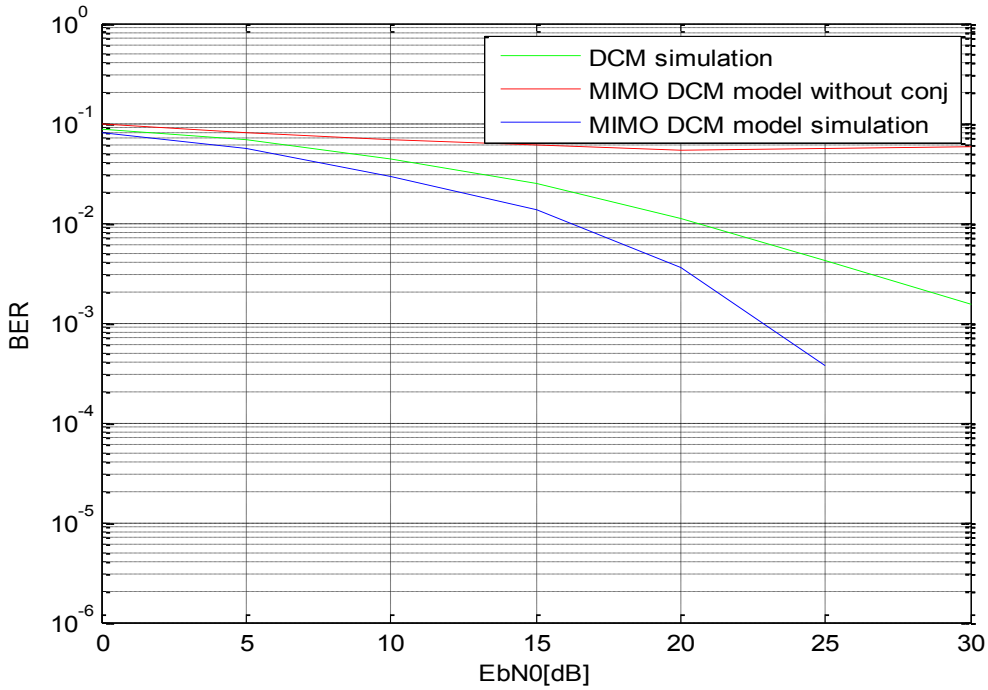

Figure (5.5.13): Spatial orthognality effect on BER of the proposed model

5.12 Comparative analyse based on increase in the order of modulation

In the following figure (5.5.14), another test had been carried out in order to investigate if increasing the number of bits in the modulation symbol and rearranging the constellation map would affect the model performance, and if so by how much and is there any explanation for that. The result had indicated clearly that the way the symbols had been scattered in the constellation diagram on the dual mapping would change the error rate performance in the models. The curves had shown that the SNR values increase slightly if the Euclidean distance between the same symbols across the two maps were further apart.

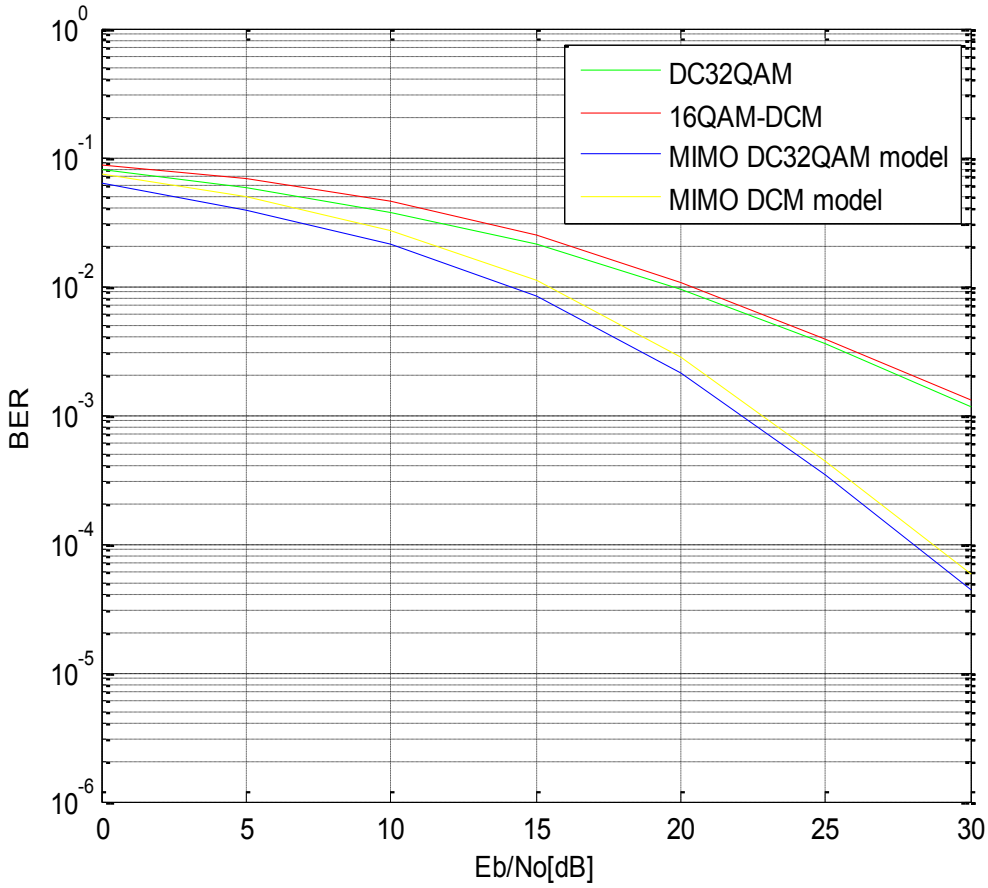

Figure (5.5.14): BER model performance based on rearranged constellation maps

5.13 Comparative analyse based on Analytical upper bound error probability

It is important to measure analytical the error performance between dual antenna system and classical single antenna structure. In this work, the upper bound error probability was evaluated in an analytical manner. The derived formula used in the design chapter was used in this simulation to evaluate mathematically the system performance in comparison with single antenna model. This evaluation was only based on numerical derivation, and statistical concepts were used to derive an upper bound on the error probability. Figure (5.5.15) shows the upper bound probability based on equation (3.4.49) in the design chapter.

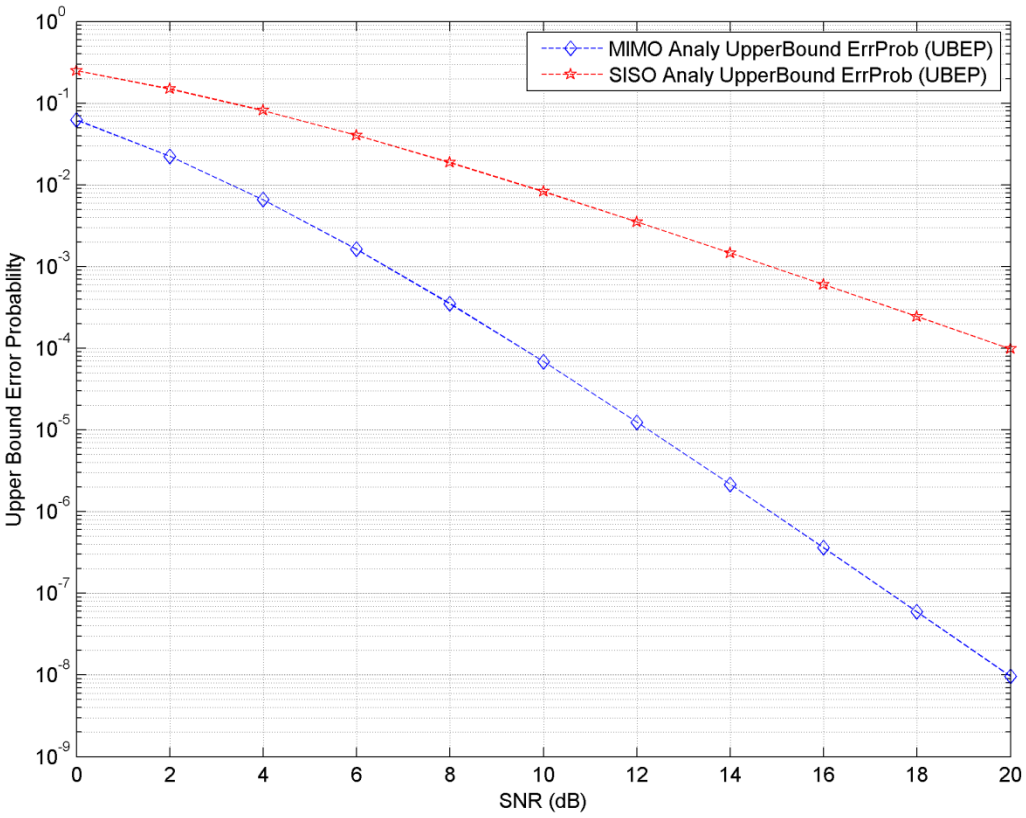

Figure (5.5.15): Analytical upper bound error probability comparison

5.14 Analysis of wireless range Evaluation

In this part, the modification of the model was evaluated to configure how the full frequency and spatial diversities was used to increase the coverage area. As the proposed aim here was to increase the receiving signal energy, and over shadowing the throughput. Therefore, the model had replaced the multiplexing technique with the use of diversity to strengthen the SNR at the receivers. The first figure (5.5.16) shows an error performance comparison between the modified model, the original designed model, and the previously proposed model (legacy model). The figure clearly shows the performance improvement the modified model achieved in comparison to the other concepts. Figure (5.5.17) on the other hand, shows the relation between the coverage area and packet error rate, and indicates the increase in the wireless range with the modification to the model that had shown in the design chapter. The calculated and simulated file data (figure 5.5.18) for the SNRs and BER values between the models were shown below.

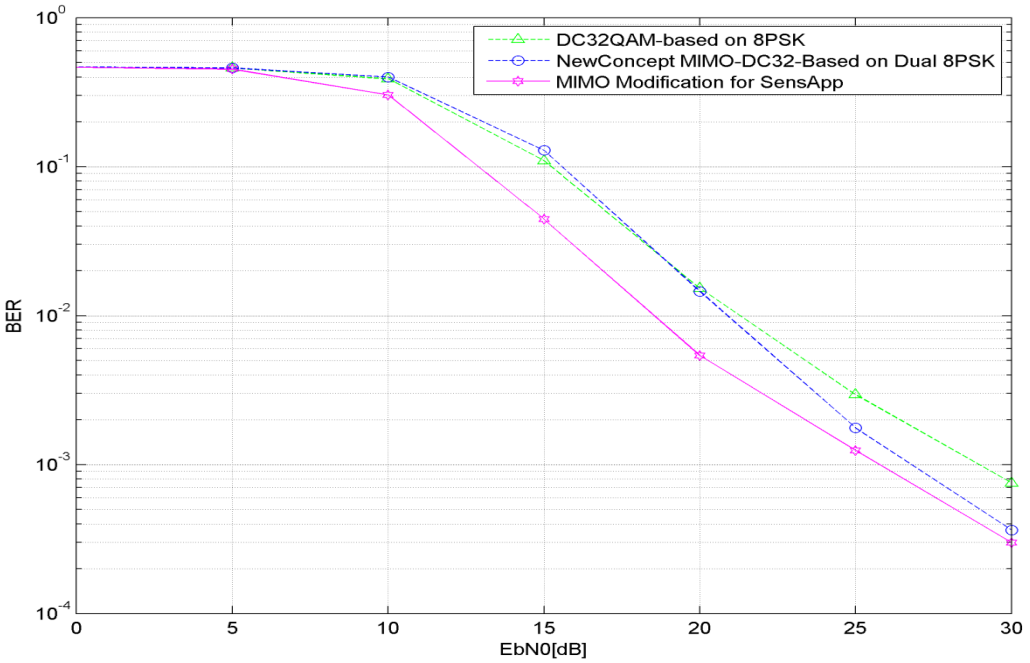

Figure (5.5.16): BER comparison between the proposed models

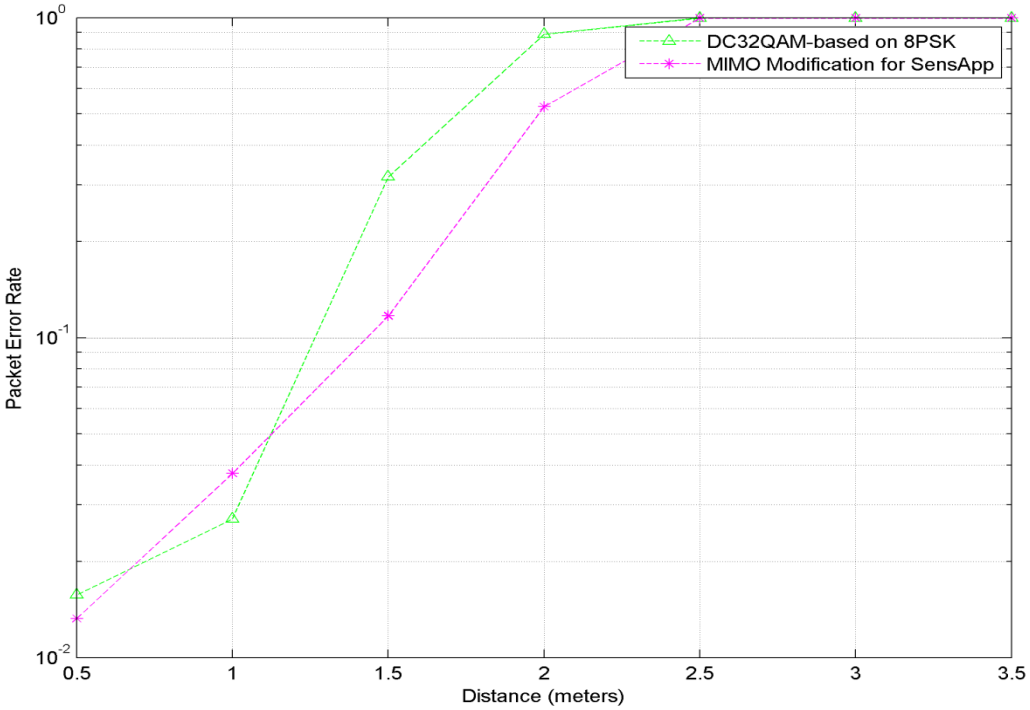

Figure (5.5.17): Performance comparison of the models over coverage area

```
EbN0  =    0[dB],  BER_for_DC32QAM-Based8PSK  =   4.649e-001,
NOE_for_DC32QAM-Based8PSK          =                  550
-------------------------------------------------------------
-----------
EbN0  =     0[dB],  BER_for_NewConpMIMO_DC32QAM-Based8PSK  =
4.691e-001,  NOE_for_NewConpMIMO_DC32QAM-Based8PSK  =    575
-------------------------------------------------------------
-----------
EbN0  =    5[dB],  BER_for_DC32QAM-Based8PSK  =   4.603e-001,
NOE_for_DC32QAM-Based8PSK          =                  543
-------------------------------------------------------------
-----------
EbN0  =     5[dB],  BER_for_NewConpMIMO_DC32QAM-Based8PSK  =
4.593e-001,  NOE_for_NewConpMIMO_DC32QAM-Based8PSK  =    522
-------------------------------------------------------------
-----------
EbN0  =   10[dB],  BER_for_DC32QAM-Based8PSK  =   3.837e-001,
NOE_for_DC32QAM-Based8PSK          =                  367
-------------------------------------------------------------
-----------
EbN0  =    10[dB],  BER_for_NewConpMIMO_DC32QAM-Based8PSK  =
4.008e-001,  NOE_for_NewConpMIMO_DC32QAM-Based8PSK  =    536
-------------------------------------------------------------
-----------
EbN0  =   15[dB],  BER_for_DC32QAM-Based8PSK  =   9.850e-002,
NOE_for_DC32QAM-Based8PSK        =                   56
-------------------------------------------------------------
-----------
EbN0  =    15[dB],  BER_for_NewConpMIMO_DC32QAM-Based8PSK  =
1.283e-001,  NOE_for_NewConpMIMO_DC32QAM-Based8PSK  =     53
-------------------------------------------------------------
-----------
EbN0  =   20[dB],  BER_for_DC32QAM-Based8PSK  =   1.167e-002,
NOE_for_DC32QAM-Based8PSK       =                    4
-------------------------------------------------------------
-----------
EbN0  =    20[dB],  BER_for_NewConpMIMO_DC32QAM-Based8PSK  =
1.125e-002,  NOE_for_NewConpMIMO_DC32QAM-Based8PSK  =      2
-------------------------------------------------------------
-----------
EbN0  =   25[dB],  BER_for_DC32QAM-Based8PSK  =   1.333e-003,
NOE_for_DC32QAM-Based8PSK       =                    0
-------------------------------------------------------------
-----------
EbN0  =    25[dB],  BER_for_NewConpMIMO_DC32QAM-Based8PSK  =
1.167e-003,  NOE_for_NewConpMIMO_DC32QAM-Based8PSK  =      0
-------------------------------------------------------------
-----------
```

```
EbN0  =   30[dB], BER_for_DC32QAM-Based8PSK  =   1.333e-003,
NOE_for_DC32QAM-Based8PSK       =                          0
-------------------------------------------------------------
-----------
EbN0  =    30[dB],  BER_for_NewConpMIMO_DC32QAM-Based8PSK  =
0.000e+000,  NOE_for_NewConpMIMO_DC32QAM-Based8PSK  =       0
-------------------------------------------------------------
-----------
```

Figure (5.5.18): File data collecting the SNRs and BER values between the models.

5.15 Conclusions

In this chapter, simulation of the proposed model was carried out and evaluation for the various setting results was identified. The simulation was performed across 2000 packets and repeated over 6 different SNR values in a Monte-Carlo simulation. In the aid of standard IEEE802.15.3.a channel model, stochastic discrete simulation had been performed using Matlab software package. The simulation work had been carried out based on integrated analysis in time and frequency domain in the first section. In the following section, frequency domain analysis was used to infer the spatial hypothesis of the proposed model and how this additional degree of freedom affects the error performance. The design and implementation included a generation of the signal, interleaving, coding, modulation and the signal transmission. Multipath channel has been used to emulate the multipath nature of the medium. Additive

White Gaussian Noise (AWGN) has been added to account for the additional distortion that includes equipment's (receiver and transmitter) and signal amplifications. The receiving block has been accomplished, and the design performance has been analysed by testing the system with predefined SNR values. The output has shown the results of the BER for the model and compared to theoretical values. In this work, MIMO techniques have been investigated in order to envisage a novel conceptual design that could be implemented in systems operating in free spectrum. The hostile indoor channel environments make these types of systems very challenging and very costly to build. Investigations of the core problems affecting the integration of multiple spatial elements has been undertaken in this work. Simulation results show the strength of the proposed model, and its operation in different Wireless and application settings with good error performance in comparison to pervious works. The proposed model design could be used as a basis for future work to address the current challenges in this field and provides a framework for future systems development

6. Conclusion

The aim of this chapter is to provide a summary of the presented results that had shown in the previous chapter, and gives a description of the proposed design along with the research objectives. A conclusion to the work, and recommendation for further research was then provided.

6.1 The research achievement

The design and implementation of the proposed multiple antennas concept applicable for WPAN applications had achieved the objectives set out in the first chapter. The model provided an increase in the transmission rate by twice the amount without the need to increase the radiating power or a decrease in the error rate performance. A successful transmission was observed with low

bit error rate, which could be used at the physical layer in low power requirement indoor wireless communication systems. In addition the model had facilitated the option of increasing the coverage area for special wireless sensor network application by making some modification to the wireless link structure.

All key objectives were achieved. A design model was developed that allows the integration of multi-antennas technique with orthogonal frequency division modulation in UWB-WPAN systems. The proposed project was designed to ensure that the goals and objectives completed by implementing low cost algorithms and digital components across at the transmitting and receiving blocks. In this aspect, the implementation had achieved its set up requirements. A conceptual algorithm was developed that allows the implementation of dual radiating elements including the modulation, coding, de-mapping, and detection at receivers that optimise the system performance in comparison with previously proposed models. The induced concept was conformed to the ECMA-368 wireless communication standard as stated in the objectives of research. In this context, the model design was based on this standard that specifies the physical and medium access control layers. The model had shown that changing the modulation scheme and the mapping method along with an optimisation to the receiving structures would result in an increase in throughput in an optimal performance. The concept used frequency diversity in the spectrum and spatial dimensions to increase the robustness of the system. The frequency diversity achieved by separating the transmitted

symbols by a large bandwidth spectrum (50 subcarriers with 206.25 MHz), taking advantage of the inherently rich multipath fading spectrum that span the UWB systems.

The Dual carrier 32QAM symbols were allocated into two individual OFDM data subcarriers with wide frequency separation ensured that deep channel fades in part of the spectrum would not affect the other used frequency band. This mapping method ensured an effective process in recovering the original signal information bits. This modulation scheme provided an increase in the transmission rate by doubling the throughputs, and this leaps enabled free license spectrum wireless link to have beyond Gigabit capability. The concept structure fits within the standard configuration without modification or changing to the transmitting and receiving modules requirements.

The coding scheme was designed to fit into the Physical Layer Service Data Unit encoding process. Phase shift keying was used in the high dimension mapping due to its unified symbol energy which reduces the noise disturbances between symbols in the signal to noise ratio. The signal points were allocated in circular loci across the constellation providing power constant for this modulation. Further, this scheme provides equal decision region for complex symbols across the map, which ensure equal energy distribution between the signal points. Allocating different signal power across the scatter diagram for modulation schemes results in variation in the probability of symbol error rates at the detection process, and that reduces the

overall error performance in the modulation schemes. This observation made the 8PSK modulation scheme an ideal candidate for the high dimension mapping, and that was observed in the performance of the model. On the other hand, higher order Quadrature amplitude modulations do not have fixed amplitude. Therefore these modulation plans tend to worsen the peak to average power ratio of the OFDM signals, and that reflected in the digital to analogue converters and the gain control mechanism.

Verification for the design was carried out with a number of tests including the IEEE802.15.3a UWB channel model standard to induce the objectives and the hypothesis requirements. The reviewing and inspection had shown that the model enables to overcome the poor radio channel condition and delivered error performance in an optimal manner in comparison to the lower rate signal that associated with single radiating element system. The model could increase the wireless coverage area by a modification to the receiving structure. The concept had achieved increased in the data rate, and system improvement while effectively maintaining low cost implementation in terms of the low power and high performance scheme. Due to the stringent power requirements set for wireless application operating at the free license spectrum (FCC regulation), this model represented a good fit that allow high rate transmission without the need to violate the standard requirements in terms of RF regulation. The design achieved good performance without an additional overhead to the ECMA standard. The contribution of this research enables multiple antennas configuration within the UWB technology within the

physical layer enabling increase in the through put, and facilitating its usability in modern indoor wireless applications.

6.2 Observation about the research process

The research and development of this project was accomplished by a number of interconnected modules. The model design of a physical layer MIMO-UWB wireless communication system operating in the free spectrum was achieved by concatenation of the transmitters, receivers and the physical channel models. The project was divided into layers and each one had its own

requirements and operational functions. The design tasks were spread across these layers with various degrees of complexity. The structure involved the transmitting module, the physical channel model and the receiver part, and this arrangement was embedded in the design. Encompassing this design structure, it is ability of backward compatibility for legacy systems with lower transmission rate. . The scheme used the inherent spatial and frequency diversities to boost the system performance by increasing the capacity, and facilitates higher throughput that dynamically varies to accommodate both the physical conditions and the type of wireless transmissions (data, videos, etc.).

The first layer of the design framework included transmitting module consisting of two spatial elements with initial design requirements. The second part of this phase constituted a multipath fading channel model designed to test and evaluates the system performance in terms of the spatial and frequency diversity presence. This in turn introduced more channels for the transmitted signal, and so improving the link budget. The receiving module represented the last sub-system within this layer, and included the decoding and estimation algorithms, as well as objects link requirements. The aim design for this layer was to evaluate the proposed concept and how to develop theoretical algorithms into working wireless systems. Therefore, a predefined metrics conditions was evaluated at the output of the receivers. In the case of not satisfying the test requirements, the design was then readjusted and modified until certain conditions are satisfied. This method enabled the development in stages with ascending order in term of complexity forming a bottom up

hierarchy.

Once this phase was completed, the next layer had included an advanced MIMO transmitting and receiving sub-systems. An additional Standardised IEEE802.15.3a channel model was included. The transmitting block included the objects within the pervious developed transmitting block, as well as stringent modulation and spatial requirements. The receiving block in this phase had included an optimised decoding and equalisation algorithms that met the desired requirements. The validation of the research hypotheses was met at this stage, and hence an iterative approach was applied. The results error performance was then compared with previous work and identified pre-set levels in the signal power. System optimisation was the third phase and covered the improvements to the model design and performance. The packet error rate (PER) for the communication link of both LOS and NLOS was further reduced in this sub-system. The complexities in the receiver were studied to make further improvement, and the overall design complexity was optimised.

Testing of the application included verification of particular conditions, by the simulation of hypothesised scenarios in order to test the fitness of the model. Additional requirements had been embedded into the model and then examined for approval purposes. Further development to the design was carried out in this stage so as to ensure practical feasibility of the system in real time environments.

The evaluation phase involved multiple tests of various indoor scenarios in

order to fulfil all the design requirements. Experimental analysis was applied to the final version of the developed design in order to validate the simulated design model against standardised and recognised approved models. Predefined parameters was used to test various fitness tests and systems requirements such as the time delay, bit error rate (BER), the signal to noise ratio (SNR) and the power profile. The necessity for this step was to match the system requirements with the achieved results and approves theoretical concepts. These results approved the design concept in increasing the link capacity, by the use of spatial element and contribute to the knowledge in this field.

The signal to noise power ratio in decibels was implemented in the simulation as know quantities. A defined vector was used to store the power ratio values in descending order. The noise power was changed based on alteration to the noise variance through the standard deviation in conjugation with the predefined SNR. The power spectral density of the AWGN was then limited by the limitation of the signal power at every time interval in the simulation. Expressing the standard deviation in terms of the SNR per transmitted signal had resulted in controlling the noise distortion on the received signals in the simulation environments.

6.3 Review of the complete proposed model

Previous work had shown that capacity could be improved by the use of multiple antenna system, and based on these researches the induced work had focused on increasing the performance with the use of dual radiating elements for WPAN. The work used multiplexing technique based on orthogonal division in the spectrum with OFDM modulation. OFDM technique gives immunity to inter-symbol interference, can be implemented at lower complexity FFT as it divides the spectrum, and could easily shape the spectrum. This scheme gave considerable improvement in the throughput and substantial increase in the SNR at the receiving end without increasing the transmission power. In this context, the work had used this proven theory to develop the concept which applicable for use in the UWB wireless indoor communication. MIMO technique strength comes in two folds, for capacity requirements systems it increases the data rate. For coverage area applications as wireless sensor network, it increases the signal power term of the snr at receivers without increasing the transmission power. This enabled increase in the coverage area for wireless systems. It is important to note that, backward compatibility is essential in developing new wireless models.

Multiple radiating elements with a pair of Dual Circular 32-QAM transmitting four complex symbols with a total of ten bits have the ability to deliver 1.2

Gb/s. The dual 8PSK symbols comes from lower dimension QPSK symbols. The most significant bit of every symbol represented the fifth bit within the original group (5 bits), and its bipolarity was used to deliver the two QPSK symbols into the upper constellation maps (8ary-PSKs). Diversity was observed in the fifth bit across both complex symbols. The scheme took a dual of 500 coded and interleaved bits across two radiating elements, and conforming to backward compatibility by spreading the mapping with 250 coded bits across every branch. The design used the defined convolutional encoder specified for the higher data rate within the standard, along with fast Fourier transform with only 128 frequency tones that is applicable for low cost analogue to digital convertors. The finalised concept provided high bit-rate wireless communication between devices which could be suitable for streaming high definition video between consumer products, without consuming high frequency clock rates.

The structure of the receivers was designed in order to translate the dimension of the received symbols according to a novel transformation process. The received symbols coming to the receivers had different channel state information reflected in the equalisation process within every group bits (a symbol has 5 bits). The proposed concept transfers the 8PSK symbols to QPSK symbols which gives a number of advantages. Firstly, this translation reduces the decoding searching subspace, and widens the de-mapping constellation. Dense constellation with high number of points tends to have large symbol error rate in comparison to the less dense constellation

modulation systems. The difference in dimension creates differences in the Euclidean powers required for the noise powers, in order to shift the received symbol to one of its neighbouring symbol's region. Error in the decoding occurs if the received symbol was shifted into another symbol's region. The larger the Euclidian distance between neighbouring symbols, the larger the noise power requirement needed to force symbol error detection the transmission. The larger the constellation dimensions with more complex symbols, the lower the Euclidian metric between constellation points. Therefore, the idea of this proposed model concept was to transfer the received symbol to a lower constellation dimension, and then performs the decoding process. This way, the Euclidean metric between symbols was increased before the de-mapping, and hence reducing the overall symbol and bit error of the system. The novelty here was increasing the error performance without increasing the receiver complexity which adds to software, hardware and overhead costs. Further, the induced method reduces the internal of the digital logic in the IFFT and FFT, and the precision of the ADC and DAC. The QPSK gives a large sub-carrier spacing in comparison to the more dense 8 points constellation, and this reflected on the noise requirement in the carrier synthesis, and improves the system robustness to synchronisation errors.

6.4 Future research recommendation

In consideration to the proposed concept, there are areas that could be taken in further research. This physical layer model was intended for a single standard, and additional work could be carried out in order to allow the multiple antennas model to be applicable with other international standards. The cross standards compatibility could make it more commercially viable, and improve the market potential for this physical layer configuration.

The framework for developing models for UWB-WPAN in the PHY centred around a low complexity and implementation cost. On the other hand, there are powerful coding schemes that give good code performance that is close to the Shannon theory limit, but have complexity and cost attached to them. Implementing an advance receiving algorithm would have cost attached to that, and therefore further research in obtaining cost effective receiving

structure is very critical in the progression of this technology. The coding algorithm could be optimised by researching a new novel concept in integrating more advanced Forward error correction methods. In this context, a further research in obtaining an optimised algorithm that reduces the complexity requirements of these strong coding methods to fit in the Wireless personal area network systems. One such scheme is the turbo code, where it represented an advanced algorithm that produces strong forward error correction code. This method improves the coding gain which is critical in optimising the error performance. The corresponding decoding process for this method requires more accurate equalisers. Therefore, additional work needed to reduce the computational complexity involves in constructing an optimised equalisers for multiple antennas systems that fits within wireless portable devices. Channel state information aided de-mapping scheme could be improved to further optimise the channel knowledge to strengthen the received signal. One way is to induce stronger algorithm at the receivers for systems with receivers only CSI configuration (No feedback CSI at transmitters). In conjunction with this, further research could be carried out to enable the use of differential modulation method that works between consecutive codes in order to overcome the channel estate information errors that results in decoding errors at receivers, and error performance degradation. One more option could be introducing feedback with the formation of transmitter side CSI, which distribute the transmitting signal power according to the channel condition

The hardware is another area that requires further research. Hardware implementation solutions for clock rates to accommodate the ever increasing data rates, and fast wireless connection would be a challenge in low cost and low sizes indoor wireless systems and portable devices. Architecture and logic design on circuit boards would be problem in low budget devices, and further research in these areas is essential to ensure the success of the technology. The wireless applications using this technology have size and power limitation, and therefore further research in the hardware architecture could further improved the implementation of the model in the physical layer. The challenges of the wireless portable devices that operate in the free license spectrum are the size limitation, limited research in the area, and the financial cost requirements (high silicon cost, and high electrical power)). In order to make high data rate transmission available in the market at affordable prices, investment in the research for improving the system clock rate, and its integration at FPGA is essential. To this end, further advanced in signal processing could enable high frequency clock to be integrated in the physical structure. The high frequency rate enables the implementation of large dimension FFT that could be fit within the PHY and MAC layer standard. Increasing the number of frequency index modulation allows the use of frequency diversity with this model across all modulated symbol bits. This in turns gives the model additional coverage area without reduction in the throughput.

The radio channel condition represents a critical parameter in degrading the performance of the wireless link in the free license spectrum. The limited current research in the area of UWB propagation makes it very challenging to obtain a physical wireless link model that operate in this large spectrum, and fully depends on existing channel models. The channel response behaviour and peculiarities are not fully defined in statistical and current measurement model and that requiring further research in order to accurately define its impulse response across the spectrum. In this context, further research in the UWB channel response particularly at upper spectrum was needed in order to test MIMO configuration model at the physical layer. As there are limited current researches in the channel behaviour, it would be useful to carry out more measurement campaign across the free licences spectrum.

6.5 Concluding Remarks

In this work, a model design was constructed that increases the throughput of indoor wireless network systems with the use of dual radiating elements at the both transmitter and receiver. A simulation model was developed that encapsulate the proposed design. Furthermore, the range of the indoor wireless network could be increased in practical wireless sensor networks. The model allows the wireless range to be extended by the use of diversity across the spatial and frequency domains, based on adjustment to the receiver structure. The outcome of the work is summarised in a MIMO model design that fits within the ECMA-368 Standard. The design enables a transmission rate of 1200 Mbps at the physical layer. In addition, the coverage area could be increased at a compromise in throughput for wireless range applications. Tests had been carried out which investigate the performance characteristics of various spatial and modulation proposals and identifies the challenges surrounding their deployments. Results analysis based on various simulation tests including the IEEE802.15.3a UWB channel model had shown a lower error rate performance in the implementation of the model. The proposed model can be integrated in commercial indoor wireless networks and devices with relatively low implementation cost. Further, the design could be used in future work to address the current challenges in this field and provides a framework for future systems development.

REFERENCES

1) “First report and order, revision of part 15 of the commission’s rules regarding ultra

-wideband transmission systems,” FCC, ET Docket 98-153, Feb. 14, 2002.

2) Batra, A.; Balakrishnan, J.; Dabak, A.; , "Multi-band OFDM: a new approach for UWB ,"Circuits and Systems, ISCAS '04. Proceedings of the 2004 International Symposium on,vol.5, no., pp. V-365- V-368 Vol.5, 23-26 May 2004.

3) Wylie-Green, M.P.; Ranta, P.A.; Salokannel, J.; , "Multi-band OFDM UWB solution for IEEE 802.15.3a WPANs," Advances in Wired and Wireless Communication, IEEE/Sarnoff Symposium on , vol., no., pp.102-105, 18-19 April 2005.

4) “Standard ECMA-368: High rate ultra wideband PHY and MAC standard,” ECMA, First Edition, Dec. 2005.

5) R. S. Sherratt, "Design issues toward a cost effective physical layer for multiband OFDM (ECMA-368) in consumer products," Consumer Electronics, IEEE Transactions on, vol.52, pp. 1179-1183, 2006.

6) R. S. Sherratt, "Design Considerations for the Multiband OFDM Physical Layer in Consumer Electronic Products," in Consumer Electronics, 2006. ISCE '06. 2006 IEEE Tenth International Symposium on, 2006, pp. 1-5.

7) T. Lunttila; S. Iraji; H. Berg; , "Advanced Coding schemes for a Multiband OFDM Ultrawideband System towards 1 Gbps ," IEEE CCNC 2006.

8) J. G. Proakis , “ Digial communications”, Fourth Edition, McGraw-Hill, International Edition, 2001.

9) B. A. Cetiner, E. Akay, E. Sengul, and E. Ayanoglu, "A MIMO System With Multifunctional Reconfigurable Antennas," Antennas and Wireless Propagation Letters, IEEE, vol. 5, pp. 463-466, 2006.

10) L. Junsheng, M. Ghavami, C. Xiaoli, B. Allen, and W. Malik, "Diversity Analysis of Multi-Antenna UWB Impulse Radio Systems with Correlated Propagation Channels," in Wireless Communications and Networking Conference, 2007.WCNC 2007. IEEE, 2007, pp. 1593-1598.

11) A. Stephan, J. F. Helard, and B. Uguen, "MIMO UWB Systems Based

on Linear Precoded OFDM for Home Gigabit Applications," in Global Telecommunications Conference, 2008. IEEE GLOBECOM 2008. IEEE, 2008, pp. 1-6.

12) J. Paulraj, D. A. Gore, R. U. Nabar, and H. Bolcskei, "An overview of MIMO communications - a key to gigabit wireless," Proceedings of the IEEE, vol. 92, pp. 198-218, 2004.

13) L. Zhiwei, P. Xiaoming, F. Chin, and P. Khiam Boon, "Enhanced MB-OFDM UWB system with multiple transmit and receive antennas," in Ultra-Wideband, 2009. ICUWB 2009. IEEE International Conference on, 2009, pp. 793-797.

14) K. Su-Nam, U. Chul-Yong, K. Dong-Wook, and K. Ki-Doo, "A study on the wireless MIMO-UWB transceiving techniques for WPAN," in Consumer Electronics, 2005. ICCE. 2005 Digest of Technical Papers. International Conference on, 2005, pp. 91-92.

15) W. P. Siriwongpairat, W. Su, M. Olfat, and K. J. R. Liu, "Space-time-frequency coded multiband UWB communication systems," in Wireless Communications and Networking Conference, 2005 IEEE, 2005, pp. 426-431 Vol. 1.

16) H. Jia and L. Moon Ho, "UWB MIMO System with Cooperative Multi-path Diversity, " in Intelligent Pervasive Computing, 2007. IPC. The 2007 International Conference on 2007, pp. 128-131.

17) H. Xu and S. Dharmendra, "Behaviors of MIMO UWB-IR Transceiver with Statistical Models," International MultiConference of Engineers & Computer Scientists 2009, pp.440-444, 2009.

18) A. Jinyoung and K. Sangchoon, "Performance of UWB MIMO Systems with Rake Receive Processing," in Communication Software and Networks, 2010. ICCSN '10.Second International Conference on, 2010, pp. 165-168.

19) Y. Cho, J. Kim, W.Yang,C. Kang , " MIMO-OFDM Wireless Communications with Matlab", John Wiley and Sons, 2010.

20) T. Koike-Akino, "Bit-Flipping Equalizer and ML Search-Space Analysis in Ultra-Wideband MIMO Channels," in Global Telecommunications Conference, 2008. IEEE GLOBECOM 2008. IEEE, 2008, pp. 1-5.

21) Z. Lin, B. Premkumar, and A. S. Madhukumar, "MMSE detection for high data rate UWB MIMO systems," in Vehicular Technology Conference, 2004. VTC2004-Fall. 2004 IEEE 60th, 2004, pp. 1463-1467 Vol. 2.

22) N. Malhouroux-Gaffet, P. Pajusco, and E. Haddad, "Effect of propagation phenomena on MIMO capacity of wireless systems between 3 and 10 GHz," in Antennas and Propagation (EuCAP), 2010 Proceedings of the Fourth European Conference on, 2010,pp. 1-5.

23) J. Chusing, L. Wuttisittikulkij, and S. Segkhoontod, "Achieving Rate Two Space-Time-Frequency Codes for Multiband UWB-MIMO Communication Systems Using Rotated Multidimensional Modulation," in Communication Networks and Services Research,2007. CNSR '07. Fifth Annual Conference on, 2007, pp. 294-301.

24) J. Adeane, W. Q. Malik, I. J. Wassell, and D. J. Edwards, "Simple correlated channel model for ultrawideband multiple-input multiple-output systems," Microwaves, Antennas & Propagation, IET, vol. 1, pp. 1177-1181, 2007.

25) M. Borgmann and H. Bolcskei, "On the capacity of noncoherent wideband MIMO-OFDM systems," in Information Theory, 2005. ISIT 2005. Proceedings. International Symposium on, 2005, pp. 651-655.

26) T. Kaiser, Z. Feng, and E. Dimitrov, "An Overview of Ultra-Wide-Band Systems With MIMO," Proceedings of the IEEE, vol. 97, pp. 285-312, 2009.

27) T. Kaiser and M. El Hadidy, "A Signal Processing Framework for MIMO UWB Channels with Real Antennas in Real Environments," in Ultra-Wideband, 2007. ICUWB 2007. IEEE International Conference on, 2007, pp. 111-116.

28) Iqbal, S. M. Riazul Islam, and K. S. Kwak, "Minimum mean square error-ordered successive interference cancellation (MMSEOSIC) in UWB-MIMO systems," in Information and Communication Technology Convergence (ICTC), 2010 International Conference on, 2010, pp. 53-54.

29) M. Jaekyun, J. Hui, J. Taehyun, and L. Sok-Kyu, "Channel estimation for MIMO-OFDM systems employing spatial multiplexing," in Vehicular Technology Conference, 2004.VTC2004-Fall. 2004 IEEE 60th, 2004, pp. 3649-3654 Vol. 5.

30) G. J. R. Kumar and K. S. Shaji, "Low complexity algorithm for channel estimation of UWB MIMO-OFDM wireless fading channels," in Emerging Trends in Robotics and Communication Technologies (INTERACT), 2010 International Conference on, 2010, pp. 125-128.

31) H. Jia and L. Moon Ho, "M-ary Signals in UWB MIMO System Using Orthogonal Space Time Block Codes," in Communication Technology, 2006. ICCT '06. International Conference on, 2006, pp. 1-4.

32) G. L. Stuber, J. R. Barry, S. W. McLaughlin, L. Ye, M. A. Ingram, and T. G. Pratt, "Broadband MIMO-OFDM wireless communications," Proceedings of the IEEE, vol. 92,pp. 271-294, 2004.

33) W. P. Siriwongpairat, S. Weifeng, M. Olfat, and K. J. R. Liu, "Multiband-OFDM MIMO coding framework for UWB communication systems," Signal Processing, IEEE Transactions on, vol. 54, pp. 214-224, 2006.

34) Alamounti, S.M. (1998) A simple transmit diversity scheme for wireless communications. IEEE J. Select. Areas Commun., 16(8), 1451–1458.

35) F. Molisch, "Ultra-Wide-Band Propagation Channels," Proceedings of the IEEE, vol. 97, pp. 353-371, 2009.

36) R. J. M. Cramer, R. A. Scholtz, and M. Z. Win, "Evaluation of an ultra-wide-band propagation channel," Antennas and Propagation, IEEE Transactions on, vol. 50, pp. 561-570, 2002.

37) F. Molisch, "Ultrawideband propagation channels-theory, measurement, and modeling," Vehicular Technology, IEEE Transactions on, vol. 54, pp. 1528-1545, 2005.

38) V. P. Tran and A. Sibille, "UWB Spatial Multiplexing by Multiple Antennas and RAKE Decorrelation," in Wireless Communication Systems, 2005. 2nd International Symposium on, 2005, pp. 272-276.

39) L. Zhiwei, P. Xiaoming, P. Khiam Boon, and F. Chin, "Kronecker Modelling for Correlated Shadowing in UWB MIMO Channels," in Wireless Communications and Networking Conference, 2007.WCNC 2007. IEEE, 2007, pp. 1583-1587.

40) F. Molisch, K. Balakrishnan, D. Cassioli, C. Chia-Chin, S. Emami, A. Fort, J. Karedal, J. Kunisch, H. Schantz, and K. Siwiak, "A comprehensive model for ultrawideband propagation channels," in Global Telecommunications Conference, 2005. GLOBECOM '05. IEEE, 2005, pp. 6 pp.-3653.

41) F. Molisch, J. R. Foerster, and M. Pendergrass, "Channel models for ultrawideband personal area networks," Wireless Communications, IEEE, vol. 10, pp. 14-21, 2003.

42) Y. Jun, A. Seyedi, D. Birru, and W. Dong, "Design and Performance of Multi-Band OFDM UWB System with Multiple Antennas," in Personal, Indoor and Mobile Radio Communications, 2007. PIMRC 2007. IEEE 18th International Symposium on, 2007, pp.1-5.

43) Batra, J. Balakrishnan, G. R. Aiello, J. R. Foerster, and A. Dabak, "Design of a multiband OFDM system for realistic UWB channel environments," Microwave Theory and Techniques, IEEE Transactions on, vol. 52, pp. 2123-2138, 2004.

44) W.Zhang,X.Xia , and K.Letaief, "Space-Time/Frequency coding for MIMO-OFDM in next generation broadband wireless system", IEEE Wireless Communications, June 2007.

45) Shu Lin, Daniel J.Costello, Error Conrtol Coding: Fundamentals and Applications ", Prentice Hall, 1983.

46) Viterbi AJ (April 1967). "Error bounds for convolutional codes and an asymptotically optimum decoding algorithm". *IEEE Transactions on*

Information Theory **13** (2): 260–269.

47) L.Bahl, J.Cocke, F.Jelinek, and J.Raviv, "Optimal Decoding of Linear Codes for minimizing symbol error rate", IEEE Transactions on Information Theory, vol. IT-20(2), pp.284-287, March 1974.

48) Jakob Dahl Andersen, “Turbo Codes Extended with Outer BCH Code”, *Electronics letters*, vol. 32 No. 22, Oct. 1996.

49) C. Soobum and P. Sang Kyu, "PAPR performance of dual carrier modulation using improved data allocation scheme," in Advanced Communication Technology (ICACT), 2011 13th International Conference on, 2011, pp. 115-118.

50) L. C. Tran and A. Mertins, "Differential Space-Time-Frequency Codes for MB-OFDM UWB with Dual Carrier Modulation," in Communications, 2009. ICC '09. IEEE International Conference on, 2009, pp. 1-5.

51) R. S. Sherratt and R. Yang, "A Dual QPSK Soft-demapper for ECMA-368 Exploiting Time-Domain Spreading and Guard Interval Diversity," in Consumer Electronics, 2007.ICCE 2007. Digest of Technical Papers. International Conference on, 2007, pp. 1-2.

52) Neogy, T. S. Chakraborty, and S. Chakrabarti, "Algorithm selection and hardware implementation for channel equalization in MB-OFDM Based UWB communications for indoor WPAN applications," in Ultra Modern Telecommunications and Control Systems and Workshops (ICUMT), 2010 International Congress on, 2010, pp. 888-895.

53) Batra and J. Balakrishnan, "Improvements to the multi-band ofdm physical layer," in Consumer Communications and Networking Conference, 2006. CCNC 2006. 3rd IEEE,2006, pp. 701-705.

54) R. Hyun-Seok, L. Jun-Seok, and C. G. Kang, "BER analysis of dual-carrier modulation (DCM) over Rayleigh fading channel," in Ultra Modern Telecommunications and Control Systems and Workshops (ICUMT), 2010 International Congress on, 2010, pp. 717-721.

55) T. H. Nguyen, T. H. Nguyen, V. T. Tran, B. G. Truong Vu, and V. D. Nguyen, "A scheme of Dual Carrier Modulation with Soft-decoding for MB-OFDM MIMO systems," in Advanced Technologies for Communications (ATC), 2011 International Conference on, 2011, pp. 220-223.

56) M. Vestias, H. Santos, and H. Sarmento, "DCM demapper for MB-OFDM on FPGA," in Consumer Electronics (ICCE), 2010 Digest of Technical Papers International Conference on, 2010, pp. 125-126.

57) Y. Runfeng and R. Sherratt, "Enhancing MB-OFDM throughput with dual circular 32-QAM," Consumer Electronics, IEEE Transactions on, vol. 54, pp. 1640-1646, 2008.

58) Z. Feng and T. Kaiser, "On the Evaluation of ChannelCapacity of

UWB Indoor Wireless Systems," Signal Processing, IEEE Transactions on, vol. 56, pp. 6106-6113, 2008.

59) B. Ray, P. K. Venkataraghavan, and B. Sriram, "Equalization for Multiband OFDM based UWB Systems," in *Vehicular Technology Conference, 2007. VTC2007-Spring. IEEE 65th*, 2007, pp. 3081-3085.

60) Parag A. Dighe, Ranjan K. Mallik, " Analysis of Transmit–Receive Diversity in Rayleigh Fading," *IEEE TRANSACTIONS ON COMMUNICATIONS, VOL. 51, NO. 4, APRIL 2003.*

61) M. Torabi, D. Haccoun, W. Ajib, " BER Performance Analysis of Multiuser Diversity with Antenna Selection in MRC MIMO Systems," IEEE Communications Society publication in the IEEE "GLOBECOM" 2009 proceedings.

Bibliography

"Digital communication over fading channels"(second edition) by Marvin Kenneth Simon 1939- Mohamed-Slim Alouini. Hoboken, N.J. : Wiley-Interscience. ISBN 0471715239

"Principles of digital communication systems and computer networks" by K.V.Prasad. Hingham Mass.: Charles River Media. ISBN 1584503297

"Wireless personal and local area networks" by Axel Sikora. Chichester : Wiley. ISBN 0470851104

"Wireless communications and networking" by Vijay Kumar Garg. Amsterdam ; Boston : Elsevier Morgan Kaufmann. ISBN 9780123735805

"Wireless networks : from the physical layer to communication, computing, sensing, and control" by Giorgio Franceschetti; Sabatino Stornelli. Burlington, MA : Academic Press. ISBN 9780080481791

"Digital Communications"(fourth edition) by John. Proakis. McGraw-Hill. ISBN 0072321113

"Error Control Coding: Fundamentals and Applications" by Shu Lin, Daniel J. Costello. Prentic-Hall. ISBN 013283796X

"MIMO-OFDM wireless communications with MATLAB" by Y. Cho, J. Kim, W. Yang, C. Kang. John Wiley & Sons (Asia) Pte Ltd, 2 Clementi Loop, # 02-01. ISBN 978-0-470-82561-7

"Space-Time Coding for Broadband Wireless Communications" by Georgios B. Giannakis, Zhiqiang_Liu, Xiaoli_Ma, Shengli_Zhou. John Wiley & Sons. ISBN 047146287X

Appendix

A summary of specified functions from the main design and implementation folders had been shown below

constellation8psk1: Generate the first 8PSK map in the DC32QAM

constellation8psk2: Generate the second 8PSK map in the DC32QAM

constellation1: Generate the first 16QAM map in the DCM

constellation2: Generate the second 16QAM map in the DCM

constellationqpsk1: Generate the QPSK map in the modulation

constellation32: Generate the first DC based on 32QAM constellation

constellation32_Qray_A: Generate the second DC based on 32QAM constellation

TransAntennas2Tx: Map two DCM symbols into four

subcarrier tones within dual antennas configuration across twice the dual constellation maps (constellation1 & constellation2).

TransDCM: Map the DCM symbol into two subcarrier tones within single antenna configuration across the dual constellation maps (constellation1 & constellation2).

TransAntennas32: Map the DC 32-QAM symbol into two subcarrier tones within single antenna configuration across the dual constellation maps (constellation32 & constellation32_Qray_A).

TransAntennas2Tx_DC32QAM: Map two DC 32-QAM symbols into four subcarrier tones within dual antennas configuration across twice the dual constellation maps (constellation32 & constellation32_Qray_A).

Mapping: Map the four bits symbol into two dimensional complex number representing a DCM symbol.

Mapping32: Map the five bits symbol into two dimensional complex number representing a DC 32-QAM symbol.

MappingD8psk1: maps the QPSK complex symbols based on the value of fifth bit to the higher PSK constellation map (the 1st 8PSK map)

MappingD8psk1: maps the QPSK complex symbols based on the value of fifth bit to the higher PSK constellation map (the 2nd 8PSK map).

tranmatrix: Applies the DCM matrix across the two complex number to produce the two DCM symbols.

tranmatrix2Tx: Applies a pair of DCM matrix across four complex numbers to produce two pair of DCM symbols.

Channlisation: Multiply the transmitted signal with the channel coeffients in the frequency domain and then adding AWGN to the end product.

Noise: Generate additive white guassin noise with a predefined power spectral density.

Decodmatrix: Reproducing the original symbol by applying the reverse DCM matrix across the dual DCM symbols and combining them.

Decodmatrix2Rx2: Reproducing the two original symbols by applying the reverse DCM matrix across the pair of the dual DCM symbols and combining them.

DataGen: This function generate the transmitted signals based on pseudo random generation method using built in algorithm stored in the library functions.

MRC_Mod_cal: Return the estimated symbol (constellation points) based on calculation of the distance metrics of each received signal from all the constellation points. Then, it finds the min distance from these metrics, and returns the constellation complex symbol with the min dis.

Channlisation: performs the frequency domain convolution by multiplying the signal with the channel confinements.

TransformConcept: Applies transformation across the dual qpsk symbols to introduce the new dual complex symbols for transmition within the MIMO configuration.

ReTransformConcept: This function readjusts the received psk symbols in order to reproduce the original qpsk symbols.

Redemap8psktoqpsk1: Remaps the 8PSK symbol to the QPSK complex

symbol based on the value of the third bit

SoftLLRDemappingqpsk: performs calculation for the Euclidean metrics used in the Log likelihood ratio method.

SoftDemappingqpsk: performs calculation for the Euclidean metrics used in in the input Viterbi function as pure metrics.

RecAntenDCMLLRSoft_QPSK: This function performs Soft Demapping using log likelihood ratio method

RecAntenDCMSoft_QPSK: This function performs Soft Demapping that used as input to the Viterbi decoder as pure soft Euclidean metrics.

RecAntennasSoft32psk1: This function performs Soft Demapping based on the DC32QAM using the first 8PSK constellation.

RecAntennasSoft32psk2: This function performs Soft Demapping based on the DC32QAM using the second 8PSK constellation.

DemappingSoft8psk1: This function performs Soft Demapping on the Euclidean metrics of the complex symbols related to the first 8PSK constellation.

DemappingSoft8psk2: This function performs Soft Demapping on the Euclidean metrics of the complex symbols related to the second 8PSK constellation.

MainSoftLLRRayleighNewConceptComparsion: The main body where the LLR decoding method was applied on the model with comparison to previous models based on multipath fading channel.

MainSoftIndoorNewConceptComparsion: The main body where the soft

decoding method was applied on the model with comparison to previous models based on standard IEEE channel for indoor wireless communication.

MainHardRayleighNewConceptComparsion: The main body where the hard decoding method was applied on the model with comparison to previous models models based on multipath fading channel with different settings.

MainSoftLLRRayleighNewConceptComparsion3: The main body where the LLR decoding method was applied on the model with comparison to previous models based on multipath fading channel with different settings.

MainSoft_LLRComparsionIndoor: The main body where the LLR and ML soft decoding methods were applied and compared on the model with comparison to previous models based on standard IEEE channel for indoor wireless communication.

MainHardIndoorNewConceptComparsion: The main body where the hard decoding method was applied on the model with comparison to previous models based on standard IEEE channel for indoor wireless communication.

MRC_calculation: Perform Maximum Ratio combining technique at the receiver.

SigShift: segment the data subcarriers into two folds and then insert the guard and pilot carries to the end of the segments, followed by reverse both sections for the IFFT operation.

ErrorCalculation: Calculate the number of errors by comparing the received samples with the transmitted samples.

ErrorPlot: Plot the error performance curve in a graphical form comparing the performance of the system as the signal to noise power in dB increases in discrete interval.

```
==========================================================
==========


clear all

% main_UWB1

%==========================================================
==========================================================
==============================================

%Initial parameters

N_tx = 2;

Nrm = sqrt(10); % DCM_QPSK Normlisation

Nrmqpsk= sqrt(6.175); % DC32-8PSK Normlisation

Nrmf32 = sqrt(210/8);%MIMO-DC32-QAM-Flip Normalisation

%Nrmf32 = sqrt(62/3);%MIMO-DC32-QAM-Flip Normalisation

frame_length = 1200;frame_length2 = 1500;

sgpsk1=0;sgpsk2=0;sgf1a=0;sgf1b=0;sgf2a=0;sgf2b=0;sgnew1a=0;sgnew1b=
0;% signal power

sgpp1=0;sgpp2=0; sgz1a=0; sgz1b=0; sgz2a=0;
sgz2b=0;sgnew2a=0;sgnew2b=0; % signal power

ThresholdErros = 1000;

Chanl = 'Multipath channel';

nfs=300; % Number of symobles
```

```
%PdB=[0 -5 -11 -13 -17 -19 -21 -25 -30 -45];

PdB=[0 -8 -17 -21 -25];

%dly = [0 3 5 6 8 9 10 11 12 13];

dly = [0 3 5 6 8];

dly1b = [0 3 5 6 8 14 16 18 19 20];

dly2a = [4 12 15 17 21];

%dly2a = [4 12 15 17 21 30 32 34 36 38];

DSM=[3.5 3 2.5 2 1.5 1 0.5];% Distance in meters

npc = 5;

powr =10.^(PdB/10);

tt=0:5:30;

fber = zeros(1,length(tt));

fEn = zeros(1,length(tt));

% Opening file

file_name=['Main_CodedUncoded_Ber_file' Chanl '_' 'Numder of Antennas' num2str(N_tx) '_' 'Frame Length' num2str(frame_length2) '.dat'];

myfileid=fopen(file_name, 'w+');

Nit = 10; % The number of iteration

%Nit = 1000; % The number of iteration

%=========================================================
=========================================================
=============================================

EBN=[0:5:30]; % EbN0 (Energy per bit to noise power ratio)

%EBN=[0:2:30]; % EbN0 (Energy per bit to noise power ratio)

for jj=1:length(EBN)


ebn = EBN(jj);

sd= sqrt(0.5/(10^(ebn/10))); % The standard deviation
```

```
nvr = sd^2;

zfqpsk1 = zeros(1,6*165+37); zfqpsk2 = zeros(1,6*165+37);% DC32-8PSK

%-------------------------------------------------------------------------------------------
-----------------

znewpsk1a = zeros(1,6*165+37); znewpsk1b = zeros(1,6*165+37);% New
Concept-MIMO-DC32-8PSK (Tx1)

znewpsk2a = zeros(1,6*165+37); znewpsk2b = zeros(1,6*165+37);% New
Concept-MIMO-DC32-8PSK (Tx2)

%-------------------------------------------------------------------------------------------
-----------------

zfd1bb = zeros(1,6*165+37); zfd2bb = zeros(1,6*165+37); % DCM1_QPSK

%-------------------------------------------------------------------------------------------
-----------------

zfqpsk1a = zeros(1,6*165+37);zfqpsk1b = zeros(1,6*165+37);% MIMO
DC32-Based on Dual 8PSK(Tx1)

zfqpsk2a = zeros(1,6*165+37); zfqpsk2b = zeros(1,6*165+37);% MIMO
DC32-Based on Dual 8PSK(Tx2)

%-------------------------------------------------------------------------------------------
-----------------

zdrf1a = zeros(1,6*165+37); zrqf1b = zeros(1,6*165+37);% MIMO-DC32-
QAM-Flip (Tx1)

zdrf2a = zeros(1,6*165+37); zrqf2b = zeros(1,6*165+37);% MIMO-DC32-
QAM-Flip (Tx2)

%-------------------------------------------------------------------------------------------
-----------------

nebb=0;neSDC8a=0;nedc1=0;nedtst=0; nefdyx1 = 0; nefdyx2=0; nencm1a=0;
nencm1atst=0;nemimo8psk=0;

randn('state',0);  rand('state',0); % rand('state',0) ensures fixed random number
gen(fixed pesudo sequence)


for jj2=1:Nit  % Start of second loop


%=========================================================
=========================================================
```

```
================================================

[codqpsk1t,codqpsk2t,codb5t] = DataGen(); % The Inforamtion data generation

[codqpsk1bt,codqpsk2bt,codb5bt] = DataGen();  % The second generation concering MIMO configration

[cod1at]=Rearrangbits(codqpsk1t,codqpsk2t,codb5t);

[cod2t]=Rearrangbits(codqpsk1bt,codqpsk2bt,codb5bt);

[cod1bt]=RearrangDCMbits(codqpsk1t,codqpsk2t);  % Proposed DCM-QAM

[cod2bt]=RearrangDCMbits(codqpsk1bt,codqpsk2bt);% Proposed DCM-QAM conscering MIMO configuration

%=================================================================
================================================

% Convoulational coding implementation

 tstr = poly2trellis(7,[133 171]);

 codqpsk1 =convenc(codqpsk1t,tstr,[1 1 1 0 0 1]); % For QPSK symbols

 codqpsk2 =convenc(codqpsk2t,tstr,[1 1 1 0 0 1]); % For QPSK symbols

 codqpsk1b =convenc(codqpsk1bt,tstr,[1 1 1 0 0 1]); % For QPSK symbols

 codqpsk2b =convenc(codqpsk2bt,tstr,[1 1 1 0 0 1]); % For QPSK symbols

 codb5 =convenc(codb5t,tstr,[1 1 1 0 0 1]); % For B5 code

 codb5b =convenc(codb5bt,tstr,[1 1 1 0 0 1]); % For B5 code

 cod1a =convenc(cod1at,tstr,[1 1 1 0 0 1]); % For DC-32QAM & MIMO-DC32QAM modulation with five bits group(G=5bits)

 cod2 =convenc(cod2t,tstr,[1 1 1 0 0 1]); % For DC-32QAM & MIMO-DC32QAM modulation with five bits group(G=5bits)

%=================================================================
================================================

%Constellation DC32-QAM

[signal11,bit11]=constellation32();

[signal22,bit22]=constellation32_Qray_A();
```

```
[signal1b,bit1b]=constellation1();

[signal2b,bit2b]=constellation2();

% Constellation QPSK

[signalqpsk1,bitqpsk1]=constellationqpsk1();

[signalqpsk2,bitqpsk2]=constellationqpsk2();

%Constellation MIMO_DC32-QAM

[signal1,bit1]=constellation32();

[signal2,bit2]=constellation32_Qray_A();

%Constellation of 8psk

[signal3,bit3]= constellation8psk1a();

[signal3b,bit3b]= constellation8psk1b();

%-------------------------------------------------------------------------------------------
----------

% % Transforming QPSK Data for DC32-Based on Dual 8PSK & DCM based
on QPSKs


[ycpsk1,ycpsk2]=TransformationQpsk(codqpsk1,codqpsk2,signalqpsk1,signal
qpsk1,bitqpsk1,bitqpsk1);

%-------------------------------------------------------------------------------------------
----------

% Transforming QPSK Data for Proposed NewConcept-MIMO-DC32-Based
on Dual 8PSK & New Concept MIMO-New DC32-Based on Dual 8PSK

[ycpsk1a,ycpsk1b]=TransformationQpsk(codqpsk1,codqpsk2,signalqpsk1,sign
alqpsk1,bitqpsk1,bitqpsk1);%Tx1

[ycpsk2a,ycpsk2b]=TransformationQpsk(codqpsk1b,codqpsk2b,signalqpsk1,si
gnalqpsk1,bitqpsk1,bitqpsk1);%Tx2

%-------------------------------------------------------------------------------------------
----------

% Transforming of Proposed NewConcept-MIMO-DC32-Based on Dual
8PSK & New Concept MIMO-New DC32-Based on Dual 8PSK

[qpnew11,qpnew12]=TransformConcept(ycpsk1a,ycpsk1b); % Generate the
new qpsk symbols coming from g1
```

```
[qpnew21,qpnew22]=TransformConcept(ycpsk2a,ycpsk2b); % Generate the new qpsk symbols coming from g2

%=========================================================================================================

%TransAnennas on MIMO-DC32-QAM-Flip

[Rf1a] = DC32SymbolCreation(cod1a,signal11,bit11,frame_length2); % group1 g1 bits

%Rf1b = conj(Rf1a);

[Rf2a] = DC32SymbolCreation(cod2,signal11,bit11,frame_length2); % group2 g2 bits

%Rf2b = -conj(Rf2a);

%-------------------------------------------------------------------------------------------------

%TransAnennas DC32-Based on Dual 8PSK

[R1qpsk1,R2qpsk2] = TransAntennasD8psk(ycpsk1,ycpsk2,signal3,signal3b,bit3,bit3b,codb5);

%-------------------------------------------------------------------------------------------------

%TransAnennas of Proposed NewConcept-MIMO-DC32-Based on Dual 8PSK & New Concept MIMO-New DC32-Based on Dual 8PSK

[ynewpsk1a,ynewpsk1b] = TransAntennasD8psk(qpnew11,qpnew12,signal3,signal3b,bit3,bit3b,codb5); % G1-8PSK

[ynewpsk2a,ynewpsk2b] = TransAntennasD8psk(qpnew21,qpnew22,signal3,signal3b,bit3,bit3b,codb5); % G2-8PSK

%-------------------------------------------------------------------------------------------------

%TransAnennas on MIMO DC32-Based on Dual 8PSK

[R1qpsk1a,R2qpsk1b] = TransAntennasD8psk(ycpsk1a,ycpsk1b,signal3,signal3b,bit3,bit3b,codb5); % Tx1

[R1qpsk2a,R2qpsk2b] = TransAntennasD8psk(ycpsk2a,ycpsk2b,signal3,signal3b,bit3,bit3b,codb5b); %
```

```
Tx2

%=================================================================
=================================================================
=================================================

% Normalisation DC32QAM-basd 8PSK

Rqpsk1 = R1qpsk1/Nrmqpsk; Rqpsk2 = R2qpsk2/Nrmqpsk;

%-------------------------------------------------------------------------

% Normalisation of Proposed NewConcept-MIMO-DC32-Based on Dual
8PSK & New Concept MIMO-New DC32-Based on Dual 8PSK

Rnewpsk1a = ynewpsk1a/Nrmqpsk; Rnewpsk1b = ynewpsk1b/Nrmqpsk; %

Rnewpsk2a = ynewpsk2a/Nrmqpsk; Rnewpsk2b = ynewpsk2b/Nrmqpsk; %

%-------------------------------------------------------------------------

% Normalisation MIMO DC32-Based on Dual 8PSK

Rqpsk1a = R1qpsk1a/Nrmqpsk; Rqpsk1b = R2qpsk1b/Nrmqpsk; % Tx1

Rqpsk2a = R1qpsk2a/Nrmqpsk; Rqpsk2b = R2qpsk2b/Nrmqpsk; % Tx2

%-------------------------------------------------------------------------

% % Normalisation MIMO-DC32-QAM-Flip

Rf1a = Rf1a/Nrmf32; %Rf1b = Rf1b/Nrmf32; % 1s Branch

Rf2a = Rf2a/Nrmf32; %Rf2b = Rf2b/Nrmf32; % 2nd Branch

%=================================================================
=================================================================
=================================================

% Channel

[hf1,hf2,hf] = Channel(nfs,2); % The operating channel

% [hf1] = IndChannelLS(Rnewpsk1a);

% [hf2] = IndChannelNLS(Rnewpsk1a);

%=================================================================
=================================================================
=================================================

%  Spatial_Channlisation- DC32QAM-basd 8PSK
```

```
[y8psk1,y8psk2,Y8psk]                                                    =
Channlisation2(hf1,hf1,Rqpsk1,Rqpsk2,sd,nfs,Nrmqpsk,hf);%     DC32QAM-
basd 8PSK

%-------------------------------------------------------------------------------------------
-------------------------------------------------------

%  Spatial_Channlisation- MIMO DC32-Based on Dual 8PSK

[ym8psk1a,ym8psk1b,Ym8psk1]                                              =
Channlisation2(hf1,hf2,Rqpsk1a,Rqpsk1b,sd,nfs,Nrm,hf);%MIMO       DC32-
Based on Dual8PSK Tx1

[ym8psk2a,ym8psk2b,Ym8psk2]                                              =
Channlisation2(hf1,hf2,Rqpsk2a,Rqpsk2b,sd,nfs,Nrm,hf);%MIMO       DC32-
Based on Dual8PSK Tx2

%-------------------------------------------------------------------------------------------
-------------------------------------------------------

%///////////////////////////////////////////////////////////////////////////////////////////
/////////////////////////////////////////

%  Spatial_Channlisation- New Concept-MIMO-DC32-Based on Dual 8PSK

[ymnpsk1a,ymnpsk1b,Ymnpsk1]                                              =
Channlisation2(hf1,hf2,Rnewpsk1a,Rnewpsk1b,sd,nfs,Nrmqpsk,hf);%New
Concept-MIMO-DC32-Based on Dual 8PSK

[ymnpsk2a,ymnpsk2b,Ymnpsk2]                                              =
Channlisation2(hf1,hf2,Rnewpsk2a,Rnewpsk2b,sd,nfs,Nrmqpsk,hf);%New
Concept-MIMO-DC32-Based on Dual 8PSK

%///////////////////////////////////////////////////////////////////////////////////////////
/////////////////////////////////////////

%///////////////////////////////////////////////////////////////////////////////////////////
/////////////////////////////////////////

%  Spatial_Channlisation- Modification for SensApp

[ysensp1a,ysensp1b,ysensp1]                                              =
Channlisation2(hf1,hf2,Rnewpsk1a,Rnewpsk1b,sd,nfs,Nrmqpsk,hf);%Modific
ation for SensApp

[ysensp2a,ysensp2b,ysensp2]                                              =
Channlisation2(hf1,hf2,Rnewpsk1b,Rnewpsk1a,sd,nfs,Nrmqpsk,hf);%Modific
ation for SensApp

%///////////////////////////////////////////////////////////////////////////////////////////
/////////////////////////////////////////
```

```
%=========================================================
=========================================================
=================================================

% Readjust Normalisation

%---------------------------------------------------------------------------------
----------------------

% Readjust Normalisation DC32QAM-basd 8PSK

y8psk1 = y8psk1*Nrmqpsk; y8psk2 = y8psk2*Nrmqpsk; Y8psk =
Y8psk*Nrmqpsk;

%---------------------------------------------------------------------------------
----------------------

% Readjust Normalisation of Proposed NewConcept-MIMO-DC32-Based on
Dual 8PSK & New Concept MIMO-New DC32-Based on Dual 8PSK

%/////////////////////////////////////////////////////////////////////////////////////////////
/////////////////////////////////////////

ymnpsk1a = ymnpsk1a*Nrmqpsk; ymnpsk1b = ymnpsk1b*Nrmqpsk;
Ymnpsk1 = Ymnpsk1*Nrmqpsk;% 1st part from the 2x2

ymnpsk2a = ymnpsk2a*Nrmqpsk; ymnpsk2b = ymnpsk2b*Nrmqpsk;
Ymnpsk2 = Ymnpsk2*Nrmqpsk;% 2nd part from the 2x2

%/////////////////////////////////////////////////////////////////////////////////////////////
/////////////////////////////////////////

% Readjust Normalisation Modification for SensApp

ysensp1a = ysensp1a*Nrmqpsk; ysensp1b = ysensp1b*Nrmqpsk; ysensp1 =
ysensp1*Nrmqpsk;% Modification for SensApp

ysensp2a = ysensp2a*Nrmqpsk; ysensp2b = ysensp2b*Nrmqpsk; ysensp2 =
ysensp2*Nrmqpsk;% Modification for SensApp

%/////////////////////////////////////////////////////////////////////////////////////////////
/////////////////////////////////////////

%---------------------------------------------------------------------------------
---------------------------------------------------------

% Readjust Normalisation MIMO DC32-Based on Dual 8PSK

ym8psk1a = ym8psk1a*Nrmqpsk; ym8psk1b = ym8psk1b*Nrmqpsk;
Ym8psk1 = Ym8psk1*Nrmqpsk;% 1st part

ym8psk2a = ym8psk2a*Nrmqpsk; ym8psk2b = ym8psk2b*Nrmqpsk;
```

```
Ym8psk2 = Ym8psk2*Nrmqpsk;% 2nd part

%=================================================================
=================================================================
=================================================

y8psk1 = y8psk1;   y8psk2 = y8psk2;  % DC32-Based on Dual8PSK

%=================================================================
=================================================================
=================================================

%
Receiver:++++++++++++++++++++++++++++++++++++++++++++++++++++++++
++++++++++++++++++++++++++++++++++++++++++++++++++++++++++++++++
++++++++++++++++++++++++++++++++++++++++

%-----------------------------------------------------------------------------------------
-----------------------------------------------------------

% Adjustment and rearrgement of Decoding DC32QAM-basd 8PSK

%y8psk1 = (y8psk1).*conj(hf1); y8psk2 = (y8psk2).* conj(hf1);%
DC32QAM-basd 8PSK

y8psk1 = (y8psk1)./(hf1); y8psk2 = (y8psk2)./(hf1);% DC32QAM-basd 8PSK

%y8psk1 = (y8psk1)./(hf1); y8psk2 = (y8psk2)./(hf2);% DC32QAM-basd
8PSK

%-----------------------------------------------------------------------------------------
-----------------------------------------------------------

% Adjustment and rearrgement of Decoding MIMO DC32-Based on Dual
8PSK

%ym8psk1a = (ym8psk1a).*conj(hf1); ym8psk1b = (ym8psk1b).* conj(hf2);%
MIMO DC32-Based on Dual 8PSK Rx1

%ym8psk2a = (ym8psk2a).*conj(hf1); ym8psk2b = (ym8psk2b).*conj(hf2);%
MIMO DC32-Based on Dual 8PSK Rx2

ym8psk1a = (ym8psk1a)./(hf1); ym8psk1b = (ym8psk1b)./(hf2);% MIMO
DC32-Based on Dual 8PSK Rx1

ym8psk2a = (ym8psk2a)./(hf1); ym8psk2b = (ym8psk2b)./(hf2);% MIMO
DC32-Based on Dual 8PSK Rx2

%///////////////////////////////////////////////////////////////////////////////////////////////
/////////////////////////////////////////

% Adjustment and rearrgement of Decoding for Modification for SensApp
```

```
ysensp1a = (ysensp1a)./(hf1); ysensp1b = (ysensp1b)./(hf2);% Modification for SensApp

ysensp2a = (ysensp2a)./(hf1); ysensp2b = (ysensp2b)./(hf2);% Modification for SensApp

%=========================================================================================

%-----------------------------------------------------------------------------------------

%/////////////////////////////////////////////////////////////////////////////////////////

% Adjustment and rearrgement of Decoding of New Concept-MIMO-DC32-Based on Dual 8PSK

%ymnpsk1a = (ymnpsk1a).*conj(hf1); ymnpsk1b = (ymnpsk1b).* conj(hf2);% Concept-MIMO-DC32-Based on Dual 8PSK Rx1

ymnpsk1a = (ymnpsk1a)./(hf1); ymnpsk1b = (ymnpsk1b)./(hf2);% Concept-MIMO-DC32-Based on Dual 8PSK Rx1

ymnpsk2a = (ymnpsk2a)./(hf1); ymnpsk2b = (ymnpsk2b)./(hf2);% Concept-MIMO-DC32-Based on Dual 8PSK Rx2

%+++++++++++++++++++++++++++++++++++++++++++++++++++++++++++++++++++++++++++++++++++++

%[b5nps1]=Bit5SoftPrevDecoding(ymnpsk1a,ymnpsk1b,signal3(8));% NewConcepMIMO-DC32QAM-B-8PSK with bit 5(g1)

%[b5nps2]=Bit5SoftPrevDecoding(ymnpsk2a,ymnpsk2b,signal3(8));% NewConcepMIMO-DC32QAM-B-8PSK with bit 5(g2)

%/////////////////////////////////////////////////////////////////////////////////////////

%=========================================================================================

% Strengthen the received through combining through process

[ysenpsk1,ysenpsk2] = SymbCombing(ysensp1a,ysensp2b,ysensp1b,ysensp2a); % Combining at the receviers for MIMO

%=========================================================================================
```

```
==============================================

%////////////////////////////////////////////////////////////////////////////////////////////////////
/////////////////////////////////////////////

% Applying symbols adjustment at the receivers before applying for
Modification for SensApp

[ysenqpsk1,ysenqpsk2]=ReTransformConcept(ysenpsk1,ysenpsk2);%
Modification for SensApp

%----------------------------------------------------------------------------------------------
-----------------------------------------------------

[ysenbit1]=Bit5SoftPrevDecoding(ysenpsk1,ysenpsk2,signal3(8));%
Modification for SensApp

%----------------------------------------------------------------------------------------------
-----------------------------------------------------

[yysenqpsk1,yysenqpsk2]                                                    =
RecAntenDCMLLRSoft_QPSK(ysenqpsk1,ysenqpsk2,signalqpsk1,bitqpsk1,si
gnalqpsk1,bitqpsk1,nvr);% Modification for SensApp

%=====================================================
=====================================================
==============================================

% Applying symbols adjustment at the receivers before applying Soft
Decoding for New Concept-MIMO-DC32-Based on Dual 8PSK

%////////////////////////////////////////////////////////////////////////////////////////////////////
/////////////////////////////////////////////

[Yqpnew1a,Yqpnew1b]=ReTransformConcept(ymnpsk1a,ymnpsk1b);%
NewConcepMIMO-DC32QAM-B-8PSK(g1)

[Yqpnew2a,Yqpnew2b]=ReTransformConcept(ymnpsk2a,ymnpsk2b);%
NewConcepMIMO-DC32QAM-B-8PSK(g2)

%++++++++++++++++++++++++++++++++++++++++++++++++++++++++++++
++++++++++++++++++++++++++++++++++++++++++++++++++++++++++++++
++++++++++++++++++++++++++++++++++++++++++++++++

[bnpk1as]=Bit5SoftPrevDecoding(ymnpsk1a,ymnpsk1b,signal3(8));%
NewConcepMIMO-DC32QAM-B-8PSK with bit 5(g1)

[bnpk2as]=Bit5SoftPrevDecoding(ymnpsk2a,ymnpsk2b,signal3(8));%
NewConcepMIMO-DC32QAM-B-8PSK with bit 5(g2)

%.....
.....
```

```
[YYnp1tas,YYnp1tbs] = RecAntenDCMSoft_QPSK(Yqpnew1a,Yqpnew1b,signalqpsk1,bitqpsk1,signalqpsk1,bitqpsk1);% NewConcepMIMO-DC32QAM-B-8PSK(g1)b5

[YYnp2tas,YYnp2tbs] = RecAntenDCMSoft_QPSK(Yqpnew2a,Yqpnew2b,signalqpsk1,bitqpsk1,signalqpsk1,bitqpsk1);% NewConcepMIMO-DC32QAM-B-8PSK(g2)b5


% [YYnp1tas,YYnp1tbs] = RecAntenDCMLLRSoft_QPSK(Yqpnew1a,Yqpnew1b,signalqpsk1,bitqpsk1,signalqpsk1,bitqpsk1,nvr);% NewConcepMIMO-DC32QAM-B-8PSK(g1)b5

% [YYnp2tas,YYnp2tbs] = RecAntenDCMLLRSoft_QPSK(Yqpnew2a,Yqpnew2b,signalqpsk1,bitqpsk1,signalqpsk1,bitqpsk1,nvr);% NewConcepMIMO-DC32QAM-B-8PSK(g2)b5

%.....

[YYnp1tastst,YYnp1tbstst] = RecAntenDCMLLRSoft_QPSKtst(Yqpnew1a,Yqpnew1b,signalqpsk1,bitqpsk1,signalqpsk1,bitqpsk1,nvr);% NewConcepMIMO-DC32QAM-B-8PSK(g1)b5

[YYnp2tastst,YYnp2tbstst] = RecAntenDCMLLRSoft_QPSKtst(Yqpnew2a,Yqpnew2b,signalqpsk1,bitqpsk1,signalqpsk1,bitqpsk1,nvr);% NewConcepMIMO-DC32QAM-B-8PSK(g2)b5

%////////////////////////////////////////////////////////////////////////////////////////////////////////////////////////////////////////

%-------------------------------------------------------------------------------------------------------------------

% Applying symbols adjustment at the receivers before applying Soft Decoding for DC32-Based on Dual 8PSK

[b5s8psk]=Bit5SoftPrevDecoding(y8psk1,y8psk2,signal3(8));% DC32QAM-B-8PSK with bit 5 of the Group

%.....

[Ytqpsk1] = RecAntennasSoft32psk1(y8psk1,signal3,bit3,y8psk2,signal3(8));% 1st 8PSK (soft)

[Ytqpsk2] = RecAntennasSoft32psk2(y8psk2,signal3b,bit3b,y8psk1,signal3(8));% 2nd 8PSK (soft)

%-------------------------------------------------------------------------------------------
```

```
------------------------------------------------------------

% Applying symbols adjustment  of Decoding MIMO DC32-Based on Dual
8PSK

[Yk8p1a]                                                        =
RecAntennasSoft32psk1(ym8psk1a,signal3,bit3,ym8psk1b,signal3(8));%
MIMO-DC32QAM-8PSK(Rx1a)

[Yk8p1b]                                                        =
RecAntennasSoft32psk2(ym8psk1b,signal3b,bit3b,ym8psk1a,signal3(8));%
MIMO-DC32QAM-8PSK(Rx1b)

[b5Ykm1]=Bit5SoftPrevDecoding(ym8psk1a,ym8psk1b,signal3(8));          %
MIMO-DC32QAM-8PSK(g1)

%

[Yk8p2a]                                                        =
RecAntennasSoft32psk1(ym8psk2a,signal3,bit3,ym8psk2b,signal3(8));%
MIMO-DC32QAM-8PSK(Rx2a)

[Yk8p2b]                                                        =
RecAntennasSoft32psk2(ym8psk2b,signal3b,bit3b,ym8psk2a,signal3(8));%
MIMO-DC32QAM-8PSK(Rx2b)

[b5Ykm2]=Bit5SoftPrevDecoding(ym8psk2a,ym8psk2b,signal3(8));          %
MIMO-DC32QAM-8PSK(g2)

%=================================================================
=================================================================
================================================

% Applying symbols adjustment at the receivers before applying  Decoding for
the Almounti Scheme

hb = sum(abs(hf).^2,2);

%=================================================================
=================================================================
================================================

% ML soft Decoding using Viterbi Decoding for New Concept-MIMO-DC32-
Based on Dual 8PSK (ML Soft)

%////////////////////////////////////////////////////////////////////////////////////////////////////
//////////////////////////////////////

YYnp11tats  =vitdec(YYnp1tas,tstr,100,'trunc','unquant',[1  1  1  0  0  1]);%
NewConcept-MIMO-DC32QAM-B-8PSK(Rx1)

YYnp12tbts  =vitdec(YYnp1tbs,tstr,100,'trunc','unquant',[1  1  1  0  0  1]);%
```

NewConcept-MIMO-DC32QAM-B-8PSK(Rx1)

bnpk1ats =vitdec(bnpk1as,tstr,100,'trunc','unquant',[1 1 1 0 0 1]);% NewConcept-MIMO-DC32QAM-B-8PSK(Rx1) b5 of g1

%..

YYnp21tats =vitdec(YYnp2tas,tstr,100,'trunc','unquant',[1 1 1 0 0 1]);% NewConcept-MIMO-DC32QAM-B-8PSK(Rx1)

YYnp22tbts =vitdec(YYnp2tbs,tstr,100,'trunc','unquant',[1 1 1 0 0 1]);% NewConcept-MIMO-DC32QAM-B-8PSK(Rx1)

bnpk2ats =vitdec(bnpk2as,tstr,100,'trunc','unquant',[1 1 1 0 0 1]);% NewConcept-MIMO-DC32QAM-B-8PSK(Rx1) b5 of g2

%~~~~~~

YYnp11tatstst =vitdec(YYnp1tastst,tstr,100,'trunc','unquant',[1 1 1 0 0 1]);% NewConcept-MIMO-DC32QAM-B-8PSK(Rx1)

YYnp12tbtstst =vitdec(YYnp1tbstst,tstr,100,'trunc','unquant',[1 1 1 0 0 1]);% NewConcept-MIMO-DC32QAM-B-8PSK(Rx1)

bnpk1atstst =vitdec(bnpk1as,tstr,100,'trunc','unquant',[1 1 1 0 0 1]);% NewConcept-MIMO-DC32QAM-B-8PSK(Rx1) b5 of g1

%..

YYnp21tatstst=vitdec(YYnp2tastst,tstr,100,'trunc','unquant',[1 1 1 0 0 1]);% NewConcept-MIMO-DC32QAM-B-8PSK(Rx1)

YYnp22tbtstst =vitdec(YYnp2tbstst,tstr,100,'trunc','unquant',[1 1 1 0 0 1]);% NewConcept-MIMO-DC32QAM-B-8PSK(Rx1)

bnpk2atstst =vitdec(bnpk2as,tstr,100,'trunc','unquant',[1 1 1 0 0 1]);% NewConcept-MIMO-DC32QAM-B-8PSK(Rx1) b5 of g2

%///

%---

% ML soft Decoding using Viterbi Decoding for DC32-Based on Dual 8PSK (ML Soft)

Ytqpsk1t =vitdec(Ytqpsk1,tstr,100,'trunc','unquant',[1 1 1 0 0 1]);%

DC32QAM-B-8PSK (soft)

Ytqpsk2t =vitdec(Ytqpsk2,tstr,100,'trunc','unquant',[1 1 1 0 0 1]);% DC32QAM-B-8PSK (soft)

b1psk1t =vitdec(b5s8psk,tstr,100,'trunc','unquant',[1 1 1 0 0 1]);% DC32QAM-B-8PSK (soft)

%---

% Decoding using Viterbi of Decoding MIMO DC32-Based on Dual 8PSK

Yk8p1avd =vitdec(Yk8p1a,tstr,100,'trunc','unquant',[1 1 1 0 0 1]);% MIMO-DC32QAM-B-8PSK (soft)

Yk8p1bvd =vitdec(Yk8p1b,tstr,100,'trunc','unquant',[1 1 1 0 0 1]);% MIMO-DC32QAM-B-8PSK (soft)

b5Ykm1vd =vitdec(b5Ykm1,tstr,100,'trunc','unquant',[1 1 1 0 0 1]);% MIMO-DC32QAM-B-8PSK (soft)

%''

Yk8p2avd =vitdec(Yk8p2a,tstr,100,'trunc','unquant',[1 1 1 0 0 1]);% MIMO-DC32QAM-B-8PSK (soft)

Yk8p2bvd =vitdec(Yk8p2b,tstr,100,'trunc','unquant',[1 1 1 0 0 1]);% MIMO-DC32QAM-B-8PSK (soft)

b5Ykm2vd =vitdec(b5Ykm2,tstr,100,'trunc','unquant',[1 1 1 0 0 1]);% MIMO-DC32QAM-B-8PSK (soft)

%==

% ML soft Decoding using Viterbi Decoding for Modification for SensApp

yysenbitsqpsk1 =vitdec(yysenqpsk1,tstr,100,'trunc','unquant',[1 1 1 0 0 1]);% Modification for SensApp

yysenbitsqpsk2 =vitdec(yysenqpsk2,tstr,100,'trunc','unquant',[1 1 1 0 0 1]);% Modification for SensApp

ysenbits1 =vitdec(ysenbit1,tstr,100,'trunc','unquant',[1 1 1 0 0 1]);% Modification for SensApp

%**

```
%/////////////////////////////////////////////////////////////////////////////////////////////////////////////////////
//////////////////////////////////////////////

%==========================================================
============================================================
==================================================

% Rearrangment the recievd bits for New Concept-MIMO-DC32-Based on Dual 8PSK

%/////////////////////////////////////////////////////////////////////////////////////////////////////////////////////
//////////////////////////////////////////////

[Ynpsk1ts]=Rearrangbits(YYnp11tats,YYnp12tbts,bnpk1ats);                    %% NewConcept-MIMO-DC32QAM-B-8PSK (the 5 bits of G1)

%~~~~~~~~~~~~~~~~~~~~~~~~~~~~~~~~~~~~~~~~~~~~~~~~~~~~~~~~~~~~~~~~~~~~~~~~~~~~~~~~~~~~~~~~~~~~~~~~~~~~~~~~~~~~~~~~~~~~~~~~~~~~~~~~~~~~~~~~~~~~~~~~~~~~~~~~~~~~~~~~~~~~~~~~~~~~~~~~~~~~~~

[Ynpsk1tstst]=Rearrangbits(YYnp11tatstst,YYnp12tbtstst,bnpk1atstst);      %% NewConcept-MIMO-DC32QAM-B-8PSK (the 5 bits of G1)

%/////////////////////////////////////////////////////////////////////////////////////////////////////////////////////
//////////////////////////////////////////////

%-----------------------------------------------------------------------------------------------
---------------------------------------------------------------

% Rearrangment the recievd bits for DC32-Based on Dual 8PSK

[Ytxa2t]=Rearrangbits(Ytqpsk1t,Ytqpsk2t,b1psk1t); %% DC32QAM-B-8PSK (the 5 bits of the Group)

%-----------------------------------------------------------------------------------------------
---------------------------------------------------------------

% Rearrangment the recievd bits for MIMO-DC32QAM-B-8PSK  Based on Dual 8PSK

[Yk8p2avdg1]=Rearrangbits(Yk8p2avd,Yk8p2bvd,b5Ykm2vd);        %MIMO-DC32QAM-B-8PSK (the 5 bits of the Group)

%==========================================================
============================================================
==============================================

% Rearrangment the recievd bits for Modification for SensApp

[Ysensg1]=Rearrangbits(yysenbitsqpsk1,yysenbitsqpsk2,ysenbits1);               % Modification for SensApp
```

```
%-----------------------------------------------------------------------------------------------------------------------------------------------------------

%=====================================================================================================================================================

% Error Calculation for New Concept-MIMO-DC32-Based on Dual 8PSK

%//////////////////////////////////////////////////////////////////////////////////////////////////////////////////////////////////////////////////////////////

% check the way the loop (jj2) works on nencm1a on both sides n(jj2) != n

[nencm1a(jj2)] = ErrorCalculation(Ynpsk1ts,cod1at); % Error calculation for New Concept of MIMO-DC32QAM-B-8PSK

%~~~~~~~~~~~~~~~~~~~~~~~~~~~~~~~~~~~~~~~~~~~~~~~~~~~~~~~~~~~~~~~~~~~~~~~~~~~~~~~~~~~~~~~~~~~~~~~~~~~~~~~~~~~~~~~~~~~~~~~~~~~~~~~~~~~~~~~~~~~~~~~~~~~~~~~~~~~~~~~~~~~~~~

[nencm1atst(jj2)] = ErrorCalculation(Ynpsk1tstst,cod1at); % Error calculation for New Concept of MIMO-DC32QAM-B-8PSK

%//////////////////////////////////////////////////////////////////////////////////////////////////////////////////////////////////////////////////////////////

%-----------------------------------------------------------------------------------------------------------------------------------------------------------

% Error Calculation for New DC32-Based on Dual 8PSK

[neSDC8a(jj2)] = ErrorCalculation(Ytxa2t,cod1at);% Error calculation for DC32QAM-B-8PSK

%-----------------------------------------------------------------------------------------------------------------------------------------------------------

% Error Calculation for MIMO-DC32QAM-B-8PSK  Based on Dual 8PSK

[nemimo8psk(jj2)] = ErrorCalculation(Yk8p2avdg1,cod1at);% Error calculation for DC32QAM-B-8PSK

%-----------------------------------------------------------------------------------------------------------------------------------------------------------

%==================================================================================================================================================

% Error Calculation for Modification for SensApp
```

[nensens(jj2)] = ErrorCalculation(Ysensg1,cod1at); % Error calculation for Modification for SensApp

%//

end % End of the second loop jj2...

%
%==

% Ber Calculation

%--

%Ber for DC32-Based on Dual 8PSK

fberdc81(jj) = sum(neSDC8a)/(nfs*4*Nit);% for DC32-Based on Dual 8PSK

PERfberdc81(jj) = 1 - power((1- fberdc81(jj)),Nit);

%--

%//

% Ber for proposed NewConcept MIMO-DC32-Based on Dual 8PSK

[Berncm1a(jj)] = sum(nencm1a)/(nfs*4*Nit); % 1st part in g1

PERBerncm1a(jj) = 1 - power((1- Berncm1a(jj)),Nit);

%~~~~~~

[Berncm1atst(jj)] = sum(nencm1atst)/(nfs*4*Nit); % 1st part in g1

%//

%---

%Ber for MIMO-DC32QAM-B-8PSK Based on Dual 8PSK

bermimo8psk1(jj) = sum(nemimo8psk)/(nfs*4*Nit);% for DC32-Based on

Dual 8PSK

```
%-------------------------------------------------------------------------------------------------------------

[Bersens(jj)] =  sum(nensens)/(nfs*4*Nit); % for Modification for SensApp

PERBersens(jj) = 1 - power((1- Bersens(jj)),Nit);

%/////////////////////////////////////////////////////////////////////////////////////////////////////////////

%-------------------------------------------------------------------------------------------------------------

%% Priniting out

%fprintf('EbN0 = %3d[dB], BER = %11.3e, Number_of_Err_for_DC32QAM = %4d\n', EBN(jj), Ber1(jj),nedc1(jj));

fprintf('EbN0 = %3d[dB], BER_for_DC32QAM-Based8PSK = %11.3e, NOE_for_DC32QAM-Based8PSK = %4d\n', EBN(jj), fberdc81(jj), neSDC8a(jj));

fprintf('-------------------------------------------------------------------------------------------------\n');

fprintf('EbN0 = %3d[dB], BER_for_NewConpMIMO_DC32QAM-Based8PSK = %11.3e, NOE_for_NewConpMIMO_DC32QAM-Based8PSK = %4d\n',  EBN(jj),Berncm1a(jj), nencm1a(jj));

fprintf('-------------------------------------------------------------------------------------------------\n');

fprintf(myfileid, 'EbN0 = %3d[dB], BER_for_DC32QAM-Based8PSK = %11.3e, NOE_for_DC32QAM-Based8PSK = %4d\n', EBN(jj), fberdc81(jj), neSDC8a(jj)); % Popluate exfile

fprintf(myfileid,'-------------------------------------------------------------------------
\n');

fprintf(myfileid, 'EbN0 = %3d[dB], BER_for_NewConpMIMO_DC32QAM-Based8PSK = %11.3e, NOE_for_NewConpMIMO_DC32QAM-Based8PSK = %4d\n',  EBN(jj),Berncm1a(jj), nencm1a(jj));

fprintf(myfileid,'-------------------------------------------------------------------------
\n');

%-------------------------------------------------------------------------------------------------------------

%%%if Ber2bb<1e-6, break; end % careful: Determine the EBN range
```

```
%%%end % End of loop refering to power of the signal sgpsk1,sgpsk2,sgnew1a,sgnew2a,and sgnew2b

end %--------------End of first loop jj-----------------------------------------------------------------------

if (myfileid~=0), fclose(myfileid); end

%=========================================================================================================

%Berncm1a_valuesssss = Berncm1a

figure(1),

%-------------------------------------------------------------------------

semilogy(EBN,fberdc81,'g--^'),hold on;

%-------------------------------------------------------------------------

semilogy(EBN,Berncm1a,'b--o'),hold on;

%-------------------------------------------------------------------------

%semilogy(EBN,Berncm1atst,'k--<'),grid on;

%-------------------------------------------------------------------------

semilogy(EBN,Bersens,'m-h'),grid on; % for Modification for SensApp

%-------------------------------------------------------------------------

%legend('DC32QAM-based on 8PSK','NewConcept MIMO-DC32-Based on Dual 8PSK','NewConcept Test MIMO-DC32-Based on Dual 8PSK','MIMO-DC32QAM-B-8PSK');

legend('DC32QAM-based on 8PSK','NewConcept MIMO-DC32-Based on Dual 8PSK','MIMO Modification for SensApp');

%legend('DC32QAM-based on 8PSK','NewConcept MIMO-DC32-Based on Dual 8PSK');

xlabel('EbN0[dB]'), ylabel('BER');

%=========================================================================================================

figure(2),

%-------------------------------------------------------------------------
```

```
semilogy(DSM,fberdc81,'g--^'),hold on;

%-------------------------------------------------------------------------

%semilogy(DSM,Berncm1a,'b--p'),hold on;

%-------------------------------------------------------------------------

semilogy(DSM,Bersens,'m--*'),grid on;

%-------------------------------------------------------------------------

%legend('DC32QAM-based on 8PSK','NewConcept MIMO-DC32-Based on
Dual 8PSK','MIMO Modification for SensApp');

legend('DC32QAM-based on 8PSK','MIMO Modification for SensApp');

xlabel('Distance (meters)'), ylabel('Error Rate');

%=========================================================
=========================================================
=========================================

figure(3),

%-------------------------------------------------------------------------

semilogy(DSM,PERfberdc81,'g--^'),hold on;

%-------------------------------------------------------------------------

%semilogy(DSM,PERBerncm1a,'b--p'),hold on;

%-------------------------------------------------------------------------

semilogy(DSM,PERBersens,'m--*'),grid on;

%-------------------------------------------------------------------------

%legend('DC32QAM-based on 8PSK','NewConcept MIMO-DC32-Based on
Dual 8PSK','MIMO Modification for SensApp');

legend('DC32QAM-based on 8PSK','MIMO Modification for SensApp');

xlabel('Distance (meters)'), ylabel('Error Rate');

%=========================================================
=========================================================
=========================================================
=================================

=========================================================
==========
```

```
%%%%%%%%%%%%%%%%%%%%%%%%%%%%%%%%%%%%%%
%%%%%%

clear all

% main_UWB1

%====================================================
========================================================
================================================

%Initial parameters

N_tx = 2;

Nrm = sqrt(10); % DCM_QPSK Normlisation

Nrmqpsk= sqrt(6.175); % DC32-8PSK Normlisation

Nrmf32 = sqrt(210/8);%MIMO-DC32-QAM-Flip Normalisation

%Nrmf32 = sqrt(62/3);%MIMO-DC32-QAM-Flip Normalisation

frame_length = 1200;frame_length2 = 1500;

sgpsk1=0;sgpsk2=0;sgf1a=0;sgf1b=0;sgf2a=0;sgf2b=0;sgnew1a=0;sgnew1b=
0;% signal power

sgpp1=0;sgpp2=0;        sgz1a=0;        sgz1b=0;        sgz2a=0;
sgz2b=0;sgnew2a=0;sgnew2b=0; % signal power

ThresholdErros = 1000;

%ThresholdErros = 500;

%PdB=[0 -5 -11 -13 -17 -19 -21 -25 -30 -45];

PdB=[0 -8 -17 -21 -25];

%dly = [0 3 5 6 8 9 10 11 12 13];

dly = [0 3 5 6 8];

dly1b = [0 3 5 6 8 14 16 18 19 20];

dly2a = [4 12 15 17 21];

%dly2a = [4 12 15 17 21 30 32 34 36 38];


npc = 5;
```

```
powr =10.^(PdB/10);

tt=0:5:30;

fber = zeros(1,length(tt));

fEn = zeros(1,length(tt));

Nit =10; % The number of iteration

%Nit = 1000; % The number of iteration

%=========================================================
=========================================================
=================================================

EBN=[0:5:30]; % EbN0 (Energy per bit to noise power ratio)

for jj=0:length(EBN)


zfqpsk1 = zeros(1,6*165+37); zfqpsk2 = zeros(1,6*165+37);% DC32-8PSK

%-----------------------------------------------------------------------------------------
-----------------

znewpsk1a = zeros(1,6*165+37); znewpsk1b = zeros(1,6*165+37);% New
Concept-MIMO-DC32-8PSK (Tx1)

znewpsk2a = zeros(1,6*165+37); znewpsk2b = zeros(1,6*165+37);% New
Concept-MIMO-DC32-8PSK (Tx2)

%-----------------------------------------------------------------------------------------
-----------------

zfd1bb = zeros(1,6*165+37); zfd2bb = zeros(1,6*165+37); % DCM1_QPSK

%-----------------------------------------------------------------------------------------
-----------------

zfqpsk1a = zeros(1,6*165+37);zfqpsk1b = zeros(1,6*165+37);% MIMO
DC32-Based on Dual 8PSK(Tx1)

zfqpsk2a = zeros(1,6*165+37); zfqpsk2b = zeros(1,6*165+37);% MIMO
DC32-Based on Dual 8PSK(Tx2)

%-----------------------------------------------------------------------------------------
-----------------

zdrf1a = zeros(1,6*165+37); zrqf1b = zeros(1,6*165+37);% MIMO-DC32-
QAM-Flip (Tx1)
```

```
zdrf2a = zeros(1,6*165+37); zrqf2b = zeros(1,6*165+37);% MIMO-DC32-QAM-Flip (Tx2)

%-------------------------------------------------------------------------------------------------

nea2=0;tnea2=0;tnebb=0;nebb=0; ne8p1=0;tn8p1=0; ne32d1=0;tn32d1=0; new1a=0;tnew1a=0; tnew1ta=0;new1ta=0;

tnew1tas=0;new1tas=0;tnew1as=0;new1as=0;tnebbs=0;nebbs=0;

randn('state',0);  rand('state',0); % rand('state',0) ensures fixed random number gen(fixed pesudo sequence)


for jj2=1:Nit  % Start of second loop


%=========================================================================================================

[codqpsk1t,codqpsk2t,codb5t] = DataGen(); % The Inforamtion data generation

[codqpsk1bt,codqpsk2bt,codb5bt] = DataGen();  % The second generation concering MIMO configration

[cod1at]=Rearrangbits(codqpsk1t,codqpsk2t,codb5t);

[cod2t]=Rearrangbits(codqpsk1bt,codqpsk2bt,codb5bt);

[cod1bt]=RearrangDCMbits(codqpsk1t,codqpsk2t);  % Proposed DCM-QAM

[cod2bt]=RearrangDCMbits(codqpsk1bt,codqpsk2bt);% Proposed DCM-QAM conscering MIMO configuration

%=========================================================================================================

% Convoulational coding implementation

 tstr = poly2trellis(7,[133 171]);

 codqpsk1 =convenc(codqpsk1t,tstr,[1 1 1 0 0 1]); % For QPSK symbols

 codqpsk2 =convenc(codqpsk2t,tstr,[1 1 1 0 0 1]); % For QPSK symbols

 codqpsk1b =convenc(codqpsk1bt,tstr,[1 1 1 0 0 1]); % For QPSK symbols
```

```
codqpsk2b =convenc(codqpsk2bt,tstr,[1 1 1 0 0 1]); % For QPSK symbols

codb5 =convenc(codb5t,tstr,[1 1 1 0 0 1]); % For B5 code

codb5b =convenc(codb5bt,tstr,[1 1 1 0 0 1]); % For B5 code

cod1a =convenc(cod1at,tstr,[1 1 1 0 0 1]); % For DC-32QAM & MIMO-DC32QAM modulation with five bits group(G=5bits)

cod2 =convenc(cod2t,tstr,[1 1 1 0 0 1]); % For DC-32QAM & MIMO-DC32QAM modulation with five bits group(G=5bits)

cod1bb =convenc(cod1bt,tstr,[1 1 1 0 0 1]); % For DCM

%=========================================================
==========================================================
==============================================

%Constellation DC32-QAM

%[signal11,bit11]=constellation32();

[signal11,bit11]=constellation32_NoGray();

%%%[signal11,bit11]=constellation();

[signal22,bit22]=constellation32_Qray_A();

[signal1b,bit1b]=constellation1();

[signal2b,bit2b]=constellation2();

% Constellation QPSK

[signalqpsk1,bitqpsk1]=constellationqpsk1();

[signalqpsk2,bitqpsk2]=constellationqpsk2();

%Constellation MIMO_DC32-QAM

[signal1,bit1]=constellation32();

[signal2,bit2]=constellation32_Qray_A();

%Constellation of 8psk

[signal3,bit3]= constellation8psk1a();

[signal3b,bit3b]= constellation8psk1b();

%-----------------------------------------------------------------------------------------
----------
```

```
% Transforming QPSK Data for DC32-Based on Dual 8PSK & DCM based on
QPSKs

[ycpsk1,ycpsk2]=TransformationQpsk(codqpsk1,codqpsk2,signalqpsk1,signal
qpsk1,bitqpsk1,bitqpsk1);

%-----------------------------------------------------------------------------------------
----------

% Transforming QPSK Data for MIMO DC32-Based on Dual 8PSK & New
Concept MIMO-New DC32-Based on Dual 8PSK

[ycpsk1a,ycpsk1b]=TransformationQpsk(codqpsk1,codqpsk2,signalqpsk1,sign
alqpsk1,bitqpsk1,bitqpsk1);%Tx1

[ycpsk2a,ycpsk2b]=TransformationQpsk(codqpsk1b,codqpsk2b,signalqpsk1,si
gnalqpsk1,bitqpsk1,bitqpsk1);%Tx2

%[ycpsk2a,ycpsk2b]=TransformationQpsk(codqpsk1b,codqpsk2b,signalqpsk2
,signalqpsk2,bitqpsk2,bitqpsk2);%Tx2

%-----------------------------------------------------------------------------------------
----------

% Transforming New Proposed Concept on MIMO-New DC32-Based on Dual
8PSK

[qpnew11,qpnew12]=TransformConcept(ycpsk1a,ycpsk1b); % Generate the
new qpsk symbols coming from g1

[qpnew21,qpnew22]=TransformConcept(ycpsk2a,ycpsk2b); % Generate the
new qpsk symbols coming from g2

%=========================================================
=========================================================
=================================================

%TransAnennas on MIMO-DC32-QAM-Flip

[Rf1a] = DC32SymbolCreation(cod1a,signal11,bit11,frame_length2); %
group1 g1 bits

%[Rf1a] = DC32SymbolCreation(cod1bb,signal11,bit11,frame_length2); %
group1 g1 bits   cod1bb

Rf1b = conj(Rf1a);

[Rf2a] = DC32SymbolCreation(cod2,signal11,bit11,frame_length2); % group2
g2 bits

%[Rf2a] = DC32SymbolCreation(cod2,signal11,bit11,frame_length2); %
group2 g2 bits
```

```
Rf2b = -conj(Rf2a);

%-------------------------------------------------------------------------------------------

%TransAnennas DCM based on QPSKs

[s1b,s2b]=tranmatrix_DCM(ycpsk1,ycpsk2);

[sx1,sx2] = TransDCM_QPSK(s1b,s2b,signal1b,signal2b,bit1b,bit2b);

%-------------------------------------------------------------------------------------------

%TransAnennas DC32-Based on Dual 8PSK

[R1qpsk1,R2qpsk2] = TransAntennasD8psk(ycpsk1,ycpsk2,signal3,signal3b,bit3,bit3b,codb5);

%-------------------------------------------------------------------------------------------

%TransAnennas of NewConcept of MIMO DC32-Based on Dual 8PSK

[ynewpsk1a,ynewpsk1b] = TransAntennasD8psk(qpnew11,qpnew12,signal3,signal3b,bit3,bit3b,codb5);
% G1-8PSK

[ynewpsk2a,ynewpsk2b] = TransAntennasD8psk(qpnew21,qpnew22,signal3,signal3b,bit3,bit3b,codb5);
% G2-8PSK

%-------------------------------------------------------------------------------------------

%TransAnennas on MIMO DC32-Based on Dual 8PSK (Without the new concept transfomation)

[R1qpsk1a,R2qpsk1b] = TransAntennasD8psk(ycpsk1a,ycpsk1b,signal3,signal3b,bit3,bit3b,codb5); %
Tx1

[R1qpsk2a,R2qpsk2b] = TransAntennasD8psk(ycpsk2a,ycpsk2b,signal3,signal3b,bit3,bit3b,codb5b); %
Tx2

%=============================================================================================

%figure(1),
```

```
%[re,im] = const_map(ynewpsk1a);


% Normalisation DC32QAM-basd 8PSK

Rqpsk1 = R1qpsk1/Nrmqpsk; Rqpsk2 = R2qpsk2/Nrmqpsk;

%-------------------------------------------------------------------------

% Normalisation New Cocept on MIMO DC32QAM-basd 8PSK

Rnewpsk1a = ynewpsk1a/Nrmqpsk; Rnewpsk1b = ynewpsk1b/Nrmqpsk; % G1

Rnewpsk2a = ynewpsk2a/Nrmqpsk; Rnewpsk2b = ynewpsk2b/Nrmqpsk; % G2

%-------------------------------------------------------------------------

% Normalisation MIMO DC32-Based on Dual 8PSK (Without the new concept transfomation)

Rqpsk1a = R1qpsk1a/Nrmqpsk; Rqpsk1b = R2qpsk1b/Nrmqpsk; % Tx1

Rqpsk2a = R1qpsk2a/Nrmqpsk; Rqpsk2b = R2qpsk2b/Nrmqpsk; % Tx2

%-------------------------------------------------------------------------

% Normalisation DCM_QPSK

RR1b = sx1/Nrm; RR2b = sx2/Nrm; % DCM_QPSK

%-------------------------------------------------------------------------

% Normalisation MIMO-DC32-QAM-Flip

Rf1a = Rf1a/Nrmf32; Rf1b = Rf1b/Nrmf32; % 1s Branch

Rf2a = Rf2a/Nrmf32; Rf2b = Rf2b/Nrmf32; % 2nd Branch

%=========================================================
=========================================================
==================

% Applying conjugatetion

%d1 = conj(d1);d2 = conj(d2);

% Constellation map

%figure(1),
```

```
%[re,im] = const_map(Rqpsk1a);

%=========================================================
==========================================================
================

%First Branch

f1=1:128; f2=128;f3 =37+[1:100]; f4=100; y1=zeros(1,640);

ff1 = 1:100; ff2=100; n1=1:50;n2=51:100;k1=1:165;k2=165;


for i=1:3


[dqpsk1(f1)] = SigShift(Rqpsk1(ff1),28,n2,n1); % DC32-8PSK1

[dqpsk2(f1)] = SigShift(Rqpsk2(ff1),28,n2,n1); % DC32-8PSK2

%-----------------------------------------------------------------------------

[dnewpsk1a(f1)] = SigShift(Rnewpsk1a(ff1),28,n2,n1); % New Concept-
MIMO-DC32-8PSK1(Tx1a)

[dnewpsk1b(f1)] = SigShift(Rnewpsk2a(ff1),28,n2,n1); % New Concept-
MIMO-DC32-8PSK2(Tx1b)

%[dnewpsk1b(f1)] = SigShift(Rnewpsk1b(ff1),28,n2,n1); % New Concept-
MIMO-DC32-8PSK2(Tx1b)

%-----------------------------------------------------------------------------

[dqpsk1a(f1)] = SigShift(Rqpsk1a(ff1),28,n2,n1);%MIMO DC32-Based on
Dual 8PSK(Tx1a) (without concept)

[dqpsk1b(f1)] = SigShift(Rqpsk1b(ff1),28,n2,n1);%MIMO DC32-Based on
Dual 8PSK(Tx1b) (without concept)

%-----------------------------------------------------------------------------

[dx1bb(f1)] = SigShift(RR1b(ff1),28,n2,n1); % DCM1_QPSK

[dx2bb(f1)] = SigShift(RR2b(ff1),28,n2,n1); % DCM2_QPSK

%-----------------------------------------------------------------------------

[drf1a(f1)] = SigShift(Rf1a(ff1),28,n2,n1); % MIMO-DC32-QAM-Flip (Tx1a)

%[drf1b(f1)] = SigShift(Rf2a(ff1),28,n2,n1); % MIMO-DC32-QAM-Flip
(Tx1b)
```

```
[drf1b(f1)] = SigShift(Rf2b(ff1),28,n2,n1); % MIMO-DC32-QAM-Flip (Tx1b)

%-------------------------------------------------------------------------------

dfqpsk1(f1) = ifft(dqpsk1(f1),128);% % DC32-8PSK1

dfqpsk2(f1) = ifft(dqpsk2(f1),128);% % DC32-8PSK2

%-------------------------------------------------------------------------------

dfnewpsk1a(f1) = ifft(dnewpsk1a(f1),128);% New Concept-MIMO-DC32-8PSK1(Tx1a)

dfnewpsk1b(f1) = ifft(dnewpsk1b(f1),128);% New Concept-MIMO-DC32-8PSK1(Tx1b)

%-------------------------------------------------------------------------------

dfqpsk1a(f1) = ifft(dqpsk1a(f1),128);%MIMO DC32-Based on Dual 8PSK(Tx1a)(without concpet)

dfqpsk1b(f1) = ifft(dqpsk1b(f1),128);%MIMO DC32-Based on Dual 8PSK(Tx1b)(without concept)

%-------------------------------------------------------------------------------

dfx1bb(f1) = ifft(dx1bb(f1),128);% DCM1_QPSK

dfx2bb(f1) = ifft(dx2bb(f1),128);% DCM2_QPSK

%-------------------------------------------------------------------------------

drqf1a(f1) = ifft(drf1a(f1),128);% MIMO-DC32-QAM-Flip (Tx1a)

drqf1b(f1) = ifft(drf1b(f1),128);% MIMO-DC32-QAM-Flip (Tx1b)

%-------------------------------------------------------------------------------

zfqpsk1(k1) = ZeroPad(dfqpsk1(f1),37); %  DC32-8PSK1

zfqpsk2(k1) = ZeroPad(dfqpsk2(f1),37); %  DC32-8PSK2

%-------------------------------------------------------------------------------

znewpsk1a(k1) = ZeroPad(dfnewpsk1a(f1),37);% New Concept-MIMO-DC32-8PSK1(Tx1a)

znewpsk1b(k1) = ZeroPad(dfnewpsk1b(f1),37);% New Concept-MIMO-DC32-8PSK1(Tx1b)

%-------------------------------------------------------------------------------
```

```
zfqpsk1a(k1) = ZeroPad(dfqpsk1a(f1),37);%MIMO DC32-Based on Dual 8PSK(Tx1a)(without concept)

zfqpsk1b(k1) = ZeroPad(dfqpsk1b(f1),37);%MIMO DC32-Based on Dual 8PSK(Tx1b)(without concept)

%-------------------------------------------------------------------------------

zfd1bb(k1) = ZeroPad(dfx1bb(f1),37); % DCM1_QPSK

zfd2bb(k1) = ZeroPad(dfx2bb(f1),37); % DCM2_QPSK

%-------------------------------------------------------------------------------

zdrf1a(k1) = ZeroPad(drqf1a(f1),37);% MIMO-DC32-QAM-Flip (Tx1a)

zrqf1b(k1) = ZeroPad(drqf1b(f1),37);% MIMO-DC32-QAM-Flip (Tx1b)

%+++++++++++++++++++++++++++++++++++++++++++++++++++++++++++++++++++++++++++++++

%Second Branch

%-------------------------------------------------------------------------------

[dqpsk2a(f1)] = SigShift(Rqpsk2a(ff1),28,n2,n1);%MIMO DC32-Based on Dual 8PSK(Tx2a)

[dqpsk2b(f1)] = SigShift(Rqpsk2b(ff1),28,n2,n1);%MIMO DC32-Based on Dual 8PSK(Tx2b)

%-------------------------------------------------------------------------------

%[dnewpsk2a(f1)] = SigShift(Rnewpsk2a(ff1),28,n2,n1); % New Concept-MIMO-DC32-8PSK1(Tx2a)

[dnewpsk2a(f1)] = SigShift(Rnewpsk1b(ff1),28,n2,n1); % New Concept-MIMO-DC32-8PSK1(Tx2a)

[dnewpsk2b(f1)] = SigShift(Rnewpsk2b(ff1),28,n2,n1); % New Concept-MIMO-DC32-8PSK2(Tx2b)

%-------------------------------------------------------------------------------

%[drf2a(f1)] = SigShift(Rf1b(ff1),28,n2,n1); % MIMO-DC32-QAM-Flip (Tx2a)

[drf2a(f1)] = SigShift(Rf2a(ff1),28,n2,n1); % MIMO-DC32-QAM-Flip (Tx2a)

[drf2b(f1)] = SigShift(Rf1b(ff1),28,n2,n1); % MIMO-DC32-QAM-Flip (Tx2b)

%-------------------------------------------------------------------------------
```

```
dfqpsk2a(f1) = ifft(dqpsk2a(f1),128);%MIMO DC32-Based on Dual 8PSK(Tx2a)

dfqpsk2b(f1) = ifft(dqpsk2b(f1),128);%MIMO DC32-Based on Dual 8PSK(Tx2b)

%-------------------------------------------------------------------------------

dfdnewpsk2a(f1) = ifft(dnewpsk2a(f1),128);% New Concept-MIMO-DC32-8PSK1(Tx2a)

dfdnewpsk2b(f1) = ifft(dnewpsk2b(f1),128);% New Concept-MIMO-DC32-8PSK1(Tx2b)

%-------------------------------------------------------------------------------

drqf2a(f1) = ifft(drf2a(f1),128);% MIMO-DC32-QAM-Flip (Tx2a)

drqf2b(f1) = ifft(drf2b(f1),128);% MIMO-DC32-QAM-Flip (Tx2b)

%-------------------------------------------------------------------------------

znewpsk2a(k1) = ZeroPad(dfdnewpsk2a(f1),37);% New Concept-MIMO-DC32-8PSK1(Tx2a)

znewpsk2b(k1) = ZeroPad(dfdnewpsk2b(f1),37);% New Concept-MIMO-DC32-8PSK1(Tx2b)

%-------------------------------------------------------------------------------

zfqpsk2a(k1) = ZeroPad(dfqpsk2a(f1),37);%MIMO DC32-Based on Dual 8PSK(Tx2a)

zfqpsk2b(k1) = ZeroPad(dfqpsk2b(f1),37);%MIMO DC32-Based on Dual 8PSK(Tx2b)

%-------------------------------------------------------------------------------

zdrf2a(k1) = ZeroPad(drqf2a(f1),37);% MIMO-DC32-QAM-Flip (Tx2a)

zrqf2b(k1) = ZeroPad(drqf2b(f1),37);% MIMO-DC32-QAM-Flip (Tx2b)

%-------------------------------------------------------------------------

f1=f1+f2;f3=f3+f4;ff1=ff1+ff2;k1=k1+k2;

end

%=========================================================
=========================================================
=============================================

%%% channel implementation
```

```
% DC32QAM-based-on-8PSK with channel effect

% [xh1qpsk1,h1a,hf1qska,hIqsk1,tqsk1]  = Channel2a(zfqpsk1);

% [xh2qpsk2,h21a,hf2qska,hIqsk2,tqsk2] = Channel2a(zfqpsk2);

[xh1qpsk1,h1a,hf1qska,hIqsk1,tqsk1]=
RayleighChannelA1_a(zfqpsk1,dly,npc,powr);

[xh2qpsk2,h21a,hf2qska,hIqsk2,tqsk2]=
RayleighChannelA1_a(zfqpsk2,dly,npc,powr);

%%%[xh2a,h21a,hf21a,hImp2a,t22a]                                    =
RayleighChannelA1_bb(zfd2a,2,10,powr,hImp1a);

%-------------------------------------------------------------------------------------
----------

% New Concept of MIMO-DC32QAM-based-on-8PSK with channel effect

%[xhnpk1a,hnew1a,hfnewpsk1a,hInewqsk1a,tnewpsk1a]                  =
Channel1a(znewpsk1a);%New Concept MIMO-DC32QAM-b8PSK(Tx1a)

[xhnpk1a,hnew1a,hfnewpsk1a,hInewqsk1a,tnewpsk1a]                  =
RayleighChannelA1_a(znewpsk1a,dly,npc,powr);%New Concept MIMO-
DC32QAM-b8PSK(Tx1a)

%[xhnpk1b,hnew1b,hfnewpsk1b,hInewqsk1b,tnewpsk1b]                  =
Channel2a(znewpsk1b);%New Concept MIMO-DC32QAM-b8PSK(Tx1b)

[xhnpk1b,hnew1b,hfnewpsk1b,hInewqsk1b,tnewpsk1b]                  =
RayleighChannelA1_a(znewpsk1b,dly,npc,powr);%New Concept MIMO-
DC32QAM-b8PSK(Tx1b)

%[xhnpk2a,hnew2a,hfnewpsk2a,hInewqsk2a,tnewpsk2a]                  =
Channel1a(znewpsk2a);%New Concept MIMO-DC32QAM-b8PSK(Tx2a)

[xhnpk2a,hnew2a,hfnewpsk2a,hInewqsk2a,tnewpsk2a]                  =
RayleighChannelA2_b(znewpsk2a,dly2a,npc,powr);%New Concept MIMO-
DC32QAM-b8PSK(Tx2a)

%[xhnpk2b,hnew2b,hfnewpsk2b,hInewqsk2b,tnewpsk2b]                  =
Channel2a(znewpsk2b);%New Concept MIMO-DC32QAM-b8PSK(Tx2b)

[xhnpk2b,hnew2b,hfnewpsk2b,hInewqsk2b,tnewpsk2b]                  =
RayleighChannelA2_b(znewpsk2b,dly2a,npc,powr);%New Concept MIMO-
DC32QAM-b8PSK(Tx2b)

%-------------------------------------------------------------------------------------
----------

 % %MIMO DC32-Based on Dual 8PSK with channel effect
```

%[xh1qpsk1a,hq1a,hf1qska1a,hIq1a,tq1a] = Channel1a(zfqpsk1a);% MIMO DC32-Based on Dual 8PSK(Tx1a)

[xh1qpsk1a,hq1a,hf1qska1a,hIq1a,tq1a] = RayleighChannelA1_a(zfqpsk1a,dly,npc,powr);% MIMO DC32-Based on Dual 8PSK(Tx1a)(without concept)

%[xh1qpsk1b,hq1b,hf1qska1b,hIq1b,tq1b] = Channel1a(zfqpsk1b); % MIMO DC32-Based on Dual 8PSK(Tx2a)<<<<<<<<<<<<<<

[xh1qpsk1b,hq1b,hf1qska1b,hIq1b,tq1b] = RayleighChannelA1_a(zfqpsk1b,dly,npc,powr); % MIMO DC32-Based on Dual 8PSK(Tx2a)(without concept)

%[xh1qpsk2a,hq2a,hf1qska2a,hIq2a,tq2a] = Channel2a(zfqpsk2a);% MIMO DC32-Based on Dual 8PSK(Tx1b)<<<<<<<<<<<<

[xh1qpsk2a,hq2a,hf1qska2a,hIq2a,tq2a] = RayleighChannelA2_b(zfqpsk2a,dly2a,npc,powr);% MIMO DC32-Based on Dual 8PSK(Tx1b)<<<<<<<<<<<<

%[xh1qpsk2b,hq2b,hf1qska2b,hIq2b,tq2b] = Channel2a(zfqpsk2b); % MIMO DC32-Based on Dual 8PSK(Tx2b)

[xh1qpsk2b,hq2b,hf1qska2b,hIq2b,tq2b] = RayleighChannelA2_b(zfqpsk2b,dly2a,npc,powr); % MIMO DC32-Based on Dual 8PSK(Tx2b)

%----------

% DCM1_QPSK with channel effect

%[xh1bb,h1bb,hf11bb,hImp1bb,t11bb] = Channel1a(zfd1bb); % DCM1_QPSK

[xh1bb,h1bb,hf11bb,hImp1bb,t11bb] = RayleighChannelA1_a(zfd1bb,dly,npc,powr); % DCM1_QPSK

%[xh2bb,h21bb,hf21bb,hImp2bb,t22bb] = Channel1a(zfd2bb); % DCM2_QPSK

[xh2bb,h21bb,hf21bb,hImp2bb,t22bb] = RayleighChannelA1_a(zfd2bb,dly,npc,powr); % DCM2_QPSK

%----------

% MIMO-DC32-QAM-Flip with channel effect

%[xhzf1a,hqf1a,hfz1a,hIf1a,tf1a] = Channel1a(zdrf1a);% MIMO-DC32-QAM-Flip (Tx1a)

```
[xhzf1a,hqf1a,hfz1a,hIf1a,tf1a] = RayleighChannelA1_a(zdrf1a,dly,npc,powr);% MIMO-DC32-QAM-Flip (Tx1a)

%[xhzf1b,hqf1b,hfz1b,hIf1b,tf1b] = Channel1a(zrqf1b); % MIMO-DC32-QAM-Flip (Tx1b)

[xhzf1b,hqf1b,hfz1b,hIf1b,tf1b] = RayleighChannelA1_a(zrqf1b,dly,npc,powr); % MIMO-DC32-QAM-Flip (Tx1b)

%[xhzf2a,hqf2a,hfz2a,hIf2a,tf2a] = Channel2a(zdrf2a);% MIMO-DC32-QAM-Flip (Tx2a)

[xhzf2a,hqf2a,hfz2a,hIf2a,tf2a] = RayleighChannelA2_b(zdrf2a,dly2a,npc,powr);% MIMO-DC32-QAM-Flip (Tx2a)

%[xhzf2b,hqf2b,hfz2b,hIf2b,tf2b] = Channel2a(zrqf2b); % MIMO-DC32-QAM-Flip (Tx2b)

[xhzf2b,hqf2b,hfz2b,hIf2b,tf2b] = RayleighChannelA2_b(zrqf2b,dly2a,npc,powr); % MIMO-DC32-QAM-Flip (Tx2b)

%================================================================================================

% Noise Part

if jj == 0 % Measuring the signal power so as to add the noise

xx11 = xh1bb(1:length(zfd1bb));xx22 =xh2bb(1:length(zfd2bb));sgpp1 = sgpp1 + xx11*xx11';sgpp2 = sgpp2 + xx22*xx22'; % DCM_QPSK

%-------------------------------------------------------------------------------------------------

xx1qsk = xh1qpsk1(1:length(zfqpsk1));xx2qsk = xh2qpsk2(1:length(zfqpsk2));sgpsk1 = sgpsk1 + xx1qsk*xx1qsk';sgpsk2 = sgpsk2 + xx2qsk*xx2qsk'; % DC32QAM-8PSK

%-------------------------------------------------------------------------------------------------

xxn1a=xhnpk1a(1:length(znewpsk1a));xxn1b=xhnpk1b(1:length(znewpsk1b));sgnew1a=sgnew1a+xxn1a*xxn1a';sgnew1b=sgnew1b+xxn1b*xxn1b';%New ConMIMODC32QAM-8PSK(Tx1)

xxn2a=xhnpk2a(1:length(znewpsk2a));xxn2b=xhnpk2b(1:length(znewpsk2b));sgnew2a=sgnew2a+xxn2a*xxn2a';sgnew2b=sgnew2b+xxn2b*xxn2b';%New
```

```
ConMIMODC32QAM-8PSK(Tx2)

%-------------------------------------------------------------------------------------------------
-----------------------------------

xq8f1a=xh1qpsk1a(1:length(zfqpsk1a));xq8f1b=xh1qpsk1b(1:length(zfqpsk1b
));sgf1a=sgf1a+xq8f1a*xq8f1a';sgf1b=sgf1b+xq8f1b*xq8f1b';%MIMO-
DC32QAM-8PSK(Tx1)

xq8f2a=xh1qpsk2a(1:length(zfqpsk2a));xq8f2b=xh1qpsk2b(1:length(zfqpsk2b
));sgf2a=sgf2a+xq8f2a*xq8f2a';sgf2b=sgf2b+xq8f2b*xq8f2b';%MIMO-
DC32QAM-8PSK(Tx2)

%-------------------------------------------------------------------------------------------------
-----------------------------------

xzf1a=xhzf1a(1:length(zdrf1a));xzf1b=xhzf1b(1:length(zrqf1b));sgz1a=sgz1a
+xzf1a*xzf1a';sgz1b=sgz1b+xzf1b*xzf1b';%MIMO-DC32-QAM-Flip(Tx1)

xzf2a=xhzf2a(1:length(zdrf2a));xzf2b=xhzf2b(1:length(zrqf2b));sgz2a=sgz2a
+xzf2a*xzf2a';sgz2b=sgz2b+xzf2b*xzf2b';continue;%MIMO-DC32-QAM-
Flip(Tx2)

end

%=================================================
================================================================
================================================

Nu = 100; % The nubmer of used fft frequency tones

N = 128;  % The number of fft frequency tones

Nbps = 4; % The number of bits per sympol

snr = EBN(jj) +10*log10(Nbps*(Nu/N));

snr2 = EBN(jj) +10*log10(Nbps*(Nu/N));

%-------------------------------------------------------------------------------------------------
--------

% Noise DC32QAM_Based on 8PSK

noise_mag1psk = sqrt((10.^(-snr/10))*sgpsk1/2);

noise_mag2psk = sqrt((10.^(-snr2/10))*sgpsk2/2);

%-------------------------------------------------------------------------------------------------
--------

yr1apsk = xh1qpsk1 +
1*noise_mag1psk*(randn(size(xh1qpsk1))+1j*randn(size(xh1qpsk1)));
```

```
yr2apsk = xh2qpsk2 +1*noise_mag2psk*(randn(size(xh2qpsk2))+1j*randn(size(xh2qpsk2)));


% yr1apsk = xh1qpsk1;

% yr2apsk = xh2qpsk2;

%=========================================================================================

% Noise New Concept of MIMO-DC32QAM_Based on 8PSK

noise_magsgnew1a = sqrt((10.^(-snr/10))*sgnew1a/2);

noise_magsgnew1b = sqrt((10.^(-snr2/10))*sgnew1b/2);

noise_magsgnew2a = sqrt((10.^(-snr/10))*sgnew2a/2);

noise_magsgnew2b = sqrt((10.^(-snr2/10))*sgnew2b/2);

%-----------------------------------------------------------------------------------------

yrnewpsk1a = xhnpk1a +1*noise_magsgnew1a*(randn(size(xhnpk1a))+1j*randn(size(xhnpk1a)));

yrnewpsk1b = xhnpk1b +1*noise_magsgnew1b*(randn(size(xhnpk1b))+1j*randn(size(xhnpk1b)));

yrnewpsk2a = xhnpk2a +1*noise_magsgnew2a*(randn(size(xhnpk2a))+1j*randn(size(xhnpk2a)));

yrnewpsk2b = xhnpk2b +1*noise_magsgnew2b*(randn(size(xhnpk2b))+1j*randn(size(xhnpk2b)));

% yrnewpsk1a = xhnpk1a;

% yrnewpsk1b = xhnpk1b;

% yrnewpsk2a = xhnpk2a;

% yrnewpsk2b = xhnpk2b;

%=========================================================================================

% Noise DCM_QPSK

noise_mag1bb = sqrt((10.^(-snr/10))*sgpp1/2); % DCM1_QPSK
```

```
noise_mag2bb = sqrt((10.^(-snr2/10))*sgpp2/2);% DCM2_QPSK

%-------------------------------------------------------------------------------------------
-------

 yr1bb                                                  =                          xh1bb
+1*noise_mag1bb*(randn(size(xh1bb))+1j*randn(size(xh1bb)));

 yr2bb                                                  =                          xh2bb
+1*noise_mag2bb*(randn(size(xh2bb))+1j*randn(size(xh2bb)));

%yr1bb  = xh1bb;

%yr2bb = xh2bb;

%=========================================================
==========================================================
==================================================

% Noise MIMO-DC32QAM-8PSK (Without the new concept transfomation)

noise_mag = sqrt((10.^(-snr/10))*sgf1a/2);

noise_mag2 = sqrt((10.^(-snr2/10))*sgf1b/2);

noise_mag221 = sqrt((10.^(-snr/10))*sgf2a/2);

noise_mag222 = sqrt((10.^(-snr2/10))*sgf2b/2);

%-------------------------------------------------------------------------------------------
------------

y8p1a=xh1qpsk1a+1*noise_mag*(randn(size(xh1qpsk1a))+1j*randn(size(xh1
qpsk1a)));%MIMO-DC32QAM-8PSK (Tx1a)(without concept)

y8p1b=xh1qpsk1b+1*noise_mag2*(randn(size(xh1qpsk1b))+1j*randn(size(xh
1qpsk1b)));%MIMO-DC32QAM-8PSK (Tx1b)(without concept)

%-------------------------------------------------------------------------------------------
------------

y8p2a=xh1qpsk2a+1*noise_mag221*(randn(size(xh1qpsk2a))+1j*randn(size(
xh1qpsk2a)));%MIMO-DC32QAM-8PSK (Tx2a)

y8p2b=xh1qpsk2b+1*noise_mag222*(randn(size(xh1qpsk2b))+1j*randn(size(
xh1qpsk2b)));%MIMO-DC32QAM-8PSK (Tx2b)



% y8p1a=xh1qpsk1a;

% y8p1b=xh1qpsk1b;
```

```
% y8p2a=xh1qpsk2a;

% y8p2b=xh1qpsk2b;

%=========================================================
=========================================================
=============================================

% Noise MIMO-DC32-QAM-Flip

noise_mag1a = sqrt((10.^(-snr/10))*sgz1a/2);

noise_mag1b = sqrt((10.^(-snr2/10))*sgz1b/2);

noise_mag2a = sqrt((10.^(-snr/10))*sgz2a/2);

noise_mag2b = sqrt((10.^(-snr2/10))*sgz2b/2);

%-----------------------------------------------------------------------------------------
------------


yqf1aa=xhzf1a+1*noise_mag1a*(randn(size(xhzf1a))+1j*randn(size(xhzf1a)))
;% MIMO-DC32-QAM-Flip (Tx1a)


yqf1bb=xhzf1b+1*noise_mag1b*(randn(size(xhzf1b))+1j*randn(size(xhzf1b))
);% MIMO-DC32-QAM-Flip(Tx1b)

  %%%-----------------------------------------------------------------------------------------
------------------


yqf2aa=xhzf2a+1*noise_mag2a*(randn(size(xhzf2a))+1j*randn(size(xhzf2a)))
;% MIMO-DC32-QAM-Flip (Tx2a)


yqf2bb=xhzf2b+1*noise_mag2b*(randn(size(xhzf2b))+1j*randn(size(xhzf2b))
);% MIMO-DC32-QAM-Flip (Tx2b)



% yqf1aa=xhzf1a;

% yqf1bb=xhzf1b;

% yqf2aa=xhzf2a;

% yqf2bb=xhzf2b;

%=========================================================
=========================================================
=============================================
```

```
% Receiver

t1 = 37+[1:165];t2=1:128;t3=1:100;n15=79:128; n14=2:51;e4=1:200;

for ss1=1:3

% First Branch

kt1apsk(t2) = GuardElimn(yr1apsk(t1),37,165);% DC32QAM_B_8PSK1

kt2apsk(t2) = GuardElimn(yr2apsk(t1),37,165);% DC32QAM_B_8PSK2

%-------------------------------------------------------------------------

knewpsk1a(t2) = GuardElimn(yrnewpsk1a(t1),37,165);% NewConceptMIMO-
DC32QAM_B_8PSK(Tx1a)

knewpsk1b(t2) = GuardElimn(yrnewpsk1b(t1),37,165);%
NewConceptMIMO-DC32QAM_B_8PSK(Tx1b)

%-------------------------------------------------------------------------

ky8p1a(t2) = GuardElimn(y8p1a(t1),37,165);% MIMO-DC32QAM-8PSK
(Tx1a)(without concept)

ky8p1b(t2) = GuardElimn(y8p1b(t1),37,165);% MIMO-DC32QAM-8PSK
(Tx1b)(without concept)

%-------------------------------------------------------------------------

 kyqf1a(t2) = GuardElimn(yqf1aa(t1),37,165);% MIMO-DC32-QAM-Flip
(Tx1a)

 kyqf1b(t2) = GuardElimn(yqf1bb(t1),37,165);% MIMO-DC32-QAM-Flip
(Tx1b)

%-------------------------------------------------------------------------

kt1bb(t2) = GuardElimn(yr1bb(t1),37,165);% DCM1_QPSK

kt2bb(t2) = GuardElimn(yr2bb(t1),37,165);% DCM2_QPSK

%-------------------------------------------------------------------------

y1apsk(t2) = fft(kt1apsk(t2),128); % DC32QAM_B_8PSK1

y2apsk(t2) = fft(kt2apsk(t2),128); % DC32QAM_B_8PSK2

%-------------------------------------------------------------------------

yknewpsk1a(t2) = fft(knewpsk1a(t2),128); % NewConceptMIMO-
DC32QAM_B_8PSK(Tx1a)
```

```
yknewpsk1b(t2) = fft(knewpsk1b(t2),128); % NewConceptMIMO-DC32QAM_B_8PSK(Tx1b)

%-------------------------------------------------------------------------

yky8p1a(t2) = fft(ky8p1a(t2),128); % MIMO-DC32QAM-8PSK (Tx1a)(without concept)

yky8p1b(t2) = fft(ky8p1b(t2),128); % MIMO-DC32QAM-8PSK (Tx1b)(without concept)

%-------------------------------------------------------------------------

 ykyqf1a(t2) = fft(kyqf1a(t2),128); % MIMO-DC32-QAM-Flip (Tx1a)

 ykyqf1b(t2) = fft(kyqf1b(t2),128); % MIMO-DC32-QAM-Flip (Tx1b)

%-------------------------------------------------------------------------

y1bb(t2) = fft(kt1bb(t2),128); % DCM1_QPSK

y2bb(t2) = fft(kt2bb(t2),128); % DCM2_QPSK

%-------------------------------------------------------------------------

y11apsk(t3) =[y1apsk(n15) y1apsk(n14)];% DC32QAM_B_8PSK1

y22apsk(t3) =[y2apsk(n15) y2apsk(n14)];% DC32QAM_B_8PSK2

%-------------------------------------------------------------------------

yyknpsk1a(t3) =[yknewpsk1a(n15) yknewpsk1a(n14)];% NewConceptMIMO-DC32QAM_B_8PSK(Tx1a)

yyknpsk1b(t3) =[yknewpsk1b(n15) yknewpsk1b(n14)];% NewConceptMIMO-DC32QAM_B_8PSK(Tx1b)

%-------------------------------------------------------------------------

yyky8p1a(t3) =[yky8p1a(n15) yky8p1a(n14)];% MIMO-DC32QAM-8PSK (Tx1a)(without concept)

yyky8p1b(t3) =[yky8p1b(n15) yky8p1b(n14)];% MIMO-DC32QAM-8PSK (Tx1b)(without concept)

%-------------------------------------------------------------------------

 yykyqf1a(t3) =[ykyqf1a(n15) ykyqf1a(n14)];% MIMO-DC32-QAM-Flip (Tx1a)

 yykyqf1b(t3) =[ykyqf1b(n15) ykyqf1b(n14)];% MIMO-DC32-QAM-Flip (Tx1b)
```

```
%-------------------------------------------------------------------------

y11bb(t3) =[y1bb(n15) y1bb(n14)];% DCM1_QPSK

y22bb(t3) =[y2bb(n15) y2bb(n14)];% DCM2_QPSK

%-------------------------------------------------------------------------

yq1apsk(t3) = y11apsk(t3)./hf1qska; % DC32QAM_B_8PSK1

yq2apsk(t3) = y22apsk(t3)./hf2qska; % DC32QAM_B_8PSK2

%-------------------------------------------------------------------------

yqnewpsk1a(t3) = yyknpsk1a(t3)./hfnewpsk1a; % NewConceptMIMO-
DC32QAM_B_8PSK(Tx1a)

yqnewpsk1b(t3) = yyknpsk1b(t3)./hfnewpsk1b; % NewConceptMIMO-
DC32QAM_B_8PSK(Tx1b)

%-------------------------------------------------------------------------

yqkp8p1a(t3) = yyky8p1a(t3)./hf1qska1a; % MIMO-DC32QAM-8PSK
(Tx1a)(without cncept)

yqkp8p1b(t3) = yyky8p1b(t3)./hf1qska1b; % MIMO-DC32QAM-8PSK
(Tx1b)(without concept)

%-------------------------------------------------------------------------

 yqyf1a(t3) = yykyqf1a(t3)./hfz1a; % MIMO-DC32-QAM-Flip (Tx1a)

 yqyf1b(t3) = yykyqf1b(t3)./hfz1b; % MIMO-DC32-QAM-Flip (Tx1b)

%-------------------------------------------------------------------------

yq1bb(t3) = y11bb(t3)./hf11bb; % DCM1_QPSK

yq2bb(t3) = y22bb(t3)./hf21bb; % DCM2_QPSK

%++++++++++++++++++++++++++++++++++++++++++++++++++++++++++++++++
++++++++++++++++++++++++++++++++++++++++++++++++++++++++

% Second Branch


ky8p2a(t2) = GuardElimn(y8p2a(t1),37,165);% MIMO-DC32QAM-8PSK
(Tx2a)

ky8p2b(t2) = GuardElimn(y8p2b(t1),37,165);% MIMO-DC32QAM-8PSK
(Tx2b)
```

```
%-------------------------------------------------------------------------

knewpsk2a(t2) = GuardElimn(yrnewpsk2a(t1),37,165);% NewConceptMIMO-
DC32QAM_B_8PSK(Tx2a)

knewpsk2b(t2) = GuardElimn(yrnewpsk2b(t1),37,165);%
NewConceptMIMO-DC32QAM_B_8PSK(Tx2b)

%-------------------------------------------------------------------------

 kyqf2a(t2) = GuardElimn(yqf2aa(t1),37,165);% MIMO-DC32-QAM-Flip
(Tx2a)

 kyqf2b(t2) = GuardElimn(yqf2bb(t1),37,165);% MIMO-DC32-QAM-Flip
(Tx2b)

%-------------------------------------------------------------------------

yky8p2a(t2) = fft(ky8p2a(t2),128); % MIMO-DC32QAM-8PSK (Tx2a)

yky8p2b(t2) = fft(ky8p2b(t2),128); % MIMO-DC32QAM-8PSK (Tx2b)

%-------------------------------------------------------------------------

yknewpsk2a(t2) = fft(knewpsk2a(t2),128); % NewConceptMIMO-
DC32QAM_B_8PSK(Tx2a)

yknewpsk2b(t2) = fft(knewpsk2b(t2),128); % NewConceptMIMO-
DC32QAM_B_8PSK(Tx2b)

%-------------------------------------------------------------------------

 ykyqf2a(t2) = fft(kyqf2a(t2),128); % MIMO-DC32-QAM-Flip (Tx2a)

 ykyqf2b(t2) = fft(kyqf2b(t2),128); % MIMO-DC32-QAM-Flip (Tx2b)

%-------------------------------------------------------------------------

yyky8p2a(t3) =[yky8p2a(n15) yky8p2a(n14)];% MIMO-DC32QAM-8PSK
(Tx2a)

yyky8p2b(t3) =[yky8p2b(n15) yky8p2b(n14)];% MIMO-DC32QAM-8PSK
(Tx2b)

%-------------------------------------------------------------------------

yyknpsk2a(t3) =[yknewpsk2a(n15) yknewpsk2a(n14)];% NewConceptMIMO-
DC32QAM_B_8PSK(Tx2a)

yyknpsk2b(t3) =[yknewpsk2b(n15) yknewpsk2b(n14)];%
NewConceptMIMO-DC32QAM_B_8PSK(Tx2b)

%-------------------------------------------------------------------------
```

```
 yykyqf2a(t3) =[ykyqf2a(n15) ykyqf2a(n14)];% MIMO-DC32-QAM-Flip (Tx2a)

 yykyqf2b(t3) =[ykyqf2b(n15) ykyqf2b(n14)];% MIMO-DC32-QAM-Flip (Tx2b)

%-------------------------------------------------------------------------

yqkp8p2a(t3) = yyky8p2a(t3)./hf1qska2a; % MIMO-DC32QAM-8PSK (Tx2a)

yqkp8p2b(t3) = yyky8p2b(t3)./hf1qska2b; % MIMO-DC32QAM-8PSK (Tx2b)

%-------------------------------------------------------------------------

yqnewpsk2a(t3) = yyknpsk2a(t3)./hfnewpsk2a; % NewConceptMIMO-DC32QAM_B_8PSK(Tx2a)

yqnewpsk2b(t3) = yyknpsk2b(t3)./hfnewpsk2b; % NewConceptMIMO-DC32QAM_B_8PSK(Tx2b)

%-------------------------------------------------------------------------

 yqyf2a(t3) = yykyqf2a(t3)./hfz2a; % MIMO-DC32-QAM-Flip (Tx2a)

 yqyf2b(t3) = yykyqf2b(t3)./hfz2b; % MIMO-DC32-QAM-Flip (Tx2b)

%-------------------------------------------------------------------------

t1=t1+165;t2=t2+128;n14=n14+128;n15=n15+128;t3=t3+100;

end

%=========================================================
=========================================================
=================================================

% Removing Conjucation

%=========================================================
=========================================================
=================================================

% Applying Spatial concept

%[yqkp8p1aa,yqkp8p1bb]                                    =
SpatialConcept(hf1qska1a,hf1qska2a,yqkp8p1a,yqkp8p1b);



%=========================================================
=========================================================
=================================================
```

```
% Readjust Normlisation for DC32QAM-B-8PSK

yq1apsk = yq1apsk*Nrmqpsk; yq2apsk = yq2apsk*Nrmqpsk;

%--------------------------------------------------------------------------

% Readjust Normlisation for New Concept MIMO-DC32QAM-B-8PSK

yqnewpsk1a=yqnewpsk1a*Nrmqpsk;yqnewpsk1b=yqnewpsk1b*Nrmqpsk; %
NewConcepDC32QAM-B-8PSK(Rx1)

yqnewpsk2a=yqnewpsk2a*Nrmqpsk;yqnewpsk2b=yqnewpsk2b*Nrmqpsk; %
NewConcepDC32QAM-B-8PSK(Rx2)

%--------------------------------------------------------------------------

% Readjust Normlisation for MIMO-DC32QAM-8PSK (Without the new
concept transfomation)

yqkp8p1a=yqkp8p1a*Nrmqpsk;      yqkp8p1b=yqkp8p1b*Nrmqpsk;%MIMO-
DC32QAM-8PSK (Tx1)

yqkp8p2a=yqkp8p2a*Nrmqpsk;      yqkp8p2b=yqkp8p2b*Nrmqpsk;%MIMO-
DC32QAM-8PSK (Tx2)

%--------------------------------------------------------------------------

% Readjust Normlisation for MIMO-DC32-QAM-Flip

 yqyf1a=yqyf1a*Nrmf32;      yqyf1b=yqyf1b*Nrmf32;%MIMO-DC32-QAM-
Flip (Tx1)

 yqyf2a=yqyf2a*Nrmf32;      yqyf2b=yqyf2b*Nrmf32;%MIMO-DC32-QAM-
Flip (Tx2)

%--------------------------------------------------------------------------

% Readjust Normlisation for DCM_QPSK

yq1bb = yq1bb * Nrm; yq2bb = yq2bb * Nrm;

%==========================================================
==========================================================
==================================================

%%% Constellation map

%figure(1),

%[re2,im2] = const_map(yq1bb);
```

```
%=================================================================
=================================================================
=================================================

% Removing  conjugatetion


%=================================================================
=================================================================
=================================================

% Decodmatrix for DCM_QPSK

[ys1bb,ys2bb]=Decodmatrix(yq1bb,yq2bb);

%=================================================================
=================================================================
=================================================

% Division for DCM_QPSK

ys1bbf = ys1bb./5;  ys2bbf = ys2bb./5;

%=================================================================
=================================================================
=================================================

% RecAntennas for DC32QAM-B-8PSK  LLR method

[Ytqpsk1] = RecAntennasSoft32psk1(yq1apsk,signal3,bit3,yq2apsk,signal3(8)); % 1st 8PSK  (soft)

[Ytqpsk2] = RecAntennasSoft32psk2(yq2apsk,signal3b,bit3b,yq1apsk,signal3(8));% 2nd 8PSK (soft)

[b5s8psk]=Bit5SoftPrevDecoding(yq1apsk,yq2apsk,signal3(8)); % b5 of the gorup

%-----------------------------------------------------------------------------------------
-------------------------------------------------

% RecAntennas for New Concept of MIMO-DC32QAM-B-8PSK ( with New 5bit idea)  LLR method

nnn2a = noise_magsgnew2a;nnn1a=noise_magsgnew1a;nnn1b = noise_magsgnew1b; nnn2b = noise_magsgnew2b;

[b5nps1]=Bit5SoftPrevDecoding(yqnewpsk1a,yqnewpsk2a,signal3(8));% NewConcepMIMO-DC32QAM-B-8PSK with bit 5(g1)
```

```
[b5nps2]=Bit5SoftPrevDecoding(yqnewpsk1b,yqnewpsk2b,signal3(8));%
NewConcepMIMO-DC32QAM-B-8PSK with bit 5(g2)

%.....

[Yqpnew1a,Yqpnew1b]=ReTransformConcept(yqnewpsk1a,yqnewpsk2a);  %
New concept for g1 with b5

[Yqpnew2a,Yqpnew2b]=ReTransformConcept(yqnewpsk1b,yqnewpsk2b);  %
New concept for g2 with b5

%.....

[YYqpnew1a,YYqpnew1b]                                              =
RecAntenDCMLLRSoft_QPSK(Yqpnew1a,Yqpnew1b,signalqpsk1,bitqpsk1,si
gnalqpsk1,bitqpsk1,nnn1a,nnn2a);%          NewConcepMIMO-DC32QAM-B-
8PSK(g1)b5

[YYqpnew2a,YYqpnew2b]                                              =
RecAntenDCMLLRSoft_QPSK(Yqpnew2a,Yqpnew2b,signalqpsk1,bitqpsk1,si
gnalqpsk1,bitqpsk1,nnn1b,nnn2b);%          NewConcepMIMO-DC32QAM-B-
8PSK(g2)b5

%-------------------------------------------------------------------------------------------
-------------------------------------------------------------

% RecAntennas for New Concept of MIMO-DC32QAM-B-8PSK  LLR
method

[bnpk1a]=Bit5SoftPrevDecoding(yqnewpsk1a,  yqnewpsk2a,signal3(8));%
NewConcepMIMO-DC32QAM-B-8PSK (g1)

[bnpk1b]=Bit5SoftPrevDecoding(yqnewpsk1b,yqnewpsk2b,signal3(8));%
NewConcepMIMO-DC32QAM-B-8PSK (g2)

%.....

[Yqpnew1ta,Yqpnew1tb]=ReTransformConcept(yqnewpsk1a,yqnewpsk2a);%
NewConcepMIMO-DC32QAM-B-8PSK (g1)

[Yqpnew2ta,Yqpnew2tb]=ReTransformConcept(yqnewpsk1b,yqnewpsk2b);%
NewConcepMIMO-DC32QAM-B-8PSK (g2)

%.....

[YYnp1ta,YYnp1tb]                                                  =
RecAntenDCMLLRSoft_QPSK(Yqpnew1ta,Yqpnew1tb,signalqpsk1,bitqpsk1,
signalqpsk1,bitqpsk1,nnn1a,nnn2a);%          NewConcepMIMO-DC32QAM-B-
8PSK (g1)

[YYnp2ta,YYnp2tb]                                                  =
RecAntenDCMLLRSoft_QPSK(Yqpnew2ta,Yqpnew2tb,signalqpsk1,bitqpsk1,
```

```
signalqpsk1,bitqpsk1,nnn1b,nnn2b);% NewConcepMIMO-DC32QAM-B-8PSK (g2)

%-------------------------------------------------------------------------------------------------------------

% RecAntennas for MIMO-DC32QAM-8PSK (Without the new concept transfomation) LLR method

[Yk8p1a] = RecAntennasSoft32psk1(yqkp8p1a,signal3,bit3,yqkp8p1b,signal3(8));% MIMO-DC32QAM-8PSK(Rx1a)

[Yk8p1b] = RecAntennasSoft32psk2(yqkp8p1b,signal3b,bit3b,yqkp8p1a,signal3(8));% MIMO-DC32QAM-8PSK(Rx1b)

[b5Ykm1]=Bit5SoftPrevDecoding(yqkp8p1a,yqkp8p1b,signal3(8)); % MIMO-DC32QAM-8PSK(g1)

%

[Yk8p2a] = RecAntennasSoft32psk1(yqkp8p2a,signal3,bit3,yqkp8p2b,signal3(8));% MIMO-DC32QAM-8PSK(Rx2a)

[Yk8p2b] = RecAntennasSoft32psk2(yqkp8p2b,signal3b,bit3b,yqkp8p2a,signal3(8));% MIMO-DC32QAM-8PSK(Rx2b)

[b5Ykm2]=Bit5SoftPrevDecoding(yqkp8p2a,yqkp8p2b,signal3(8)); % MIMO-DC32QAM-8PSK(g2)

%-------------------------------------------------------------------------------------------------------------

% RecAntennas for DCM_QPSK LLR method

[Ytx1bb,Ytx2bb] = RecAntenDCMLLRSoft_QPSK(ys1bbf,ys2bbf,signalqpsk1,bitqpsk1,signalqpsk1,bitqpsk1,nnn1a,nnn2a);

%-------------------------------------------------------------------------------------------------------------

% Readjusting the received symbol for %MIMO-DC32-QAM-Flip LLR method

 ydcf1a  = conj(yqyf2b);

 ydcf2a = -conj(yqyf1b);
```

```
[y32dc1] = SymbolsCombining(yqyf1a,ydcf1a); % getting back group 1 g1

[y32dc2] = SymbolsCombining(yqyf2a,ydcf2a); % getting back group 2 g2

%-------------------------------------------------------------------------------------------
---------

%RecAntennas for %MIMO-DC32-QAM-Flip   LLR method

[Yx32dc1] = RecAntennas32(y32dc1,frame_length2,signal11,bit11); % First
estimated symbol

[Yx32dc2] = RecAntennas32(y32dc2,frame_length2,signal11,bit11); %
Second estimated symbol

%=========================================================
=========================================================
=================================================

%/////////////////////////////////////////////////////////////////////////////////////////////////
/////////////////////////////////////

%=========================================================
=========================================================
=================================================

% RecAntennas for New Concept of MIMO-DC32QAM-B-8PSK ( with New
5bit idea)

[b5nps1s]=Bit5SoftPrevDecoding(yqnewpsk1a,yqnewpsk2a,signal3(8));%
NewConcepMIMO-DC32QAM-B-8PSK with bit 5(g1)

[b5nps2s]=Bit5SoftPrevDecoding(yqnewpsk1b,yqnewpsk2b,signal3(8));%
NewConcepMIMO-DC32QAM-B-8PSK with bit 5(g2)

%.....

[Yqpnew1as,Yqpnew1bs]=ReTransformConcept(yqnewpsk1a,yqnewpsk2a); %
New concept for g1 with b5

[Yqpnew2as,Yqpnew2bs]=ReTransformConcept(yqnewpsk1b,yqnewpsk2b);
% New concept for g2 with b5

%.....

[YYqpnew1as,YYqpnew1bs]                                    =
RecAntenDCMSoft_QPSK(Yqpnew1as,Yqpnew1bs,signalqpsk1,bitqpsk1,sign
alqpsk1,bitqpsk1);% NewConcepMIMODC32QAMB-8PSK(g1)b5

[YYqpnew2as,YYqpnew2bs]                                    =
RecAntenDCMSoft_QPSK(Yqpnew2as,Yqpnew2bs,signalqpsk1,bitqpsk1,sign
alqpsk1,bitqpsk1);% NewConcepMIMODC32QAMB-8PSK(g2)b5
```

```
%-------------------------------------------------------------------------------------------
-------------------------------------------------------

% RecAntennas for New Concept of MIMO-DC32QAM-B-8PSK

[bnpk1as]=Bit5SoftPrevDecoding(yqnewpsk1a, yqnewpsk2a,signal3(8));%
NewConcepMIMO-DC32QAM-B-8PSK (g1)

[bnpk1bs]=Bit5SoftPrevDecoding(yqnewpsk1b,yqnewpsk2b,signal3(8));%
NewConcepMIMO-DC32QAM-B-8PSK (g2)

%.....

[Yqpnew1tas,Yqpnew1tbs]=ReTransformConcept(yqnewpsk1a,yqnewpsk2a);
% NewConcepMIMO-DC32QAM-B-8PSK (g1)

[Yqpnew2tas,Yqpnew2tbs]=ReTransformConcept(yqnewpsk1b,yqnewpsk2b);
% NewConcepMIMO-DC32QAM-B-8PSK (g2)

%.....

[YYnp1tas,YYnp1tbs]                                                    =
RecAntenDCMSoft_QPSK(Yqpnew1tas,Yqpnew1tbs,signalqpsk1,bitqpsk1,sig
nalqpsk1,bitqpsk1);% NewConcepMIMO-DC32QAM-B-8PSK (g1)

[YYnp2tas,YYnp2tbs]                                                    =
RecAntenDCMSoft_QPSK(Yqpnew2tas,Yqpnew2tbs,signalqpsk1,bitqpsk1,sig
nalqpsk1,bitqpsk1);% NewConcepMIMO-DC32QAM-B-8PSK (g2)

%-------------------------------------------------------------------------------------------
-------------------------------------------------------

% RecAntennas for MIMO-DC32QAM-8PSK (Without the new concept
transfomation)

[Yk8p1a]                                                               =
RecAntennasSoft32psk1(yqkp8p1a,signal3,bit3,yqkp8p1b,signal3(8));%
MIMO-DC32QAM-8PSK(Rx1a)

[Yk8p1b]                                                               =
RecAntennasSoft32psk2(yqkp8p1b,signal3b,bit3b,yqkp8p1a,signal3(8));%
MIMO-DC32QAM-8PSK(Rx1b)

[b5Ykm1]=Bit5SoftPrevDecoding(yqkp8p1a,yqkp8p1b,signal3(8));          %
MIMO-DC32QAM-8PSK(g1)

%

[Yk8p2a]                                                               =
RecAntennasSoft32psk1(yqkp8p2a,signal3,bit3,yqkp8p2b,signal3(8));%
MIMO-DC32QAM-8PSK(Rx2a)
```

```
[Yk8p2b] = RecAntennasSoft32psk2(yqkp8p2b,signal3b,bit3b,yqkp8p2a,signal3(8));% MIMO-DC32QAM-8PSK(Rx2b)

[b5Ykm2]=Bit5SoftPrevDecoding(yqkp8p2a,yqkp8p2b,signal3(8)); % MIMO-DC32QAM-8PSK(g2)

%-------------------------------------------------------------------------------------------

% RecAntennas for DCM_QPSK

[Ytx1bbs,Ytx2bbs] = RecAntenDCMSoft_QPSK(ys1bbf,ys2bbf,signalqpsk1,bitqpsk1,signalqpsk1,bitqpsk1);

%-------------------------------------------------------------------------------------------

% Readjusting the received symbol for %MIMO-DC32-QAM-Flip

 ydcf1a  = conj(yqyf2b);

 ydcf2a = -conj(yqyf1b);

 [y32dc1] = SymbolsCombining(yqyf1a,ydcf1a); % getting back group 1 g1

 [y32dc2] = SymbolsCombining(yqyf2a,ydcf2a); % getting back group 2 g2

%-------------------------------------------------------------------------------------------

%RecAntennas for %MIMO-DC32-QAM-Flip

 [Yx32dc1] = RecAntennas32(y32dc1,frame_length2,signal11,bit11); % First estimated symbol

 [Yx32dc2] = RecAntennas32(y32dc2,frame_length2,signal11,bit11); % Second estimated symbol

%=============================================================================================

% Viterbi decoding for DC32QAM-B-8PSK (soft)   LLR method

Ytqpsk1t =vitdec(Ytqpsk1,tstr,100,'trunc','unquant',[1 1 1 0 0 1]);% DC32QAM-B-8PSK (soft)

Ytqpsk2t =vitdec(Ytqpsk2,tstr,100,'trunc','unquant',[1 1 1 0 0 1]);% DC32QAM-B-8PSK (soft)

b1psk1t =vitdec(b5s8psk,tstr,100,'trunc','unquant',[1 1 1 0 0 1]);% DC32QAM-
```

B-8PSK (soft)

%----------

% Viterbi decoding MIMO-DC32QAM-8PSK (soft) (Without the new concept transfomation) LLR method

Ytk8p1at =vitdec(Yk8p1a,tstr,100,'trunc','unquant',[1 1 1 0 0 1]);% MIMO-DC32QAM-8PSK(Rx1) (soft)

Ytk8p1bt =vitdec(Yk8p1b,tstr,100,'trunc','unquant',[1 1 1 0 0 1]);% MIMO-DC32QAM-8PSK(Rx1) (soft)

b1psk1at =vitdec(b5Ykm1,tstr,100,'trunc','unquant',[1 1 1 0 0 1]);% MIMO-DC32QAM-8PSK(Rx1) (soft)

%

Ytk8p2at =vitdec(Yk8p2a,tstr,100,'trunc','unquant',[1 1 1 0 0 1]);% MIMO-DC32QAM-8PSK(Rx2) (soft)

Ytk8p2bt =vitdec(Yk8p2b,tstr,100,'trunc','unquant',[1 1 1 0 0 1]);% MIMO-DC32QAM-8PSK(Rx2) (soft)

b1psk2at =vitdec(b5Ykm2,tstr,100,'trunc','unquant',[1 1 1 0 0 1]);% MIMO-DC32QAM-8PSK(Rx2) (soft)

%----------

% Viterbi decoding for NewConcept-MIMO-DC32QAM-B-8PSK (soft) (with New 5bit idea) LLR method

YYnp1at =vitdec(YYqpnew1a,tstr,100,'trunc','unquant',[1 1 1 0 0 1]);% NewConcept-MIMO-DC32QAM-B-8PSK with b5(Rx1)

YYnp1bt =vitdec(YYqpnew1b,tstr,100,'trunc','unquant',[1 1 1 0 0 1]);% NewConcept-MIMO-DC32QAM-B-8PSK with b5(Rx1)

b5nps1t =vitdec(b5nps1,tstr,100,'trunc','unquant',[1 1 1 0 0 1]);% NewConcept-MIMO-DC32QAM-B-8PSK with b5(Rx1)

YYnp2aaat =vitdec(YYqpnew2a,tstr,100,'trunc','unquant',[1 1 1 0 0 1]);% NewConcept-MIMO-DC32QAM-B-8PSK with b5(Rx2)

YYnp2bbt =vitdec(YYqpnew2b,tstr,100,'trunc','unquant',[1 1 1 0 0 1]);% NewConcept-MIMO-DC32QAM-B-8PSK with b5(Rx2)

b5nps22t =vitdec(b5nps2,tstr,100,'trunc','unquant',[1 1 1 0 0 1]);%

NewConcept-MIMO-DC32QAM-B-8PSK with b5(Rx2)

%----------

% Viterbi decoding for NewConcept-MIMO-DC32QAM-B-8PSK (soft) LLR method

YYnp1tat =vitdec(YYnp1ta,tstr,100,'trunc','unquant',[1 1 1 0 0 1]);% NewConcept-MIMO-DC32QAM-B-8PSK(Rx1)

YYnp1tbt =vitdec(YYnp1tb,tstr,100,'trunc','unquant',[1 1 1 0 0 1]);% NewConcept-MIMO-DC32QAM-B-8PSK(Rx1)

bnpk1at =vitdec(bnpk1a,tstr,100,'trunc','unquant',[1 1 1 0 0 1]);% NewConcept-MIMO-DC32QAM-B-8PSK(Rx1)

%----------

% Viterbi decoding for DCM_QPSK (soft) LLR method

% Ytx1bbt =vitdec(Ytx1bb,tstr,96,'trunc','unquant',[1 1 1 0 0 1],erasures);% DCM_QPSK

Ytx1bbt =vitdec(Ytx1bb,tstr,100,'trunc','unquant',[1 1 1 0 0 1]);% DCM_QPSK

Ytx2bbt =vitdec(Ytx2bb,tstr,100,'trunc','unquant',[1 1 1 0 0 1]);% DCM_QPSK

%----------

% Viterbi Decoding for MIMO-DC32-QAM-Flip LLR method

Yx32dc1 =vitdec(Yx32dc1,tstr,100,'trunc','hard',[1 1 1 0 0 1]);% MIMO-DC32-QAM-Flip (Rx1)

Yx32dc2 =vitdec(Yx32dc2,tstr,100,'trunc','hard',[1 1 1 0 0 1]);% MIMO-DC32-QAM-Flip (Rx1)

%----------

% Vetribi decoding implementation (Soft bit decoding) LLR method

%decoded = vitdec(code,trellis,tblen,opmode,'soft',nsdec);

%==========

```
%////////////////////////////////////////////////////////////////////////////////////////////////////////////
////////////////////////////////////

%=========================================================
==========================================================
==================================================

%  Viterbi decoding for NewConcept-MIMO-DC32QAM-B-8PSK (soft) ( with New 5bit idea)

YYnp1ats =vitdec(YYqpnew1as,tstr,100,'trunc','unquant',[1 1 1 0 0 1]);% NewConcept-MIMO-DC32QAM-B-8PSK with b5(Rx1)

YYnp1bts =vitdec(YYqpnew1bs,tstr,100,'trunc','unquant',[1 1 1 0 0 1]);% NewConcept-MIMO-DC32QAM-B-8PSK with b5(Rx1)

b5nps1ts =vitdec(b5nps1s,tstr,100,'trunc','unquant',[1 1 1 0 0 1]);% NewConcept-MIMO-DC32QAM-B-8PSK with b5(Rx1)



YYnp2aaats =vitdec(YYqpnew2as,tstr,100,'trunc','unquant',[1 1 1 0 0 1]);% NewConcept-MIMO-DC32QAM-B-8PSK with b5(Rx2)

YYnp2bbts =vitdec(YYqpnew2bs,tstr,100,'trunc','unquant',[1 1 1 0 0 1]);% NewConcept-MIMO-DC32QAM-B-8PSK with b5(Rx2)

b5nps22ts =vitdec(b5nps2s,tstr,100,'trunc','unquant',[1 1 1 0 0 1]);% NewConcept-MIMO-DC32QAM-B-8PSK with b5(Rx2)

%-----------------------------------------------------------------------------------------------
-----------------------------------

%  Viterbi decoding for NewConcept-MIMO-DC32QAM-B-8PSK (soft)

YYnp1tats =vitdec(YYnp1tas,tstr,100,'trunc','unquant',[1 1 1 0 0 1]);% NewConcept-MIMO-DC32QAM-B-8PSK(Rx1)

YYnp1tbts =vitdec(YYnp1tbs,tstr,100,'trunc','unquant',[1 1 1 0 0 1]);% NewConcept-MIMO-DC32QAM-B-8PSK(Rx1)

bnpk1ats =vitdec(bnpk1as,tstr,100,'trunc','unquant',[1 1 1 0 0 1]);% NewConcept-MIMO-DC32QAM-B-8PSK(Rx1)

%-----------------------------------------------------------------------------------------------
-----------------------------------

%  Viterbi decoding for DCM_QPSK (soft)

% Ytx1bbt =vitdec(Ytx1bb,tstr,96,'trunc','unquant',[1 1 1 0 0 1],erasures);% DCM_QPSK
```

```
Ytx1bbts =vitdec(Ytx1bbs,tstr,100,'trunc','unquant',[1 1 1 0 0 1]);% DCM_QPSK

Ytx2bbts =vitdec(Ytx2bbs,tstr,100,'trunc','unquant',[1 1 1 0 0 1]);% DCM_QPSK

%=========================================================================================================

% Rearrangments

[Ytxa2t]=Rearrangbits(Ytqpsk1t,Ytqpsk2t,b1psk1t); % for DC32QAM-B-8PSK  LLR method

%%-------------------------------------------------------------------------------------------------------

[Ym8p1]=Rearrangbits(Ytk8p1at,Ytk8p1bt,b1psk1at); %MIMO-DC32QAM-8PSK(Rx1)(Without the new concept transfomation) LLR method

[Ym8p2]=Rearrangbits(Ytk8p2at,Ytk8p2bt,b1psk2at); %MIMO-DC32QAM-8PSK(Rx2)(Without the new concept transfomation) LLR method

%%-------------------------------------------------------------------------------------------------------

[ydcmqpsk1]=RearrangDCMbits(Ytx1bbt,Ytx2bbt); % Proposed DCM-QAM (Soft Decoding) LLR method

%%-------------------------------------------------------------------------------------------------------

[Ynpsk1]=Rearrangbits(YYnp1at,YYnp1bt,b5nps1t); % NewConcept-MIMO-DC32QAM-B-8PSK with b5(G1)(With new bit5 idea) LLR method

%%-------------------------------------------------------------------------------------------------------

[Ynpsk1t]=Rearrangbits(YYnp1tat,YYnp1tbt,bnpk1at); %% NewConcept-MIMO-DC32QAM-B-8PSK (G1)  LLR method

%=========================================================================================================

%/////////////////////////////////////////////////////////////////////////////////////////////////////////

%%=========================================================================================================
```

```
[ydcmqpsk1s]=RearrangDCMbits(Ytx1bbts,Ytx2bbts);  % Proposed DCM-QAM (Soft Decoding)

%%-------------------------------------------------------------------------------------------------------------

[Ynpsk1s]=Rearrangbits(YYnp1ats,YYnp1bts,b5nps1ts);  % NewConcept-MIMO-DC32QAM-B-8PSK with b5(G1)(With new bit5 idea)

%%-------------------------------------------------------------------------------------------------------------

[Ynpsk1ts]=Rearrangbits(YYnp1tats,YYnp1tbts,bnpk1ats); %% NewConcept-MIMO-DC32QAM-B-8PSK (G1)

%=============================================================================================================

 % Error calculation for DC32QAM-B-8PSK  LLR method

 %%%[tnea2,nea2] = ErrorCalc(b1psk1t,codb5t,nea2,tnea2); % Test for bit5

 [tnea2,nea2] = ErrorCalc(Ytxa2t,cod1at,nea2,tnea2);

 %-------------------------------------------------------------------------------------

 % Error calculation for New Concept of MIMO-DC32QAM-B-8PSK  LLR method

 [tnew1ta,new1ta] = ErrorCalc(Ynpsk1t,cod1at,new1ta,tnew1ta);

 %[tnew1a,new1a] = ErrorCalc(b5nps1t,codb5t,new1a,tnew1a); % Bit 5 decoding test

 %-------------------------------------------------------------------------------------

 % Error calculation for New Concept of MIMO-DC32QAM-B-8PSK (With new bit5 idea)  LLR method

 [tnew1a,new1a] = ErrorCalc(Ynpsk1,cod1at,new1a,tnew1a); % New 5bit idea

 %%%[tnew1a,new1a] = ErrorCalc(Ynpsk1,cod1bt,new1a,tnew1a); % 4 bits (2QPSK) test

 %-------------------------------------------------------------------------------------

 % Error calculation for MIMO-DC32QAM-8PSK (Without the new concept transfomation)  LLR method

 [tn8p1,ne8p1] = ErrorCalc(Ym8p1,cod1at,ne8p1,tn8p1); % Rx1

 %-------------------------------------------------------------------------------------
```

```
 % Error calculation for MIMO-DC32-QAM-Flip  LLR method

 [tn32d1,ne32d1] = ErrorCalc(Yx32dc1,cod1at,ne32d1,tn32d1); % Rx1

 %-------------------------------------------------------------------------------

 % Error calculation for DCM_QPSK  LLR method

 [tnebb,nebb] = ErrorCalc(ydcmqpsk1,cod1bt,nebb,tnebb);

%=================================================================
=================================================================
=============================================

%/////////////////////////////////////////////////////////////////////////////////////////////////
/////////////////////////////////////

%%=================================================================
=================================================================
=============================================

 % Error calculation for New Concept of MIMO-DC32QAM-B-8PSK

 [tnew1tas,new1tas] = ErrorCalc(Ynpsk1ts,cod1at,new1tas,tnew1tas);

 %[tnew1as,new1as] = ErrorCalc(b5nps1ts,codb5t,new1as,tnew1as); % Bit 5
decoding test

 %-------------------------------------------------------------------------------

 % Error calculation for New Concept of MIMO-DC32QAM-B-8PSK (With
new bit5 idea)

 [tnew1as,new1as] = ErrorCalc(Ynpsk1s,cod1at,new1as,tnew1as); % New 5bit
idea

 %%%[tnew1as,new1as] = ErrorCalc(Ynpsk1s,cod1bt,new1as,tnew1as); % 4
bits (2QPSK) test

 %-------------------------------------------------------------------------------

 % Error calculation for DCM_QPSK

 [tnebbs,nebbs] = ErrorCalc(ydcmqpsk1s,cod1bt,nebbs,tnebbs);

%=================================================================
=================================================================
=============================================

%Comparison

if ne8p1>ThresholdErros, break; end % BER for MIMO-DC32QAM-
8PSK(Without the new concept transfomation)
```

if nebb>ThresholdErros, break; end % BER for DCM_QPSK

if new1ta>ThresholdErros, break; end % BER for New Concept of MIMO-DC32QAM-B-8PSK

if new1a>ThresholdErros, break; end % BER for New Concept of MIMO-DC32QAM-B-8PSK (New 5bit idea)

if nea2>ThresholdErros, break; end % BER for DC32QAM-B-8PSK

if ne32d1>ThresholdErros, break; end % BER for MIMO-DC32-QAM-Flip % Carfull for the use of ne32d1

end % jj2 close of the second loop (generate the randomisation in noise & ch 100 times)

%==========
==========
==========

if jj==0, sgpp1= sgpp1/165/3/Nit;sgpp2=sgpp2/165/3/Nit; % for DCM_QPSK

sgpsk1= sgpsk1/165/3/Nit; sgpsk2= sgpsk2/165/3/Nit; % for DC32QAM-8PSK

sgz1a= sgz1a/165/3/Nit; sgz1b= sgz1b/165/3/Nit; % for MIMO-DC32-QAM-Flip(Tx1)

sgz2a= sgz2a/165/3/Nit; sgz2b= sgz2b/165/3/Nit; % for MIMO-DC32-QAM-Flip(Tx2)

sgf1a= sgf1a/165/3/Nit; sgf1b= sgf1b/165/3/Nit; % for MIMO-DC32QAM-8PSK (Without the new concept transfomation)

sgf2a= sgf2a/165/3/Nit; sgf2b= sgf2b/165/3/Nit; % for MIMO-DC32QAM-8PSK (Without the new concept transfomation)(Tx2)

sgnew1a= sgnew1a/165/3/Nit; sgnew1b= sgnew1b/165/3/Nit; % for New Concept of MIMO-DC32QAM_Based on 8PSK (Tx1)

sgnew2a= sgnew2a/165/3/Nit; sgnew2b= sgnew2b/165/3/Nit; % for New Concept of MIMO-DC32QAM_Based on 8PSK (Tx2)

else

%==========
==========
==========

```
% BER for DC32QAM-B-8PSK  LLR method

Ber22 = nea2/tnea2; %

fber22(jj) = Ber22;

fEn2(jj)  = EBN(jj);

%-----------------------------------------------------------------------------------------------------------

% BER for New Concept of MIMO-DC32QAM-B-8PSK LLR method

Bernew1ta = new1ta/tnew1ta; %

fbernew1ta(jj) = Bernew1ta;

%-----------------------------------------------------------------------------------------------------------

% BER for New Concept of MIMO-DC32QAM-B-8PSK ( with New 5bit idea) LLR method

Bernew1a = new1a/tnew1a; %  New 5bit idea

fbernew1a(jj) = Bernew1a;%  New 5bit idea

%-----------------------------------------------------------------------------------------------------------

% BER for MIMO-DC32QAM-8PSK(Without the new concept transfomation) LLR method

Ber8p1 = ne8p1/tn8p1; % MIMO-DC32QAM-8PSK (Rx1)

fBer8p1(jj) = Ber8p1;

%-----------------------------------------------------------------------------------------------------------

% BER for MIMO-DC32-QAM-Flip   LLR method

Ber32d1 = ne32d1/tn32d1; % MIMO-DC32-QAM-Flip (Rx1)

fBer32d1(jj) = Ber32d1;

%-----------------------------------------------------------------------------------------------------------

% BER for DCM_QPSK   LLR method

Ber2bb = nebb/tnebb; %
```

```
fber2bb(jj) = Ber2bb;

%=================================================================
=================================================================
=================================================

%/////////////////////////////////////////////////////////////////////////////////////////////////
/////////////////////////////////////

%%================================================================
=================================================================
=================================================

% BER for New Concept of MIMO-DC32QAM-B-8PSK

Bernew1tas = new1tas/tnew1tas; %

fbernew1tas(jj) = Bernew1tas;

%-----------------------------------------------------------------------------------------
----------------------

% BER for New Concept of MIMO-DC32QAM-B-8PSK ( with New 5bit
idea)

Bernew1as = new1as/tnew1as; %  New 5bit idea

fbernew1as(jj) = Bernew1as;%  New 5bit idea

%-----------------------------------------------------------------------------------------
----------------------

% BER for DCM_QPSK

Ber2bbs = nebbs/tnebbs; %

fber2bbs(jj) = Ber2bbs;

%================================================================
=================================================================
=================================================

fprintf('EbN0=%3d[dB],          BER=%4d/%8d          =%11.3e\n',
EBN(jj),nea2,tnea2,Ber22);

if Ber2bb<1e-6, break; end % careful: Determine the EBN range

end

 end %  jj loop  % ----End of the first loop----------------------------

%================================================================
=================================================================
```

```
==============================================

%%%figure(2),

semilogy(fEn2,fber22,'gs-'); hold on % DC32QAM-B-8PSK

%%%-----------------------------------------------------------------------------------------------------

 semilogy(fEn2,fBer8p1,'b'); hold on % MIMO-DC32QAM-8PSK (Rx1)(Without the new concept transfomation)

% %%%-----------------------------------------------------------------------------------------------------

 semilogy(fEn2,fBer32d1,'r'); hold on % MIMO-DC32-QAM-Flip (Rx1)

% %%%-----------------------------------------------------------------------------------------------------

%%% semilogy(fEn2,fbernew1ta,'m*'); hold on % New Concept of MIMO-DC32QAM-B-8PSK LLR method

% %%%-----------------------------------------------------------------------------------------------------

% semilogy(fEn2,fber2bb,'k'); hold on % BER for DCM_QPSK  LLR method

%%%-----------------------------------------------------------------------------------------------------

semilogy(fEn2,fbernew1a,'c--'); grid on % New Concept of MIMO-DC32QAM-B-8PSK with New 5bit idea LLR method

%=====================================================
=============================================================
=============================================

%/////////////////////////////////////////////////////////////////////////////////////////////////////
/////////////////////////////////////

%%=====================================================
=============================================================
=============================================

%semilogy(fEn2,fbernew1tas,'y*'); hold on % New Concept of MIMO-DC32QAM-B-8PSK

% %%%-----------------------------------------------------------------------------------------------------

% semilogy(fEn2,fber2bbs,'ks'); hold on % BER for DCM_QPSK
```

```
%%%-------------------------------------------------------------------------------------------
----------------------

semilogy(fEn2,fbernew1as,'b--o'); grid on % New Concept of MIMO-DC32QAM-B-8PSK with New 5bit

%%=================================================================
=================================================================
=================================================

%%%legend('DC32QAM-B-8PSK(soft)','MIMO-DC32-QAM-Flip','BER for DCM-QPSK LLR','NewConceptMIMO-DC32QAM-8PSK1 5b(soft)with LLR');

%legend('DC32QAM-B-8PSK(soft)','MIMO-DC32QAM (Soft)','NewConceptMIMO-DC32QAM-8PSK1 5b(soft)with LLR');

legend('DC32QAM-B-8PSK(soft)','MIMO-DC32QAM (Soft)','MIMO-DC32-QAM-Flip','NewConceptMIMO-DC32QAM-8PSK1 5b with LLR','NewConceptMIMO-DC32QAM-8PSK1 5b(soft)');

xlabel('Eb/N0[dB]'), ylabel('BER');

%%%=================================================
=================================================================
=================================================

=================================================================
==========
```